A PETROLOGICAL AND GEOCHEMICAL STUDY REGARDING THE SUITABILITY OF THE VAALPUTS RADIOACTIVE WASTE DISPOSAL FACILITY

by

HERMANUS JOHANNES BRYNARD

Thesis submitted in partial fulfilment
of the requirements for the degree

PHILOSOPHIAE DOCTOR

in the Faculty of Science

University of Pretoria

NOVEMBER 1988

Page

ABSTRACT

The National Radioactive Waste Disposal Facility at Vaalputs in Bushmanland was selected for the disposal of intermediate- to low-level radioactive waste. The selection followed intensive investigations involving a wide spectrum of the earth sciences. Amongst others, mineralogical, petrological and geochemical studies were applied to study the rocks as a natural analogue to waste disposal. The aim of the investigation was mainly to identify the geochemical processes in the geological environment which gave rise to the present element distribution and furthermore to assess the extent to which the processes could retard element mobility. Using this knowledge, supported by experimental data, it was attempted to predict how these processes could contribute to retard the migration of radionuclides, comprising mainly Cs, Sr and Co, from the buried waste to the biosphere in the event of accidental release. The suitability of the rocks for the disposal of high-level radioactive waste was only briefly investigated.

The geological investigations led to the identification of an argillaceous surficial succession overlying a crystalline basement, comprising mainly granitic gneiss of the Namaqualand Metamorphic Complex, into which noritic rocks of the Koperberg Suite, amongst others, are intrusive. The surficial succession consists of a rock unit of argillaceous character, termed the white clay, overlying the weathered basement and is suggested to have been derived by in situ weathering of the basement. The white clay is overlain by a red clay unit, informally named the Vaalputs Formation, in which the SiO_2/Al_2O_3 ratio is significantly higher than that of the white clay indicating its more arenaceous character. Calcrete development is evident at various horizons through the entire surficial succession, but is especially prominent near the present ground surface. The red clay is significantly more depleted

with respect to most elements, except Ca and Mg in the calcrete, when compared to the white clay. The entire succession is covered by a thin veneer of red sand belonging to the Gordonia Formation.

The main clay minerals of the red clay are illite with subordinate kaolinite and smectite, while smectite predominates in the white clay and in the weathered and fresh basement, with subordinate kaolinite and illite. Smectite and kaolinite generally increase in depth while illite decreases, but exceptions to these trends occur. The former two formed by hydrolysis of the feldspar minerals and their stability is confirmed by the ground water chemistry. Illite presumably formed by physical and chemical reconstitution of micaceous minerals of which especially biotite is abundant in the Vaalputs rocks. These clay minerals, especially smectite and illite, have good adsorption and ion-exchange properties and can account for high concentrations of many elements, including the natural isotopes of the radionuclides. High concentrations of notably Nb, V, Cr, Th, Ni, Co, Zn and Pb can probably be attributed to adsorption onto, or co-precipitation with Ti-, Fe- and Mn-oxide minerals, which are known to be "scavengers" of these elements. Some trace elements such as Sr, Ba, Pb and Y are concentrated in a similar manner as above by calcretes, while the alkaline environment in the vicinity of calcrete layers is considered to be responsible for the immobilisation of Cs, Rb, Ba and V. The sediments are generally impoverished with respect to uranium, except for a few instances where locally favourable physico-chemical conditions were possibly conducive to its adsorption onto clay minerals. Iron-oxide minerals have also been shown to adsorb uranium, but hardly any correlations of Fe with U were found. Zirconium and hafnium are thought to be present mainly in zircon. Their correlation with Ti-, Fe- and Mn-oxides towards the base of the red clay suggests their presence in heavy mineral concentrations.

Cobalt is frequently correlated with the Ti-, Fe- and Mn-oxides, but its adsorption by clay minerals is also possible. The above-mentioned empirical observations of element retardation mechanisms are supported by experiments of radionuclide sorption by clay minerals and calcretes of Vaalputs. The experiments indicate that Co adsorption on clay and calcrete is maximal in the pH range 5,5 - 8 and sorption of U on clay is a maximum in the pH range 5 - 6,5. Sorption maxima of U on calcrete occur at pH4 and pH>8.

The red clay at Vaalputs is considered to constitute the distal portion of an alluvial fan which originated to the south-west of Vaalputs. The presence of blue quartz pebbles and iron-oxides nodules in the red clay suggests its origin as being partly reworked Dasdap Formation rocks, which outcrop to the south of Vaalputs and form the proximal portion of the Dasdap fan mentioned above. The conditions under which the red clay was deposited are thought to be humid coupled with good drainage, which changed during time to the present arid conditions. The white clay is considered to be the result of in situ weathering of the basement rocks, although a portion may have been derived from local reworking of weathered basement. The irreconciliable geochemistry of the white clay and the Dasdap Formation rocks precludes the latter as a precursor for the white clay sediments.

The calcretes at Vaalputs are considered to be of non-pedogenic origin i.e. due to precipitation from ascending ground water due to soil suction. A periodically fluctuating ground water level would explain the multiple calcrete layers in the succession. The red sand covering the entire sequence is of aeolian origin. The physico-chemical conditions in the rocks are oxidising, as inferred from the ubiquitous presence of iron-oxide coatings around mineral grains in the red clay. The absence of iron-oxides coatings in the white clay suggests that conditions in it were probably of a more

reducing nature. The slightly higher pH in the red clay, when compared to that in the white clay, further explains the paucity of iron-oxides in the latter.

The weathering at Vaalputs is considered to be mainly of a chemical nature with very little physical disintegration of the rocks having taken place. The most important factor which could influence the future migration of elements, including the radionuclides, is climate. However, dramatic changes in climate over relatively short periods (300 years) during which the waste is to be stored safely, have not been recorded and the Vaalputs site is therefore considered to be eminently suitable for the purpose for which it was chosen.

Despite the oxidation conditions in the basement rocks minor redistribution of uranium has taken place. It occurs mainly in refractory accessory minerals in the basement rocks. Argillic alteration products play an important role in immobilising this labile uranium. Under the anoxic conditions which would presumably prevail in a deep high-level waste repository, uranium would be expected to be even less mobile and the Vaalputs rocks therefore seem to be suitable for the disposal of high-level waste at least from a geochemical point of view.

SAMEVATTING

Die Nasionale Radioaktiewe Afvalwegdoeningsfasiliteit te Vaalputs in Boesmanland is geselekteer vir die wegdoening van medium- tot laagaktiewe radioaktiewe afval. Die keuse het gevolg op intensiewe ondersoeke wat 'n wye spektrum van die aardwetenskappe betrek het. Onder andere is mineralogiese, petrologiese en geochemiese studies toegepas om die gesteentes as 'n natuurlike analogie vir afvalwegdoening te bestudeer. Die doel van die ondersoek was hoofsaaklik die identifisering van geochemiese prosesse in die geologiese omgewing wat aanleiding gegee het tot die hedendaagse elementverspreiding en verder om die mate waarin hierdie prosesse die mobiliteit van elemente kan vertraag te bepaal. Deur van hierdie kennis gebruik te maak, gerugsteun deur eksperimentele data, is 'n voorspelling gewaag hoedanig hierdie prosesse sou bydra om die migrasie van radionukliede, wat hoofsaaklik Cs, Sr en Co behels, vanaf die begraafde afval na die biosfeer te vertraag in die geval van toevallige vrylating. Die geskiktheid van die gesteentes vir die wegdoening van hoogaktiewe afval is ook kortliks ondersoek.

Die geologiese ondersoeke het gelei tot die identifisering van 'n kleiige oppervlak-opeenvolging bo-op 'n kristallyne vloer, bestaande uit hoofsaaklik granitiese gneis van die Namakwaland Metamorfe Kompleks, waarin onder andere noritiese gesteentes van die Koperberg Suite intrusief is. Die oppervlak-opeenvolging bestaan uit 'n gesteente-eenheid met 'n kleiige karakter wat die verweerde vloer oordek en waarvan die oorsprong toegeskryf word aan <u>in situ</u> verwering van die vloer. Hierdie klei-eenheid word oordek deur 'n rooi klei-eenheid, informeel bekend as die Vaalputs Formasie, waarin die SiO_2/Al_2O_3 verhouding beduidend hoër is as die van die wit klei en wat dui op sy meer sandige karakter. Kalkreetontwikkeling is sigbaar op verskeie horisonne deur die hele oppervlak-

opeenvolging, maar is veral prominent naby die hedendaagse grondoppervlak. Die rooi klei is beduidend meer verarm met betrekking tot die meeste elemente, behalwe Ca en Mg in die kalkreet, wanneer dit met die wit klei vergelyk word. Die hele opeenvolging word oordek deur 'n dun lagie van rooi sand wat tot die Gordonia Formasie behoort.

Die hoof kleiminerale van die rooi klei is illiet met ondergeskikte kaoliniet en smektiet, terwyl smektiet in die wit klei oorheers en ook in die verweerde en vars vloer, met ondergeskikte kaoliniet en illiet. Smektiet en kaoliniet neem oor die algemeen toe met diepte terwyl illiet afneem, maar uitsonderings op hierdie patroon kom voor. Eersgenoemde twee het onstaan deur hidrolise van die veldspaatminerale en hulle stabiliteit word deur die waterchemie gestaaf. Illiet het vermoedelik gevorm deur die fisiese en chemiese herordening van die glimmers, waar veral biotiet volop is in die Vaalputs gesteentes. Hierdie kleiminerale, veral smektiet en illiet, besit goeie adsorpsievermoë en ioon-uitruileienskappe en kan rekenskap gee vir hoë konsentrasies van baie elemente, insluitende die natuurlike isotope van die radionukliede. Hoë konsentrasies van veral Nb, V, Cr, Th, Ni, Co, Zn en Pb kan waarskynlik toegeskryf word aan adsorpsie deur ko-presipitasie met Ti-, Fe- en Mn-oksied-minerale, wat as "opruimers" van hierdie elemente bekend is. Sommige spoorelemente soos Sr, Ba, Pb en Y word op soorgelyke wyse deur kalkrete gekonsentreer, terwyl die alkaliese omgewing in die nabyheid van kalkreetlae as synde verantwoordelik vir die immobilisering van Cs, Rb, Ba en V beskou word. Die sedimente is algemeen verarm in uraan, behalwe vir enkele gevalle waar plaaslike gunstige fisies-chemiese toestande bevordelik vir die adsorpsie daarvan op kleiminerale was. Daar is ook aangetoon dat ysteroksiedminerale uraan kan adsorbeer, maar nouliks enige korrelasies van Fe met U is gevind. Sirkonium en hafnium word vermoed as synde teenwoordig hoofsaaklik in sirkoon. Hulle

korrelasie met Ti, Fe- en Mn-oksied naby die basis van die rooi klei suggereer hulle teenwoordigheid in swaarmineraalkonsentrasies.

Kobalt is dikwels gekorreleer met die Ti-, Fe- en Mn-oksiede, maar adsorpsie daarvan deur kleiminerale is ook moontlik. Die bogenomemde empiriese waarnemings van element-vertragingsmeganismes word deur die resultate van eksperimente op radionukliedsorpsie deur klei-minerale en kalkreet vanaf Vaalputs gerugsteun. Die eksperimente toon dat Co-adsorpsie op klei en kalkreet maksimaal is in die pH bereik van 5,5 - 8 en U-sorpsie op klei 'n maksimum is in die pH bereike van 5 - 6,5. Sorpsie maksima van U op kalkreet kom by pH4 en pH>8 voor.

Die rooi klei op Vaalputs word as die verwyderde gedeelte van 'n alluviale waaier, wat sy oorsprong suidwes van Vaalputs gehad het, beskou. Die teenwoordigheid van blou kwartsrolstene en ysteroksied nodules in die rooi klei suggereer die oorsprong daarvan as synde gedeeltelik herwerkte Dasdap Formasie-gesteentes, wat suid van Vaalputs dagsoom en die nabye gedeelte van die Dasdap alluviale waaier, hierbo genoem, vorm. Die toestande waaronder die rooi klei afgeset is word beskou as hoë humiditeit gekoppel aan goeie dreinering wat met die loop van tyd verander het na die hedendaagse droë toestande. Die wit klei word beskou as die produk van <u>in situ</u> verwering van die vloergesteentes, alhoewel 'n gedeelte daarvan toegeskryf kan word aan plaaslike herwerking van verweerde vloergesteentes. Die onversoenbare geochemie van die wit klei en die Dasdap Formasie gesteentes sluit laasgenoemde gesteentes as brongesteente vir die sedimente van die wit klei uit.

Die kalkrete te Vaalputs word as van nie-pedogene oorsprong beskou, dit wil sê as gevolg van presipitasie uit stygende grondwater as gevolg van grondvakuum. 'n Periodieke wisselvallige grondwatervlak sou die veelvuldige kalkreetlae in die opeenvolging verklaar. Die

rooi sand wat die hele opeenvolging bedek is van windafsettings (eoliese) oorsprong.

Die fisies-chemiese toestande in die gesteentes is oksiderend, soos afgelei uit die wye teenwoordigheid van ysteroksied-deklagies om mineraalkorrels in die rooi klei. Die afwesigheid van sulke ysteroksiedlagies in die wit klei suggereer dat toestande daarin waarskynlik van 'n meer reduserende aard was. Die effens hoër pH in die rooi klei, wanneer dit met die wit klei vergelyk word, verklaar die afwesigheid van ysteroksiedlagies in laasgenoemde verder.

Die verwering te Vaalputs word as hoofsaaklik van 'n chemiese aard met baie min fisiese disintegrasie van die gesteentes beskou. Die mees belangrike faktor wat 'n invloed kan hê op die toekomstige migrasie van elemente, wat die radionukliede insluit, is klimaat. Dramatiese klimaatsveranderinge oor die betreklike kort periode van 300 jaar waarin die afval geberg sal moet word is nog nie aangeteken nie en die Vaalputsterrein word derhalwe as uitmuntend geskik beskou vir die doel waarvoor dit gekies is.

Nieteenstaande die oksiderende toestande in die vloergesteentes het geringe herverspreiding van uraan, wat hoofsaaklik in weerstandbiedende bykomstige minerale in die vloergesteentes voorkom, in die vloergesteentes plaasgevind. Kleiige veranderingsprodukte speel 'n belangrike rol in die immobilisering van hierdie beskikbare uraan. Onder die anoksiese toestande wat vermoedelik in 'n diepwegdoeningsfasiliteit vir hoogaktiewe afval sal heers, word uraan verwag om selfs minder mobiel te wees en die Vaalputs gesteentes blyk uiters geskik vir die wegdoening van hoogaktiewe afval te wees gesien uit 'n geochemiese oogpunt.

List of Figures

List of Tables

CHAPTER 1

INTRODUCTION

By generating electricity at the 1 842 MW Koeberg nuclear power station, the national electricity generating and supply utility, Eskom, became South Africa's largest producer of radioactive waste. In preparing for this eventuality, Eskom and the Atomic Energy Corporation of South Africa Limited (AEC) studied the requirements for the safe disposal of Koeberg nuclear waste, after which the AEC agreed to embark on a site selection programme for a national radioactive waste repository. This work culminated in the establishment of the National Radioactive Waste Disposal Facility at Vaalputs in Bushmanland (Spencer et al., 1986), (Fig. 1).

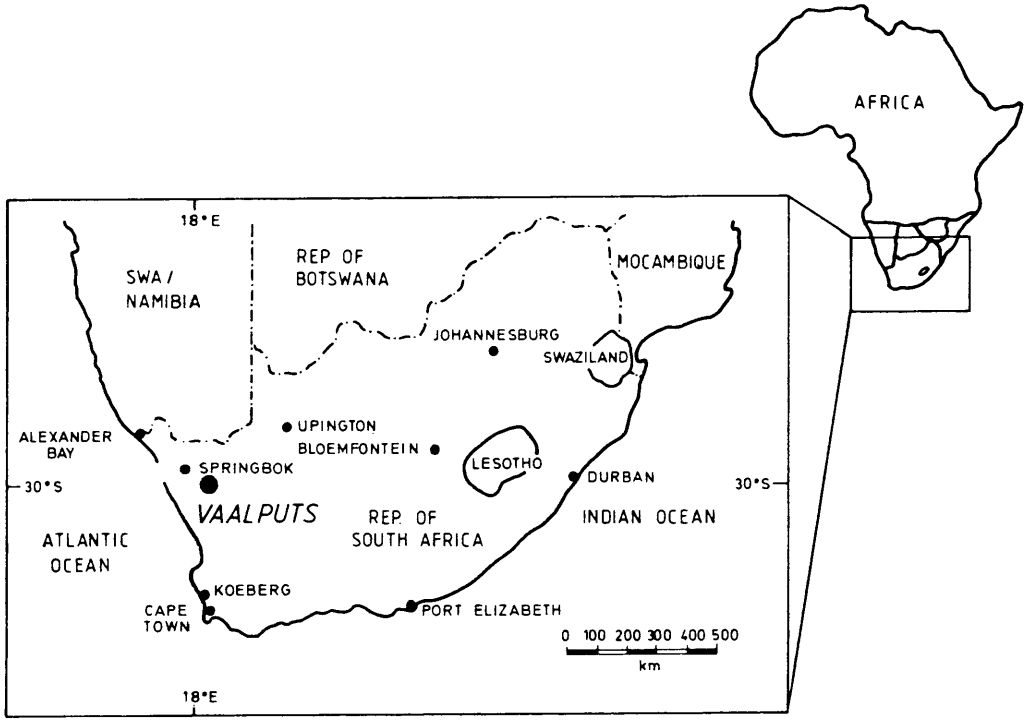

Figure 1 Location of the Vaalputs National Radioactive Waste Disposal Facility in Bushmanland.

The general geology of the Vaalputs vicinity comprises a basement of metasedimentary rocks into which granites are intrusive. These together with the metasediments belong to the Namaqualand Metamorphic Complex. This basement is overlain by an argillaceous sequence with an average thickness of 30 m consisting of a lower white clay unit and an upper red clay unit covered by a thin veneer of sand. Several layers of calcrete with varying thickness are developed within the argillaceous sequence.

1.1 Nature of the Radioactive Waste

The Vaalputs facility which received its first waste in November 1986 makes provision for the storage of intermediate- and low-level waste only, although some consideration is being given by the AEC to the possibility of storing spent fuel and high-level waste at the same site in the future.

Low- and intermediate-level radioactive waste generated in the normal operation of nuclear installations is defined as follows:

- Low-level waste mainly consists of trash such as gloves, clothing and paper.

- Intermediate-level waste comprises particulate filters and ion-exchange resins used in the various clean-up systems of a nuclear power station. Approximately 95% of the radioactivity is contained in the resins.

The low-level waste is compacted into 200 litre metal drums, while the intermediate level waste is immobilised in concrete containers (Fig. 2) lined with metal to absorb possible deformation of the container. The container is capped with concrete and weighs approximately 5 tons.

The amounts of radioactive waste are measured in terms of activity of which the standard unit is the Becquerel (Bq). The more important radionuclides produced annually by the Koeberg nuclear

power station are ^{60}Co, ^{90}Sr, ^{137}Cs and ^{134}Cs, while some ^{238}U may also be present. The amounts of activity from these radionuclides and their half-lives are given in Table I.

Figure 2 The stacking of intermediate-level waste containers in a disposal trench located in red clay at the Vaalputs Radioactive Waste Disposal Facility.

Table I Activity of the more important radionuclides produced annually by the Koeberg nuclear power station

Radionuclide	Activity per annum *(Bq x 10^{12})	Half-life (years)
^{60}Co	39,26	5,3
^{90}Sr	0,19	28,1
^{134}Cs	360,05	2,3
^{137}Cs	177,45	30,2

*The standard SI-unit for radioactivity is the Becquerel (Bq)

The volumes of waste to be disposed of from three nuclear power stations in the 60 year proposed life time of the repository are given in Table II.

Table II Volumes of waste to be disposed of in the 60 year proposed life-time of the Vaalputs repository

Waste generator	Type of container	Container volume (m^3)	Number of containers per year per station	Total volume disposed of in 60 years*
Eskom	Concrete	2	500	120 000
Eskom	Metal	0,2	1 500	36 000
Eskom	Filters	-	-	14 400
AEC	Metal	0,1	1 700	10 200

* In this calculation it was assumed that waste from a second power station will be received after 10 years of operation of the facility and from a third station after 20 years.

High-level waste will not be stored at Vaalputs in the foreseeable future. It comprises mainly the waste products generated during the re-processing of spent fuel elements to recover unfissioned uranium and possibly transuranic products such as ^{239}Pu for use as nuclear fuel in a breeder reactor. The waste includes highly toxic and long-lived isotopes and stringent precautions are required for their permanent storage or disposal. The most commonly envisaged repository for this type of waste is a deep excavation in basement rocks. No decision has been made by the appropriate authorities to reprocess spent fuel, therefore very little attention has been given in the present treatise to the suitability of the Vaalputs rocks for disposal of this type of waste.

1.2 Purpose and Scope of this Study

The most likely means for radionuclides, disposed as solid waste in geological repositories, to reach the biosphere, is through dissolution of the solid waste and subsequent radionuclide transport by circulating ground water. Licensing criteria require information regarding the physico-chemical interactions between radionuclides present in ground water with the waste package and rocks, since these processes can significantly delay or constrain the mass transport of radionuclides relative to ground water movement. Although the literature on radionuclide migration and adsorption by

clay minerals and other phases is voluminous, this knowledge cannot summarily be applied to the site in question, and there is therefore a need for site-specific data to evaluate its suitability for the disposal of radioactive waste.

When Vaalputs was chosen as a suitable candidate site, detailed geophysical and geological investigations were initiated to gain site-specific data. The preliminary mineralogical work indicated that the geological environment in which the waste was to be buried was eminently suitable to retard the migration of radionuclides in the unlikely event of accidental release. However, the need arose to investigate this environment also from a geochemical point of view, the aim being to model the migration of elements, particularly the naturally occurring isotopes of the radionuclides present in the waste, through geological history and to attempt a prediction as to their likely future behaviour. The predictions regarding nuclide migration based on the current investigations should be valid for at least 300 years, the period required for the radioactivity in the waste to decay to safe levels.

The approach in this investigation has been to study the geological environment at Vaalputs as a natural analogue to radionuclide behaviour and as such the study has been a qualitative assessment of the suitability of the rocks for the disposal of low- to intermediate-level radioactive waste, with some consideration of the potential suitability of the site for the storage or disposal of high-level waste. The use of mathematical models was intentionally avoided as this forms the study material of a thesis by Levin (1988) on the geohydrology of the site.

The prediction of radionuclide migration over the long time-scales during which radioactive wastes are stored is difficult to model with confidence without an understanding of the processes involved. Generic research models, supporting a probabilistic risk assessment for a particular proposed repository site, need to be tested with data and measurements belonging to natural geochemical systems. The role and applications of natural analogues in radioactive waste

assessments have been described by Chapman and Smellie (1986). To be of optimum use, a natural analogue study of radionuclide mobilisation, migration and retardation is best confined to a particular process. These authors stated that in selecting an analogue, the geochemical process should be clearly measurable, that the natural elements studied should behave like the radionuclides of interest, that the physico-chemical parameters should be quantifiable, and that the time scale factor should be defined. These constraints determine the validity of an analogue in the modelling exercise (Chapman et al., 1984).

Finally the observations and conclusions of the study could make some contribution to the knowledge concerning the geochemistry and mineralogy of weathering in an arid environment.

CHAPTER 2

METHODS USED IN THIS STUDY

In the present study rock is regarded as any consolidated or unconsolidated material (but not soil) with one or more minerals or a representative sample of such material (Glossary of Geology, 1972).

2.1 Sampling

2.1.1 Basement rocks

A suite of basement rocks were sampled from outcrops in the vicinity of the waste disposal facility with the following aims in mind:

- To test the continuity of basement rocks, outcropping on Vaalputs, underneath the argillaceous succession by mineralogical, geochemical and petrological comparison with rocks encountered in percussion boreholes on the site.

- To evaluate the possibility of these rocks being the source rocks of the argillaceous succession on Vaalputs by comparison of their mineralogy and geochemistry.

- To evaluate the suitability of basement rocks for high-level waste disposal by studying their uranium distribution and mobility.

The paucity of outcrops limited the number of rock types that could be sampled. The sample locations are shown in Appendix A. Although diamond drill core became available at a later stage during the study, chips from percussion boreholes on the Vaalputs site were mostly utilised for this part of the investigation.

2.1.2 Surficial rocks

The samples for the greater part of the geochemical study were derived from percussion boreholes in the area around the waste disposal site and were chosen to best represent the different rock types of the argillaceous succession.

Sampling of percussion boreholes was carried out simultaneously with the drilling operations. Samples were collected in 1 m long PVC sausage bags using a cyclone sample blower. During subsequent logging by the field geologist, lithological variations were noted and the coarse fraction (>1mm) of the sediments was investigated by means of a hand lens and dilute hydrochloric acid for the presence of calcite. Lithologically different layers were sampled separately and a representative portion was derived by repetitive splitting with a 25 mm sample splitter. Eventually a 1 kg sample was obtained for storage and an equal quantity was kept as reference material. In the laboratory a 100 g sample was taken from the former sample by repetitive splitting using a 10 mm sample splitter. Of this sample 25 g was weighed out for mineralogical and chemical analysis.

2.1.3 Calcrete

Twenty-four samples of calcrete and silcrete were collected at various depths in the vertical walls of the waste disposal trenches at Vaalputs. The horizons sampled comprised fairly continuous bands of calcrete nodules. In addition, a vertical crack, lined with calcrete, in the trench wall was sampled for comparison.

Trench 1 is currently used for the storage of low-level waste in metal drums, while intermediate-level waste is stored in concrete drums in trench 2. The samples are numbered consecutively from the top to the bottom in trench 2 with sample 2T1 representing the top-most sample. The suffix A-E denotes a different lateral position on a particular calcrete horizon. Sample 1T1 was taken midway down the red clay unit in trench 1 and the rest consecutively downwards and laterally. The calcretes all occur within the red sand and red

clay units at depths ranging from 0,5 m to 7 m.

Thin sections were prepared of the calcrete samples described above and portions were crushed to a grain size of a few millimeters in diameter. These portions were submersed in an ultrasonic bath and cleaned for several minutes to release excessive detrital material from the surface of the samples.

2.2 Calcrete Dissolution

A portion of each sample, between 30 to 80 g in mass, was weighed out after drying at 110^{o}C and placed in a conical flask. Dilute nitric acid was added to dissolve the sample. As most samples effervesced vigorously, care had to be taken to prevent the sample from bubbling out of the flask. Acid was continually added over a period of days, until no further effervescence was observed, even after the addition of concentrated acid. A few drops of methyl-tymol blue indicator were added and the solutions were neutralised by the addition of ammonia, until a colour change from red to yellow was observed, which represents a pH of approximately 7.

The solutions were subsequently filtered through Whatman No. 541 filter paper, which was washed with demineralised water, to give a clear solution free of gelatinous or suspended material. The solutions were made up to a volume of 1 000 ml in a volumetric flask and submitted for analysis of Ca, Mg, Sr, Ba, Co, Cu, Pb, V, Y and Zr by inductively coupled plasma analysis (ICP). A control sample of analytical grade calcium carbonate was treated in the same way as the calcrete samples and the solution was also analysed by ICP.

The insoluble residues were dried at 110^{o}C in the filter paper and weighed. These together with representative portions of the original calcretes were submitted for X-ray fluorescence analyses of major and trace elements. The percentages of dissolved rock were calculated and the analyses of the aliquots were recalculated to the mass of dissolved rock.

2.3 Analytical Techniques

Analyses for major and trace elements of borehole chip samples were carried out by two different laboratories using the X-ray fluorescence method. Major element analyses were done on fused glass discs and did not initially include Na_2O and MgO due to technical difficulties with the apparatus. These two elements were later analysed for by another laboratory. This may be the reason for the poor totals in some cases (Appendix D). The calcrete analyses were carried out at a later date by a private laboratory and their totals are within acceptable limits (Appendix F). The FeO values reported in all the tables in this thesis were determined by means of X-ray fluorescence analysis.

All trace element analyses of surficial rocks, except Ga, Cs, Cr and Hf, were done by a multi-element X-ray fluorescence method using pressed powders. A duplicate set of samples from borehole W40N0 was analysed to check for precision. A good correlation (0,93 at the 95% confidence level) was found between the two sets of analyses and the results, using the first method, are considered adequate for the present purpose. The reason for using multi-element X-ray fluorescence analysis in preference to more accurate methods was to analyse as many samples as possible within monetary constraints and to obtain a picture as representative as posssible of the spatial distribution of elements even though this may be at the expense of accuracy.

The detection limits and accuracy of trace element analyses by means of the X-ray fluorescence method are listed in Table III (De Villiers, 1983). He used ten briquettes of pressed powders (not Vaalputs samples) which were analysed for 17 elements, some of which are listed in Table III. The concentrations and standard deviations for the different elements are reported in Table III. In general the relative standard deviation is exponentially proportional to the reciprocal of the concentration of the element. Analyses for some elements, particularly U, Th and Cu are generally considered to be of low accuracy because of their low concentrations in the surficial rocks.

Ga, Cs, Cr and Hf in surficial rocks and all trace elements in the suite of regional basement rocks were determined by the neutron activation technique.

Table III Detection limits and accuracy of trace element analyses by X-ray fluorescence

Element	Detection limit (ppm)	Concentration (ppm)	Standard deviation	Relative standard deviation (%)
Ba	9,8	599	12,3	2,1
Co	3,2	23	0,9	4,0
Cu	2,5	6	0,7	12,5
Nb	1,5	5	0,5	9,4
Ni	2,8	38	1,2	3,1
Pb	4,9	22	1,2	5,5
Rb	2,1	58	1,0	1,6
Sr	2,0	264	3,8	1,4
Th	4,2	9	0,5	5,6
U	3,5	98	1,5	1,5
V	3,8	86	2,1	2,5
Y	1,8	18	0,6	3,5
Zn	2,1	34	1,0	3,1
Zr	1,7	116	2,6	2,3

De Villiers (1983)

Solutions derived from calcrete were analysed by induced coupled plasma analysis, which is accurate at the low concentration levels of the elements analysed for. The accuracy of the major element analyses was controlled by the inclusion of a control sample comprising analytical grade $CaCO_3$ for which a Ca value of 39,37% was obtained, 0,63% below the theoretical value of 40% for pure $CaCO_3$. This represents an analytical error of 1,6%, which is within acceptable limits.

To assess the reliability of the calcrete trace element analyses the analyses of whole rock, insoluble fractions and solutions were applied to calculate the theoretical concentrations of elements in the whole rock by using a mass balance equation:

$$Ci_{\text{whole rock}} = c1Ci_{\text{soluble}} + c2Ci_{\text{insoluble}}$$

where Ci is the concentration of element i in a fraction;
c1 = fraction of soluble rock; and
c2 = fraction of insoluble rock = (1-c1).

The calculated concentrations for Ca and Mg were on average within 6% of the analysed values. The trace elements showed a greater but systematic variation and correlation coefficients ranging between 0,59 and 0,96 were calculated for the two sets of values (Table IV). Only Pb values showed no correspondence in the two sets of values. The discrepancy between calculated and analysed values could probably be attributed to the small quantity of material in the insoluble fraction which was available for analysis.

Table IV Correlation coefficients for calculated and analysed concentrations of elements in calcrete whole rock analyses

Element	Co	Cu	Sr	Zr	V	Y	Pb	Ba	Mg	Ca
Correlation coefficient	0,59	0,63	0,82	0,93	0,91	0,63	0,05	0,66	0,92	0,96

2.4 Clay Mineral Analyses

2.4.1 Pre-treatment for mineralogical analysis

Pre-treatment for mineralogical analysis involves the removal of undesirable constituents in the sediments such as carbonate minerals, organic matter and free iron oxides which may adversely affect dispersion of the clay. Furthermore, the degree of crystal orientation required for X-ray diffraction analysis may be reduced significantly by the presence of these constituents on clay particles. The pre-treatment methods are designed to have a minimal undesirable effect on the physical properties of the sediments (Kunze, 1965).

Calcite was dissolved by using sodium acetate at a concentration of 1 mole per litre adjusted to pH 5 with acetic acid. The samples were treated with 80 ml of acetate at 80°C in glass beakers on a water bath for 8 hours. Following acetate treatment the samples were allowed to settle, the clear supernatant liquid was decanted and the samples were transferred to 100 ml plastic bottles in which it remained for all the subsequent procedures.

Organic material in sediments has an aggregating effect and its removal is necessary for good dispersion. Hydrogen peroxide is commonly used to oxidise organic matter. Each sample was treated with 20 to 30 ml of hydrogen peroxide (30%) in the plastic bottles which were heated to 80°C in an oven for 8 hours. Since no strong effervescence occurred the organic content in the sediments is evidently low.

The term "free oxides", refers to compounds having only a single species of co-ordinating cation such as silicon or iron. Free iron-oxides usually occur as discrete particles or as coatings on mineral grains and may cause fluorescence background during X-ray diffraction analysis when using Cu-Kα radiation, resulting in poor peak-to-background ratios. In addition they may prevent dispersion and good orientation of the sample (Kunze, 1965). The need to

remove iron-oxide was not investigated systematically, but trial X-ray diffraction studies on two iron-rich samples showed the presence of poor 14 Å peaks on the X-ray diffractograms, possibly due to a lack of clay mineral orientation. Iron removal in these samples resulted in the appearance of distinct 14 Å peaks. All samples were therefore deferrated by the addition of 40 ml each of sodium citrate (0,3 mole per litre) and sodium bicarbonate (1 mole per litre) at pH 8,4 to which 1,5 - 6 g of sodium dithionite was added. The latter acts as a reducing agent for iron and the sodium citrate acts as a chelating agent. The samples were allowed to react at 70°C for a few hours. The bottles with samples were then centrifuged and the supernatant liquid was decanted.

Interlayer cations retain different amounts of water of hydration and it is necessary to saturate the clay homo-ionically to ensure uniform expansion. In the present study magnesium chloride (0,5 mole per litre) was added to each sample and the sample was shaken for approximately four hours. The samples were subsequently repeatedly centrifuged, washed with demineralised water and tested with silver nitrate until they were free of chloride ions.

After magnesium saturation the sample was wet-sieved through a 45 µm sieve to separate the sand from the silt and clay fraction. The sample bottles containing the latter fraction were filled with demineralised water, shaken, and allowed to stand for three hours and twelve minutes at 20°C, which is the time required for particles of 2 µm in diameter to settle through 40 mm in water, according to the equation of Stokes. After this period the top 40 mm of each sample was siphoned off and collected in a separate container.

It is well known that equivalent spherical particle diameter theory is not necessarily applicable to the settling velocity of plate-shaped particles such as clay. Therefore, the unpredictable settling behaviour of clay-sized particles may lead to some mineralogical variation due to inaccurate size segregation (Birch, 1978).

2.4.2 Sample mounting and X-ray diffraction

The clay fraction was mounted on semi-porous tiles measuring 30 mm by 37 mm and 2 mm thick, cut from unglazed ceramic tiles. The clay suspension was dropped onto the tile to cover an area of 30 mm by 20 mm and dried under a heat lamp until a thickness of approximately 80 µm was obtained. This was found to be the optimum thickness to give a good peak-to-background ratio on diffractograms and simultaneously prevented curl-up of the clay as a result of drying.

The samples were analysed using a Philips diffractometer with a Geiger detector employing Co-Kα radiation and an iron filter. The instrumental settings were as follows : KV = 40; mA = 25; attenuation = 2^4; time constant = 4; slits $^1/_2^\circ$, $^1/_2^\circ$/0,1 mm. The rate meter settings varied from 4 x 10^2 to 2 x 10^3 counts per second. Thirty samples were scanned from 2° to 35° 2θ and since no appreciable peaks were observed at angles exceeding 15° 2θ all subsequent samples were scanned from 2° to 15° 2θ. Expansion of smectite clays was achieved by the application of glycerol to dried clays by means of a soft brush. A mixture containing 150 ml ethanol, 10 ml glycerol and 5 ml demineralised water was used. Untreated clay mounts were heated to 300°C and 550°C for one hour and scanned from 2° to 15° 2θ to observe changes in the structure of the clay minerals.

2.4.3 Mineral identification

Mineral identification was made by means of the characteristic basal reflections at interplanar spacings of 7 Å, 10 Å, 12,5-14 Å and 17 Å.

Illite was characterised by its 001 reflection due to a d - spacing of 10 Å which was enhanced subsequent to heating to 300°C and also persisted after heating to 550°C. Smectite clay was identified by a reflection corresponding to the 001 d-spacing of 12,5-14 Å which shifted to 17 Å on glycerol treated mounts and collapsed almost wholly to 9 Å after heating to 300°C and completely after heating to 550°C. Kaolinite characteristically shows prominent peaks at 7,1 Å

and 3,57 Å. Both these peaks become broader and more diffuse with increasing structural disorder (Wilson, 1987). Kaolinite was positively identified by heating the slides to 550°C for 1 hour which destroys the crystallinity of nearly all kaolinites, resulting in the total collapse of the strong basal reflection at 7 Å. This is a useful confirmatory test for kaolinite, except where chlorite is present in which case there is only partial collapse of this peak (Wilson, 1987). The chlorite can then be decomposed by 6N hydrochloric acid (at 90°C for 30 minutes), whereas kaolinite will resist this treatment.

2.4.4 Semi-quantitative analyses

Quantitative estimates of the amounts of clay minerals in sediments have been stated by various authors to be probably accurate to about 5 to 10% (Carroll, 1970). The semi-quantitative analyses carried out in the present study were based on methods investigated by Johns et al. (1954) and Schultz (1964).

Semi-quantitative estimates were made by comparison of integrated peak areas on glycerol-treated diffractograms. The areas under peaks were measured with a planimeter. The area under the 7 Å peak was totally assigned to kaolinite, the 10 Å peak area to illite and the 17 Å peak area to smectite. The intensity data for illite and smectite could not be compared directly due to the fact that the efficiency with which a sheet-type silicate mineral scatters X-rays along the 001 plane varies with sin θ according to a form factor function (Johns et al., 1954). It has been shown by Bradley (1953) that the reflections due to clay minerals with a d - spacing corresponding to 17 Å, exceeds the intensity of reflection of similar material with a d - spacing of 10 Å, by a factor of four. Therefore the peak area of illite at 10 Å must be multiplied by four to facilitate comparison with the 17 Å smectite peak area. Similarly the ratio of peak areas corresponding to 7 Å and 10 Å, which represent kaolinite and illite respectively, ranges from 1:1 for poorly developed kaolinite to 2:1 for well crystallised kaolinite (Schultz, 1964).

The sharpness of the 7 Å kaolinite peak, as expressed by its area-to-height ratio was used to evaluate the crystallinity of kaolinite. The average value of 0,4 mm indicated good crystallinity. The modified peak areas of each constituent can then be expressed as a percentage of the sum of the modified peak areas:

% mineral x = 100[(modified peak area of mineral x) ÷ {0,5(7 Å peak area) + 4(10 Å peak area) + (17 Å peak area)}].

To test the accuracy of the clay mineral analyses, mixtures were analysed of pure <2 µm clay mineral species from Vaalputs. Three mixtures were prepared in which pure fractions of each of the three major clay minerals i.e. smectite, illite and kaolinite, comprised the major constituent (50%) and the other two clay minerals 25% each. X-ray diffractograms were obtained of the glycolated clay mixture mounts, which were prepared following the same procedures as for the samples. Diffractograms were also obtained of the pure species. The results indicated that the smectite peaks in all the mixtures were greatly exaggerated at the expense of illite, which showed an anomalously low peak when compared to that of the pure component, even in the slide in which it is the major component. The smectite peaks of pure material and that of the mixture in which it forms the major component showed relatively small differences in peak areas on diffractograms, using identical instrument settings.

By solving for the three unknown coefficients in three linear equations of calculated mass percentages and measured peak areas of the clay minerals, a formula was derived according to which the clay mineral composition could be calculated from the measured peak areas as described previously. The results are presented in Table V. The coefficients for smectite, illite and kaolinite were found to be 0,5, 5 and 2 respectively compared to 1, 4 and 0,5 which are widely quoted in the literature (Johns et al., 1954, Schultz, 1964, Pierce and Segal, 1969). The ideal formula for calculating the composition of Vaalputs clay mineral mixtures then becomes:

% mineral x = 100[(modified peak area of mineral x) ÷ {2(7 Å peak area) + 5(10 Å peak area) + 0,5(17 Å peak area)}].

Although the results of this experiment are probably not statistically significant it is considered that it represents a more reliable approach to determining the true clay mineral composition than summarily applying the formulas given in the literature. However, the important aspect as pointed out by Pierce and Segal (1979) is "that although calculation methods differ and give significantly different results, if used with the same diffractograms, each method (of analysis) is internally consistent for a given study and can give results that suggest meaningful geological trends."

Table V Calculated and analysed compositions of clay mineral mixtures from Vaalputs

Sample	Calculated value (mass %) A	B	C	Analysed value (mass %) A	B	C
Smectite	50,5	25,3	24,3	49,7	26,4	23,9
Illite	24,5	50,0	24,8	21,2	47,1	27,8
Kaolinite	25,0	24,8	51,0	29,0	26,5	48,3

2.5 Fission-track Micro-mapping

The study of uranium distribution in rocks is complicated by the often finely disseminated nature of the uranium and the fact that it is usually present in concentrations far below the detection limit of the electron microprobe.

Solid-state track-detector methods for studying uranium distribution in geological material include autoradiography, alpha-track and fission-track methods. Of these methods fission-track micro-mapping is preferable in that it is rapid, much more sensitive and specific in detecting uranium or uranium together with thorium, depending on the experimental conditions. Fission-track detection in solids was initiated by Price and Walker, (1962) who followed up the direct electron microscopic observation of tracks by Silk and Barnes (1959). A disadvantage of the method is the fact that the investigator must have access to an intense source of neutrons such

as a nuclear reactor. In addition, only small samples (~4 cm^2) can be studied.

2.5.1 Theory of fission-track micro-mapping

In essence tracks are produced when ^{238}U, or ^{235}U irradiated by thermal neutrons, fission into two fragments which move away from the original site in opposite directions. If these fission fragments are allowed to bombard an overlay of a dielectric solid they leave trails of damage to the atomic structure of the solid. These damage trails may be rendered visible under an optical microscope after treatment with a properly chosen chemical, usually a strong acid or alkali, which preferentially attacks the damaged area and removes the surrounding matrix. This enlarges the etched hole and marks the trail of the particle which is commonly known as a track and a record of the uranium site is obtained. When these tracks are sufficiently dense their distribution may be visible to the unaided eye. Dielectric solids commonly used in the study of nuclear track distribution are polycarbonate plastics, of which Lexan is most commonly used, cellulose nitrate and muscovite.

Low intensity ionising radiation such as that produced by alpha- and beta-decay is not recorded so that internal tracks in crystals or in solid state detectors are entirely due to either fission of uranium or thorium or to recoil nuclei much heavier than alpha particles. If the neutron dose is accurately monitored, the density of tracks induced by irradiation in the detector can be used to determine the uranium content of the material, otherwise standards of known uranium concentration can be included in the sample holder to be irradiated.

2.5.2 Methodology

The techniques employed in the present study involved the preparation of polished thin sections on glass and on specially prepared resin discs. The use of polished thin sections is convenient as they can be viewed by both incident and reflected

light. The presence of sodium in the glass slides causes them to become highly radioactive and several days are required for the radioactivity to decay to a level which permits safe handling of the slides.

Discs made of cold-setting resin have been found to work satisfactorily for irradiation times not exceeding fifteen minutes, after which the resin shows colouration, often to such an extent as to render viewing in transmitted light impossible. However, irradiation times up to five minutes have proved to be sufficient to yield visible prints, even with very low concentrations of uranium (Brynard, 1983, 1986).

Discs of mica sheet less than 100 µm thick or Lexan polycarbonate plastic approximately 100 to 250 µm thick were placed onto the thin sections after location holes were pierced through the detector and into the thin section surface to facilitate subsequent reorientation. Alternatively marks with radioactive ink can be made. Wrapping of the section and its detector overlay in "lunch wrap" plastic has been found to be of great advantage in securing close contact between sample and detector, resulting in enhanced resolution (Brynard, 1986). Muscovite consistently proved to be a superior detector to Lexan polycarbonate due to its better resolution for fission-tracks.

This assembly was then irradiated by means of the pool-side rotating facility (PROF) in the SAFARI-1 reactor. After cooling down to a permissible level of radiation the discs and detectors were removed to the laboratory. The detectors were etched in 6N KOH in the case of Lexan and 40% hydrofluoric acid in the case of mica, after which the detectors were dried and reorientated by superimposing the location marks on the disc on their corresponding holes. The fission-tracks on the detector were then studied by viewing in normal transmitted light under the optical microscope. The matching precision between the print and sample was generally about 50 µm but with care this was reduced to about 10 µm. No attempt was made to quantitatively determine the uranium content of the rocks in the present study.

2.6 Grain Size Analyses

One representative borehole, W40N0, was chosen for a grain size distribution analysis. A 100 g representative portion of each sample from this borehole was weighed into a 250 ml plastic bottle and 150 ml of Calgon (sodium hexametaphosphate which is commercially available as a water softener) was added to facilitate dispersion.

The sample was shaken for 4 hours to disperse the sediment after which it was wet-sieved through a series of sieves with apertures of 45, 63, 125, 250, 425, 850 and 1 700 µm. The suspension which passed the 45 µm sieve was collected in a container. The other fractions were dried in an oven at 100°C and weighed. The mass of each fraction was expressed as a percentage of the original sample.

2.7 Multivariate Statistical Techniques

To assess the interrelationships of variables in a large data set is often a difficult task. To achieve this goal the construction of variation diagrams is often used. Choosing the two or three correct variables among the many possibilities is a major problem and this choice could either be dictated by simplicity or by some preconceived idea on how the data behave. In this way much of the raw data is not used resulting in a loss of information (Le Maitre, 1982). Various multivariate statistical techniques exist to aid the investigator in interpreting these interrelationships. Most of the techniques rely on interpreting the structure within the variance-covariance matrix or the correlation matrix of either the observations (samples) or the variables of the data set. Two useful multivariate techniques in geochemical interpretation are principal components analysis and cluster analysis.

2.7.1 Principal components analysis

Principal components analysis (PCA) entails nothing more than extracting the eigen vectors of either the variance-covariance matrix or a correlation matrix of either the observations (samples)

or the variables. In contrast to factor analysis, which is commonly regarded as a true statistical technique, principal components analysis is regarded as a purely mathematical manipulation. A discussion of eigen analysis is a prerequisite to the understanding of principal components analysis.

Assume a set of bivariate observations in two dimensional space where the variables are X1 and X2. If **a** is the variance of X1, **b** the variance of X2 and their covariance is **c**, the structure of the variances can be represented by plotting them on the same coordinate system as the observations. The coordinates of the variances and their common covariance is shown in Figure 3, where each co-ordinate defines a vector. The same structure can be defined by a 2 x 2 matrix, termed the variance-covariance matrix:

$$\begin{bmatrix} \mathbf{a} & \mathbf{c} \\ \mathbf{c} & \mathbf{b} \end{bmatrix}$$

Mathematically the elements of an m x m matrix define points lying on an m-dimensional ellipsoid where the eigen vectors of the matrix yield the principal axes of the ellipsoid and the eigen values represent their magnitude or length. Because an m x m matrix is symmetrical the principal axes or eigen vectors will always be orthogonal. Eigen analysis and therefore PCA is concerned with finding these axes and their magnitudes.

The eigen vectors or principal components are defined by a linear equation of coefficients or elements commonly called loadings. Each coefficient corresponds to a variable. Each of the original observations, plotted on the same coordinate system as the variances can now be projected onto the principal axes of the ellipsoid by multiplication with the coefficients of the eigen vectors.

If the first eigen vector is defined by the coordinate set $(\alpha_1 X_1, \alpha_2 X_2)$ as follows:

$$Y_1 = \alpha_1 X_1 + \alpha_2 X_2$$

then the projection of observation i on this vector is defined as:

$$Y_{1i} = \alpha_1 X_{1i} + \alpha_2 X_{2i}$$

commonly called the score of variable i on the first principal axis, or first eigen vector.

Usually the first eigen vector will account for a much larger percentage of the variance in the data than the second orthogonal eigen vector, and the variance along this vector will be greater than along any other possible straight line drawn through the data points. The plane defined by the two principal axes or eigen vectors can usually be expected to account for at least two thirds of the variance in the data set. If the first set of principal component co-ordinates accounts for a high proportion of the variance, the remainder may be discarded, thereby reducing the number of variables that need to be considered (Le Maitre, 1982). In geological and other problems the number of variables are usually numerous and constitute an n-dimensional space, which compounds the problem.

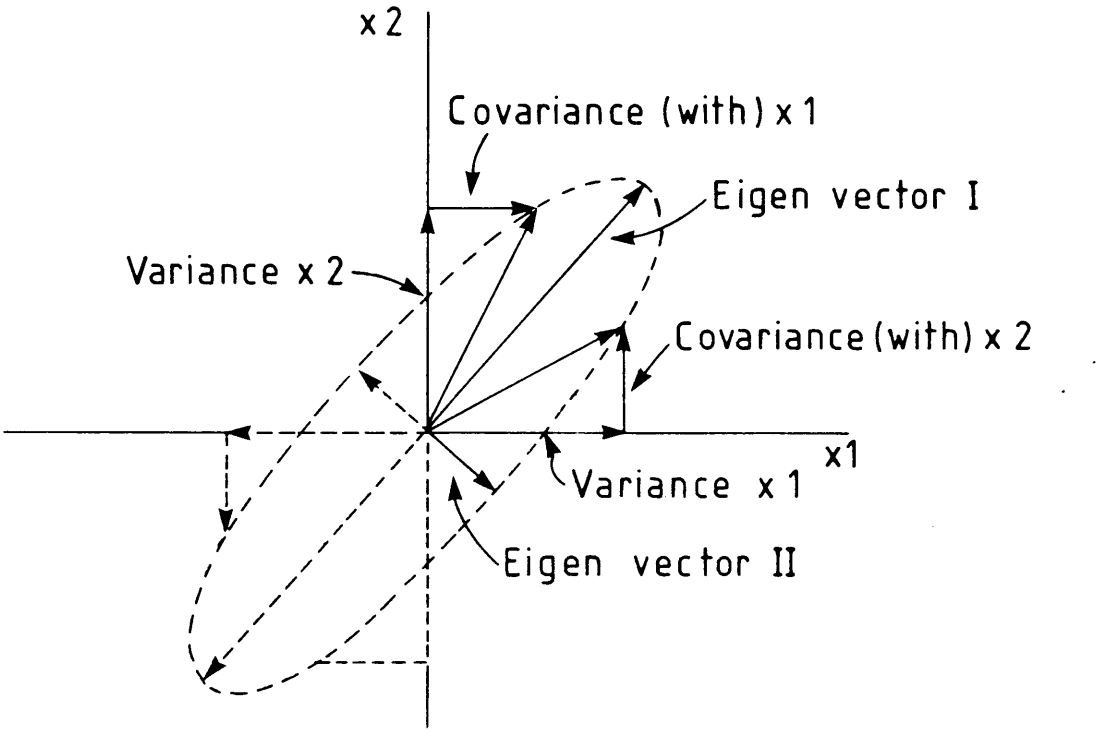

Figure 3 The relationship of variance-covariance to the principal eigen vectors of PCA in two-dimensional space.

In order to use both major and trace elements of which the units of measurement differ, it is necessary to convert the data to unitless or standardised form. This standardisation of the data set is achieved by subtracting its mean from each value of a variable or observation and the difference is divided by the standard deviation. The transformed variables will then have a mean of zero and a variance of one. In this case the eigen vectors and eigen values are extracted from the correlation matrix. Since most of the variables in the data set are to some extent normally distributed the logarithm to the base 10 of the values were used in the calculation of the correlation matrix.

As PCA is a type of linear curve fitting, a well defined curved trend in p-dimensional space may be indistinguishable from an ellipsoidal distribution and the data should therefore always be plotted and examined before deciding upon the cause of the variability (Le Maitre, 1982). It is commonly considered that PCA only gives meaningful results when a large data set in terms of number of samples is used. However, the author is at variance with this viewpoint and this is borne out by the simple examples used by Le Maitre (1982) to illustrate the method. As in all numerical methods, results obtained by PCA can be erroneous if due cognisance is not taken of the geology. Positive element correlations in one rock unit may be cancelled by strong negative correlations of the same elements in another unit, and it is therefore important to base the distinction of units on sound geological observation.

In this study the FORTRAN program for PCA by Davis (1970) was adapted to the author's requirements e.g. to use all or only certain of the variables of a data set to interpret the correlations of variables in the various rock units.

2.7.2 Cluster analysis

The most simplistic way to correlate multi-element data is to generate a matrix of correlation coefficients between all possible pairs of variables. However, some degree of subjectivity is

involved in deciding on the mutually correlated groups of variables. A more objective approach is to choose those mutually correlated variables which exhibit the greatest within-group correlation relative to the between-groups correlation. This is the principle of cluster analysis and the method is well adapted for situations in which the underlying causes of correlations among the variables are unknown. In practice a matrix of mutual correlations is generated from which the highest correlations are weighed and a sub-matrix of correlations generated until all the highest correlating groups are effectively clustered. The result is presented in a tree-like diagram termed a dendogram (Levinson, 1974). In the present study the FORTRAN program for the weighted-pair group average-linking method (Davis, 1970), has been adapted to the author's requirements.

CHAPTER 3

THE VAALPUTS RADIOACTIVE WASTE DISPOSAL FACILITY

3.1 Geographical Setting

The Vaalputs Radioactive Waste Disposal Facility is located on the Bushmanland Plateau, close to the escarpment, approximately 90 km south-east of Springbok and about 120 km from the Atlantic Ocean. The facility is bounded by 30°05' and 30°10' south latitude and 18°25' and 18°37' east longitude.

The climate is characterised by anticyclonic conditions throughout the year and extreme temperatures are experienced, varying between 7°C and 36°C in summer and between -1°C and 22°C during winter. The western part of the Bushmanland Plateau lies in the rain shadow of the higher mountain land to the west resulting in minimal winter precipitation, and in summer the interior winds lack moisture resulting in low summer rainfall. Although the area lies in the transitional zone between the summer and winter rainfall regions, precipitation averages 74 mm per annum (Redding and Hutson, 1983).

The extremes of temperature coupled with low precipitation have a profound effect on the weathering process in the region and the resultant migration of the constituent elements of the rocks; the migration of radionuclides which may be accidentally released from the buried waste will be similarly affected by the climate.

Vegetation is sparse both on the sand covered plateau and on the rocky outcrops in the hills to the west of the disposal site. Due to the paucity of vegetation, soils are thin and show hardly any profile development. Biogeochemical activity is therefore not considered to have a profound effect on the weathering process and the resultant migration of elements.

3.2 Stratigraphy

Precambrian crystalline rocks of the Namaqualand Metamorphic Complex form the basement to shallow veneers of late Palaeozoic (Karoo) and Tertiary terrigenous rocks. All the crystalline rocks, with the possible exception of some late pegmatites, bear the imprint of a penetrative fabric, which is most intense in the older banded gneisses and weakest in the syntectonic granites and in the late-syntectonic basic intrusives of the Koperberg suite (Andersen, research in progress). A metamorphic age of 1 100 ±50 Ma is widespread in the metamorphosed crystalline rocks irrespective of their position in the stratigraphy (H Welke and I Evans, unpublished data).

The geology of the Vaalputs vicinity is shown in Figure 4 and Table VI summarises the stratigraphic relationships on the Bushmanland Plateau in the area adjacent to the waste disposal site. The following condensed geological description has largely been taken from Andreoli et al. (1987).

3.2.1 Basement rocks

Light-coloured biotite gneiss and quartzo-feldspathic rocks are the most widespread rock types and may represent ancient arkosic-pelitic formations and have therefore been termed "supracrustal" by Joubert (1971). In a number of localities rocks regarded as supracrustal quartzo-feldspathic gneisses by Joubert (1971) comprise charnockite, a variety of granitoids and orthogneisses. The supracrustal rocks at Vaalputs and environment belong to the **Garies Subgroup** of the **O'Okiep Group** (Table VI).

3.2.2 Intrusive rocks

Rocks of granitic bulk composition containing relic granite textures are the most common in the Vaalputs area. They are regarded as intrusive and were termed "infracrustal" by Joubert (1971). Table VI lists the intrusive suites recognised at Vaalputs.

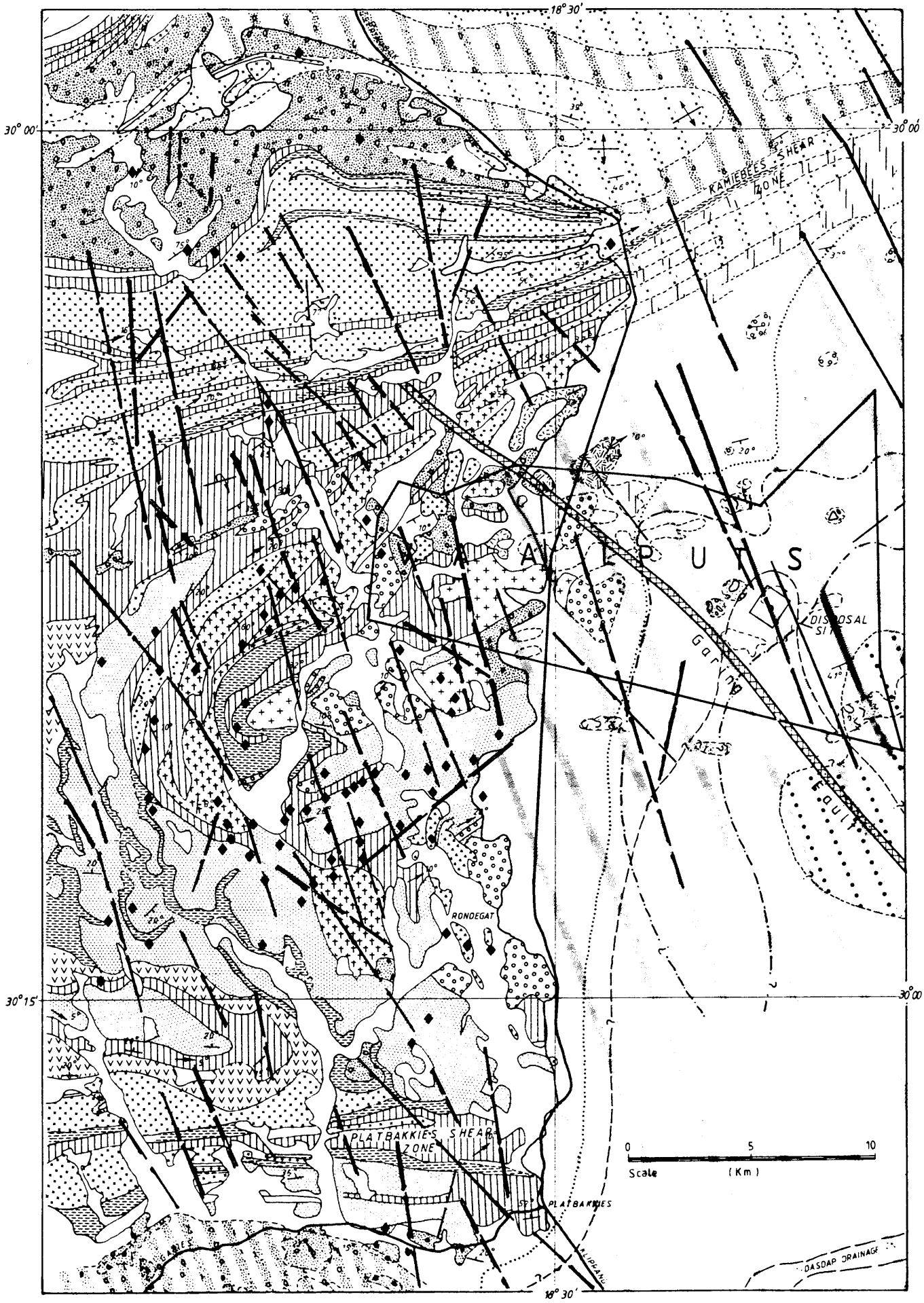

Figure 4 Geological map of the Vaalputs vicinity.

(After Andersen, 1987)

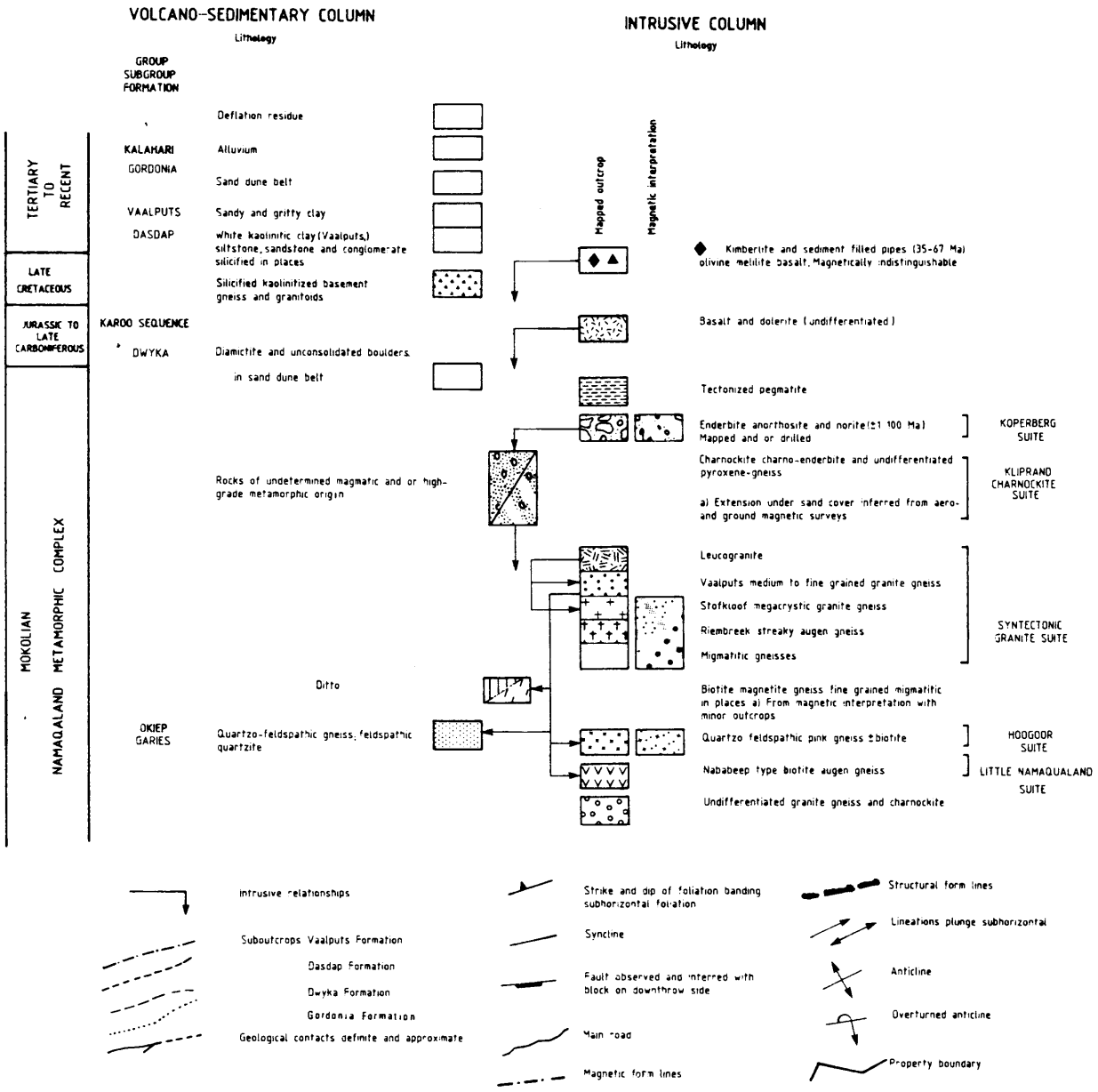

Legend to geological map of the Vaalputs vicinity.

(After Andersen 1987)

TABLE VI THE LITHOSTRATIGRAPHY AT VAALPUTS

(Modified after Andreoli et al., 1987)

Sequence Group/sub-group Suite	Formation/ Granite type	Lithology	Approximate Age(Ma)	Origin
	Gordonia	Red sand	20 - 5	Aeolian
		Unconformity		
	Vaalputs (Red Clay)	Calcrete and silcrete nodules	35 - 0	Chemical precipitate
		Brown, grey and white sandy to gritty clay with intercalated pebble bands	35 - 20	Alluvial fan and fluvial sheet wash
		Unconformity		
	White Clay	Grey-white sandy to gritty clay and weathered basement Siliceous sandstone	35 - 20	In-situ weathering of basement rocks
		Unconformity		
	Dasdap	Conglomerate Immature cross-bedded arkosic grits	38 - 20	Alluvial fan
		Unconformity		
		Olivine-melilite basalt Kimberlite	35 - 67	Intrusives
		Unconformity		
Karoo Sequence		Basalt and dolerite	180	Intrusives
		Unconformity		
Koperberg Suite		Pegmatites		Syn- to late-tectonic intrusives
		Diorite, norite Hypersthenite, enderbite Quartzolite, nelsonite		Late-tectonic basic intrusives into the Garies Group
Kliprand Charnockite Suite		Charnockite		
Syntectonic Granite Suite	Leucogranite Vaalputs Stofkloof Riembreek	Various granitoids	1100 ± 50	Syn- to late-tectonic granitic intrusives into the Garies Group
Hoogoor Suite		Undifferentiated quartzo-feldspathic (pink) gneisses		
Little Namaqualand Suite	Nababeep	Augen gneiss		
O'Okiep Group Garies Subgroup		Quartzo-feldspathic gneiss	>1 100	Metamorphism of ancient arkosic-pelitic gneisses

In the Vaalputs area the **Little Namaqualand Suite** is represented by the **Nababeep Augen Gneiss** which is well-foliated and streaky, with well-developed augen consisting of aggregates of quartz and feldspar surrounded by biotite. The matrix is fine-grained and consists of interstitial quartz and feldspar. The presence of xenoliths of supracrustal rocks in the O'Okiep area indicates its intrusive nature.

The **Hoogoor Granite Suite** refers to the rock type which in the past has generally been called a pink gneiss. Pink quartzo-feldspathic gneisses outcropping north of 30^{o} latitude and to the west of the facility were tentatively correlated with the Hoogoor Suite by Andreoli et al. (1987).

Several intrusive granite types, collectively known as the **Syntectonic Granite Suite** occur at Vaalputs. The **Riembreek granite gneiss** is generally characterised by the lack of garnet, by the abundance of biotite, and by a very persistent streakiness caused by the concentrations of the femic minerals. Feldspar augen are frequently present and the rock may superficially resemble the Nababeep Augen Gneiss. The **Stofkloof granite gneiss** is typically coarse-grained to megablastic and porphyroblastic and in a number of localities it displays rapakivi-textured K-feldspar megacrysts; garnet-bearing leucosomes also occur. The relative scarcity of garnet and biotite, the often fine-grained texture and a rather uniform pinkish colour distinguish the **Vaalputs granite gneiss** from the other syntectonic intrusives. Leucocratic granite, characterised by the absence of biotite, the frequent presence of large garnets, an off-white colour and rapid changes in grain size from aplitic to coarse-grained, forms a broad NE-striking belt of intrusive sheets within the older granites.

Charnockites are defined as (meta)plutonic rocks of granitic bulk composition, but characterised by a dark green to black colour, as well as by the diagnostic orthopyroxene-perthite pair. The Vaalputs charnockites, referred to as the **Kliprand Charnockite Suite** often contain more biotite than pyroxene and thus may have more than one mode of origin.

A suite of basic rocks correlated with the **Koperberg Suite** of the Springbok area outcrop at Vaalputs and were also encountered below the surficial succession during drilling. Typical Koperberg Suite rocks of the Vaalputs area include hypersthenite, norite, nelsonite (hypabyssal rocks composed chiefly of ilmenite and apatite with or without rutile), quartzolite (plutonic rock with more than 90% quartz), enderbite (plagioclase-rich charnockite) and anorthosite. A petrogenetic process defined as the "nelsonite cycle", which links these rock types, has been proposed by Andreoli et al. (1987).

In the Vaalputs area only scattered and small pegmatite bodies, occasionally displaying prominent muscovite books, occur. However, quartz-rich rock of gray colour and with occasional scattered feldspars are fairly common.

Phanerozoic intrusive rocks comprise dolerite and olivine-melilitite. Kimberlites and melilite-basalt occur at Vaalputs and are characterised by a ground-mass containing chrome diopside, ilmenite, phlogopite, olivine (monticellite) and melilite.

3.2.3 Karoo Sequence

The Dwyka Formation in the north-western Cape comprises massive diamictite, basement derived breccia, glaciogenic argillite and sandstones (Visser, 1985). Dwyka float consisting of faceted sandstone pebbles has been observed in two areas just south of Vaalputs, indicating the presence of an isolated outlier of Dwyka rocks underlying the sand.

3.2.4 Tertiary formations

During the radioactive waste site selection programme an extensive alluvial fan was noted by Levin and Raubenheimer (1983) on the LANDSAT image of the Bushmanland Plateau (Fig. 5). Outcrops of conglomerates and sandstones were mapped by them on Banke and Burtonsputs (shown in Appendix A), south of Platbakkies, where they are exposed along the Dasdap drainage, part of which is shown

in Figure 4. The name **Dasdap Formation** has been proposed for these sediments, (Levin et al., 1986) but the name has not yet been acknowledged by the South African Committee on Stratigraphy (SACS). References to these outcrops date back as far as 1911 (Rogers, 1911); Reuning (1930) referred to outcrops, coincident with the Dasdap Formation as "deposits of pre-surface quartzite age".

In the type area at Banke, south of Vaalputs, the exposures of Dasdap Formation rocks generally lie on a floor of kaolinised gneiss and consist of a basal conglomerate, followed upward by conglomerate and sandstone grading into trough cross-bedded grits, and massive sandstone with intercalations of silicified siltstone. Pervasive ferruginisation of the upper part of the formation has occurred and iron-oxide nodules are commonly found scattered around the outcrops. Much of the conglomerate consists of blue quartz pebbles derived from local quartz veins. On Rondegat, south of Vaalputs, an outlier of Dasdap Formation with a similar succession occurs (Fig. 6).

At Banke the outcrops display a consistent palaeocurrent direction towards the south-east and a genetic link with the alluvial fan shown in Figure 5 is not so obvious (Levin et al., 1986). Further north there seems to be a wider range of palaeocurrent directions, suggesting a fan-shaped distributory system.

Percussion boreholes drilled on Platbakkies penetrated up to 35 m of gritty silicified sandstones, and a borehole in the south-east corner of Bok-Puts intersected about 20 m of yellowish to white sandstones, assumed to belong to the Dasdap Formation. Small exposures of silicified sandstone occur throughout the area in small pans and deflation areas between dunes.

At Vaalputs drilling revealed white gritty to sandy clay sediments on the western half of the farm. In the central disposal area up to 21 m of alluvial material, resembling in part rocks of the Dasdap Formation, rests on weathered basement and is overlain by red gritty to sandy clays.

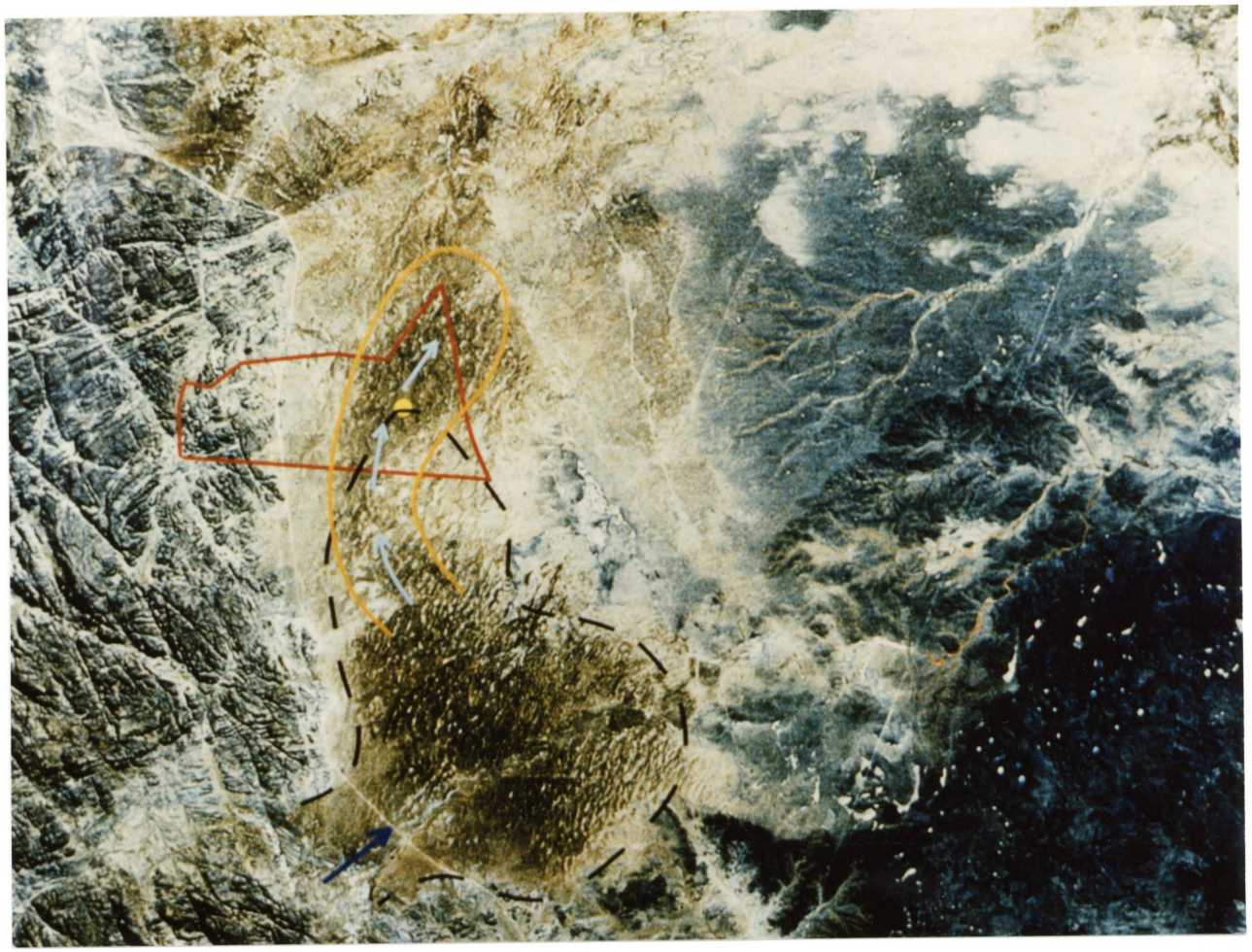

0 1 2 3 4 km

Scale

Figure 5 Landsat image of the Vaalputs area showing the extent of an alluvial fan originating in the Kamiesberge and from which some of the sediments at Vaalputs are believed to have been derived. The outline of the Vaalputs Facility is superimposed on the image.

This basal formation has been correlated with the Dasdap Formation by Levin et al. (1986). However, the author is at variance with this point of view on the basis of their different geochemistry. In this study the rock unit is consistently referred to as **white clay**, albeit rather loosely.

Extensive drilling at Vaalputs revealed a channel-like depression cut into the basal sediments and basement which is filled by red gritty to sandy clay (Fig. 7). In areas where the basal formation is absent the sediments lie directly on the weathered basement. The name **Vaalputs Formation** has been proposed by Andersen et al. (1983) for this clay unit but the name has not been acknowledged by the SACS and in this study the term **red clay** is loosely used for the rock unit.

Three cycles of deposition, each followed by calcretisation, are recognised in the red clay. Grey sandy to gritty clay-loam with large calcrete nodules (Fig. 7) indicates humid conditions, while the overlying brown sandy to gritty clay loam with small calcrete and silcrete nodules at the top points to increased desiccation. An upper ferruginised and laminated sandy gritty clay loam is followed by the present-day calcrete layer below the sand veneer covering the area (Fig. 7). Iron-oxide nodules and blue quartz pebbles, very conspicious in the Dasdap Formation, occur concentrated in thin layers in the clay of the early cycle and they are also scattered throughout the rest of the succession. There is little doubt that these accumulations represent reworking of the sediments of the Dasdap Fan by surface processes which include fluvial action and bioturbation. Fossil evidence from the Koa Valley to the north-west suggests that this reworking was well advanced by the Late Tertiary and was followed by aridification and dune sand transgression.

3.2.5 Younger surficial deposits

Most of the Bushmanland Plateau is covered by a veneer of sand which overlies remnants of the red clay and white clay. The sand cover is between 0,5 and 2 m thick although the topography gives the

impression of hummocky longitudinal dunes (5 m high) orientated in a north-easterly direction. McCarthy et al. (1984) concluded that the coarse sand, the low relief of the dunes, and the presence of small pans and deflation surfaces on the dunes all point to an advanced state of degradation. The sand cover has tentatively been correlated with the **Gordonia Formation** (SACS, 1980). Various types of sand are distinguished and include red-brown sand typical of the dune crests and valleys and light-brown sand which occurs mainly in the western portion and closer to the area of outcrop. The transition zone between the red-brown sand and the light-brown sand, as developed in the central Vaalputs site, is marked by elongated calcrete outcrops. Intermediate sand occurs as a transition zone between the red-brown and the light-brown sand, and is better developed south and north of Vaalputs, being absent on the site. This sand tends to occur as elongated patches parallel to the dunes in the area. It is suggested that the colour differences of the sands are due to different iron contents.

Isolated outcrops of calcrete between 1 and 5 m in thickness and consisting of nodular calcrete with occasional silcrete occur at Vaalputs. They are parallel to the dunes and seem to be associated with the slopes of the dunes but this is considered as the result of wind deflation.

Deposits of alluvium characterise the infill of depressions and valleys in the rejuvenated area west of the escarpment. They are incoherent and of sandy character and in several places they are slightly ferruginised, leading to a light brown to brown colour. These are considered to be of Recent age.

3.3 Geomorphology

Physiographically the Vaalputs area comprises two broad regions which are separated by the north-south escarpment into the gently undulating Bushmanland Plateau to the east and the rugged mountainous granitic terrane of Namaqualand to the west. The former is characterised by intermittent and discontinuous valleys and

Figure 6 Outlier of the Dasdap Formation sediments in a broad valley on the farm Rondegat south of Vaalputs.

Figure 7 View of a disposal trench side wall at Vaalputs showing red clay with layers of isolated calcrete nodules. The trench height is 7 metres.

extensive pan development in the largely sand covered area. The area in which the Vaalputs site is located consists of an extensive dune field dominated by low, longitudinal dunes, orientated in a north-easterly direction. The eastern end of the dune field is terminated by a low scarp of calcretised Dwyka tillite and further east outcrops of basement rocks become prominent, but in the area of Vaalputs outcrops are scarce (McCarthy et al., 1984).

To the west of the facility outcrops of basement rocks in the form of tors and bornhardts form the largest part of the surface. A prominent geomorphological feature of the western part is represented by light-coloured steep-sided cliffs rising several tens of metres above the talus-covered plain (Fig. 8). These ridges are flat-topped and consist of silicified and kaolinised crystalline basement rocks which represent relics of the receding Bushmanland Plateau. The origin of these silicified and kaolinised basement rocks is related to a period of planation under humid conditions in late Cretaceous to early Tertiary times (60 Ma) (McCarthy et al., 1984).

3.4 Geohydrology

Three major watersheds intersect in the Vaalputs region and separate the drainage basins of the Buffels River to the west, the Olifants River to the south and the Koa River to the north-east (McCarthy et al., 1984). The Vaalputs Facility is located well within the Koa River basin, which is a palaeodrainage with no active surface drainage features. The disposal site is located in an area with a relatively deep ground water level of between 50 and 60 m, and this is considered favourable for the location of a repository (Levin, 1988).

Carbon-14 dating of ground water revealed ages of up to 10 000 years on Vaalputs and up to 14 700 years on Platbakkies to the south. These ages are explained by slow movement and lack of recharge due to the thick overburden. Rates of ground water movement as low as 2 m per year are quoted for similar environments (Levin, 1983).

The inferred slow water movement within the basin makes it eminently suitable for the location of a waste disposal site.

Figure 8 Silicified cappings overlying kaolinised basement rocks to the west of the Vaalputs site.

CHAPTER 4

PETROLOGY AND MINERALOGY

A sound knowledge of the petrology and mineralogy of both the surficial and basement rocks constitutes the basis for a geochemical interpretation of element distribution in the surficial rocks. Regarding the basement rocks it is important to know the composition and relative amounts of their constituent minerals. In the case of the surficial rocks it is also important to know their grain size distributions because the silt and clay fractions may play an important role in the adsorption of elements, with a consequent bearing on the retardation potential of the rocks for some elements.

A suite of basement and surficial rocks from Vaalputs was studied with the following objectives in mind:

- To assess their petrological nature.
- To study the uranium distribution in the rocks.
- To test the possibility of the surficial succession being derived (at least in part) from the basement rocks.
- To attempt a prediction of the suitability of the rocks for the retardation of radionuclides.

4.1 Petrology and Mineralogy of Basement Rocks

In this section petrographic and mineralogical descriptions of typical rock types which are volumetrically important on Vaalputs are given.

4.1.1 O'Okiep Group

This Group comprises lithologically heterogeneous rocks ranging from kinzigite to fine grained two-feldspar gneisses with biotite and quartz. The kinzigite is characterised by coarse sillimanite nematoblasts, green zincian spinel (gahnite), and red biotite. The biotite-gneisses are characterised by quartz, microcline and albite as main constituents. Biotite, locally chloritised, is a major constituent and accessory minerals are magnetite with exsolved ilmenite, zircon and occasional apatite. Mineral textures e.g. platy quartz and partly microclinised orthoclase, indicate that the rocks experienced a high-strain episode under upper amphibolite facies conditions, probably followed by a deuteric episode during which they were partly chloritised.

4.1.2 Hoogoor Suite

The main rock type of this Suite is referred to as pink gneiss. It is a fine to medium grained, leucocratic, granulitic rock, characterised by perthitic K-feldspar, ranging from orthoclase to microcline, and amoeboid to platy quartz, as typical major constituents. Minor constituents are albite, biotite, garnet and hornblende may also be present. Accessory minerals are ilmenite and magnetite with lamellae of a Ti-phase (probably brookite) and rims of sphene. Zircon is characteristically zoned with the outer shell often appearing more metamict than the inner idiomorphic core, due to a higher uranium content. Xenoblastic radioactive monazite and apatite are occasionally present. Ilmenite occurs in the magnetite and the reddening of the feldspar by hematitisation is evident. Chloritisation of biotite is common but this latter process is likely to be post-metamorphic in nature.

4.1.3 Syntectonic Granite Suite

The rocks in this Suite are mostly distinguished by their field relationships and minor mineralogical variations occur which are not considered relevant to the topic under discussion. The following

general description applies to most of the rocks in the Suite.

The rocks are massive, crudely lineated orthogneiss of variable grain size from fine (<1 mm) to coarse grained (>10 mm), occasionally porphyroblastic. The main constituents are perthitic K-feldspar (orthoclase and microcline) and quartz, frequently in amoeboid or platy grains. Myrmekitic and micrographic intergrowths of quartz and perthitic feldspar are common. The feldspars are moderately altered to sericite.

Minor constituents are biotite (often replaced by chlorite and fluorite), albite and in places, xenoblastic interstitial hornblende. Accessory minerals are typically magnetite with ilmenite lamellae and sometimes with laths of leucoxene. Zircon is the most abundant accessory mineral while sphene, ilmenite, and occasionally monazite occur. Other unidentified radioactive minerals are present, as shown by fission-track micro-mapping; but are also evident through the ubiquitous pleochroic halos at the margins of, or within biotite flakes. Zircon is characterised by idiomorphic, highly birefringent cores and a partly metamict, subspherical, multi-layered outer shell. Monazite occurs as xenoblastic grains and unzoned fluorite with a marked purple hue is characteristically associated with chloritised biotite, suggesting its formation from the breakdown of a fluorine-bearing biotite.

4.1.4 Kliprand Charnockite Suite

With respect to major rock forming minerals, accessory minerals and texture this rock suite is similar to the previously described rocks. It differs mainly with respect to fabric and the presence of a mafic component, mostly hornblende and pyroxene, formed during charnockitisation.

4.1.5 Koperberg Suite

The Suite comprises a variety of rocks ranging from pure anorthosite, leuconorite, norite to hypersthenite. The plagioclase

is of intermediate composition; potassium, detected by energy dispersive X-ray analysis occurs as antiperthite which is common. The pyroxenes are mainly, hypersthene and augite. Biotite is a common phase and apart from Fe and Mg contains Ti as a major constituent. In some thin sections, neoformed prograde biotite occurs at an orientation different to that of altered retrograde biotite. Some biotites seem to have a high Cs content.

Spinels with Fe, Al, Zn and Mn as main constituents are common and are typically emerald green in very thin sections. These probably belong to the dysluite or Zn-Mn-Fe-gahnite group of spinels (Ford, 1949). Magnetite with varying proportions of Ti, V and Cr as minor elements in the structure is common and almost invariably has exsolution lamellae of both spinel (Fe-, Al-rich) and ilmenite. Other accessory minerals include zircon, monazite with a high Th content, xenotime, sphene and apatite.

4.2 Petrology and Mineralogy of Surficial Rocks

4.2.1 Dasdap Formation

The following petrological and mineralogical description of Dasdap Formation on the farm Rondegat, south of Vaalputs (Fig. 4 and Appendix A) is typical of the whole formation. It is included here due to its importance to the interpretation of the geochemistry and petrogenesis of the terrigenous succession on Vaalputs.

Weathered, kaolinised granite gneiss (RGT1 and -2) with pure white weathered feldspar and abundant blueish quartz grains forms the basement to the succession. The remnant gneissic rock texture is clearly discernible. The feldspars are completely altered to kaolinite, which occurs as fan-like books, resulting in a felt-textured matrix. Remnant myrmekitic textures can be seen with only quartz blebs remaining in the matrix, portions of which have been completely silicified. Abundant accessory minerals include zircon, apatite, monazite, magnetite and ilmenite, all of which are unaffected by the alteration. Some quartz grains have been broken

due to the forceful injection of clay minerals into cracks. Some unknown titaniferous phases have been completely altered to form anatase (identification confirmed by XRD) and the exsolution texture of the remaining framework grain can still be seen.

The basal rock of the Dasdap Formation is a rudite (RGT3) with pebbles of blueish quartz and silicified and kaolinised weathered granite in a grit-sized quartz matrix. The weathered rock clasts have a vague outline and are not rounded. The matrix consists of opal which is very ferruginous in places. Ribbon-like ferruginous opal characterised by dessication cracks, lines fissure walls. Minor quantities of kaolinite books as described above and anatase are also present in the interstices. Heavy minerals include zircon, euhedral apatite, hematite, magnetite and ilmenite.

The rudite is followed upwards by very fine-grained (RGT4) silicified sandstone with blueish quartz grains in a matrix consisting of opal, fine-grained quartz, kaolinite and heavy minerals similar to those in the above-mentioned rocks.

Brown-pink to white grit (RGT5) with distinct layering follows the silicified sandstone upwards. Liesegang banding is present in the whole rock unit. The grit sized quartz grains occur together with hematite, ilmenite and anatase or brookite in a matrix of opal. All the detrital grains are rimmed by ferruginous opal.

A layer, several metres thick, overlies the above-mentioned succession and consists of ferruginised rudite (RGT6) with alternating layers, $\pm$ 3-5 cm thick, of grit which is strongly ferruginised in places. The layers are made up of quartz grains, 2-4 mm in diameter and less, set in a matrix of kaolinite and opal. These layers alternate with layers of quartz-pebbles in a similar matrix. The pebble diameter may reach 10 mm. Larger clasts of silicified material are also present and strongly hematitised patches occur in places. Heavy minerals are abundant and comprise mainly the above-mentioned suite and pyroxene.

Nodules of iron-oxide and ferruginised opal (RGT8) occur scattered on surfaces around the outcrops. Microscopically the rock consists of small quartz grains in a ferruginous opal matrix ranging from a core of sulphur-rich iron-oxide, through limonite to hematite. In places the matrix is free of interstitial quartz. Veins of chert traverse some pebbles.

4.2.2 White clay

The white clay varies in composition from gritty to sandy clay-loam to silty-loam in the textural classification of Hillel (1971). The main constituents are clay minerals, which include smectite, kaolinite and illite in order of abundance. The mineralogical variation of the white clay is illustrated in Figure 9 (a - 1). The silt- and sand-sized fraction consists mostly of quartz, fresh to altered K-feldspar, plagioclase, biotite, fresh to altered pyroxene and rock fragments in varying stages of alteration. Some blueish quartz pebbles occur and in two boreholes W40S10 and W83N0 (Figs. 9c and 9k) iron-oxide nodules occur only in the upper half of the white clay.

4.2.3 Red clay

The red clay could be classified as gritty to sandy clay to sandy clay-loam in terms of the textural classification of Hillel (1971). Clay minerals are the major constituents and include illite, kaolinite and smectite in order of abundance. The silt and sand fractions consist mainly of quartz, minor fresh to altered K-feldspars and plagioclase, heavy minerals similar to those found in the basement rocks and iron-oxide nodules. The occurrence of blue quartz grains and iron-oxide nodules on certain horizons suggests a petrogenetic link between the red clay and the Dasdap Formation to the south of Vaalputs.

The mineralogy of the red clay differs from that of the white clay in several aspects. Illite and kaolinite are the major clay minerals in the red clay, with subordinate smectite, but smectite

predominates in the white clay with kaolinite and illite being more or less equally abundant (Table VII). Biotite is absent and muscovite scarce in the red clay and feldspars are less common and more altered.

The red clay is readily distinguished by its red colour which is due to iron-oxide in and around mineral grains. The mineralogical variation in boreholes on Vaalputs is shown in Figure 9 (a - 1).

4.2.4 Gordonia Formation

The red sand as it is loosely referred to in this study, comprises mainly quartz sand of which the grains are well rounded and typically iron-oxide coated, giving it a red appearance. A host of heavy minerals similar to those in the basement rocks occur in the sand. Several colour variations of sand occur at Vaalputs, which are thought to be due to varying Fe content. Clay minerals, mainly illite, smectite and kaolinite form minor components of the red sand.

4.2.5 Calcrete and silcrete

Calcrete according to the definition of Netterberg (1969) comprises any material formed by the cementation and/or partial or complete replacement of a pre-existing soil by (dominantly) $CaCO_3$. The boundary between calcified soils and calcrete is set at 50% total carbonate (calcite plus dolomite) by weight. Three textural types of calcrete have been identified in the samples collected at Vaalputs:

(i) Nodular calcretes collected near surface south of the Garing homestead, are typical of all near-surface calcretes. They comprise a concentrically zoned very fine grained matrix, containing abundant rock fragments. In the nodules collected at Garing the fragments are noritic in character; quartz is virtuallly absent. The rock fragments are probably derived from the Koperberg Suite and are rich in pyroxene, plagioclase and magnetite. They have been resorbed to varying extents and are rimmed by coarse grained calcite. The fine

grained nodular core is generally surrounded by calcite grains, coated with iron-oxides, and has a very high content of fine detrital grains predominantly quartz, magnetite and zircon and to a lesser extent K-feldspar and plagioclase. This core is covered by a zoned shell consisting of concentric iron-oxide rich calcite layers, containing fine-grained detrital grains, alternating with pure white calcite layers free of detrital grains and iron-oxide. Occasional concentric layers of laminar chalcedony occur. Dendritic Mn-oxide occurs abundantly in the ferruginous zone.

(ii) The upper samples collected in trench 1 are pure calcretes with a high calcium carbonate content and a low detrital mineral component. Although some textural variations occur with respect to grain size, these calcretes are essentially characterised by a fine grained matrix of calcite with crystal diameters ranging from 4 µm to more than 30 µm. The crystallites are subhedral to euhedral and are randomly orientated. The rock texture is commonly nodular with very fine grained nodules ranging from 0,5 to 1 mm in diameter cemented by coarser grained calcite crystals 20-40 µm in diameter containing iron-oxides, thus enhancing the nodular texture. This texture may be attributable to the effect of dessication after which the cracks are filled in with detrital minerals. Quartz is the most common detrital phase with sub-ordinate K-feldspar, plagioclase, magnetite and ilmenite. The most common accessory mineral is zircon. The grain size of the detrital minerals varies greatly. The detrital grains are commonly resorbed by the calcite (Fig. 10), often to such an extent that only ghost-like relicts of the original grains remain, showing the original texture such as twinning in plagioclase and rutile needles in quartz. The grains are commonly rimmed by calcite, of which the grain size is several diameters larger than the surrounding matrix.

The calcretes appear to be iron rich, but this is not substantiated by the chemical analysis, the reason being that iron-oxide is present as microscopic coatings on grains, (Fig. 11) causing a marked colouration of the rock. The matrix is sometimes traversed by veinlets which remain white after staining with Alizarin Red S

(Friedman, 1959) and presumably consist of dolomite. Fissures within the calcrete are filled with detrital grains, which are coated with ribbon-like ferruginous opal which also lines the inner walls of the fissures.

(iii) A third textural variety of calcrete consists of a matrix of interlocking spherulites, up to 1 mm in diameter, containing iron-oxide on their peripheries, resulting in a concentration of iron-oxide rich material in the interstitial space between spherulites. Coarse grained elongated calcite crystals also grow radially from detrital grains which are being resorbed by the calcite.

The calcretes occurring at Vaalputs correspond to the nodular and hardpan calcretes described by Netterberg (1969). Hardpan calcrete is defined as a firm to hard, sheetlike, relatively impervious layer of calcrete normally underlain by softer or looser material.

Silcretes occur at Vaalputs, but are not abundant. Their fine grained matrix consists entirely of opal and fissures in the silcrete are filled with a variety of detrital minerals; mainly quartz, K-feldspar, magnetite and zircon. Their interstices are usually filled to a varying degree with ferruginous opal, forming a concentric coating around grains and also lining the walls of the fissures.

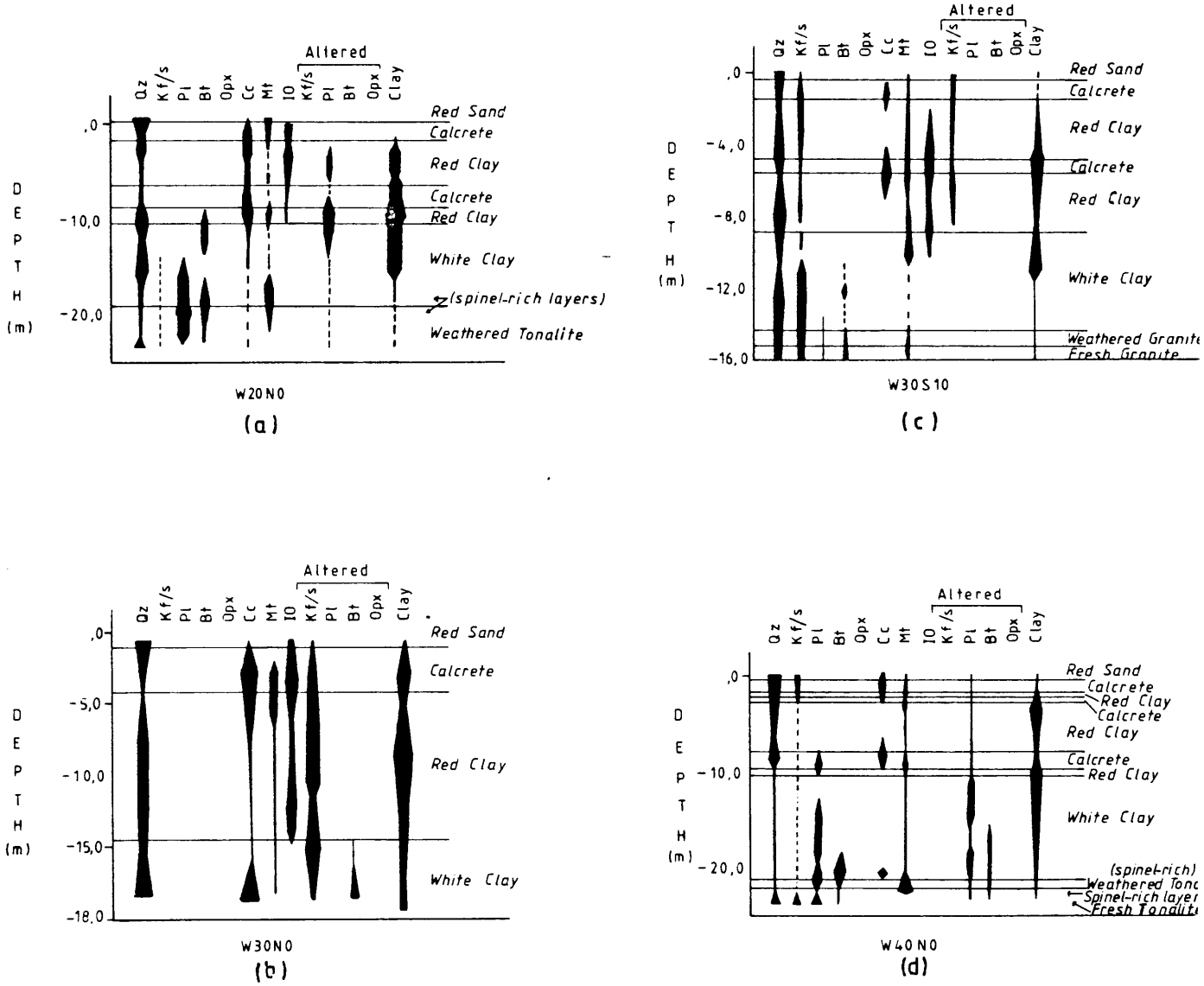

Figure 9 Mineralogical variation with depth in percussion boreholes from Vaalputs.

Abbreviations: Qz = quartz
K f/s = K-feldspar
Pl = plagioclase
Bt = biotite
Opx = pyroxene
Cc = calcrete
Mt = magnetite
IO = iron-oxide

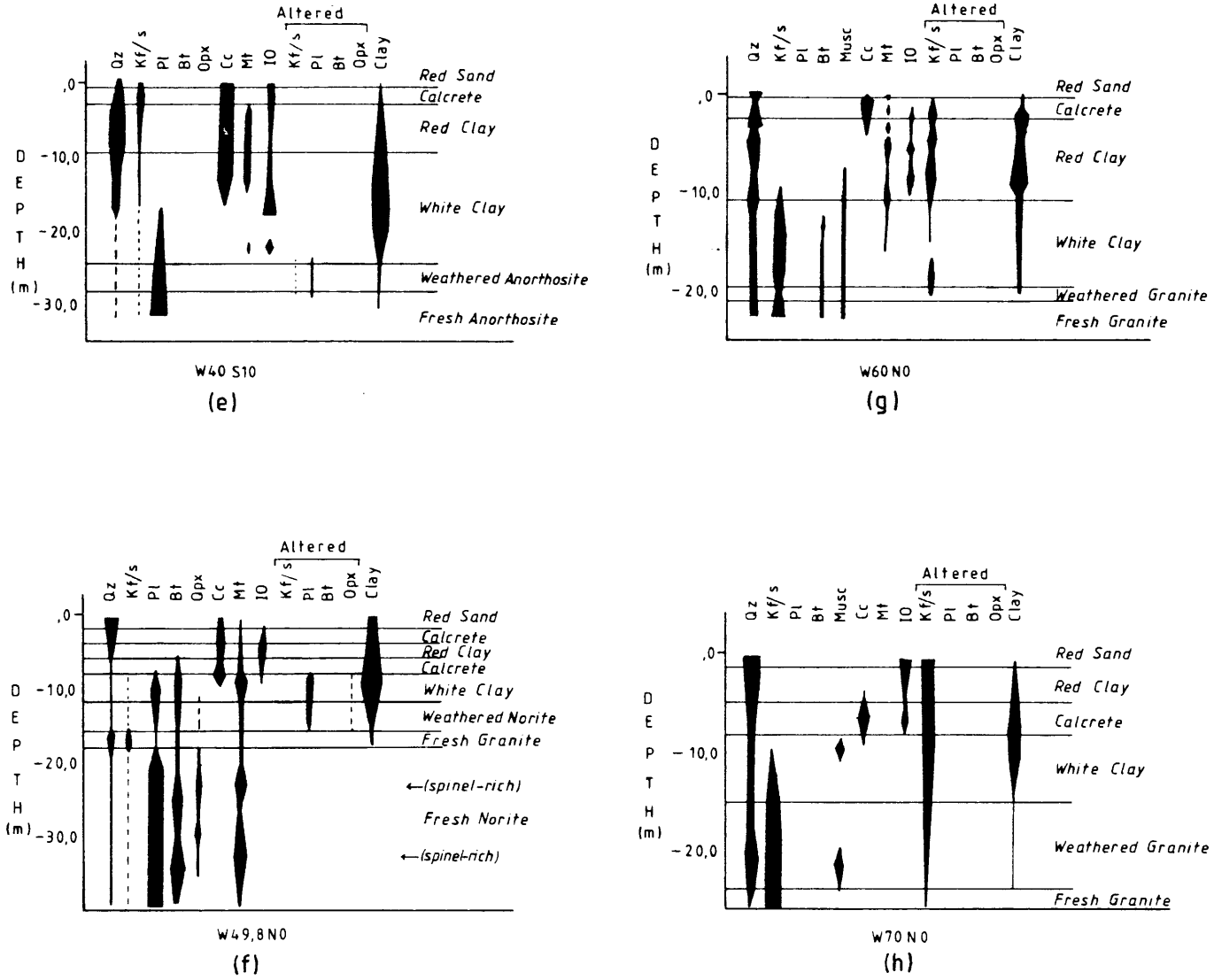

Figure 9(cont.) Mineralogical variation with depth in percussion boreholes from Vaalputs.

Abbreviations: Qz = quartz
K f/s = K-feldspar
Pl = plagioclase
Bt = biotite
Opx = pyroxene
Cc = calcrete
Mt = magnetite
IO = iron-oxide

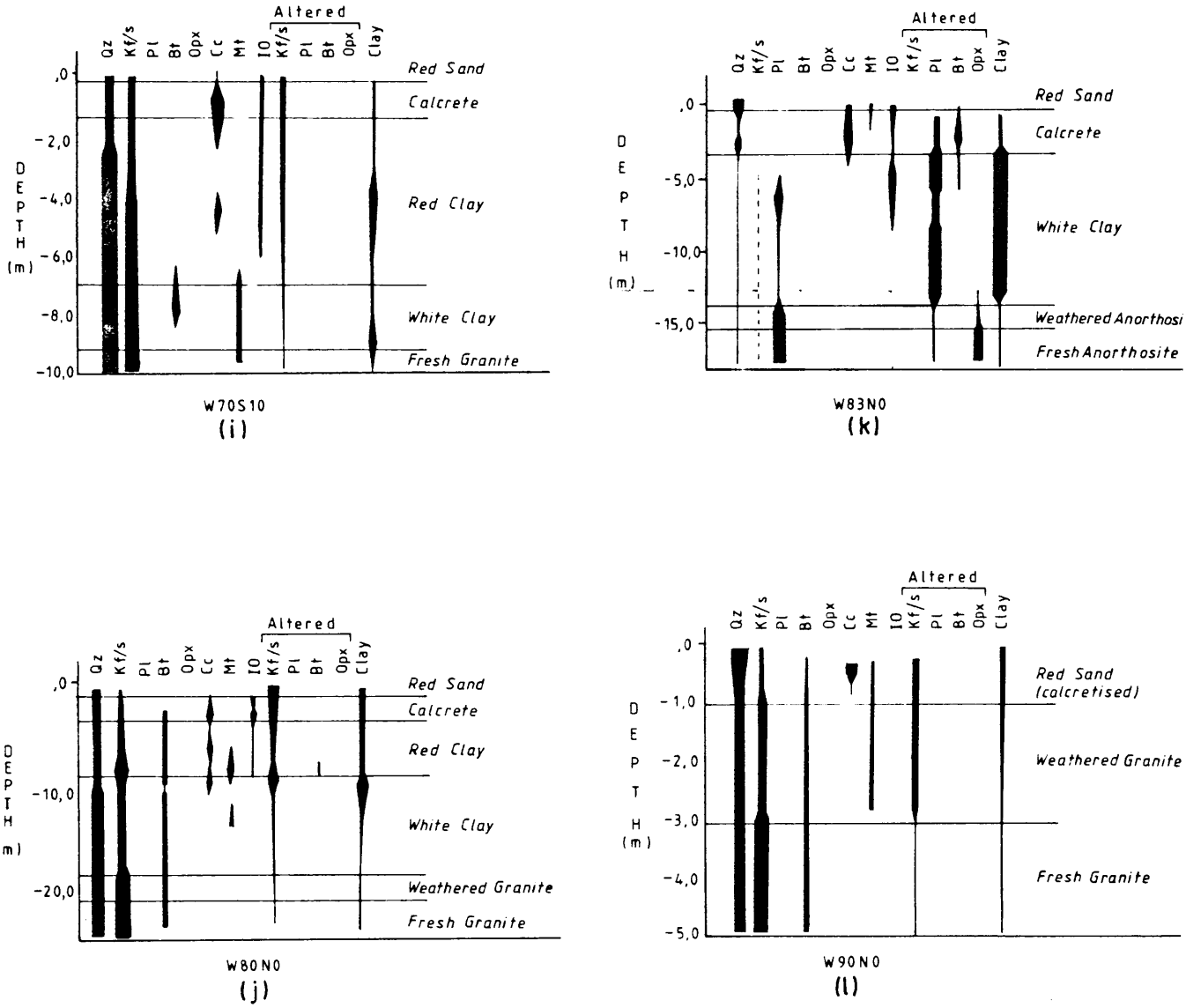

Figure 9(cont.) Mineralogical variation with depth in percussion boreholes from Vaalputs.

Abbreviations: Qz = quartz
Pl = plagioclase
Opx = pyroxene
Mt = magnetite
K f/s = K-feldspar
Bt = biotite
Cc = calcrete
IO = iron-oxide

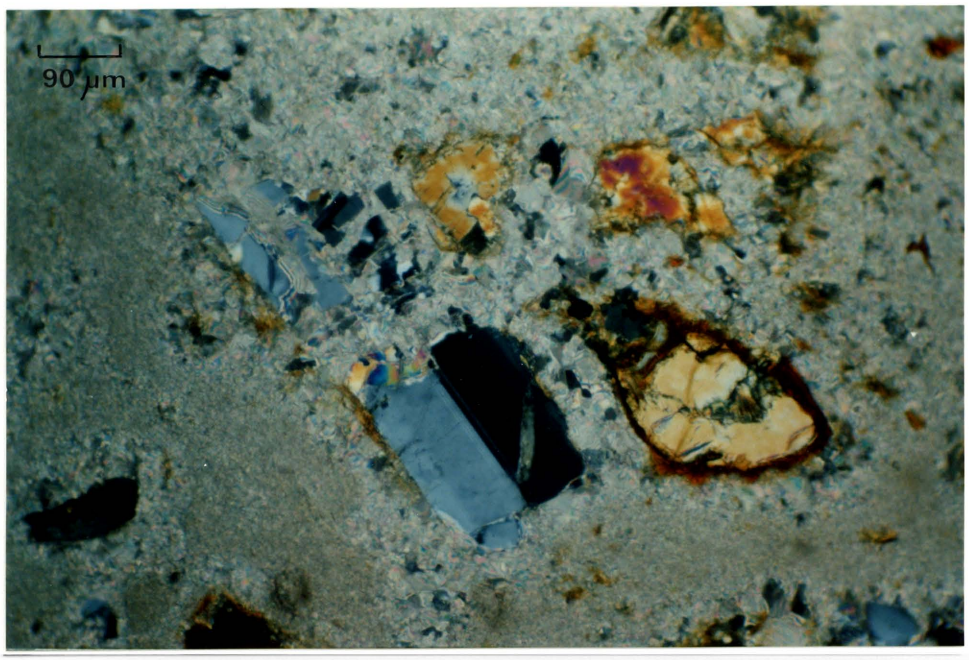

Figure 10 Partial resorption of twinned plagioclase and pyroxene by calcite in a calcrete nodule. Coarse grained calcite rims the resorbed grains. (crossed nicols)

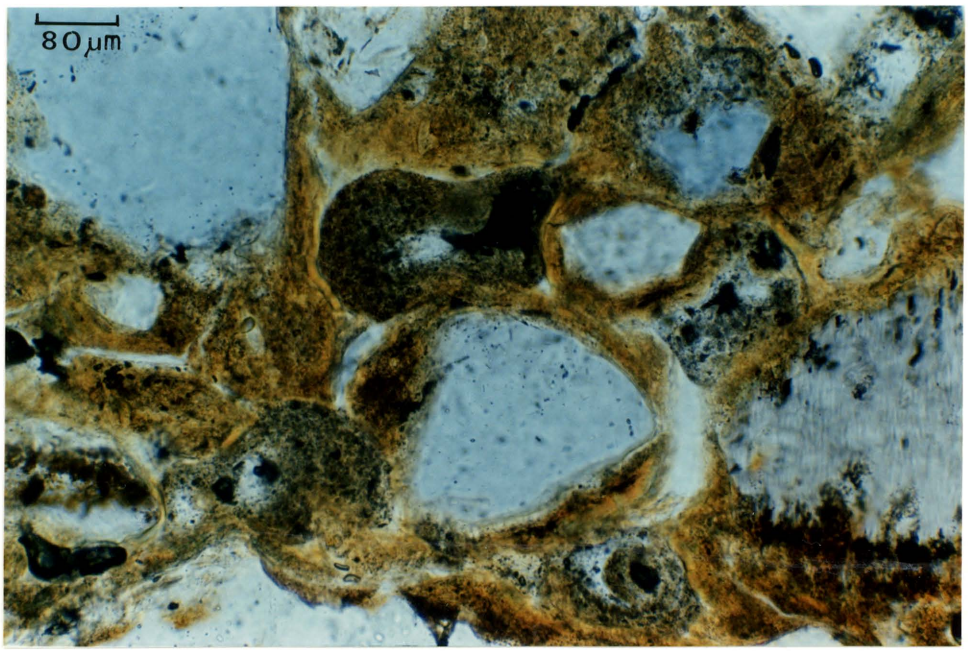

Figure 11 Ferruginous opal rimming detrital grains in a fissure in calcrete. (plane polarised light)

4.3 Clay Mineralogy

Clay mineralogical investigations on 107 samples from 6 boreholes, representing the surficial materials at Vaalputs were undertaken (Brynard, 1983) to aid the selection of the location of the waste disposal site. The clay mineral composition of the <2µm fraction of the sediments is expected to be a major factor in governing the geochemical behaviour of radionuclides in the surficial environment in the event of accidental release. The location of boreholes which were investigated is shown in Figure 12.

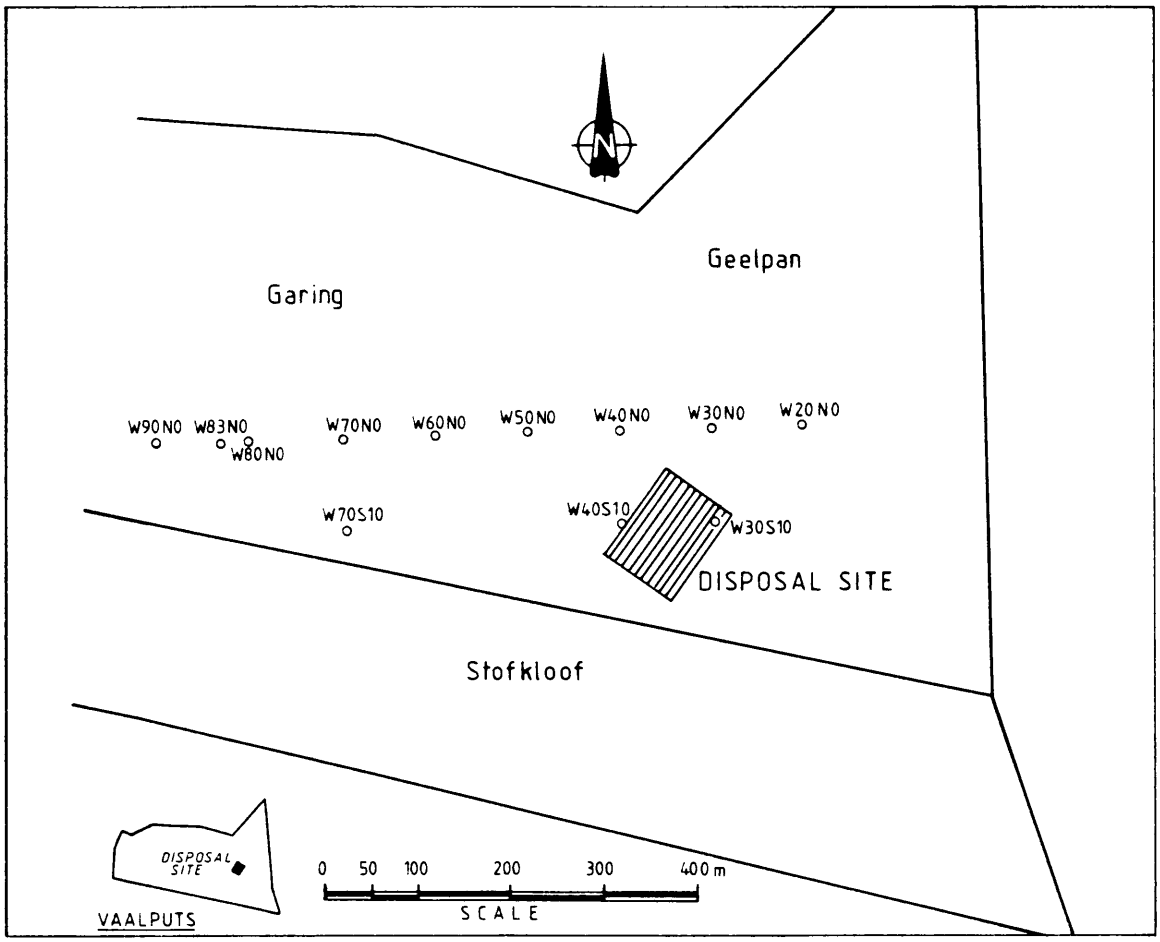

Figure 12 Location of percussion boreholes used in the study at the Vaalputs Facility.

4.3.1 Clay mineral variation

The variation in clay mineral composition with depth for each of the boreholes analysed is depicted in Figures 31, 33, 35, 37, 45 and 49.

The mean clay composition of each lithological unit in each of the six boreholes analysed is summarised in Table VII and the data from which it has been compiled are tabulated in Appendix B. Illite is the main clay mineral in the red sand and near-surface calcrete, with varying smectite and kaolinite contents. Smectite and illite predominate in the red clay, while smectite and kaolinite are the main components in the white clay. In most of the boreholes in which granite forms the fresh basement, illite decreases with depth and smectite and kaolinite gradually increase, except in W70S10 (Fig. 37) where kaolinite is scarce. In boreholes W40S10 and W40N0 (Figs. 45 and 49) in which the basement is anorthosite and tonalite, kaolinite decreases with depth and smectite increases while illite is also abundant. Generally in the weathered and fresh basement, irrespective of lithology, smectite is the major clay mineral with subordinate kaolinite and illite. A marked feature of the clay mineral variation in virtually all the borehole profiles is the antipathetic relationship between kaolinite and illite and the prominent dually increasing trends of smectite.

The diffractograms invariably show weak peaks for all the clay minerals in samples taken close to the surface, indicating poor crystallinity. X-ray diffraction analyses of silt fractions of three samples also showed an abundance of the above-mentioned three clay mineral groups. Furthermore it was observed that the fraction <2 µm constituted the major part of the grain-size fraction less than 45 µm in diameter, except in the fresh basement rocks. Although it is not expected to find clay minerals in the fresh basement, some clay minerals occur, possibly in minor fractures.

4.3.2 Discussion

Among the most important constituents of soils and sediments are the clay minerals, which are mainly hydrous aluminium silicates commonly with some replacement by Fe, Mg, Na and Ca. The clay minerals mentioned in this study are not specific mineral names, but colloquial terms designating groups of minerals, the general characteristics of which have been summarised by Krumbein and Sloss (1963) (Table VIII).

Table VII The mean clay mineral composition of the <2 µm fraction and mean mass percentage of the <45 µm fraction in six boreholes from Vaalputs

		Mean clay content (<2 µm) (mass %)			Mean mass of (<45 µm) fraction
Borehole	Rock unit	Smectite	Illite	Kaolinite	(%)
W30S10	Red sand	10	66	24	20,4
	Calcrete	15	45	40	50,4
	Red clay	25	48	27	52,3
	White clay	19	15	67	53,3
	Weathered granite	42	19	39	38,4
	Fresh granite	40	19	41	39,6
W40N0	Red sand	21	32	47	26,0
	Calcrete	17	70	13	36,2
	Red clay	24	42	34	44,5
	White clay	74	11	15	45,3
	Weathered tonalite	79	10	11	27,8
	Fresh tonalite	87	3	10	27,8
W40S10	Red sand	7	87	6	21,8
	Calcrete	12	72	16	22,4
	Red clay	23	52	25	51,4
	White clay	33	60	7	61,4
	Weathered anorthosite	54	37	9	12,4
	Fresh anorthosite	51	40	9	9,6
W60N0	Red sand	3	85	12	8,8
	Calcrete	12	70	18	36,4
	Red clay	29	38	33	42,0
	White clay	31	14	55	23,4
	Weathered granite	43	28	29	19,6
	Fresh granite	37	27	36	21,2
W70N0	Red sand	3	89	7	31,6
	Calcrete	27	53	19	42,4
	Red clay	24	62	14	46,8
	White clay	25	25	50	34,6
	Weathered granite	43	17	39	31,5
	Fresh granite	28	42	31	26,8
W70S10	Red sand	0	96	4	29,2
	Calcrete	9	72	19	27,2
	Red clay	33	41	26	31,9
	White clay	47	18	35	39,6
	Weathered granite	65	26	9	26,4

* During percussion drilling some material may be comminuted to a grain size less than 45 µm, which explains the high percentage of this fraction in fresh basement samples.

Table VIII Summary of properties and occurrence of the major clay mineral groups

Property	Kaolinite Group	Illite Group	Smectite Group
Particle size (in μm)	4,0-0,3	0,3-0,1	0,2-0,02
Cation-exchange capacity (in meq/100 g) at pH 7*	3 - 15	10 - 70	50 - 150
Relative water adsorption	Slight	Moderate	Very Large
Relative permeability	Large	Moderate	Small
Relative plasticity	Slight	Moderate	Large
Occurrence in recent sediments	Common	Abundant	Common
Occurrence in ancient sediments	Common	Abundant	Common

After Krumbein and Sloss, (1963)
*Data from Carroll (1959) and Rösler and Lange (1972)

The ideal formula for each of the three mineral groups under discussion is given by Schröcke and Weiner (1981) as follows:

Smectite group:
Montmorillonite -
$(Al_{1,67},Mg_{0,33})[(OH)_2/Si_4O_{10}]\cdot Na_{0,33}(H_2O)_4$

Saponite -
$Mg_3[(OH)_2/Al_{0,33}Si_{3,67}O_{10}]\cdot Na_{0,33}(H_2O)_4$

Illite group - $(K,H_2O)Al_2[(H_2O,(OH)_2/AlSi_3O_{10}]$

Kaolinite - $Al_2[(OH)_4/Si_2O_5]$

Clay minerals are layer type aluminosilicates and owing to their small particle size they have great surface activity, reflected by their high ion adsorption capacity and cohesiveness. Smectite has high ion-exchange capacity arising through the accumulation of exchangeable cations in the interlayer positions between each unit cell as well as on the flat surfaces of each crystal. The cations balance a negative charge which is due to extensive substitution of Al^{3+} for Si^{4+} in the tetrahedral layers and extensive substitution of Mg^{2+} (and to a lesser extent Fe^{3+} and Fe^{2+}) for Al^{3+} in the octahedral layer. Illite, which can be considered to be a compositional variant of the mineral muscovite, has intermediate ion-exchange capacity due to the presence of a limited number of interlayer exchange sites resulting from some octahedral substitution, a lesser amount of tetrahedral substitution of Al^{3+} and some replacement of K^{+} by exchangeable cations. In kaolinite there is little ionic substitution for Al^{3+} or Si^{4+}, and as a result interfacial electrical double layers due to substitution are unimportant and therefore it has correspondingly low ion-exchange capacity. Exchangeable cations in all the above-mentioned reactions are predominantly the common cations in natural waters, K^{+}, Na^{+}, Ca^{2+} and Mg^{2+} (Berner, 1971).

The specific clay minerals in sediments are a reflection of some combination of conditions that existed in the area of weathering of the parent rocks and later in the area of accumulation. Since the clay minerals are highly aluminous they require aluminous precursors such as K-feldspar, plagioclase, biotite and muscovite (Berner, 1971). Of the four minerals, plagioclase, because of its high reactivity and abundance, appears to be the principal source of the cations and silica found in most ground waters in contact with igneous rocks (Garrels, 1967). The hydrolysis of albite can be represented by the reaction (Berner, 1971):

$$2NaAlSi_3O_8(\text{albite}) + 2H_2CO_3 + 9H_2O \rightleftharpoons 2Na^{+} + 4H_4SiO_4 + Al_2Si_2O_5(OH)_4(\text{kaolinite}) + 2HCO_3^{-}$$

Berner, (1971) has emphasised the importance of water flow as a

controlling factor in determining the types of clay minerals likely to form during weathering. At moderate flow rates albite is changed to kaolinite by the above reaction. High flow rates promote the formation of gibbsite instead of kaolinite. When flow rates are slow, material is removed slowly from the weathering site and, provided Mg^{2+} is available, smectite is formed by the reaction (Berner, 1971):

$$3NaAlSi_3O_8(\text{albite}) + Mg^{2+} + 4H_2O \rightleftharpoons$$
$$2Na_{0,5}Al_{1,5}Mg_{0,5}Si_4O_{10}(OH)_2(\text{smectite}) + 2Na^+ + H_4SiO_4$$

Smectite forms as a result of alteration of feldspar in an alkaline environment (Lukashev, 1970). In arid conditions it will be stable (Perel'man, 1967), but during chemical leaching in a humid climate and where good drainage occurs, kaolinite is the stable clay mineral. The formation of illite requires an abundance of potassium either in the source rock or in solutions with which they are in contact (Jackson, 1970). Biotite and muscovite often weather to illite (Brownlow, 1979).

The occurrence of clay minerals at Vaalputs is generally in accordance with the results of a survey of clay minerals in soils of semi-arid to arid regions in South Africa by van der Merwe and Heystek (1955) who found illite, smectite, and mixed-layer clays to be the main clay minerals. Smectite increased in depth, but kaolinite was found to be scarce or absent. The abundance of illite and smectite in the upper part of the sedimentary sequence at Vaalputs is in agreement with the mineralogy of soils of arid to semiarid regions, where these minerals predominate (Krauskopf, 1967). The presence of illite in the red clay of Vaalputs indicates incomplete leaching of the sediments or that abundant potassium was available for its formation from muscovite. It is evident that the abundance of smectite at Vaalputs can be attributed to the alteration in an alkaline environment of feldspars in the basement rocks and sediments. The basement rocks underlying the surficial sediments are mainly of granitic and noritic composition. Their constituent minerals which include K- and Na-feldspar, pyroxene and biotite, which are also abundant in the surficial sediments, are the

main precursors of the clay minerals. The abundance of kaolinite in the white clay suggests that the water flow in this unit has been higher than in the red clay, where smectite and illite predominate. The paucity of iron-oxide grain coatings in the white clay and the lower pH of this unit (pH 7,3 - 7,8) when compared to that of the red clay (pH 8,5) supports this idea. The co-existence of kaolinite and smectite with feldspars in the rocks was found to be compatible with the ground water chemistry at Vaalputs, but illite does not seem to form from the interaction of the feldspar minerals and ground water. Its presence is thought to be due to the physical breakdown and chemical reconstitution of biotite or muscovite, which was shown to be feasible by Brownlow (1979). It is evident that climate and relief play an important role in the control of the composition of the clay minerals.

With regard to the antipathetic relationship between kaolinite and illite it is possible to describe the mineral reactions involving them during weathering in terms of three chemical components i.e. Si, Al and K. Considering the major rock forming minerals of the Vaalputs basement rocks i.e. quartz, K-feldspar and muscovite, the two variables Si and Al are relatively inert and K has a varying chemical potential in the system (Velde, 1985). The key reactions during weathering with increasing alkali (potassic) potential involve K-feldspar, kaolinite, smectite and illite. Under low fluid flow conditions illite will crystallise at the grain edges of K-feldspar and muscovite (in the presence of K-feldspar), but with lowered alkali potential the clay mineral assemblage formed will change to illite plus smectite (or smectite only, where only K-feldspar is present) and then to smectite plus kaolinite and eventually to kaolinite (Velde, 1985).

Plagioclase reacts directly to form kaolinite since all calcium goes into solution and little alkali is present in the solution so that the high Si-Al concentration immediately provokes the crystallisation of kaolinite (Velde, 1983). However, plagioclase in the Vaalputs rocks has a substantial K-content as inferred from the abundance of antiperthite and kaolinite does not always form

directly from anorthosites as in borehole W40S10 (Fig. 45).

When the stability field diagram involving illite is considered (Fig. 62c) the major factors determining the formation of kaolinite and illite from feldspar alteration are potassium activity, pH and silica activity. However, for the reaction illite-kaolinite, if such a rection exists, only potassium activity and pH are important. The result of this is illustrated in the clay variation diagrams where illite is generally the major phase in the red clay in the proximity of calcrete layers in boreholes W30S10, W60N0, W70N0, W70S10, W40S10 and W40N0 (Figs. 31, 33, 35, 37, 45 and 49). The kaolinite content of these layers is generally subordinate to illite and the factor which appears to determine illite formation is potassium activity, which is generally high in these boreholes. Some illite could also be of detrital origin as in borehole W30S10 where its high concentration at the base of the red clay correlates with high Zr and Hf, probably representing zircon. However, high kaolinite contents are to be found within or directly below the calcrete in boreholes W30S10, W60N0, W70N0, W40S10 and W40N0 (Figs. 31, 33, 35, 45 and 49).

Smectite trends reach maxima towards the base of the red clay and towards the top of the fresh basement in boreholes W30S10, W60N0, W70N0 and W30S10 (Figs. 31, 33, 35 and 37). In borehole W40S10 the upper-most maximum occurs somewhat lower than the red clay - white clay interface, but coincides with a definite break in the trends of most of the elements, which is interpreted as representing an unconformity. This unconformity marks the base of reworking of the upper part of the white clay. This interpretation is supported by coinciding maxima of TiO_2, Fe_2O_3, Zr, Hf, Nb, and Th all of which are constituents of heavy minerals. The total silt and clay contents are slightly lower in these samples. The absence of smectite maxima in the surficial lithologies of borehole W40N0 could be explained by the total reworking of the white clay in this borehole which is located in an erosion channel (Levin and Raubenheimer, 1983).

It is therefore suggested that the lower smectite peak is due to smectite forming from the alteration of feldspars in the fresh basement under present day arid conditions. This is substantiated by the ground water chemistry. The peak at the interface of the red and white clay units could be explained as follows: smectite is expected to be the main clay phase to form under the arid conditions which are believed to have prevailed during the formation of the red clay sediments. During their transportation to the present site, however, constituent cations of smectite such as calcium, magnesium and potassium would have been partially lost to solution, while sodium, being a very mobile element would have been lost to a greater extent. In the post-depositional period upward migration of elements occurred, resulting in the formation of calcrete layers. The clay minerals forming in the upper portion of the red clay would then have comprised kaolinite or illite due to the paucity of cations to form smectite.

The coexistence of the diversity of clay minerals at Vaalputs are compatible in terms of ground water chemistry. The predominance of one constituent over the others appears to be primarily a function of the prevailing geochemical conditions during any given period and the available cations for its formation.

During logging in the field the geologist has to rely on visual observations and testing of physical properties of minerals. The distinction between smectite, illite and kaolinitic clays cannot be made readily without X-ray diffraction analysis. As a result much of what has been regarded as kaolinite during initial borehole logging has now been proven to be either smectite or illite, or a mixture of the three minerals. The clay minerals are the single most important mineral group which could influence the migration of elements and could therefore have an important bearing on radionuclide migration.

4.4 Grain Size Analyses

Borehole W40N0 was chosen for a grain-size analysis due to the fact

that it represents the spectrum of lithological variation on Vaalputs and is situated near the final disposal site (Fig. 12). The percentage variation of each grain size fraction with depth is shown in Figure 13. The mass percentages of the sized fractions for each sample are tabulated in Appendix C. The sand and coarser fractions (+63µm) consist of quartz, which usually predominates, with varying quantities of feldspar, calcrete and heavy minerals. Only the size fractions greater than 45 µm are represented in the diagram. The total mass of these fractions represents between 25 and 50% of the rock mass, the rest being silt and clay (<45 µm).

The low percentages in the +45 µm fraction mark a sharp transition from sand to silt size material. The high percentage of coarse grained material at a depth of 1 to 2 m is due to the presence of a calcrete layer. In general there is an increase in percentage with depth in the smaller size fractions (+45 to +250 µm) and a corresponding decrease in percentage in the larger fractions (+425 µm). This confirms the arenaceous character of the red clay unit in contrast to the more argillaceous white clay.

4.5 Conclusions

Several features distinguish the surficial lithological units at Vaalputs. The characteristics of the red sand and the calcrete are obviously high quartz sand and calcite contents respectively. The distinction between the red clay and the white clay units is less obvious. The red clay is distinguished from the white clay mainly by its red colour which is due to iron-oxide coatings on mineral grains, but which are absent in the white clay. In addition iron-oxide nodules and blue quartz pebbles occur in the red clay but not in the white clay, which has petrogenetic implications. Biotite is mostly absent in the red clay, as it was probably weathered to illite, but it is often present in the white clay. Feldspar, quartz and other mineral grains occur in both units and clay minerals are abundant, although different clay minerals predominate in each unit, namely smectite and illite with subordinate kaolinite in the red clay, while the main clay minerals of the white clay are smectite

and kaolinite with less illite. The red clay is also more arenaceous than the white clay. The high clay content of both units is important from the point of view of element migration and therefore radionuclide retardation. The similarity in the mineralogical constituents of the fresh and weathered basement and that of the surficial rocks indicates that the basement rocks could have constituted the source rocks for the sediments.

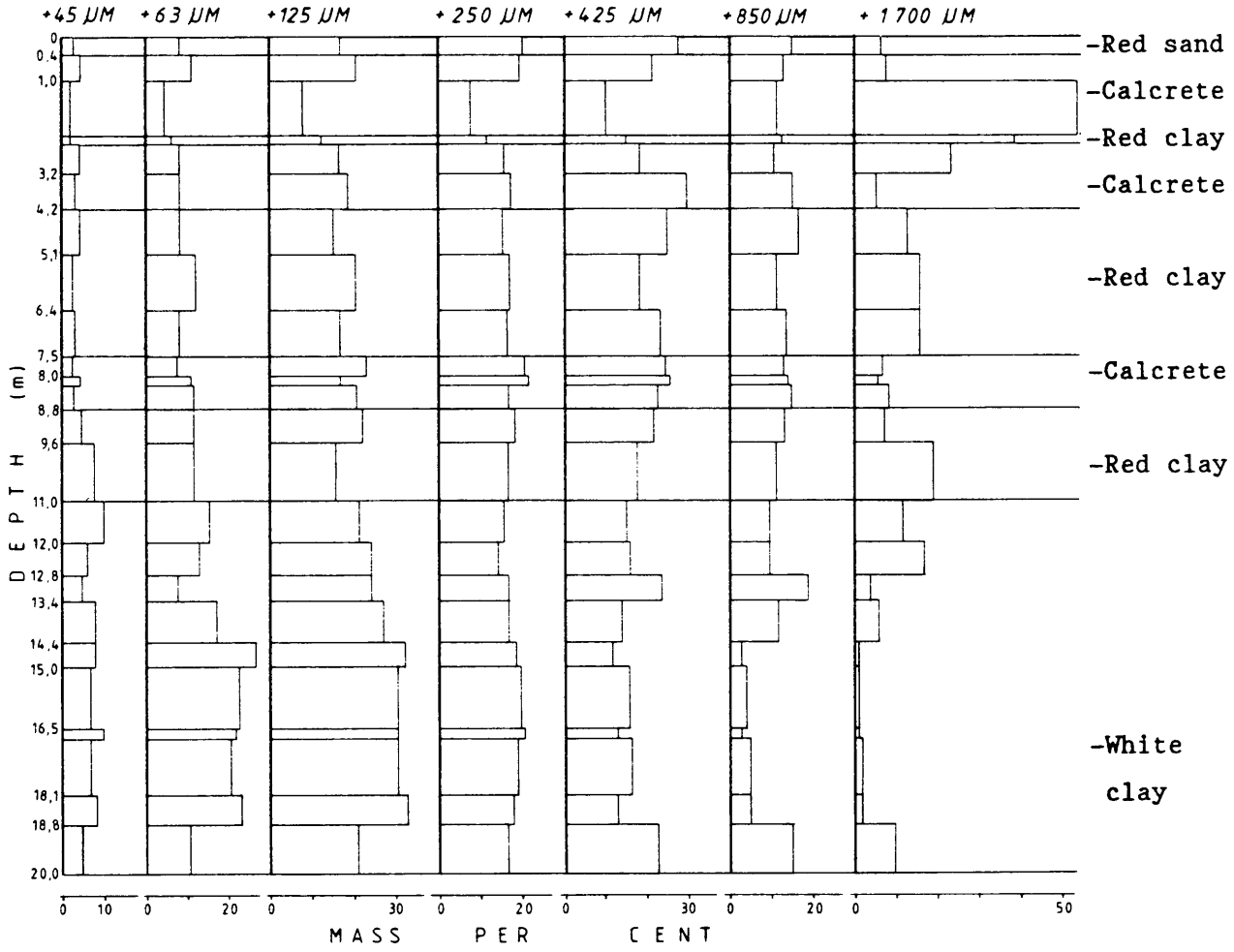

Figure 13 Mass percentage variation with depth of grain size fractions in borehole W40N0.

CHAPTER 5

URANIUM DISTRIBUTION

An evaluation of the uranium distribution in the geological environment at Vaalputs is a prerequisite to establish the suitability of the rocks for retaining this element which is present mostly in high-level radioactive waste. The three-dimensional uranium distribution on a macroscopic scale is discussed under the appropriate section dealing with element distribution. The technique of fission-track micro-mapping allows the microscopic distribution of uranium in both basement and surficial rocks to be established and also the degree to which uranium has been mobilised in the basement rocks.

The following description is based on work done by the author, but some descriptions, notably of the uranium distribution in Koperberg Suite rocks were taken from Robb (1987).

5.1 Uranium in Basement Rocks

Samples of the rocks were taken towards the western portion of Vaalputs where reasonably fresh outcrops occur. A summary of uranium distribution in specific rock types is given in Table IX.

Zircon invariably contains U in very high concentrations (Fig. 14) and being the most abundant uranium-bearing mineral, probably accounts for most of the uranium present. It commonly occurs as roundish, zoned grains with the outer zone having the highest uranium content. It is generally associated with patches of mafic minerals especially magnetite and biotite, but grains totally enclosed in feldspars are also common.

Other accessory phases containing high uranium values are monazite, sphene and xenotime, all of which are almost always associated with

patches of biotite and magnetite. Sphene, with irregularly distributed uranium, occurs as euhedral grains. No zoning is optically discernible but distinctly higher uranium concentrations are present on grain boundaries (Fig. 15). The areas with highest uranium concentration have higher (yellow) interference colours than the remainder of the grain, however, this is not clearly visible in Figure 15.

In magnetite, U is most often concentrated along the periphery of grains which display an argillic alteration rim at the contact with feldspar (Fig. 16). However, some purple fluorite can also sometimes be seen to be present along the magnetite periphery and can account for the uranium. Occasionally U occurs evenly distributed in the magnetite. Lath-like grains of leucoxene occur intergrown with the magnetite (Figs. 16 and 17) and these usually contain a higher U content. Discrete concentrations of U within the magnetite are probably due to its presence in leucoxene alteration products. An opaque phase, possibly uraninite, with an extremely high uranium content was noticed, but is not abundant.

Biotite <u>per se</u> does not seem to accommodate much uranium, but high concentrations are associated with fluorite which shows the characteristic purple colour due to radiation (Fig. 17). High concentrations of uranium are also associated with an unidentified phase in the biotite, where it is especially associated with areas with yellow interference colours in the biotite (Fig. 18). In some rocks prograde biotite, which post-dates the retrograde mafic minerals, hosts a small amount of uranium, in contrast to the barren retrograde assemblages (Robb, 1987).

Uranium has been mobilised to some extent in the rocks and now occurs in microcracks in quartz grains adjacent to the biotite (Fig. 19). The cracks usually contain argillaceous material which has adsorbed the U. Uranium was also observed to occur in cracks in extensively sericitised K-feldspar and seems to have originated from a proximal magnetite-leucoxene association.

5.2 Uranium in Surficial Rocks

A suite of thin sections of rocks representative of the surficial cover at Vaalputs was also investigated with respect to uranium distribution. Samples of the sedimentary sequence were obtained from the auger boreholes and were impregnated prior to preparation of thin sections. This process does not seem to have affected the micro-mapping technique detrimentally. The red sand was not investigated due to its very loose unconsolidated nature.

5.2.1 White clay

These rocks consist mostly of detrital grains like quartz, feldspar, and heavy minerals including zircon, monazite, sphene, magnetite etc. in a clay matrix. Uranium is present in low concentrations in the argillaceous matrix and in some heavy minerals e.g. magnetite and sphene, but very abundant in zircon and monazite. Titaniferous minerals, probably leucoxene, have very high U contents.

5.2.2 Red clay

The uranium distribution in the red clay is similar to that in the white clay. In addition, grains of red hematite with small inclusions of detrital grains are found in the matrix of the red clay and these have a U content several orders of magnitude higher than the matrix.

5.2.3 Calcrete

Calcrete and calcretised clay from the upper layers have a very low U content. The U generally occurs disseminated in the matrix, but ferruginous portions usually have a substantially higher U content. Detrital U-bearing minerals such as zircon occur, but are scarce in the calcrete. Relicts of basement material are abundant in the calcrete. Coarse calcite surrounds these relict grains which show a distinctly higher U content than the finer grained calcite matrix. K-feldspar resorbed by calcite shows a high U content and

chloritised feldspar with very high U was noticed in one sample (Fig. 20).

5.3 Discussion

In the basement rocks uranium is present predominantly in the accessory minerals and in phases which have formed as the result of hydrothermal alteration e.g. leucoxene. Zircon is the most important U bearing phase and most grains contain abundant uranium, even in the meta-sediments where the zircons are remnants of the sedimentary source rocks. The prominent zoning of zircon in which the outer zones are more uraniferous, is probably the result of overgrowths during metamorphism.

Uranium seems to be more labile in the titaniferous phases from which it has been redistributed as a result of oxidation in a subaerial environment. The presence of U in cracks and fractures and along grain boundaries could alternatively be explained by flushing of the rock by U-bearing fluids, but this is considered unlikely. There is little additional evidence that uranium has been mobilised in the basement rocks. Some of the mobilised U has been adsorbed by argillic alteration products and it seems that mechanisms exist to retard the relatively minor migration of U in the basement rocks. In a deep waste repository it would be expected that anoxic conditions, and probably lower permeability as a result of lithostatic pressure, will inhibit migration of uranium even further. From this point of view the basement rocks seem to be eminently suitable for the disposal of high-level waste.

In the surficial rocks uranium is present in detrital heavy minerals, finely disseminated in the argillaceous matrix and adsorbed onto Fe- and Ti-oxides. Although the latter are better concentrators of uranium when compared to the clay matrix, the higher abundance of clay probably accounts for the bulk of the uranium in the surficial rocks. The surficial rocks therefore possess good retardation properties for uranium, provided that the physico-chemical conditions allow its adsorption.

Table IX A summary of uranium distribution in the basement rocks of Vaalputs

Mineral Assemblage	Stratigraphy	Occurrence of uranium	Characteristics
Quartz-plagioclase-biotite-K-feldspar-magnetite gneiss	Koperberg	Accessories including xenotime, zircon and apatite; microfractures and grain boundaries	Abundant accessories associated with biotite and magnetite; no U in rock-forming minerals like biotite or magnetite.
K-feldspar quartz (leucogranite)	Koperberg	Zircon, apatite; minor U in hematite and ilmenite exsolution bodies	Pervasively sericitised feldspar
Quartz-plagioclase	Koperberg	Sphene, zircon, sphene rims around magnetite; no redistribution of U	Minor chlorite and perthite feldspar; myrmekite abundant; feldspar fresh; mafics highly propylitised; high magnetite content
K-feldspar-chlorite-biotite	Stofkloof Megacrystic Granite	Zoned zircon, monazite, altered magnetite and biotite; microfractures and grain boundaries	Myrmekitic intergrowths of plagioclase and quartz; biotite altered to chlorite/epidote; feldspars argillitised
Garnet-K-feldspar chlorite-biotite	Stofkloof Megacrystic Granite	Zircon; less in magnetite, little U in fractures	Garnet-biotite assemblage rock
Quartz-plagioclase-orthoclase-perthite-biotite-chlorite	Kliprand Charnockite Suite	Zircon, minor U in chlorite; Ti-magnetite with ilmenite exsolution bodies	Biotite/chlorite pseudomorphous after hornblende; fabric of orientated quartz blebs; biotite fresh.
Quartz-microcline perthite-magnetite-zircon	Kliprand Charnockite Suite	Zircon; small amounts in prograde biotite; none in altered biotite	Prograde biotite postdates altered biotite
Quartz-plagioclase clinopyroxene-magnetite	Hoogoor Suite	Zircon, apatite, monazite low U in magnetite; little remobilisation.	Red brown accessory minerals resembling monazite; granoblastic texture
Quartz-plagioclase-biotite-orthoclase-magnetite-zircon	Hoogoor Suite	Zircon; U generally low	Biotite and quartz define prominent foliation
Quartz-orthoclase-microcline-perthite-chlorite-biotite-magnetite with minor plagioclase	Hoogoor Suite	Zircon, apatite (zoned), significant U in magnetite-ilmenite exsolution altered to leucoxene; chloritised-biotite; microfractures and grain boundaries	Feldspars turbid, especially along grain boundaries; weak foliation defined by altered biotite and opaque minerals

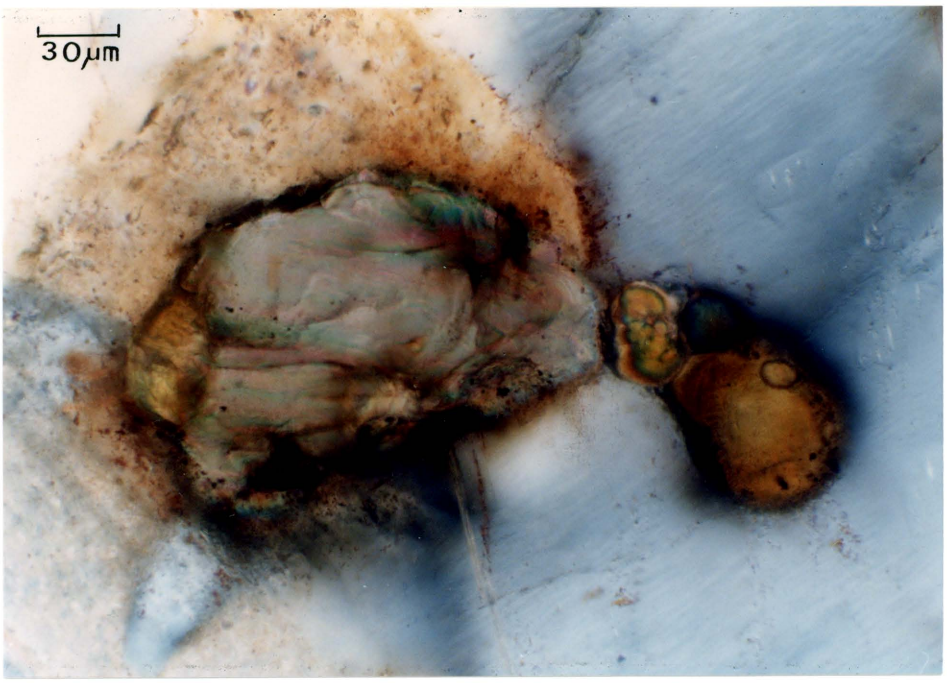

Figure 14(a) Zircon group in Vaalputs granite gneiss.
(crossed nicols)

Figure 14(b) Fission-track image showing high concentration of U in zircon especially along the grain periphery.
(plane polarised light)

Figure 15(a) Photomicrograph of Stofkloof Megacrystic Granite showing biotite with fluorite along cleavages (lower left), subhedral sphene (upper centre), magnetite, leucoxene and zircon (upper right). (crossed nicols)

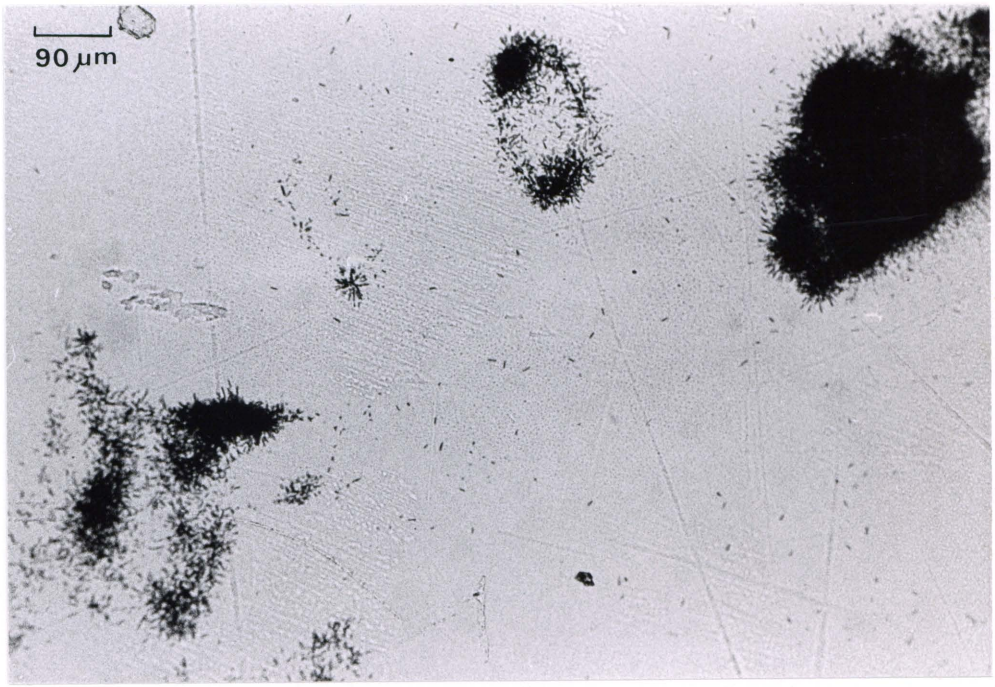

Figure 15(b) Fission-track image showing high U in biotite (lower left) and along grain boundaries of sphene (upper centre). Very high U occurs in zircon and leucoxene associated with magnetite (upper right). (plane polarised light)

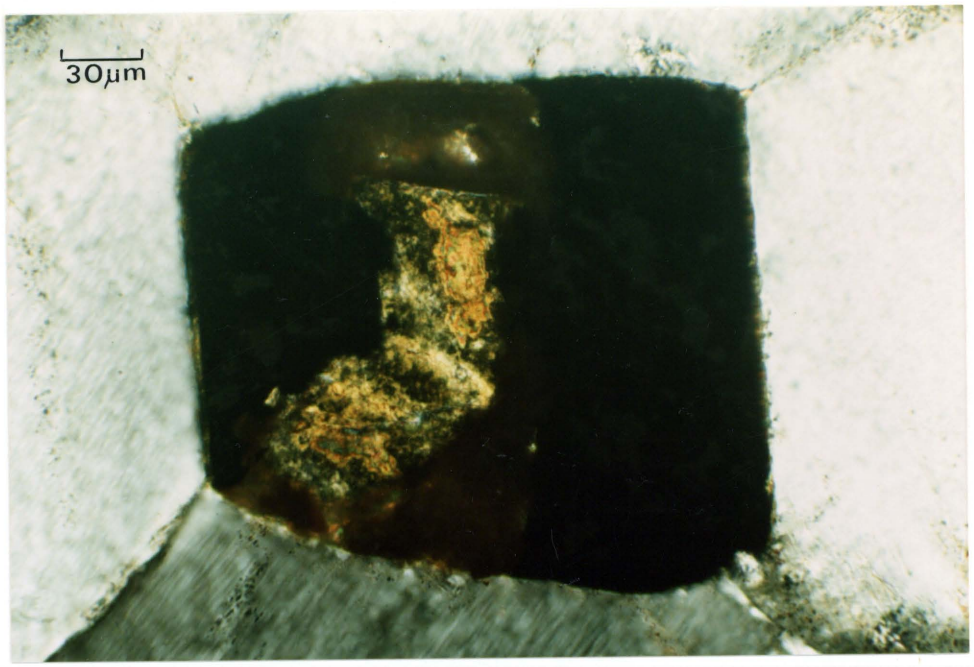

Figure 16(a) Photomicrograph of Stofkloof Megacrystic Granite showing titaniferous magnetite and leucoxene alteration (top and bottom of grain) and a Ti-alteration phase in the centre. Argillic alteration along the magnetite grain boundary is discernible. (crossed nicols)

Figure 16(b) Fission-track image showing U distribution along magnetite grain boundary and mobilised U in a micro-fracture (lower right corner). High U in the Ti-alteration phases (top centre) is evident. (plane polarised light)

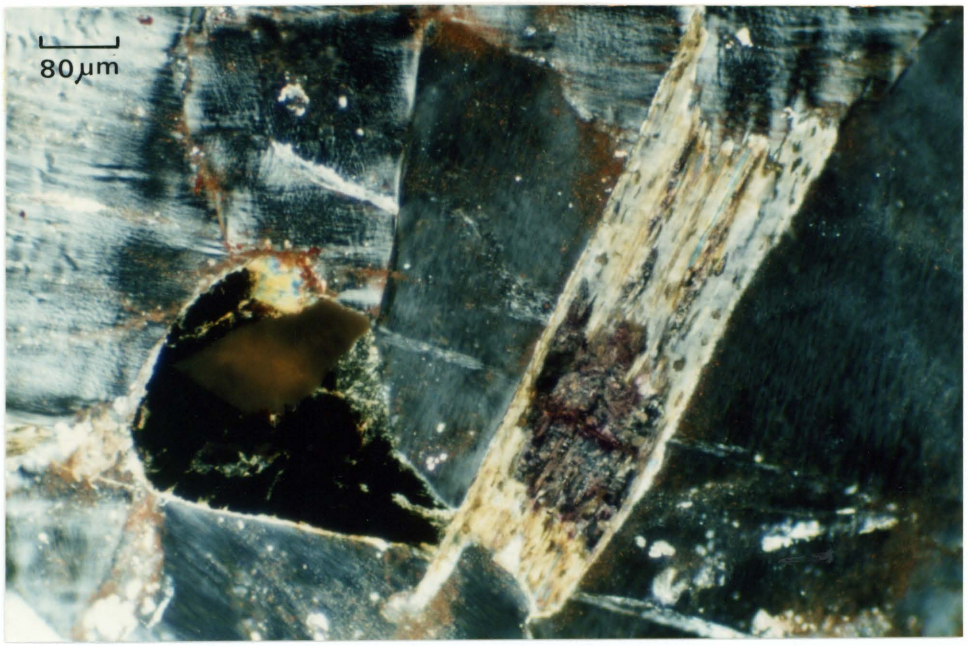

Figure 17(a) Photomicrograph of Stofkloof Megacrystic Granite showing biotite (right) with fluorite along cleavage (top right) and purple fluorite in the centre. Magnetite (left) with leucoxene (middle left) and zircon (above leucoxene) are commonly associated with biotite. (crossed nicols)

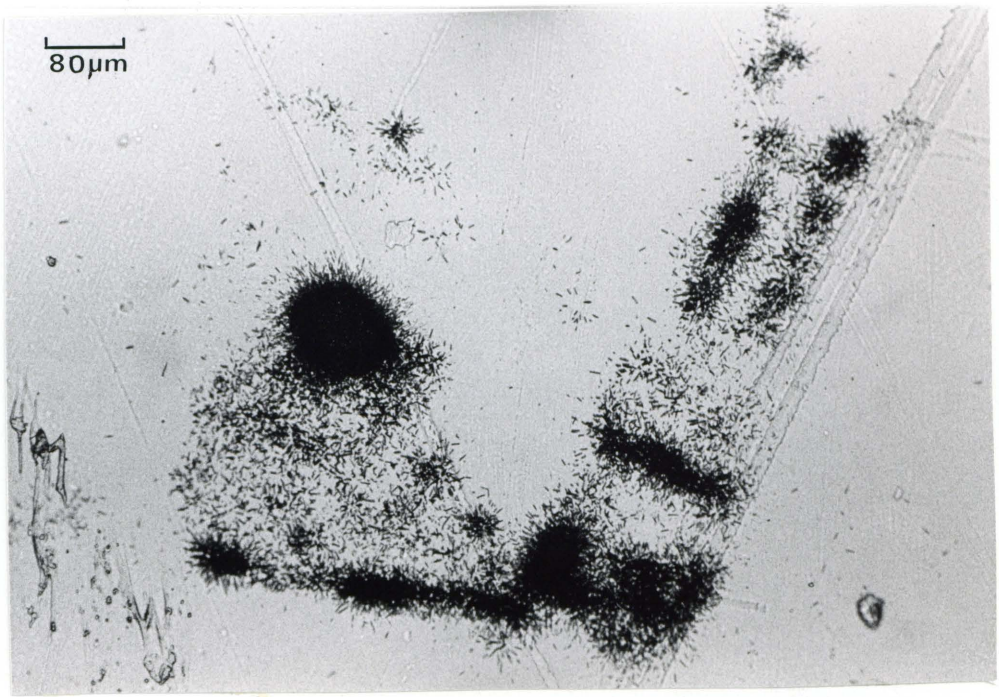

Figure 17(b) Fission-track image showing U associated with fluorite along cleavage and associated with argillic alteration along the bottom of the magnetite grain on left. U contents of leucoxene and zircon are evidently high compared to magnetite (left). (plane polarised light)

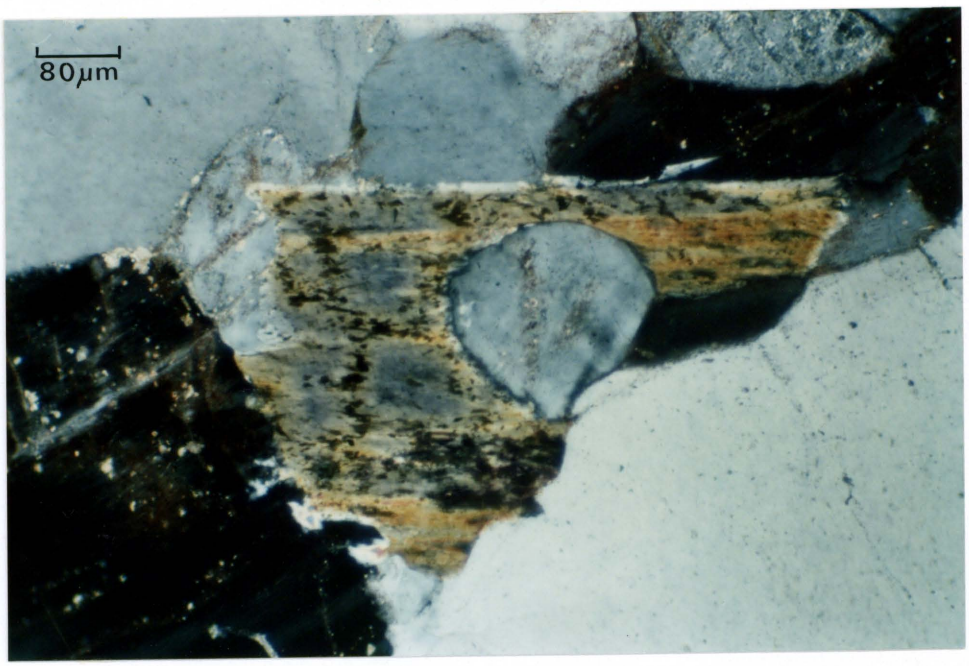

Figure 18(a) Titaniferous biotite with leucoxene (black phases) along cleavages. An unidentified phase causing marked yellow interference colours in biotite is evident in places (top right and lower centre). (crossed nicols)

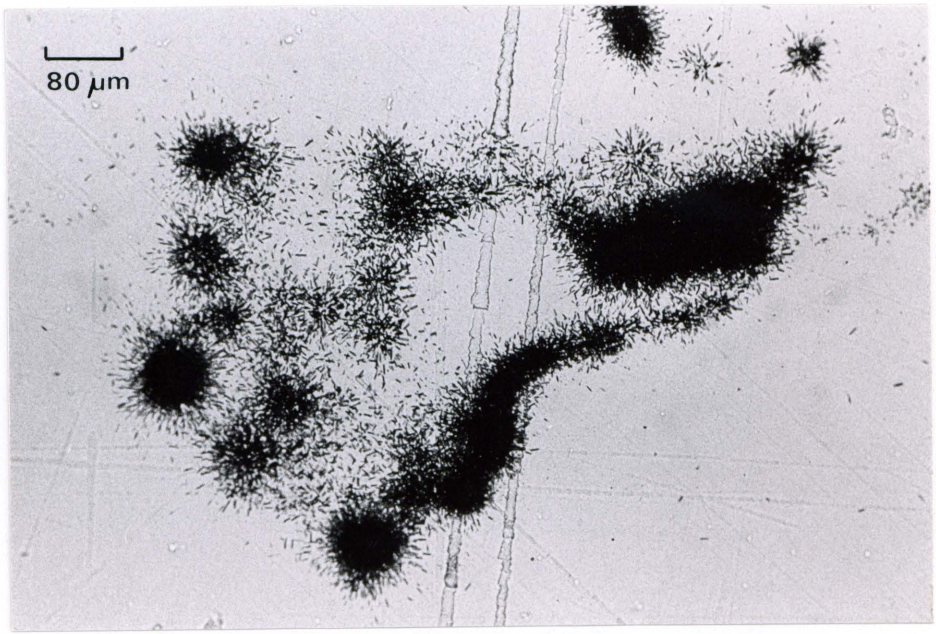

Figure 18(b) Fission-track image showing U in biotite associated with leucoxene along cleavages and very high U associated with the yellow coloration mentioned in Fig. 18(a) and purple fluorite (lower right). Partly mobilised U occurs along biotite grain boundary (right). (plane polarised light)

biotite grain boundary (right). (plane polarised light)

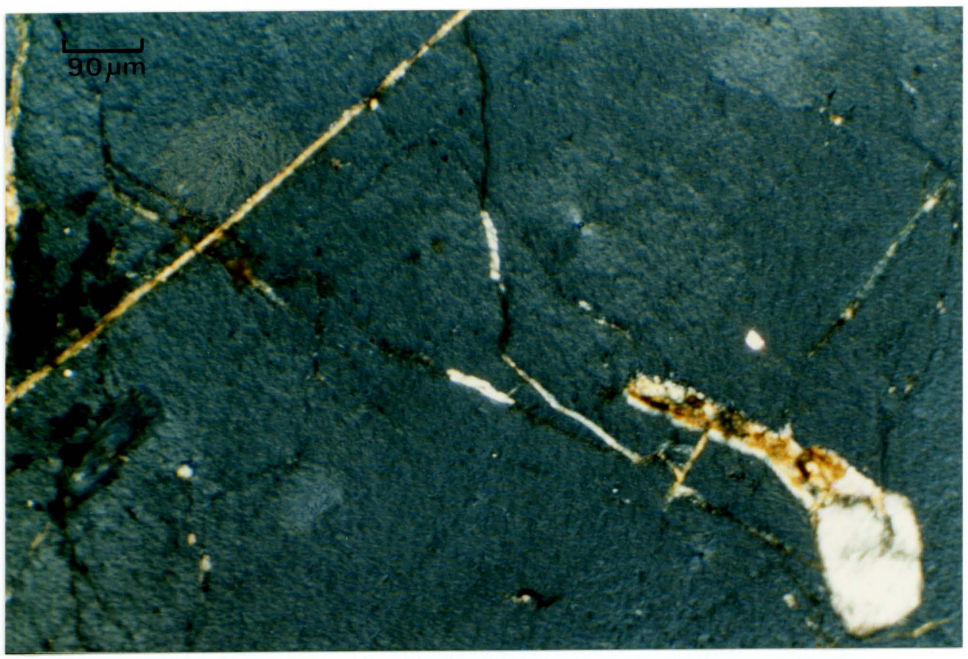

Figure 19(a) Iron-rich argillic alteration along micro-fractures in quartz in basement rocks. (crossed nicols)

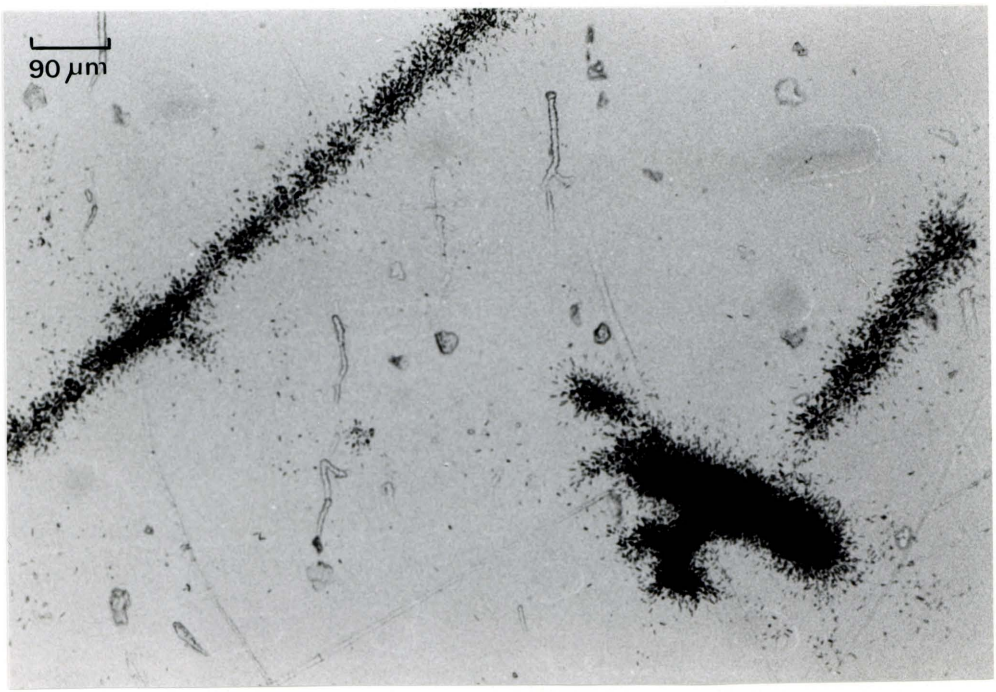

Figure 19(b) Corresponding fission-track image showing high content of mobilised uranium in microfractures. (plane polarised light)

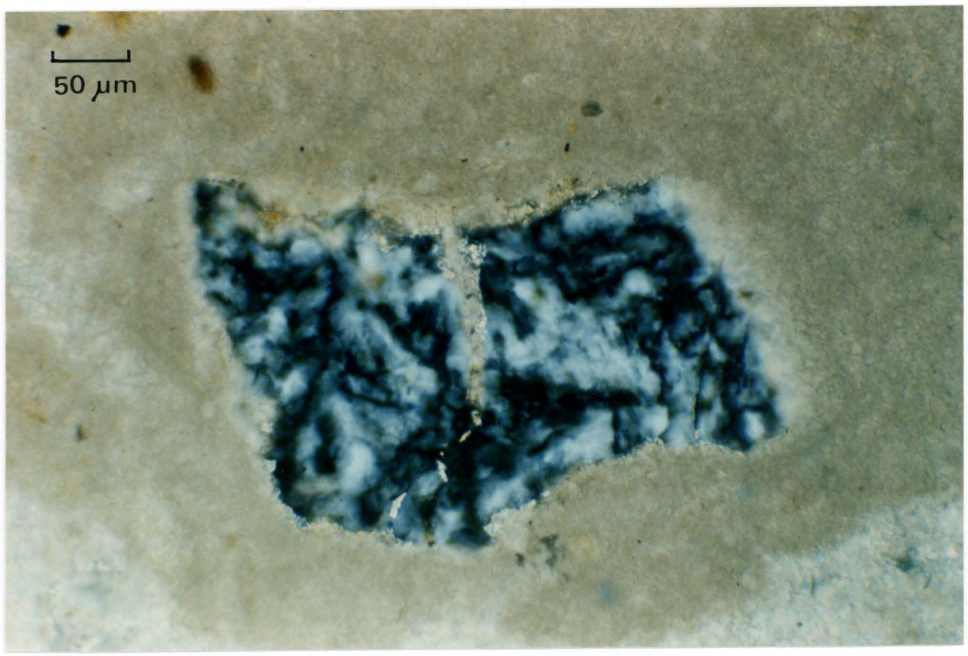

Figure 20(a) Photomicrograph of altered feldspar in calcrete. (crossed nicols)

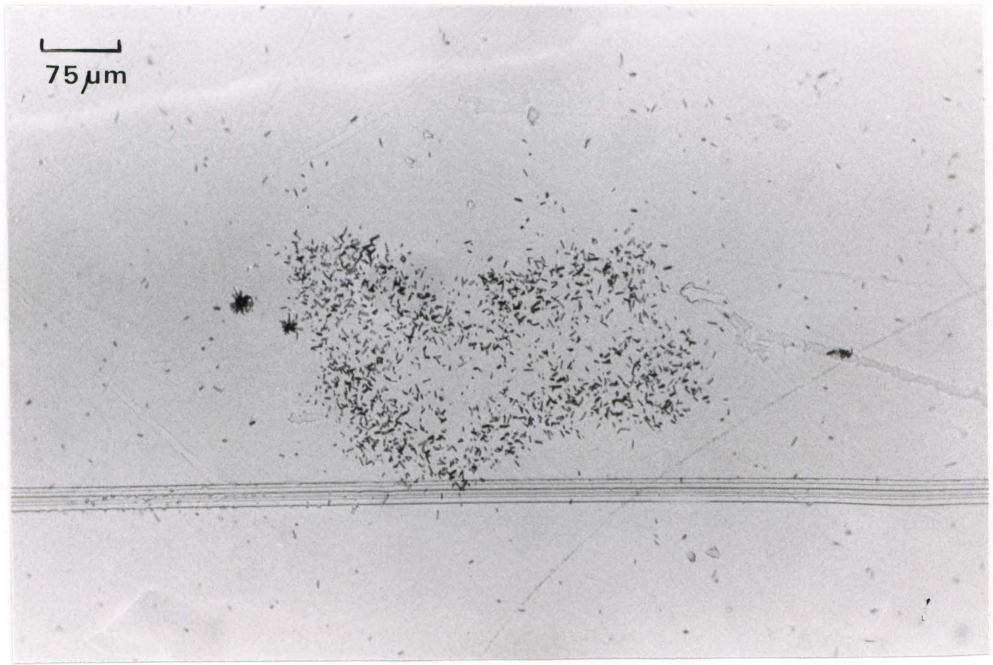

Figure 20(b) Fission-track print showing U distribution in altered feldspar with slightly higher U near the grain edges. (plane polarised light)

CHAPTER 6

GEOCHEMISTRY

The most likely mechanism for the migration of radionuclides from a repository to the biosphere is in solution in groundwater. Hydrothermal interactions with the waste will be controlled by geochemical reactions and reaction kinetics which will determine the composition of this transported solution. These reactions are controlled by temperature, pressure and compositional parameters. The subsequent behaviour of this solution and precipitation or adsorption of its constituents will be affected by reactions similar to those that have been operating in the geological history of the rocks, and which account for the present three dimensional distribution of elements.

To understand and eventually model element migration, geochemical studies must focus on the characterisation of the prevailing in situ physico-chemical conditions, the groundwater-rock alteration reactions and particularly the radionuclide precipitation and/or sorption reactions in this environment.

As the stratigraphy of the surficial rocks has not been formally described, these rocks will be loosely referred to as red sand, calcrete, red clay and white clay for the sake of brevity.

6.1 Geochemistry of the Basement Rocks

The geochemistry of the basement rocks plays an important role in the interpretation of the geochemistry of the surficial cover, because it constitutes the source rocks from which the mineralogical constituents of the surficial rocks are ultimately derived.

6.1.1 Classification of basement rocks in boreholes

To aid the interpretation of the geochemistry of the Vaalputs basement rocks underlying the surficial sediments or in boreholes,

principal components analysis, involving ten major and eighteen trace element analyses of basement rocks, was undertaken. The total variance accounted for by the first three eigen vectors of the analysis is 76,9%. Four distinct geochemical groups could be identified (Fig. 21) comprising:

Basement rocks with granitic composition in the westerly group of boreholes i.e. W90N0, W80N0, W70N0, W70S10, W60N0, W30S10 and the top-most fresh basement sample in W49,8N0.

Anorthositic basement rocks in boreholes W83N0 and W40S10.

Noritic basement comprising samples in borehole W49,8N0.

Tonalitic rocks consisting of one sample in W40N0 and four samples in W49,8N0.

The inclusion of sample 11 (from borehole W49,8N0) in the group of granitic rocks suggests that the granitic rocks in this borehole represent an enclave in noritic rocks. Although not included in the analysis, the weathered basement rocks of W20N0 probably belong to the fourth group as inferred from their mineralogy. It is not known to what extent the surficial cover at Vaalputs is underlain by noritic and anorthositic rocks, but the presence of several bodies at Vaalputs were inferred from an aeromagnetic survey (Andersen et al., 1986). The high frequency of incidence of these bodies intersected in boreholes is probably incidental for there is a paucity of outcrops of these rocks in the Vaalputs vicinity.

6.1.2 Element associations

The interpretation of the trace element associations with rock-forming minerals was undertaken by applying principle components analysis of major and trace elements (Appendices D and E) in the fresh and weathered basement. The PCA-scores plotted on the principal plane, comprising the first two eigen vectors, using major and trace element data of boreholes W49,8N0 and W20N0 are shown in

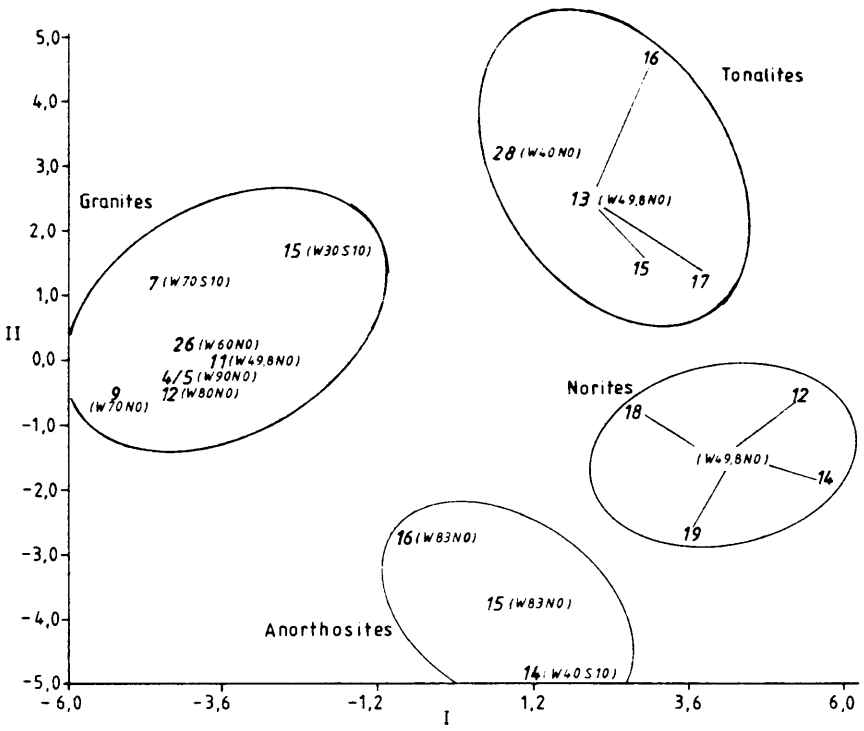

Figure 21 Principal component scores of samples on the plane of the first two eigen vectors using major and trace element data for basement rocks in boreholes. Sample numbers refer to the fresh basement samples in Appendices D and E.

Figures 22 and 23 respectively. The fresh basement in W49,8NO is mainly noritic in character. The weathered basement of W20NO is tonalitic in composition. The element distributions shown are typical of all the basement rocks. It can be seen in the figures that trace elements occur in groupings together with major elements which represent plagioclase, K-feldspar, clay minerals and the accessory minerals biotite, magnetite, zircon, xenotime and titaniferous phases such as sphene (and sulphide minerals in the case of W49,8NO). Some trace elements can have multiple associations with minerals. Cesium for instance can enter potassium positions in both K-feldspar and biotite and is associated with groups representing both these minerals in the plots of boreholes W49,8NO and W20NO respectively.

The close correlation of gallium with iron and zinc in Figure 23 is of interest. This group of elements is thought to represent the Zn-rich spinel, dysluite, in whic Al is a main constituent and Ga would therefore be expected to be high.

CC = calcite

LOI = loss-on-ignition

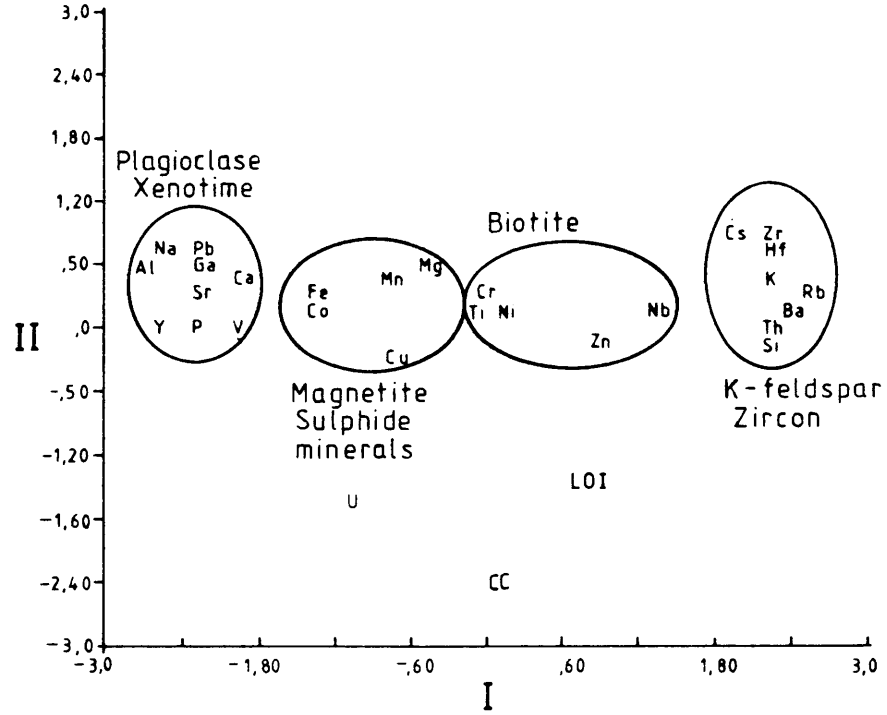

Fig 22 Principal component scores on the plane of the first and second eigen vectors using major and trace elements of fresh basement in borehole W49,8NO.

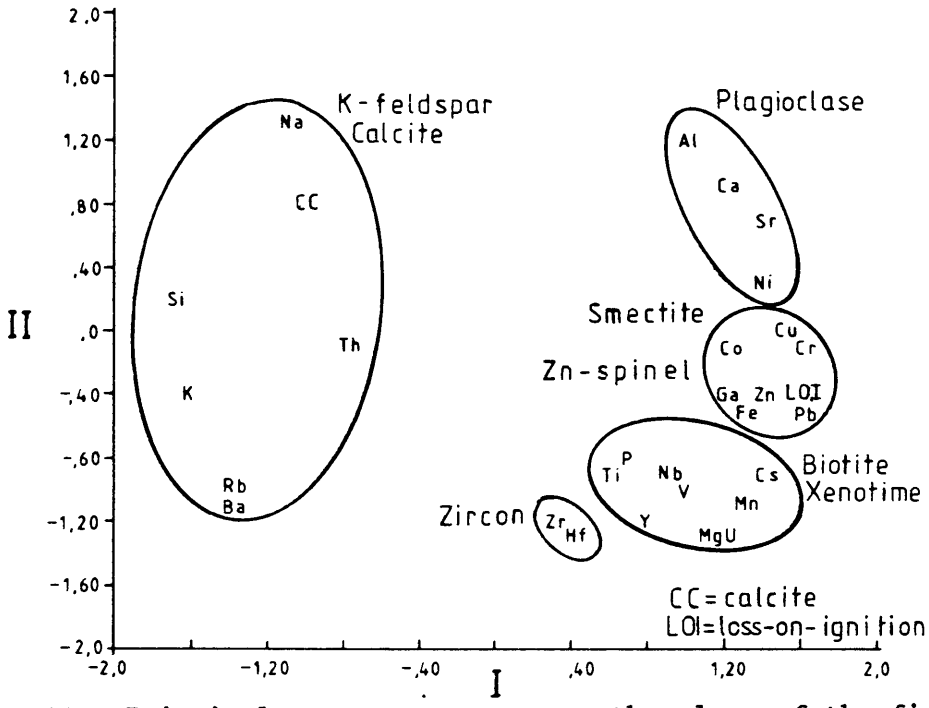

Figure 23 Principal component scores on the plane of the first and second eigen vectors using major and trace elements of weathered tonalitic basement in borehole W20NO.

High Al_2O_3 contents in the weathered and fresh basement usually correlate with high feldspar contents. Corresponding high CaO and/or Na_2O contents as in W20N0, W40S10, W49,8N0 and W83N0 (Figs. 43, 45, 51 and 47) imply plagioclase, while corresponding high Na_2O and K_2O concentrations imply K-feldspar and/or albite.

6.2 Geochemistry of the Dasdap Formation

Rocks representing the basal portion of the Dasdap Formation on Rondegat south of Vaalputs (Fig. 4 and Appendix A) provide valuable insight into the role of various processes in the concentration of key elements. This information could serve as a base line for the interpretation of the geochemistry as found in the terrigenous sequence at Vaalputs.

Isolated inselbergs comprising inliers of Dasdap Formation occur in a broad erosion valley on Rondegat. The highly silicic nature of these rocks probably accounts for their preservation. The rocks were deposited on a basement of granite gneiss, the exact stratigraphic relationship of which can only be inferred as being quartzo-feldspathic gneiss of the Garies Sub-group, due to their location. The basement is well exposed and highly altered. The major weathering process involving kaolinisation and silicification probably took place prior to the deposition of the sediments since silicified clasts of sandstone occur in an unsilicified matrix of the sandstones and grits. The alternative explanation would require a process of selective silicification which affected only certain horizons of the sedimentary succession, but this seems unlikely.

Chemical analyses of the Dasdap rocks on Rondegat are presented in Table X. The major element analyses confirm the weathered basement mineralogy which comprises mainly quartz and kaolinite with minor smectite and subordinate unaltered feldspar. If their degree of alteration is considered these rocks have fairly high contents of most trace elements especially Y, Zr, U, Th and Cr, and the rare earths La, Ce and Nd, when compared to the mean values of these elements in the rocks of the Namaqualand Province (Holland and

Table X Major and trace element analyses of Dasdap Formation rocks from the farm Rondegat, South of Vaalputs

	RGT1	RGT2	RGT3	RGT4	RGT5	RGT6	RGT8
	Major elements (%)						
SiO_2	73,81	72,48	78,03	64,06	82,05	72,23	60,60
TiO_2	0,27	0,26	8,11	0,94	0,42	7,02	0,15
Al_2O_3	16,88	18,07	4,27	19,25	9,03	5,55	0,57
Fe_2O_3	0,10	0,08	0,62	0,07	0,09	1,33	3,71
FeO	0,69	0,55	4,48	0,53	0,63	9,60	26,75
MnO	0,03	0,03	0,12	0,02	0,02	0,16	0,04
MgO	0,12	0,00	0,24	0,19	0,10	0,00	0,00
CaO	0,07	0,16	0,13	0,50	0,24	0,02	0,21
Na_2O	0,08	0,16	0,20	0,89	0,41	0,00	0,00
K_2O	0,84	0,36	0,02	0,07	0,08	0,00	0,00
P_2O_5	0,17	0,25	0,54	0,40	0,20	0,32	0,26
Cr_2O_3	0,04	0,04	0,09	0,05	0,04	0,05	0,07
NiO	0,00	0,00	0,00	0,00	0,00	0,01	0,02
H_2O	0,50	0,36	0,37	0,40	3,40	0,43	0,93
LOI	6,24	7,58	2,53	12,61	3,30	3,13	6,20
Total	99,82	100,38	99,74	100,00	99,99	99,84	99,53
	Trace elements (ppm)						
Zn	14	13	25	27	20	57	209
Cu	0	32	0	9	10	8	25
Ni	12	11	36	14	7	27	105
Co	20	3	39	5	16	8	75
Ga	20	18	1	17	6	6	2
Mo	3	2	378	10	3	57	105
Nb	17	14	212	20	10	139	7
Zr	276	290	4960	716	232	1200	34
Y	112	99	429	51	30	137	6
Sr	34	49	65	340	62	78	23
Rb	52	25	6	11	9	6	8
U	11	16	48	5	2	27	75
Th	68	65	737	58	21	278	6
Pb	60	50	76	159	24	69	21
Cr	198	134	276	91	186	241	329
V	<16	19	157	<14	<14	274	145
Ba	131	63	147	228	139	193	245
Sc	<2	15	45	<10	<13	45	<1
La	170	162	1115	579	233	662	78
Ce	237	269	2207	886	275	1121	105
Nd	131	178	1116	511	140	491	55
Sn	<1	14	20	<1	<1	25	<33
W	10	159	18	177	<1	177	250

RGT1 Weathered gneiss
RGT2 Weathered gneiss
RGT3 Rudite
RGT4 Silicified sandstone
RGT5 Ferruginous grit
RGT6 Ferruginous rudite
RGT8 Ferruginous opal

Analyses by Rocklabs cc.

Marais, 1987). Elements present in low concentrations include Zn, Cu, Sr and V (in the case of RGT1).

In the basal rudite (RGT3) a detrital component comprising quartz and heavy minerals as observed by mineralogical examination is confirmed by high TiO_2, Zr, Th, Y and P_2O_5 contents. The rock also has high concentrations of virtually all other trace elements except Cu, Ga, Rb and Sr, when compared to the other rock types in the succession.

The silicified sandstone (RGT4) is of interest in the respect that it contains very low K_2O and is highly aluminous due to kaolinite in the matrix. With regard to trace element composition it contains much higher Zn, Zr, Sr, Pb, Ba and REE but lower Co, Cr, Rb, Th, U and Y when compared with the kaolinised basement rocks (RGT1/2). Adsorption onto kaolinite and colloidal SiO_2 (opal) is suggested to account for the high contents of the above-mentioned trace elements. The silicified grit of sample RGT5 has a lower clay content than RGT4, but a similar trace element composition, except for higher Sr and REE and lower Y, Rb, U, Th, and Pb than in the weathered basement.

The role of iron in concentrating elements is evident in the ferruginised rudite sample (RGT6) in which low Al_2O_3 suggests a low clay content. When compared to a mineralogically similar rock type (RGT3), the major element content is similar except for higher Fe_2O_3 and FeO in RGT6 and much higher contents of Zn, Cu, V and Ba. However, when compared to the weathered basement rocks RGT1 and RGT2, it is noted that in addition to these elements the rock is rich in Ti, Ni, Mo, Nb, Y, Zr, Sr, U, Th, Cr and the REE. The adsorbing role of iron is further exemplified by the analysis of the ferruginous opaline nodules (RGT8) which occur so abundantly on surface near the Dasdap Formation and also in the red clay (Vaalputs Formation). The major element chemistry of the nodules confirms their mineralogical composition. When compared to the weathered basement, a marked enrichment is noted with respect to the chalcophile elements Zn and Cu, the siderophile Ni and Co together

with Mo, U, Cr, V and Ba, while the lithophile elements Sr, Rb, Zr, Nb, Pb, Th, Y and the REE are lower in concentration. The abundance of these trace elements is suggested to be due to adsorption by, or co-precipitation with an anhydrous Fe-phase and to a lesser extent also with titaniferous phases such as leucoxene, brookite and ilmenite, which have been identified in the sample. An apparent increase in the $Ga:Al_2O_3$ ratio, proportional to Fe_2O_3 content, is noted in the above-mentioned samples. In samples RGT1, RGT2, RGT4, RGT5 and RGT6 it is 0,03; 0,23 in RGT3; 1,9 in RGT7, and 3,5 in RGT8.

The Dasdap Formation represents deposition during the late-Cretaceous, (McCarthy et al., 1984) under humid conditions which were responsible for the kaolinisation and silicification of basement rocks and large scale leaching of the major elements, except Al. However, some trace elements have been retained efficiently in the rocks, probably by clay minerals, opal and iron-oxide.

6.3 Geochemistry of the Surficial Rocks

6.3.1 White clay

In the white clay the element associations deviate substantially from those of the weathered and fresh basement. The mineralogy of this rock unit shows that many minerals are in varying stages of alteration and trace elements will show less coherence to groups of elements representing particular minerals. Element associations in the white clay are typified by borehole W40S10 of which the PCA-scores are shown in Figure 24. Collectively the PCA-scores plots of white clay show that calcite formation is evident in the rock, suggested by the close mutual correlation between Ca, Mg, calcite and loss-on-ignition. A consistent element group in the white clay comprises K, Rb and Cs, representing either K-feldspar or smectite or illite. In PCA analyses comprising white clay in other boreholes Cs is sometimes associated with other element groups e.g. representing biotite. Yttrium and phosporus are present in zircon

and xenotime respectively. The remaining trace and major elements in this unit either belong to groups representing plagioclase and accessory minerals or show no consistent grouping.

In almost all the element variation profiles (Figs. 31 to 54), high Al_2O_3 both in the white and red clay generally correlates with a high clay content, unless it is accompanied by high K_2O or Na_2O, which indicates a high feldspar content. In the white clay the SiO_2/Al_2O_3 content is much lower than in the red clay (Fig. 25 and Table XI), indicating the predominantly arenaceous character of the latter and suggesting a detrital origin.

Table XI SiO_2/Al_2O_3 ratios in Vaalputs rocks

Lithological unit	SiO_2/Al_2O_3 Mean	S.Dev.	Number of samples
Red sand	13,6	5,8	12
Calcrete	9,0	2,0	7
Red clay	8,8	2,4	63
White clay	4,2	1,9	67
Weathered basement	4,9	1,4	16
Fresh basement	4,5	1,6	22

6.3.2 Red clay

More systematic groupings of elements appear in the PCA-scores plot using elements in the red clay, when compared to those in the white clay. Borehole W20N0 represents a typical example (Fig. 26), where three distinct major groupings emerge. The first represents calcite in calcrete where Ca, Mg, Sr, Ba and Pb are generally highly correlated, and sometimes Y, although this is not shown by Figure 26. A second group represents the alkali metals which are present in K-feldspar and clay mineral crystal structures or adsorbed onto the latter. This group includes K, Rb, Cs and a host of other elements. A third group representing the hydrolysate

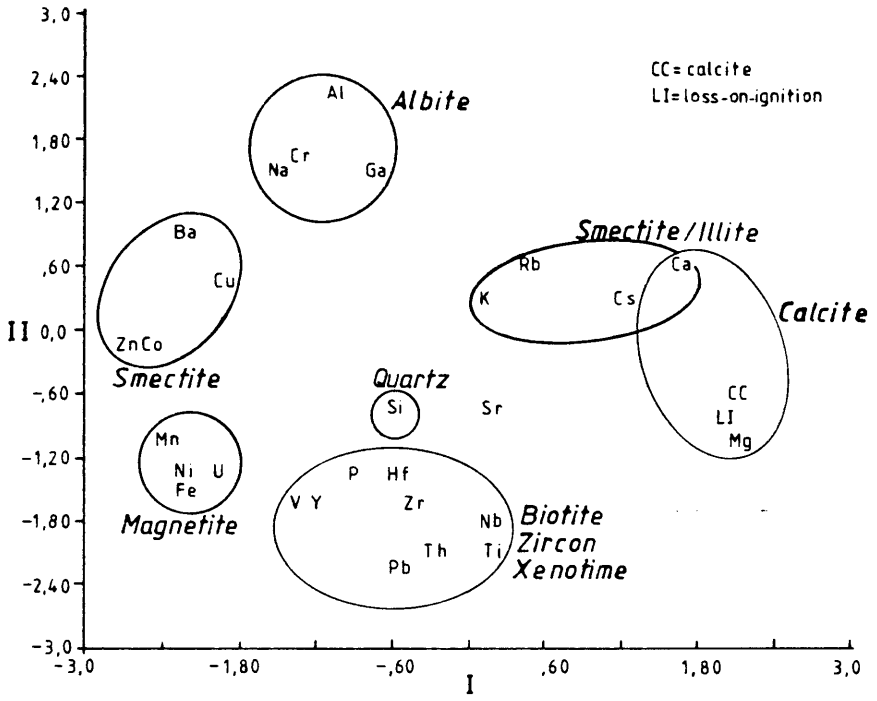

Figure 24 Principal component scores on the plane of the first and second eigen vectors using major and trace elements of white clay in borehole W40S10.

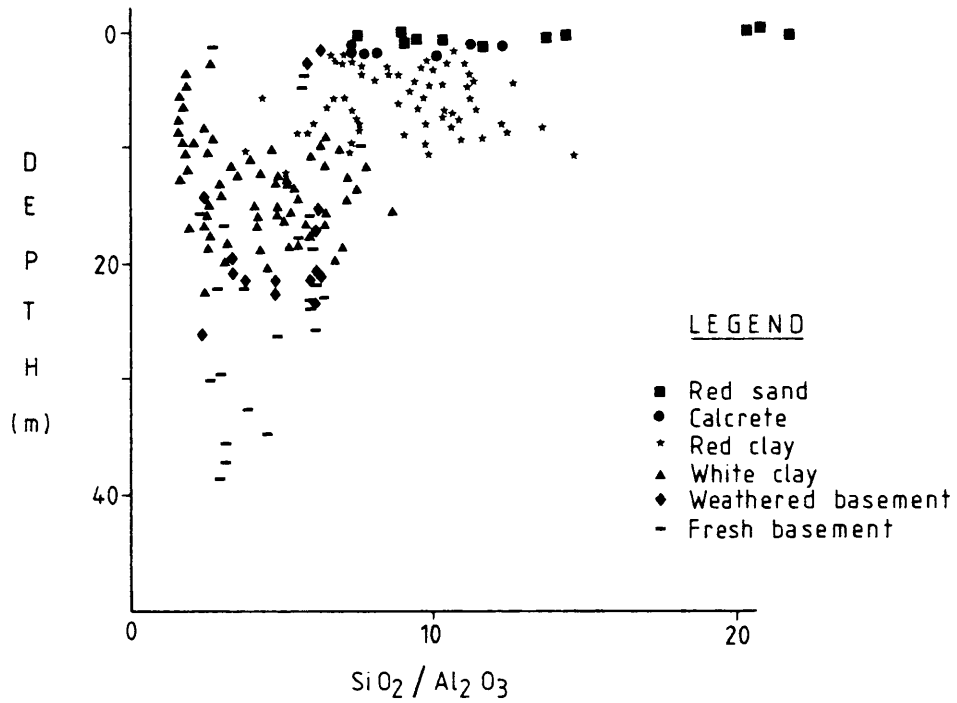

Figure 25 SiO_2/Al_2O_3 ratios in Vaalputs rocks.

elements (Barth, 1962) (Fig. 27), comprises Mn, Ti, Th, Nb, Zr and Hf and Fe.

In the element variation diagrams (Figs. 31 to 54) the concentrations of most elements are generally visibly lower in the red clay when compared to the other rock units, except Ca and trace elements associated with calcrete e.g. Ba, Sr, Pb and Y.

6.3.3 Calcrete

The geochemistry of calcretes in the disposal trenches at Vaalputs was studied by comparing the whole rock composition with that of the soluble (epigenetic) and insoluble (detrital) fractions. These findings were then applied to interpret element migration during the process of calcrete formation and to predict the likely behaviour of radionuclides in an analogous situation.

The analyses of the dissolved portion of the calcrete samples are presented in Table XII together with the mass percentages of dissolved rock. The complete analyses of calcrete whole rock samples and insoluble residues are given in Appendix F. The mass percentages of dissolved rock generally vary between 58,6% and 92,0% with a mean of 82,38% for trench 1 and 74,08% for trench 2. Two silcrete samples, 1T4C and 2T1, have low solubility and during dissolution the latter sample actually showed an unaccountable mass increase, which is probably too high to be within analytical error.

As would be expected, CaO contents of the whole rock samples are proportional to their solubility, but the same relationship does not hold for the CaO contents of the solutions. Calcium contents of six of the whole rock samples exceed the theoretical maximum of 56% CaO for pure $CaCO_3$, indicating that calcium is present in other phases in addition to calcite, probably in plagioclase and accessory phases, e.g. sphene and apatite. It is notable that the dissolved sample with the lowest CaO content (Table XII) also has the highest MgO content, i.e. 6,9%. Magnesium values of the soluble rock average 0,45% for samples from trench 1 and 0,41% for those from

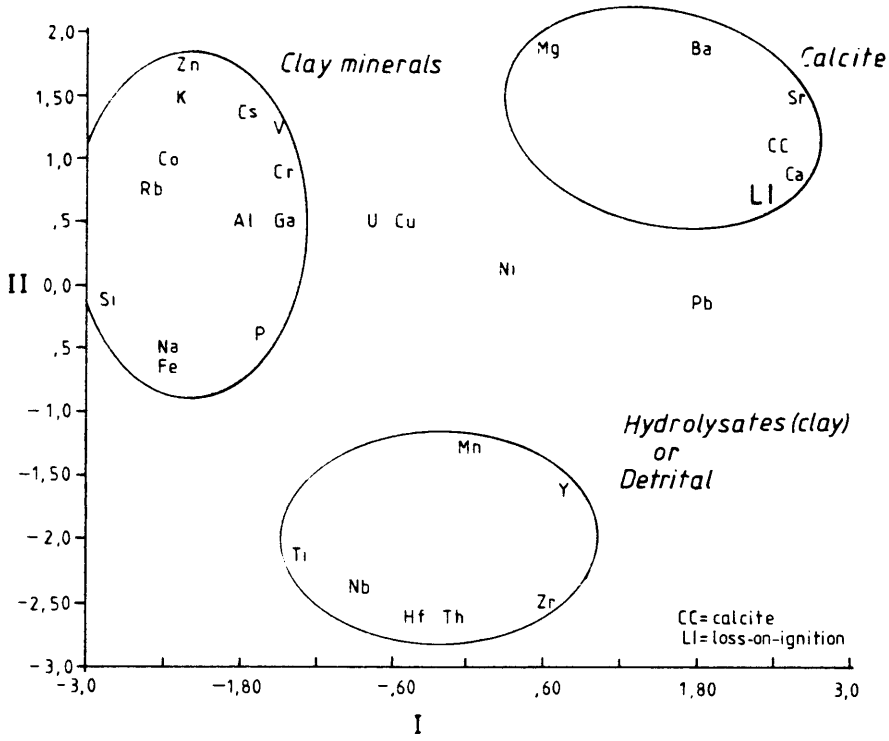

Figure 26 Principal component scores on the plane of the first and second eigen vectors using major and trace elements of red clay in borehole W20N0.

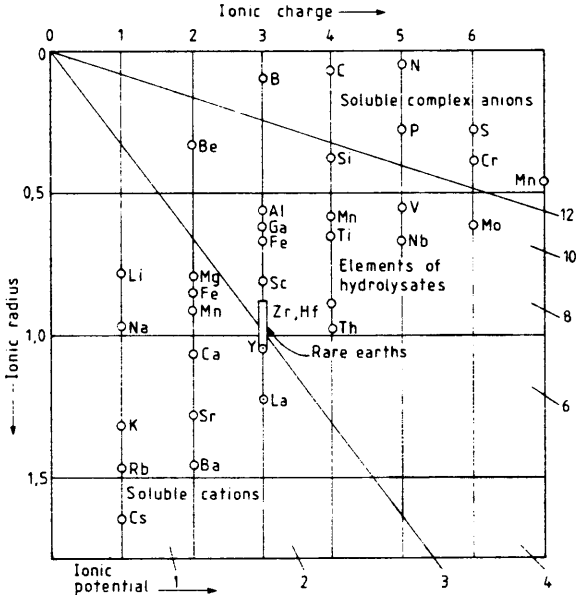

Figure 27 The properties of chemical elements in relation to ionic potentials (Barth,1962).

trench 2, with three very low values in samples 1T3C, 2T2 and 2T3. The Ba contents of the samples are variable, with the samples from trench 2 having significantly higher mean values of Ba (148,69 ppm) than those in trench 2 (68,86 ppm).

Table XII Trace and major element analyses of the soluble fraction of calcrete samples from Vaalputs.

Sample	Co	Cu	Sr	Zr	V	Y	Pb	Ba	MgO	CaO	% DISSOLVED
			mg/l						%		ROCK
1T1	3,68	2,28	93,76	1,05	2,80	2,10	19,10	106,38	,51	52,80	90,7
1T1B	3,44	1,98	95,11	,93	2,38	2,78	21,30	12,70	,68	46,43	90,6
1T2	3,53	2,08	78,04	,96	2,56	2,24	19,71	166,19	,42	54,23	84,2
1T2B	4,83	2,42	83,09	,48	3,86	6,28	,48	40,10	,44	55,80	92,0
1T2C	3,90	2,67	105,13	1,03	2,87	3,49	12,32	49,08	,58	54,33	78,9
1T3	3,59	2,56	111,97	,85	2,74	2,05	21,03	10,77	,46	48,89	84,5
1T3B	3,44	2,29	127,33	,98	2,62	2,13	21,28	31,10	,26	52,79	77,5
1T3C	3,67	2,57	122,55	1,10	2,57	2,20	17,45	180,61	,13	59,68	68,5
1T4	4,46	3,29	110,33	,94	3,99	2,35	7,51	22,30	,38	49,26	73,6
1T4B	3,86	2,31	108,48	,77	2,57	61,70	9,00	20,05	,62	55,03	83,1
1T4C	17,15	5,72	186,75	1,91	5,72	1,91	1,91	118,15	6,90	25,88	10,7
2T1*	,16	,08	1,99	,01	,04	,01	,01	12,41	291,00	,12	-
2T2	4,12	2,83	159,70	,77	3,09	2,83	10,82	126,73	,04	58,42	58,6
2T3	4,05	2,63	149,37	,81	2,63	2,43	16,39	179,53	,05	58,66	68,2
2T4	3,51	2,28	108,79	1,58	3,16	2,11	20,39	243,23	,28	54,03	80,3
2T4B	3,56	2,25	122,28	,94	2,43	2,06	20,41	173,41	,39	55,37	78,4
2T4C	3,29	2,26	103,29	,82	2,47	3,50	11,52	13,99	,71	51,05	83,5
2T4D	4,71	2,55	115,10	,98	2,75	2,35	14,51	242,55	,51	57,24	78,5
2T4E	3,92	2,45	124,80	,74	2,70	4,17	7,85	336,40	,55	52,04	79,8
2T5	3,75	2,68	116,79	1,07	2,50	2,14	20,00	168,39	,18	56,80	63,1
2T5B	3,72	2,60	122,12	,93	2,60	2,04	17,66	82,16	,66	56,18	79,8
2T5C	3,23	2,15	102,79	,90	2,51	1,97	20,09	27,09	,60	50,08	83,7
2T5D	3,87	2,64	117,96	,88	2,64	2,29	22,89	176,06	,33	49,74	65,7
2T6	4,59	3,21	96,87	,46	4,13	2,30	,46	14,69	,57	51,48	69,4
CTRL	4,31	3,02	496,98	1,08	2,59	2,16	12,07	6,47	,16	55,12	92,8

* - Due to the insolubility of the sample the analysis of the solution is given in mg/l.

CTRL - Control sample (pure $CaCO_3$)

Analyses by Atomic Energy Corporation Ltd.

By comparing analyses of the whole rock with those of the insoluble fractions the relative enrichment or depletion of elements in the latter were determined. The elements Si, Al, K, P, Zr, Y and Nd are largely insoluble and are therefore concentrated in the detrital fraction. Other elements which are enriched to some extent in this fraction include Ti, Fe, Mg, Zn, Ga, Rb, Ba and La while elements

with variable enrichment are Mn, Ni, Nb, Pb and V. Elements which are depleted in the detrital fraction include Na, Cu, Sr, Cr, Ce, S and Cl, the latter element with two exceptions. These elements are thought to be either adsorbed by or co-precipitated with $CaCO_3$. Elements such as Co, Ga, U and Th, for which the X-ray fluorescence analyses are generally of low accuracy, show extreme variations. Gallium is to be expected to follow Al in its behaviour, while U and Th are present in resistate minerals such as monazite, zircon, apatite and titaniferous minerals which occur in the calcretes.

Principal components analysis using major and trace element data of the whole rock and insoluble residues of the calcretes reveals some interesting element associations. In the PCA-scores plot on the principal eigen vector plane using data of the whole rock analyses, three well defined groups of elements emerge (Fig. 28). The first comprises Ba, Sr and Cl which correlate to some extent with Ca. The second distinct group consists of the light REE, Y, La and Nd. A third broad group includes SiO_2, K_2O, Na_2O, Al_2O_3, Fe_2O_3, Rb, Zn, Ti, Zr, V, Th, Ni, Cu and P_2O_5 and a host of other elements poorly correlated with the major group, but showing high mutual correlations e.g. Mn and MgO.

The main element group is considered to represent K-feldspar and Fe-oxyhydroxides, which fill interstices between detrital grains in the calcrete and voids in the calcrete. The trace elements are considered to be adsorbed on either the clay material constituting the matrix in the voids, or on Fe-oxides, or contained in accessory minerals such as zircon, sphene, ilmenite or rutile. The association of the light REE with CaO is thought to reflect their presence in apatite, which is known to retain light REE to a large extent (Allegre and Hart, 1978). These element associations also occur in the PCA-scores plot using analytical data of the insoluble residues.

Many of these element associations in the whole rock are shown by PCA to exist also in the detrital fraction (Fig. 29), e.g. Ba, Sr, Cl (now including MgO); SiO_2, K_2O, Rb, Fe_2O_3 and Al_2O_3.

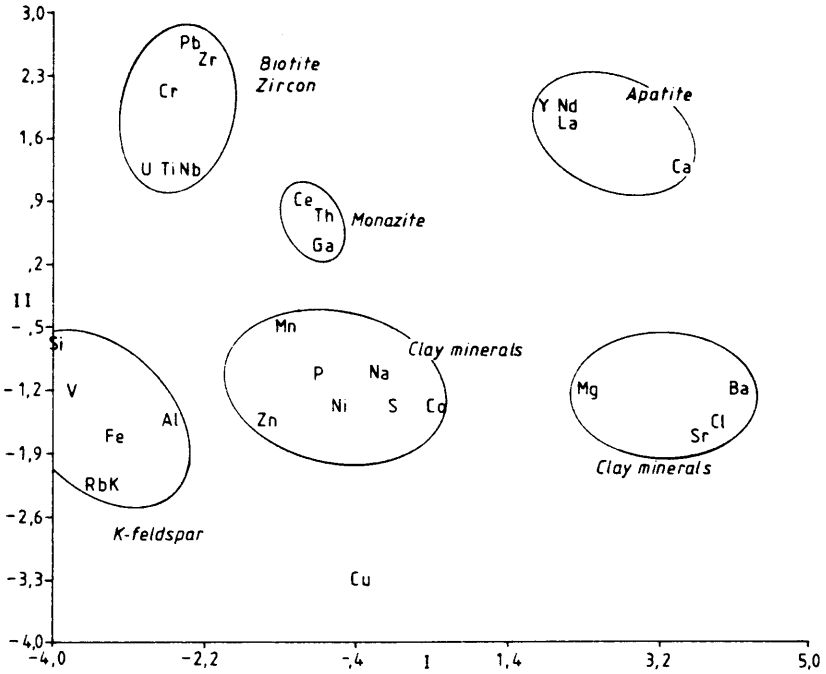

Figure 28 Principal component scores plot on the plane of the first and second eigen vectors using major and trace element data of Vaalputs calcrete whole rock samples.

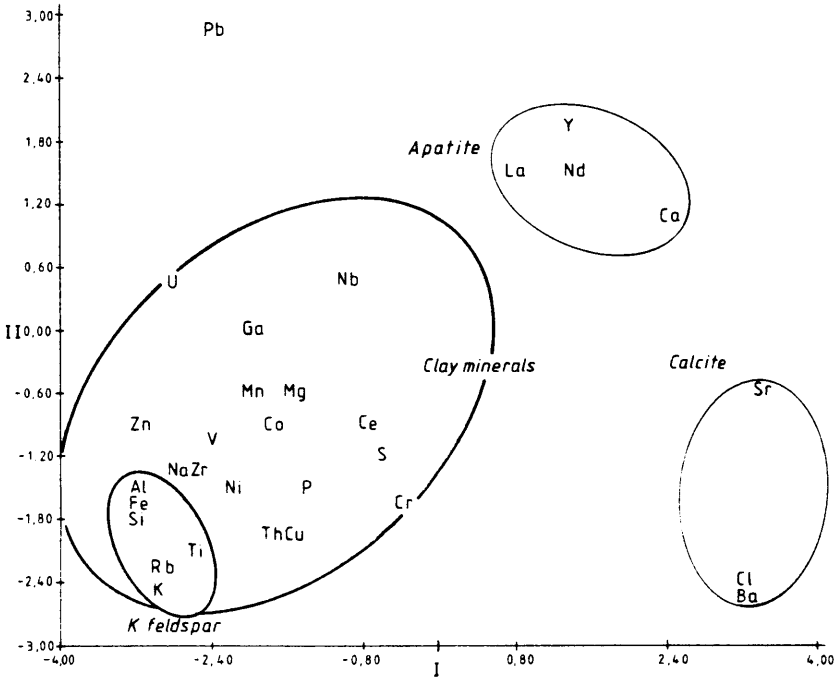

Figure 29 Principal component scores plot on the plane of the first and second eigen vectors using major and trace element data of leached calcrete samples (detrital fraction).

Additional groups emerge comprising Pb, Zr, Cr, U, Ti and Nb, possibly present in zircon and titaniferous phases or associated with biotite; Ce, Th and Ga, probably in monazite and a more diffuse group representing elements probably adsorbed on clay or Mn-oxides, as inferred from their close correlation with the major elements present in these minerals e.g. Mn and Na. The correlation of Ba, Sr and Cl with Ca in the whole rock samples could be attributed to their presence in calcite. Since calcite does not exist in the detrital fraction the persistent mutual correlation of Ba, Sr and Cl and their correlation with magnesium in this fraction could suggest their presence in smectite clay of which Mg can be a major constituent. All the above-mentioned correlations are substantiated by cluster analysis, which quantitatively displays the mutual correlations among elements (Fig. 30).

Scrutiny of Table XII reveals that the silcretes (sample 1T4C and 2T1) contain values of Co, Cu, Sr, Zr, V and Mg higher than the mean of the calcrete samples. Examination of thin sections of the silcretes shows the presence of abundant Fe-rich colloidal material which occurs interstitially between detrital grains or as linings in voids in the calcrete. Many of these constituents are probably adsorbed onto this interstitial colloidal material or onto feldspars and clay minerals or the colloidal silica constituting the matrix.

The occurrence of calcretes at Vaalputs is of importance to the problem of radioactive waste disposal, because it reflects conditions in the geological environment which may have an important bearing on the migration and retardation of radionuclides. Calcium, the major constituent of calcrete, is considered to have been largely derived from weathering of the immediate underlying rocks through vertical movement. During this process other elements with high mobility could have accompanied calcium to be co-precipitated with, or be adsorbed onto the calcrete. Two important elements in this respect are Sr and Ba which have been shown to have a good mutual correlation and also with Cl and Mg in both whole rock and the insoluble residue. The high correlation of Ba and Sr with Cl would suggest them to be present as their respective chlorides, but

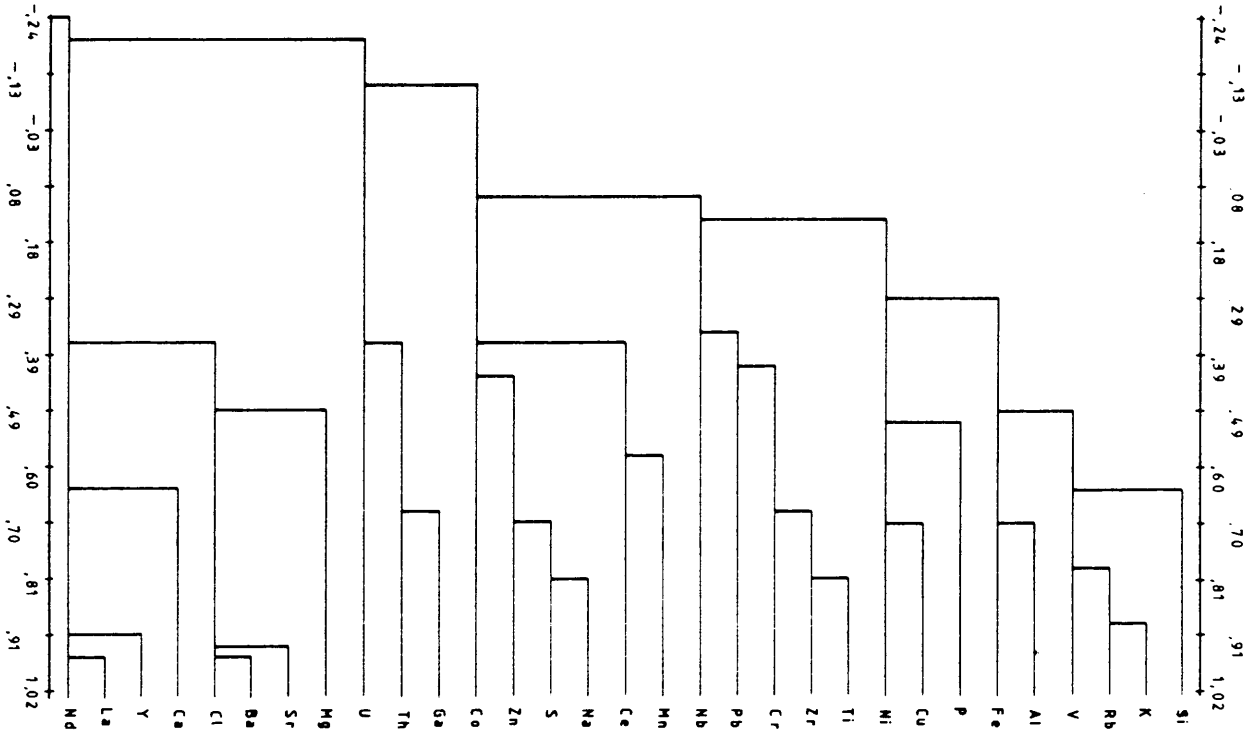

Figure 30 Cluster analysis dendogram showing the mutual correlation groupings of major and trace elements in the insoluble fractions of calcretes from Vaalputs.

Levin (1988) considers their presence as carbonates or sulphates. The latter possibility seems doubtful in view of the low correlation of these elements with sulphur, but the chlorides of Ba and Sr are water soluble (Levinson, 1974), which renders their presence as chlorides improbable. Barium and strontium are therefore considered to have co-precipitated with the calcrete as their respective sulphates or carbonates. Barite is singled out as the most important Ba-bearing mineral in sedimentary rocks and may contain considerable amounts of Sr in solid solution (Dragunov and Katchenkov 1958, quoted by Graf, 1960). Analyses of the insoluble fractions of calcretes indicate that Ba is highly enriched in some samples where it is considered to be adsorbed onto clay minerals or present in feldspars, which abound in the calcrete. Strontium in contrast is present predominantly in the epigenetic fraction. A portion is probably present in plagioclase in the detrital fraction. Strontium, despite being a highly mobile element, is

retained to a large extent in calcretes at Vaalputs.

From the element variation diagrams (Figs. 31 to 54) it is noted that the trace elements associated most frequently with calcrete layers are Ba, Sr, Pb and Y. They may have been co-precipitated with the calcrete, or occur in feldspars or are adsorbed onto clay minerals in the calcrete. Other elements seem to reach peak concentrations in the proximity of calcrete layers e.g. V and Ba and a group comprising K, Rb, Cs, Sr and Zn, which show a consistent mutual correlation in almost all profiles. Their presence near the calcrete could be explained by their preferential adsorption onto clay under alkaline conditions. This alkaline environment preserves feldspars to some extent, due to the paucity of exchanging H^+, which is considered the prime factor in the removal of cations from feldspars during weathering. It has been observed though in thin sections of calcrete that resorption of feldspar by calcite occurs.

The fact that calcite can adsorb elements, particularly barium, magnesium and copper (Morse, 1986), and strontium by either ion-exchange or co-precipitation, and the assumption that these prqcesses are still in progress at Vaalputs, implies that calcrete could constitute an excellent barrier to radionuclides, either when applied as a base to the waste package or in-situ in the trench walls, where it is present in abundance.

In addition, the locally impervious calcrete cappings found near surface would serve to limit the infiltration of water to the subsurface. If a calcrete layer is applied as a capping to the trenches, the dissolution and re-cementing of this calcrete may in time form a partly impervious layer over the trenches to impede the infiltration of rain water. The fact that calcrete appears to be in chemical equilibrium with its environment implies that the intermediate-level waste concrete containers will probably be chemically stable, thus minimising the possibility of leaching of their included waste.

Other elements not discussed so far are present to a varying degree

in the calcretes, but are not considered to be of major importance from a petrogenetic point of view or to have any implications for the waste disposal problem. The major presence of these elements in the detrital fraction is ascribed to the fact that they are either major components of, or adsorbed onto other minerals.

The paucity of silcretes at Vaalputs is compatible with a low rainfall which is favourable for the disposal of radioactive waste. The silcretes are, however, also considered to be good barriers to radionuclide migration. The abundance of elements associated with the two silcrete samples analysed, suggests their adsorption by, or co-precipitation with the silcretes. This probably takes place onto the Fe-rich colloidal material which forms a major constituent of the detrital component. Co-precipitation of elements is also possible in silcretes according to Thiry and Millot (1987) and control the degree of order in opal. Various elements were found by these authors to be present in various forms of silica. e.g. Ti occurs as a fine brown pigment in opal, some forms of which contain abundant aluminium and potassium.

6.3.4 Gordonia Formation

Insufficient samples were available for an interpretation of the element associations in red sand in any particular borehole, but the PCA-scores plot of the collective samples in all boreholes reveals a relationship similar to that in the red clay.

6.4 Element Variation

The variation in chemical composition of bulk samples in various stages of weathering, intersected in twelve percussion boreholes at Vaalputs are presented graphically in Figures 31 to 54. The major and trace element data are presented in Appendices D and E respectively. The upward chemical variation from fresh basement rocks to surficial rocks is discussed in terms of major and trace elements.

6.4.1 Major Elements

Silicon

Silicon expressed as SiO_2, generally decreases upwards in the transition from fresh through weathered basement into the overlying white clay. In some boreholes this decrease seems to follow a smooth trend partially or wholly into the white clay unit, suggesting that at least a portion of the white clay unit represents in-situ weathering of basement rock. In borehole W60N0 (Fig. 33), SiO_2 remains constant upwards and in W20N0 and W40N0 (Figs. 43 and 49) there are distinct breaks in the variation trends of virtually all elements at the boundary between fresh and weathered basement. Towards the top of the white clay unit SiO_2 increases again in boreholes W30S10, W40S10, W60N0, W70S10, W80N0 (Figs. 31,45, 33, 37 and 39) whereas Al_2O_3 decreases. The striking consistent antipathetic variation of SiO_2 and CaO through the entire profile in almost all boreholes is due to a dilution effect as they comprise two of the major chemical constituents. In the red clay unit the SiO_2 content is variable, but it usually increases towards the base of the red clay and in the sand cover it is invariably high.

Silicon is the second most abundant element of the earth's crust (after oxygen) and forms the major constituent of most rock-forming minerals, where it occurs in fourfold co-ordination with oxygen. This co-ordination limits the number of metals which can replace it in crystal lattices and also the number of trace elements which can enter the lattices. In complex silicate lattices some cations can be accommodated (Day, 1963). For these reasons SiO_2 shows few consistent correlations with other elements.

Titanium, iron and manganese

The behaviour of the oxides, TiO_2, Fe_2O_3 (total iron) and MnO is very similar in all the profiles. These oxides may decrease (3 boreholes) or increase (6 boreholes) in passing from fresh

basement through weathered basement into white clay; two other boreholes, W20N0 and W40N0 (Figs. 43 and 49) show no significant variation. In the red clay the trends are variable, but the concentration levels are generally higher than in the underlying rock units. Notable exceptions with respect to Fe_2O_3 and MnO occur in W20N0, W40S10 and W49,8N0 (Figs. 43, 45 and 51) and with respect to TiO_2 in W49,8N0 and W83N0 (Figs. 51 and 47). All three oxides generally form high concentrations at the base of the red clay, probably in heavy minerals marking an unconformity.

Titanium is markedly lithophile in character. It forms a limited number of independent minerals e.g. perovskite, ilmenite and sphene all of which are both igneous minerals and residual minerals in sands (Day 1963). Sphene is also a common deuteric and even an authigenic mineral in sedimentary rocks. Titanium is also a minor constituent in many other rock-forming minerals such as biotite. Sphene and biotite are the most favoured host minerals of titanium in magmatic rocks. Sphene is also a host for Nb, Sr, Pb, Y, U, Th, Al, Fe and the rare earth elements (Goldschmidt, 1958). Much of the Ti in soils seems to be associated with the hydrolysate minerals, probably not as an adsorbed constituent, but as tiny rutile needles (Goldschmidt, 1958).

Titanium occurs in detrital minerals in the surficial rocks of Vaalputs, notably in ilmenite, leucoxene, sphene, anatase and as an exsolution phase in magnetite. In addition it is abundant in biotite as rutile needles in fresh basement rocks.

Iron being typically siderophile, may also be distinctly thiophile or lithophile. The Fe^{2+} ionic radius of 0,86Å (sixfold co-ordination, high spin) is somewhat larger than the Mg^{2+} ion (0,80 Å, sixfold co-ordination) (Whittaker and Muntus, 1970) and diadochy between the two is not uncommon (Day, 1963). The Fe^{2+} ion cannot replace Ca^{2+} in feldspars for thermochemical reasons, but it is possible for Fe^{3+} to replace Al^{3+} in these minerals to a limited extent (Day, 1963). The minerals of iron are numerous and abundant and include primary oxides and sulphide minerals,

primary silicate minerals and secondary oxygen compounds of iron including oxides, hydroxides and oxy-salts other than silicates (Day, 1963).

The most common mode of occurrence of iron at Vaalputs is as ferric-oxide or -hydroxide in the surficial rocks, occurring as a coating on sand grains or finely disseminated in red clay and calcrete, as detrital grains in red clay and possibly as a constituent of the smectite species nontronite. Ferruginous opal also occurs in the above-mentioned rock types. In addition iron occurs in magnetite, gahnite (in granitic and anorthositic rocks), ilmenite and biotite, the latter mineral mostly restricted to the white clay and weathered and fresh basement.

As a transitional element, manganese is well known for its multiplicity of oxidation states, but the ion is probably confined to the two-, three- and four-valent states in nature. It could be classified as a lithophile element with some thiophile tendencies. The element is essentially cationic and Mn^{2+} ions are characteristic of igneous rocks, with the higher oxidation state Mn^{4+} being more characteristic of the sedimentary environment, while Mn^{3+} seems to occur only in a limited number of minerals. The ionic radii of Mn^{2+} (0,75 Å, low spin or 0,91, high spin) are only slightly larger than that of Fe^{2+} (0,69 Å, low spin or 0,86, high spin) (Whittaker and Muntus, 1970) and considerable interchange between these elements can take place. Other elements with similar ionic radii are Ca, Mg and several other metals so that the element is widely present in trace or minor quantities in minerals containing these elements, especially the silicates (Day, 1963).

Apart from occurring with iron in oxides and hydroxides, manganese oxide is visibly present in the Vaalputs rocks as dendritic layers on fracture planes in clay and calcrete. Manganese and zinc show good correlation in some boreholes, which could possibly be ascribed to their presence in spinels particularly gahnite, in which they have been identified with iron as major constituents by means of energy dispersive X-ray analysis.

Aluminium and gallium

These two elements form what is termed a classical pair by virtue of their frequent close association. A discussion of the behaviour of Al_2O_3 therefore generally applies equally well to gallium and only the variation of Al_2O_3 is discussed except where major deviations in their association occur.

In the fresh and weathered basement and often in the white clay, Al_2O_3 generally exhibits a trend antipathetic to that of SiO_2, but exceptions occur as in W70NO and W90NO (Figs. 35 and 41). In the red clay this relationship changes, with Al_2O_3 trends in this unit being less erratic than that of SiO_2. The Al_2O_3 content of the white clay unit is significantly higher than that of the red clay. Generally there is a nett upward decrease in Al_2O_3 in all profiles, which is indicative of increasing upward weathering of the rocks or could also be due to a dilution effect resulting from the abundance of CaO.

In borehole W30NO (Fig. 53/54) a deviation in the behaviour of Ga with respect to Al_2O_3 occurs where the Ga/Al_2O_3 ratio in the red sand is higher (0,11) compared to the mean of 0,03 in the other rock units. Minor deviations in the ratio also occur in the fresh and weathered basement of W30S10 and W40NO (Figs. 31/32 and 49/50) where a higher ratio (0,05 to 0,23) is found when compared to 0,03 in the surficial rock units. The very high ratio of 0,23 is associated with an abundance of magnetite and Zn-rich spinels in W40NO (Fig. 49).

Aluminium is the dominant metal in the Earth's crust and is about one third as abundant as silicon. It occurs widespread due to the fact that Al can exist in both fourfold and sixfold co-ordination. It is therefore able to enter into a great range of silicate structures as well as forming a variety of other oxygen compounds. It is a strongly lithophile element. The ionic radius of Al^{3+} is 0,61 Å for sixfold co-ordination which compares with 0,63 Å (low spin) or 0,73Å (high spin) for Fe^{3+}, 0,70 Å for Cr^{3+} and 0,48 Å

for Si^{4+} (Whittaker and Muntus, 1970). In minerals where Al is in this co-ordination it is usually possible for diadochy to take place, particularly with Fe^{3+} and Cr^{3+}. It is possible for Al to enter into sixfold and fourfold co-ordination and both of these may sometimes exist in the same mineral e.g. muscovite.

Undoubtedly the most important rock forming minerals in which Al occurs are the feldspars with structures in which up to one-half of the tetrahedral positions in the framework are occupied by the element and positive ions are present in sufficient numbers to neutralise the negative charge of the $(Si,Al)O_2$ framework (Day, 1963). In addition it forms a major component of the clay minerals and some spinels and has been detected as a major constituent in grains of iron-oxide or -hydroxide (presumably laterite) and in colloidal coatings around detrital grains in calcrete at Vaalputs.

Gallium differs from aluminium in several notable respects. Ga^{3+} is 17% larger than the Al^{3+} ion if the ionic radii by Whittaker and Muntus (1970) of 0,47 Å for Al^{3+} and 0,55 Å for Ga^{3+} are used. It forms a more covalent bond than Al^{3+} and readily enters sulphide minerals, mainly sphalerite. It is close in size to Fe^{3+} and the Ga-O bond is more ionic than the Fe-O bond. Ga^{3+} should enter Fe^{3+} positions more readily than Al^{3+} positions and should exhibit a close association with Fe^{3+}. Three distinct features may thus be distinguished in the geochemical behaviour of gallium:

Substitution for Al^{3+};
Substitution for Fe^{3+};
Entry into zinc sulphide.

The large amount of Al^{3+}, compared to Fe^{3+}, is usually sufficient to mask the tendency of Ga to be associated with the latter element (Taylor, 1966). Its mode of occurrence at Vaalputs is essentially similar to that of Al. High ratios of Ga to Al correlate well with Fe-content both in the rocks of Vaalputs and the Dasdap Formation sediments.

Magnesium and calcium

Magnesium-oxide like calcium-oxide, almost invariably shows an upward increase through all rock units to form local concentrations in calcrete layers or calcretised sand and clay. The levels of MgO are much lower than those of CaO. The upper calcrete layers usually have a higher CaO content when compared to the lower layers. Deviations in this close relationship occur in most boreholes. Magnesium is thought to be co-precipitated with calcium as dolomite, which was identified in cracks in the calcrete. Peak concentrations of MgO not associated with CaO are thought to represent the presence of smectite clay, of which MgO is an important constituent. In addition to the above-mentioned modes of occurrence magnesium has been detected by X-ray energy dispersive analysis in iron-oxide and -hydroxide minerals in the Vaalputs rocks.

Magnesium is the least abundant of the major rock forming elements. It is characteristically the cation which goes into the chain-silicate minerals e.g. pyroxenes, but is also present in granitic rocks mainly in biotite. The large difference in radii for sixfold co-ordination of Mg^{2+} (0,80 Å) and Ca^{2+} (1,08 Å) (Whittaker and Muntus, 1970) is unfavourable for diadochy, as in dolomite where Mg and Ca are alternately substituted in the calcite lattice. The readily hydrated Mg-ion, like Na, becomes too large for adsorption on soil colloids and is therefore easily lost in solutions, in contrast to the less easily hydrated K ion which is readily adsorbed (Day, 1963).

Calcium as a rock-forming element tends to be concentrated in the basic and intermediate types of igneous rocks for several reasons:

It forms the plagioclase feldspar, anorthite, which readily forms an isomorphous series with the Na-feldspar, albite.

Calcium readily enters into certain ino-silicate structures together with Mg^{2+} and Fe^{2+}, characteristic of basic and intermediate rocks.

Residual calcium in a magma is often taken into accessory minerals e.g. apatite, monazite, sphene and calcite.

The ubiquity of Ca ions in igneous rocks is due largely to their ionic radius (1,08 Å, sixfold co-ordination) for which a large number of other ions of similar co-ordination can deputise e.g. Na^{+}, (1,10 Å); Mn^{2+},(0,91 Å, high spin); Sm^{3+},(1,04 Å); Sr^{2+}, (1,33 Å, eightfold co-ordination) and the lanthanides e.g. Lu^{3+},(0,94 Å) (Whittaker and Muntus, 1970). Barium (1,50 Å), however, does not easily proxy for calcium (Day, 1963).

In addition to being the major constituent of the calcrete layers, Ca is present in the Vaalputs rocks in all of the above-mentioned modes and also as a minor constituent of zircon, as shown by energy dispersive analysis.

Sodium and potassium

Sodium-oxide, like potassium-oxide, shows a general upward decrease through all rock units, the former, except in borehole W30S10, almost invariably so, but K_2O, being more effectively retained locally by clay minerals, occasionally increases slightly upwards in the profile of W40N0, W49,8N0, W83N0 (Figs. 49, 51 and 47).

Sodium is present in the earth's crust in mainly three modes:

In a limited number of complex aluminohalide minerals;

In a large number of complex silicate minerals;

In a considerable variety of soluble, simple and complex salts mainly in evaporite deposits.

The sodium ion Na^{+} (1,24 Å, eightfold co-ordination) differs markedly from K^{+} (1,59 Å) (Whittaker and Muntus, 1970) and is less frequently associated with K^{+} in rocks than would be expected. The ion is much nearer in size to Ca^{2+} (1,20 Å, eightfold co-ordination) with which it is more frequently associated in

silicate minerals. Furthermore they are nearly equally abundant in the crust and are often met with in solid solution series of isomorphous minerals e.g. the plagioclase feldspars and clino-pyroxenes. Among the secondary minerals containing Na, the zeolites are the most important. Few micas, however, contain Na while K is more abundant. Many typical sedimentary rock forming minerals are devoid of Na because it readily passes into solution during weathering and there is no natural process by which it can be rendered insoluble and immobilised (Day, 1963). Most of the sodium in the Vaalputs rocks occurs in feldspars, smectite clay and halite in the surficial rocks.

Potassium stands between sodium and magnesium on the rank of abundance in the Earth's crust, and the mode of occurrence of its compounds is rather similar to those of sodium. The elements do tend to separate from each other for several reasons, largely related to their difference in ionic radius, ease of hydration in solution, which in turn determines their degree of adsorption on colloids, and the relative solubility of the different salts. The K-bearing minerals, like those of Na, fall into the three classes of complex halides, silicates and soluble salts in evaporites. The most important of the silicate minerals are the K-feldspars, the micas and clays, all of which occur in the Vaalputs rocks.

During weathering of igneous rocks, K initially passes into solution, where the relative ease of release of K depends on the mineral. Biotite and leucite are rather easily decomposed whereas K-feldspar is more resistant. The K-ion, being less easily hydrated, is readily adsorbed onto colloids and micas and the element is readily retained on clay minerals (Day, 1963).

Phosphorus

Phosphorus, analysed as P_2O_5, remains fairly constant in concentration throughout all Vaalputs profiles, and does not show a consistent correlation with any other element.

The oxygen-rich conditions of the earth's crust lead to the

exclusive existence of phosphorus as the PO_4-ion, which on account of the stability of its tetrahedral structure presents analogies with the SiO_4-ion. Silica is in fact substituted for by phosphorus. This only seems to happen among the orthosilicates such as zircon. Phosphorus can be regarded as a lithophile and an oxyphile element. As much as 95% of the phosphorus in the Earth's crust is contained in minerals of the apatite group, which constitute common accessory minerals in granite. Other important minerals are xenotime and monazite (Day, 1963). In addition to the above-mentioned modes of occurrence, phosphorus has also been detected in iron-oxides and -hydroxides in the red clay and calcrete of Vaalputs.

6.4.2 Trace Elements

Rubidium

The variation of Rb, due to its chemical behaviour similar to K, follows this element most closely in all the profiles through all rock units. Minor deviations from this rule are to be found in W60N0 (Fig. 51/52) where in the white clay unit, Rb decreases much more rapidly upward than K_2O. In W49,8N0 a peak concentration of K_2O in the calcrete (upper red clay sample) is not accompanied by a corresponding rise in Rb concentration. At the boundary between white and red clay in W30N0 (Fig. 53/54) the elements show opposite trends.

This element is usually present at levels from ten to several hundred parts per million in acid igneous rocks. The ionic radii, electro-negativities and ionisation potentials of potassium and rubidium are very similar, although Rb enters the K positions in micas such as biotite in preference to those in feldspars. The bulk of Rb in rocks is, however, contained in the K-feldspars, due to their predominance over biotite. It is of interest to note that the albite lattice can accommodate excess Rb and Cs relative to K (Taylor, 1966). Due to its intimate relationship with potassium, the mode of occurrence of rubidium at Vaalputs is similar to that of potassium.

Cesium

The behaviour of Cs is variable and seems to depend to a great deal on the degree of weathering of the rocks. In the fresh basement it most often correlates well with Rb and K and to some extent with Ba. This is particularly evident in boreholes W30N0 and W30S10 (Figs. 53/54 and 31/32). The best correlation is with Rb in all rock units, however, an exception is found in W70S10 (Fig. 37/38) where the upward trend of Cs is opposite to that of Rb and K_2O in passing from fresh basement to white clay, in which case a moderate correlation with Fe_2O_3 and Nb is evident. This is possibly due to its presence in biotite rather than in K-feldspar. In fresh noritic basement of W49,8N0 (Fig. 52) cesium concentrations are up to an order of magnitude higher than the mean contents of regional basement rocks. Here Cs clearly correlates well with a host of elements including Rb, Zr, Hf, Cr, Th, Ni, Cu, Zn and to a lesser extent Nb and Ba, some of which are constituents of biotite which is present in very high concentrations in some samples of noritoid rocks. There is a definite upward increase in Cs concentration in most boreholes and a correlation with illite and kaolinite contents seems evident, especially in boreholes W70N0, W60N0 and W40N0 (Figs. 35/36, 33/34 and 49/50). Although the latter mineral has a low cation-exchange capacity it is known that it can adsorb Cs to some extent (Nesbitt et al., 1980). High Cs concentrations are also found in W20N0 and W40N0 (Figs. 43/44 and 49/50) where it is associated with other elements such as Fe, Ca, Y, Zr, Hf, V, Th, Ni, Cu, Zn and Pb at the base of the white clay layer where abundant magnetite and other heavy minerals are present.

Cs is so much rarer than Rb, yet on account of its large ionic radius (1,96 Å) it tends to concentrate in the residual liquids of magmatic crystallisation and is able to form the distinct mineral pollucite, $(Cs,Na)AlSi_2O_6.nH_2O$ (where $n<1$) (Day, 1963). It is the largest of all cations and can substitute only for K among the major elements, but being very much larger than K it substitutes for this element with difficulty. In common with Rb, Cs enters the twelvefold co-ordination positions in micas in preference to the

smaller site in feldspars (Taylor, 1966).

In addition to being present in K-feldspars and biotite, Cs is adsorbed onto clay minerals and also secondary iron-oxides and -hydroxides at Vaalputs.

Barium

The behaviour of Ba, like that of Cs, is very variable. It is the most abundant trace element and attains high levels of concentration especially in boreholes W20N0 and W40N0 (Figs. 44 and 50). In many boreholes notably W20N0, W30N0, W60N0 and W90N0 (Figs. 43/44, 53/54, 33/34 and 41/42) the element shows moderate correlation with Ca throughout the profile, but mostly with calcrete in boreholes W70S10 and W80N0 (Figs. 37/38 and 39/40). Only in a few instances a correlation with K is evident e.g. W83N0 (fig. 47/48) and in the lower rock units of W30S10 (Fig. 31/32). Although a good correlation of Ba with Sr is evident in most boreholes, an exception is found in W49,8N0 (Fig. 52) where the Ba trend is opposite to that of Sr. Extreme values of Ba are found in upper portions of the weathered basement of boreholes W40N0 and W20N0 (Figs. 50 and 44).

The geochemical behaviour of Ba is comparatively simple since it substitutes for K^+ among the common cations. Ba^{2+} is nearly identical in size to K^+ but the Ba-O bond is somewhat more covalent in character. According to data of Nockolds and Mitchell (1948, quoted by Taylor, 1966) it enters K-feldspar more readily than biotites, the concentration ratio being about two. This is possibly due to the difficulty of charge balance, where adjustment is necessary in two independent silicate sheets linked by the planes of K^+ ions. Rb and Cs show the reverse behaviour, partly due to their large size, as well as to the single charge (Taylor, 1966).

Barium is predominantly lithophile in character. The difference in ionic radius between Ca and Ba is such that Ba does not commonly enter into Ca-minerals and is less likely to enter Mg-minerals. The Ba-ion extends its resemblance to K also in its ability to be

adsorbed by colloids, hence Ba-ions are fairly readily retained by soils or are precipitated with hydrolysates such as hydrated manganese-oxides (Day, 1963).

Barium has been found, in addition to the above-mentioned modes, to be present as barite in iron-oxides and -hydroxides. It may be present as barium sulphate or carbonate in calcretes of Vaalputs.

Strontium

Strontium exhibits a dual behaviour in most profiles. In those boreholes of which the basement consists of basic rocks e.g. W40N0, W40S10, W49,8N0 and W83N0 (Figs. 50, 46, 52 and 48), and in W20N0 (Fig. 44) of tonalitic composition, the Sr content of the basement and white clay is high, decreasing rapidly upwards. Although the Sr levels in the red clay unit in these boreholes are higher than in the remainder of the boreholes, the correlation of Sr with Ba and Ca is not readily visible in the profiles, however, PCA shows a good correlation to exist. In the remainder of boreholes where the basement consists of granitic or gneissic rocks, the Sr content remains constant upwards or may increase and then usually correlates well with Ba and Ca.

The peculiarities of the geochemistry of Sr is related to its ionic size compared to those of Ca, Ba and K, their ionic radii for eightfold co-ordination being: Ca^{2+}, (1,20 Å); Sr^{2+}, (1,83 Å); K^{+}, (1,59 Å) and Ba^{2+}, (1,50 Å) (Whittaker and Muntus, 1970). Due to its ionic radius being similar to those of Ca^{2+} and Ba^{2+} there is an equal tendency for Sr-ions to enter Ca-minerals or Ba-minerals, but on account of the greater abundance of the former, Sr is more often found in small amounts in Ca-minerals. Barium, however, even though it has a larger ionic radius than strontium, replaces potassium more readily than the latter. Generally Sr is frequently found in Ca-minerals of the alkalic and basic types of igneous rocks, but to a lesser extent in the silicates of granitic rocks. There is a marked deficiency of Sr in the complex silicates containing Ca, Mg and Fe^{2+} and it is only rarely found in

K-feldspars (Day, 1963). The reason for the paucity of Sr in these silicates is the fact that Ca^{2+} enters into sixfold co-ordination with oxygen, whereas Sr^{2+} enters into eightfold or tenfold co-ordination (Taylor, 1966). However, it appears that calcite is one of the few minerals where Ca occurs in sixfold co-ordination. The available data for co-existing K-feldspar and plagioclase indicate that Sr enters K positions more readily than Ca and the Sr/Ca ratio is about ten times as great in K-feldspar as in co-existing plagioclase. Strontium does not enter micas (except margarite) to a great extent, in which, due to its small ionic radius it occupies twelvefold co-ordination with difficulty. Lead, with nearly the same size as strontium shows analogous behaviour (Taylor, 1966).

The above-mentioned modes of occurrence are thought to apply to Sr in the rocks at Vaalputs, where it is probably also present as the sulphate in calcretes and adsorbed onto clay minerals.

Yttrium

In almost all the profiles where fresh basement is present, yttrium shows an increasing trend from fresh basement through weathered basement and partially into the white clay, where the maximum concentration is usually towards the middle or top of the unit. From this maximum upwards the trend is a decreasing one into the red clay, calcrete and red sand. There is one exception where Y decreases significantly towards the middle of the white clay i.e. W40N0 (Fig. 50). In W60N0 and W90N0 (Figs. 34 and 42) the trend from fresh basement through weathered basement to white clay is opposite to the above-mentioned trend. In the proximity of calcrete layers the Y content is slightly higher e.g. W60N0 (Fig. 33/34).

Yttrium is a member of the rare earth element group, of which the whole family is characteristically lithophile and occurs in accessory minerals of granitic rocks such as apatite, xenotime and sphene which are also detrital minerals in sands (Day 1963). Y^{3+} is closest in size to Ca^{2+} among the major cations and could be

expected to substitute for Ca in early crystallising magmatic minerals. However, it concentrates in later apatite and titanite due to the more covalent character of the Y-O bond compared to the Ca-O bond (Taylor, 1966). The Y-Eb group predominate in certain minerals such as xenotime. There is some degree of camouflage of the lanthanide ions in alkaline earth minerals and in some lead minerals (Day, 1963). The silicate allanite, an accessory mineral in some Vaalputs basement rocks, may contain trivalent rare earths replacing Ca.

On account of the general tendency for the rare earths to separate in the later stages of crystallisation, particularly in pegmatites, they are quite often associated with elements like Th, U, Nb and Ta (Day, 1963). During the process of weathering, soil formation and sedimentation all the rare earth elements, including Y, are assembled in the hydrolysate minerals e.g. the various clay and shale components, the bauxite minerals and the oxidates of Fe and Mn (Goldschmidt, 1958).

Zirconium and Hafnium

Zirconium and hafnium are closely associated elements, the Zr/Hf ratio being about 55 (Taylor, 1966). The elements generally increase in concentration from fresh basement through weathered basement to white clay where a maximum usually occurs. In boreholes W83N0, W90N0 and W49,8N0 (Figs. 48, 42 and 52) there is a decreasing upward trend within these rock units. From the white clay unit the trend is generally decreasing towards the base of the red clay where a high concentration occurs in most boreholes. From the red clay upwards the contents of these elements decreases again. In two boreholes i.e. W20N0 and W40N0 (Figs. 44 and 50) anomalous concentrations occur at or near the boundary between weathered basement and fresh basement where zircon is abundant. The only exception to the generally high correlation between Hf and Zr occurs at the base of the red clay unit in borehole W70N0 (Fig. 36). This may be due to analytical error.

Zirconium and hafnium exhibit marked lithophile and oxyphile characters and all of their natural compounds appear to contain oxygen. They occur as accessory minerals in igneous rocks. Zircon, the usual mineral of these elements in granite, is highly resistant to weathering and consequently concentrates as a heavy mineral in the weathering products of granite, in which it shows greatest abundance (Day 1963). It can accommodate a substantial Hf content. With the exception of Fe^{2+}, no common cation is close in size to Zr^{4+}. Tetravalent hafnium and zirconium may be expected to substitute to some extent for Ti^{4+} and hence they accompany this element in substituting for Fe^{2+} (Taylor, 1966).

Most of the Zr in the Vaalputs rocks is thought to occur in the mineral zircon, but some Zr derived from the dissolution of zircon is probably present in hydrolysate minerals in the surficial rocks.

Vanadium

Vanadium generally increases upward in all boreholes with peak concentrations in the red clay unit, often near the top, close to calcrete layers. Occasional high concentrations also occur in the white clay unit and anomalous concentrations occur at the boundary between fresh and weathered basement in W20N0 and W40N0 (Fig. 44 and 50).

The element occurs principally as V^{3+} (0,72 Å) and should substitute for Fe^{3+} (0,73 Å, sixfold co-ordination) in late crystallising magmatic minerals or Fe^{2+} in early crystallising minerals. Vanadium is both lithophile and biophile and exists in at least three oxidation states, V^{3+}, V^{4+} and V^{5+} and it shows a tendency to form complexes with oxygen and sometimes sulphur. To a limited extent the vanadium in igneous rocks may occur as the VO_4^{3-}-ion as a replacement in silicate minerals. Vanadium is more commonly present in magmatic rocks as V^{3+}, often associated with Fe^{3+} in magmatic iron ores, e.g. magnetite. Vanadium is readily oxidised to the five-valent state (V^{5+}) in the weathering cycle and even perhaps in the late magmatic stages. Trivalent

vanadium, like Fe^{3+} and Cr^{3+}, is relatively immobile due to precipitation as the very sparingly soluble hydroxide even at rather low pH values, whereas soluble vanadates $(VO_4)^{3+}$ are very mobile over a wide range of acidity or alkalinity (Goldschmidt, 1958). Local precipitation of soluble vanadate ions is frequently caused by hydroxides of aluminium or of ferric iron. Another mode of occurrence of vanadium is in the uraniferous mineral carnotite, which has been identified at Vaalputs, but is rare.

Vanadium has been identified by X-ray energy dispersive analysis in magnetite and in iron-oxides and -hydroxides at Vaalputs.

Lead

Lead generally exhibits an upward decreasing trend from fresh through weathered basement with very low concentrations in the red clay. Towards the top of the red clay, below and within calcrete layers lead tends to show peak values. In W20N0 (Fig. 44) these peaks do not seem to coincide with calcareous layers. In borehole W90N0 (Fig. 42) lead shows an upward increasing trend.

Divalent lead, Pb^{2} with an ionic radius of 1,37 Å, is closely associated with Sr^{2+} with a similar ionic radius (1,33 Å) (Whittaker and Muntus, 1970). It is intermediate in size between Ca^{2+} and K^{+} and may thus be expected to substitute for K in feldspars and micas, and for Ca in plagioclase. Apatite and other minerals containing large lattice sites should be particularly favoured hosts (Taylor 1966).

Lead ores are commonly associated with zinc, but in weathering processes they become separated to a large extent. In soils, Pb-ions can be adsorbed onto clay minerals in the same way as K-ions (Day, 1965). In addition to being present in K-feldspars this is considered to be the main mode of occurrence of Pb in the Vaalputs rocks.

Niobium

Although the behaviour of niobium is somewhat variable, the common characteristic in virtually all the boreholes is a high concentration in the red clay. The general tendency is an increase in Nb from fresh to weathered basement into the white clay, occasionally with maximum values near the middle of the white clay and decreasing upwards towards the white clay - red clay boundary. Three exceptions to the above-mentioned trends are found in W90N0, W49,8N0 and W60N0 (Figs. 42, 52 and 34) where there is a decrease upwards from fresh basement, through weathered basement into white clay. The only borehole where the red clay is depleted relative to the other units is W30S10 (Fig. 32). In W40N0 (Fig. 50) an anomalously high Nb content occurs at the top of the fresh basement.

Pentavalent niobium, Nb^{5+} and its associated element Ta^{5+} may substitute for Ti^{4+}, Sn^{4+}, Zr^{4+}, Mo^{6+} and W^{6+} on the basis of their similar ionic radii. The bulk of the Nb and Ta in granites is present in biotites and the Nb/Ta ratio decreases in the sequence biotite, ilmenite and zircon (Taylor, 1966). Niobium and tantalum do not easily substitute for elements in silicate minerals, probably due to the difficulty to fit a pentavalent ion into these structures (Day, 1963).

During weathering a small fraction of Nb remains in resistant minerals such as cassiterite, rutile etc. and as such is arrested in residual sediments. Most of the Nb is precipitated with hydrolysate sediments, such as clays along with most of the Ti and Zr (Goldschmidt, 1958) and this is also considered to be its mode of occurrence in the surficial rocks of Vaalputs.

Chromium

In the westerly located boreholes W49,8N0 to W90N0 and W30S10 (Figs. 52, 42 and 32) on Vaalputs, the Cr content shows a consistent upward increase from fresh through weathered basement into white clay and red clay. In borehole W70N0 (Fig. 36) there is a peak concentration

in the calcrete while in W70S10 (Fig. 38) it is relatively depleted. In W80N0 (Fig. 40) the red sand has a high Cr concentration. The most easterly boreholes W40N0 to W20N0 (Figs. 50 and 44), except W30S10 (Fig. 32), show a decrease in Cr content upwards. These boreholes also have high chromium values in the weathered basement.

The most important concentrations of chromium occur in oxide minerals of a refractory character with rather high density such as chromite. Owing to their similarity in ionic size, some replacement of Fe^{3+}- and Al^{3+}-ions by Cr^{3+} can occur and Cr is therefore found in small amounts in a number of common silicate minerals (Day 1963).

The oxidation state and the behaviour of chromium during weathering and subsequent soil and sediment formation is not known with certainty. It is probable that the element passes into solution and in the Cr^{3+} valency state it is probably not very mobile. There is a certain amount of concentration of Cr^{3+} in hydrolysate sediments, particularly those containing alumina, but not to any extent in oxidate sediments e.g. iron ores (Day 1963).

It is probable that the bulk of Cr in the sedimentary sequence occurs in the common hydrolysate sediments (Goldschmidt, 1958) and this is also believed to be the case at Vaalputs. Chromium was, however, detected by means of energy dispersive X-ray analysis in exsolution lamellae in titaniferous magnetite and as minute chromite grains in Koperberg Suite rocks in borehole W20N0.

Thorium and uranium

Thorium shows a somewhat variable behaviour in all boreholes, but some general characteristics can be derived. The Th concentration is almost invariably highest in the fresh basement and decreases upward through the entire succession. Occasional slight peaks occur near the top of the red clay. An anomalously high value is found e.g. in W40N0 (Fig. 50). In three boreholes W40S10, W70N0 and W83N0

(Figs. 46, 36 and 48) the trend is increasing upward from fresh basement, through weathered basement into the white clay, where it reaches a peak value and then decreases upward. Where higher values occur these are almost invariably in the lower rock units, either fresh or weathered basement or white clay, with a decreasing trend upwards. Both Th and U are abundant in heavy minerals of which zircon, monazite and sphene are the most important U- and Th-bearing phases and they account for much of these elements in the rocks. Anomalous U values occur in W20N0 and W40N0 (Figs. 44 and 50) in the weathered basement and white clay, where a correlation with high smectite and illite contents is evident.

The tetravalent cations U^{4+} and Th^{4+} occur closely associated in igneous rocks due to their similar ionic radii of 1,08 Å and 1,12 Å respectively (Whittaker and Muntus, 1970). They commonly occur in accessory minerals such as zircon, monazite, sphene, apatite and allanite (Ahrens, 1965). Although the behaviour of U and Th is very similar in igneous rocks rocks, this is certainly not valid in the sedimentary environment where U^{4+} is readily oxidised to U^{6+} which is highly soluble and mobile as $(UO_2)^{2+}$. Thorium is not oxidised and remains immobile (Taylor, 1966), which is evident in the variation profiles of Th. Six of the twelve boreholes show a depletion of U, where the values are probably below the detection limit of X-ray fluorescence analysis. Thorium and uranium hardly ever show corresponding high concentrations.

Copper

Copper is present at levels much higher than nickel in virtually all the boreholes. Apart from this, the tendency for Cu is to increase from fresh through weathered basement into the white clay and even into the red clay in six of the boreholes. In the other six boreholes the red clay is depleted in Cu relative to the underlying rocks. The two boreholes W70N0 and W70S10 (Figs. 36 and 38) show slight enrichments of Cu in the calcrete. The noritic basement in W49,8N0 (Fig. 52) contains much higher Cu values than granitic basement in the same borehole.

Copper is characteristically chalcophile, the largest concentrations of the element are in the form of various sulphur compounds, but many other stable forms occur (Day 1963). Cu^{2+} is closer in size to Fe^{2+} among the major elements, but Cu^{+} is similar in size to Na^{+}. Cu^{+} will enter plagioclase and apatite, substituting for Na^{+} and Ca^{2+}, and will enter minerals containing Fe^{2+}. Copper may thus be expected in most of the common rock forming minerals (Taylor, 1966). Being a transition element its geochemical behaviour, like that of nickel, is strongly influenced by crystal-field effects.

Nickel

Nickel generally occurs in low concentrations except in two boreholes where values of up to 100 ppm are found. In five boreholes the element could not be detected. Where high values occur, the tendency for Ni is to increase from fresh basement, through weathered basement to white clay, and then to decrease upwards. In the red clay the element is almost invariably depleted, an exception being in W80N0 (Fig. 40) where slightly higher values occur (≃3 ppm), than in the underlying rock units.

Nickel is normally siderophile in character like iron and cobalt. It is probably mostly contained in accessory sulphide minerals. In weathering processes Ni^{2+} is generally stable. Its mobility depends on the associated anions; it is soluble as $NiSO_4$, but insoluble as $Ni_3As_2O_8.8H_2O$ (annabergite). It is largely retained in hydrous silicate minerals analogous to serpentine, chlorite and smectite (Day 1963).

Cobalt

Cobalt increases in concentration upwards in the profiles from fresh through weathered basement to white clay, where it peaks towards the top of the unit and then rapidly decreases in the red clay and red sand units. Three exceptions to this general behaviour occur e.g. in W60N0 and W80N0 (Figs. 34 and 40) where Co is depleted in the

lower rock units, but peaks in the red clay and in the latter borehole also in the red sand. In W70N0 (Fig. 36) there is an overall upward increase in Co values with a peak in the calcrete. Cobalt has a siderophile character and does not easily constitute the major component of minerals except in sulphides and arsenides. It has little tendency to enter silicate lattices but on account of similar atomic and ionic radius to iron it is fairly commonly present as a camouflaged element in sulphide minerals. Most of the natural compounds of Co exhibit the lower oxidation state Co^{2+}, but a few oxide minerals seem to contain the Co^{3+}-ion. The much higher potential (1,84 V) required to effect this oxidation, when compared to iron, explains the paucity of natural cobaltic compounds (Day 1963).

Zinc

Zinc shows a somewhat variable behaviour in the various profiles. In five boreholes containing fresh basement, the tendency is to increase from fresh basement through weathered basement into the white clay in boreholes W40S10, W49,8N0, W70S10, W80N0, W83N0, (Figs. 46, 52, 38, 40 and 48). In six other boreholes the upward trend is decreasing. In the one borehole in which neither fresh nor weathered basement was sampled, Zn decreases upward from the base of the red clay to the red sand. Anomalous Zn values occur in the weathered basement of W20N0 and W40N0 (Figs. 44 and 50) and also in fresh basement of the latter borehole where it is present in Zn-rich spinel. Peaks of Zn concentration also occur in the calcrete in most of the boreholes. In some of the boreholes showing an upward decreasing trend in the lower rock units, Zn increases in the red clay towards the top e.g. W30S10, W40S10, W60N0 (Figs. 32, 46 and 34).

In the upper parts of the crust Zn shows some lithophile character (Day, 1963). It commonly occurs in four- to sixfold co-ordination in its minerals, consequently there is doubt about the amount of Zn which actually enters the silicate mineral lattices. Tauson and Kravchenko (1956) found that Zn apparently entered biotites in

preference to other minerals in granites and to a lesser extent in feldspars (Taylor, 1966).

In the weathering process Zn would pass into solution and would subsequently be precipitated in various forms such as carbonates, silicates, phosphates etc. (Goldschmidt, 1958). It is not unlikely that Zn in soils is bound by ion-exchange to the hydromicas and smectite even more strongly than K, with the same ionic size (Goldschmidt, 1958, Day, 1963).

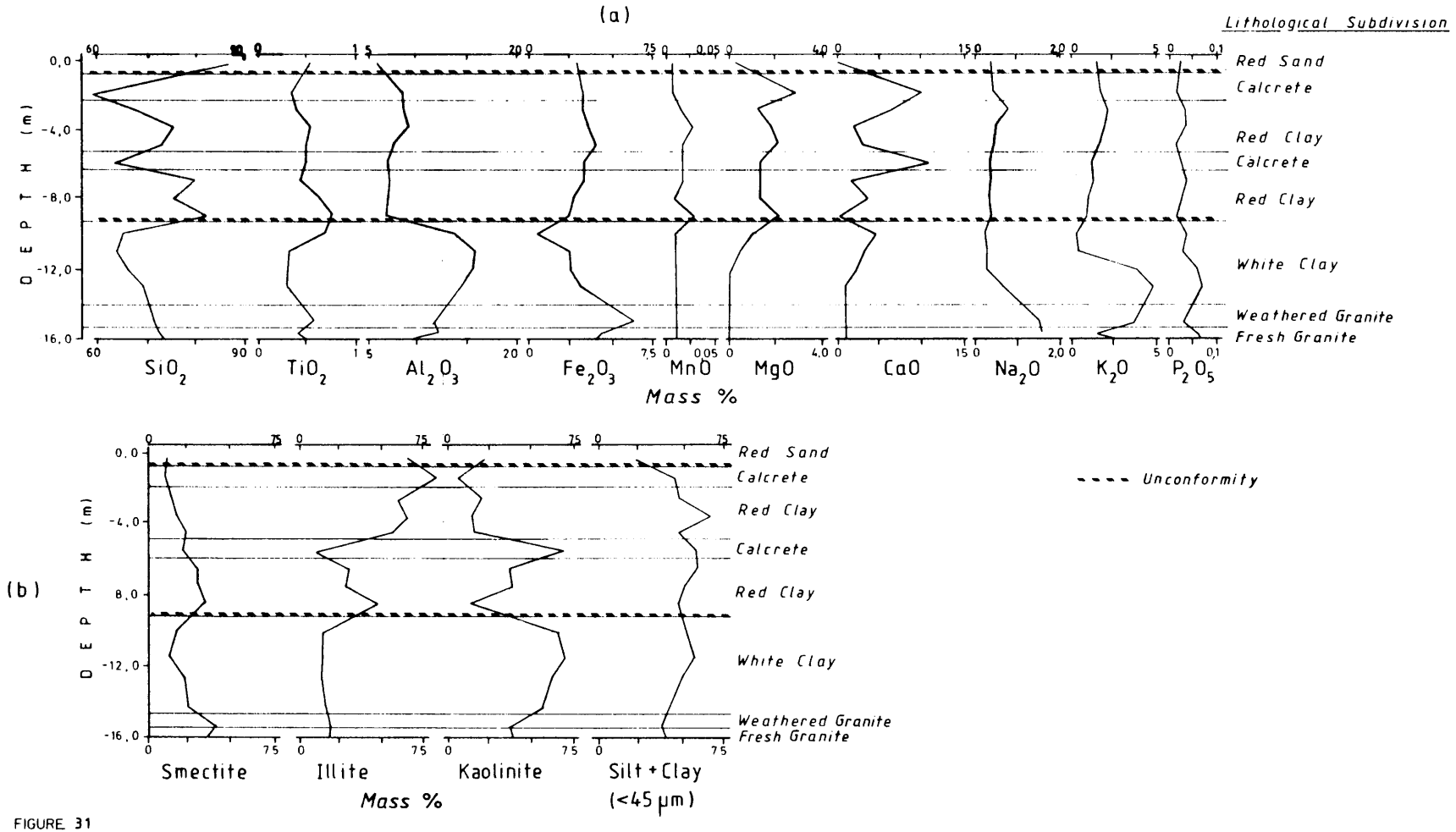

FIGURE 31

(a) MAJOR ELEMENTS VARIATION WITH DEPTH IN PERCUSSION BOREHOLE W30 S10 ON VAALPUTS.

(b) CLAY MINERAL AND TOTAL SILT AND CLAY VARIATION.

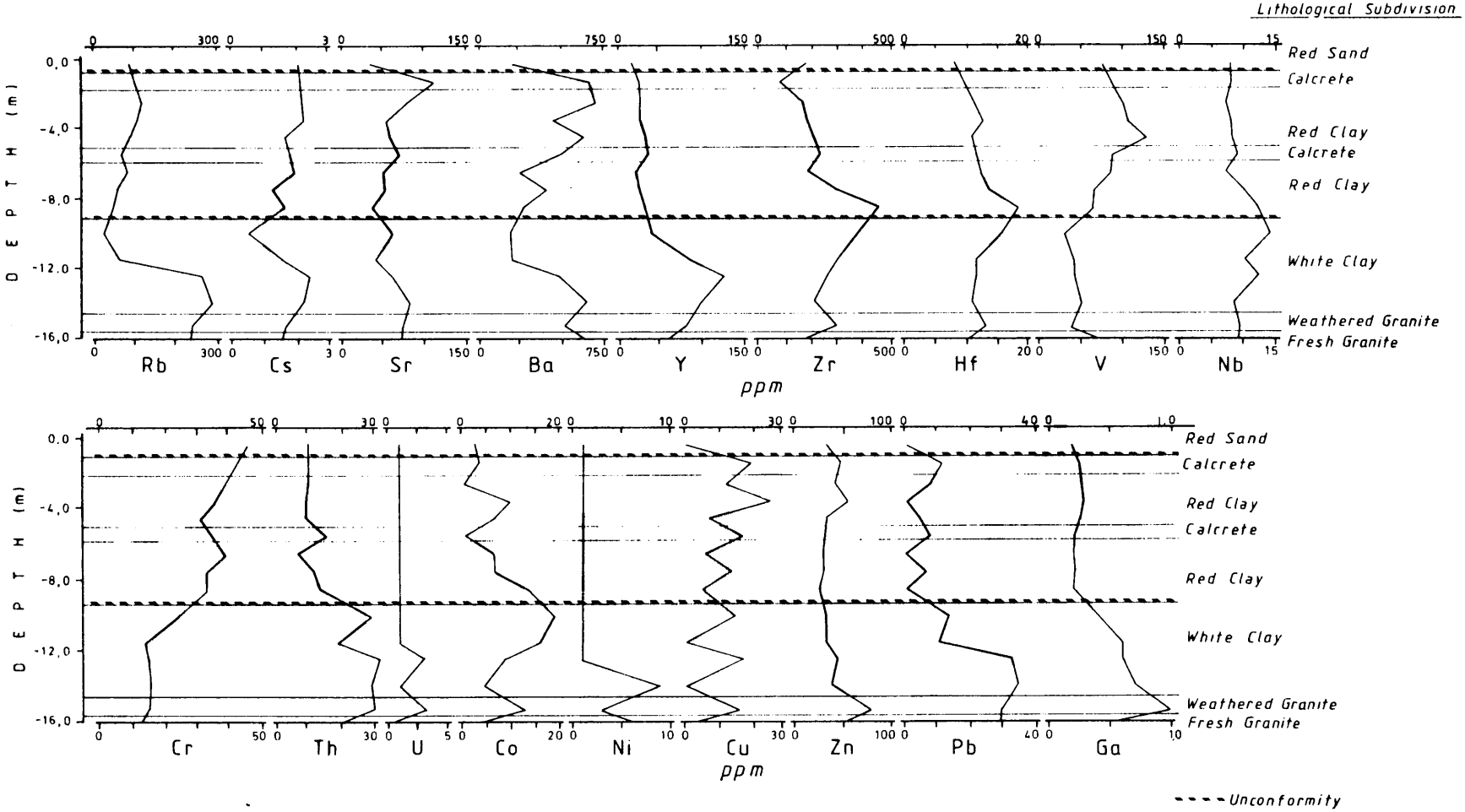

FIGURE 32

TRACE ELEMENTS VARIATION WITH DEPTH IN PERCUSSION BOREHOLE W30 S10 ON VAALPUTS.

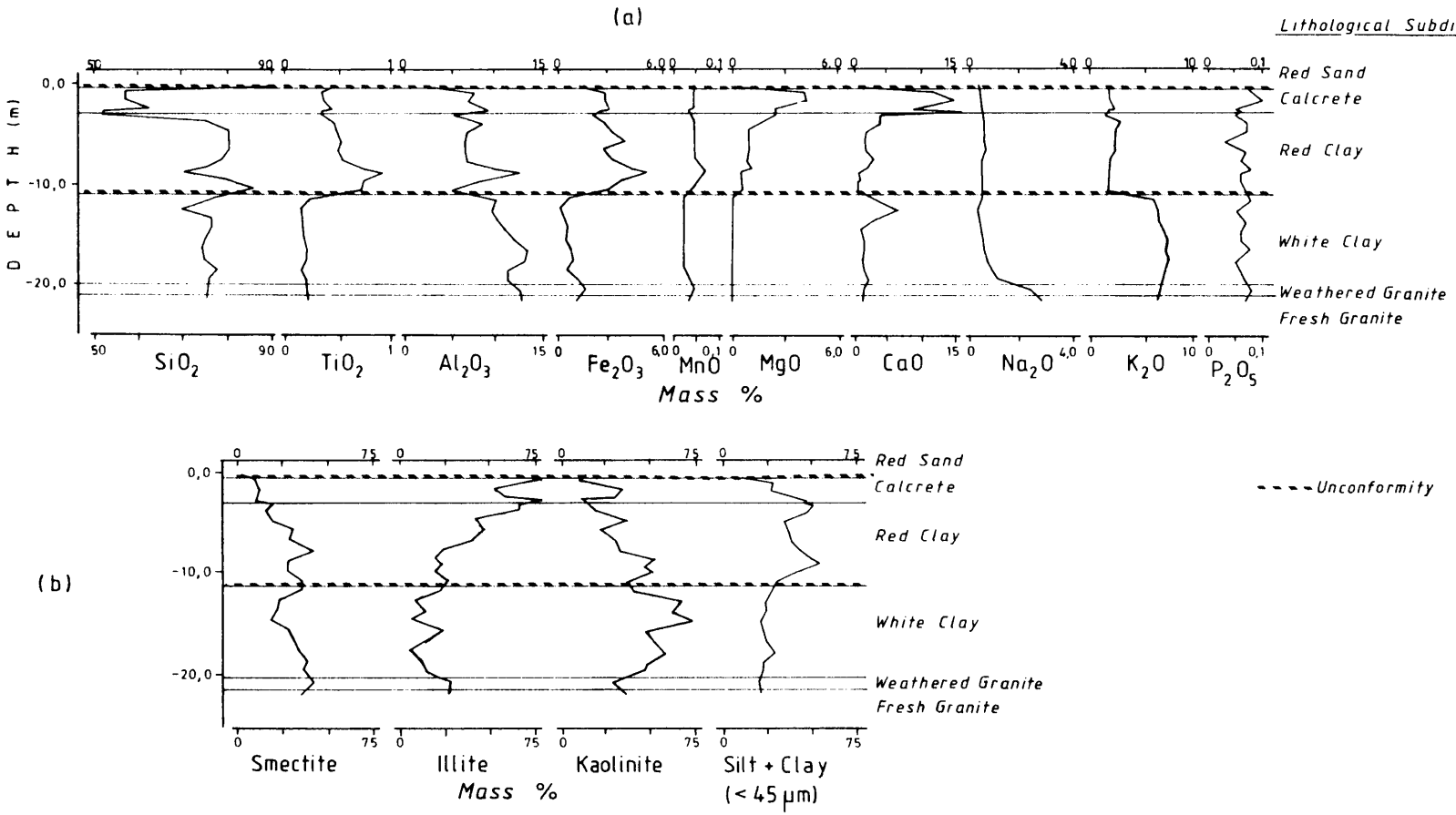

FIGURE 33

(a) MAJOR ELEMENTS VARIATION WITH DEPTH IN PERCUSSION BOREHOLE W60 N0 ON VAALPUTS.

(b) CLAY MINERAL AND TOTAL SILT AND CLAY VARIATION.

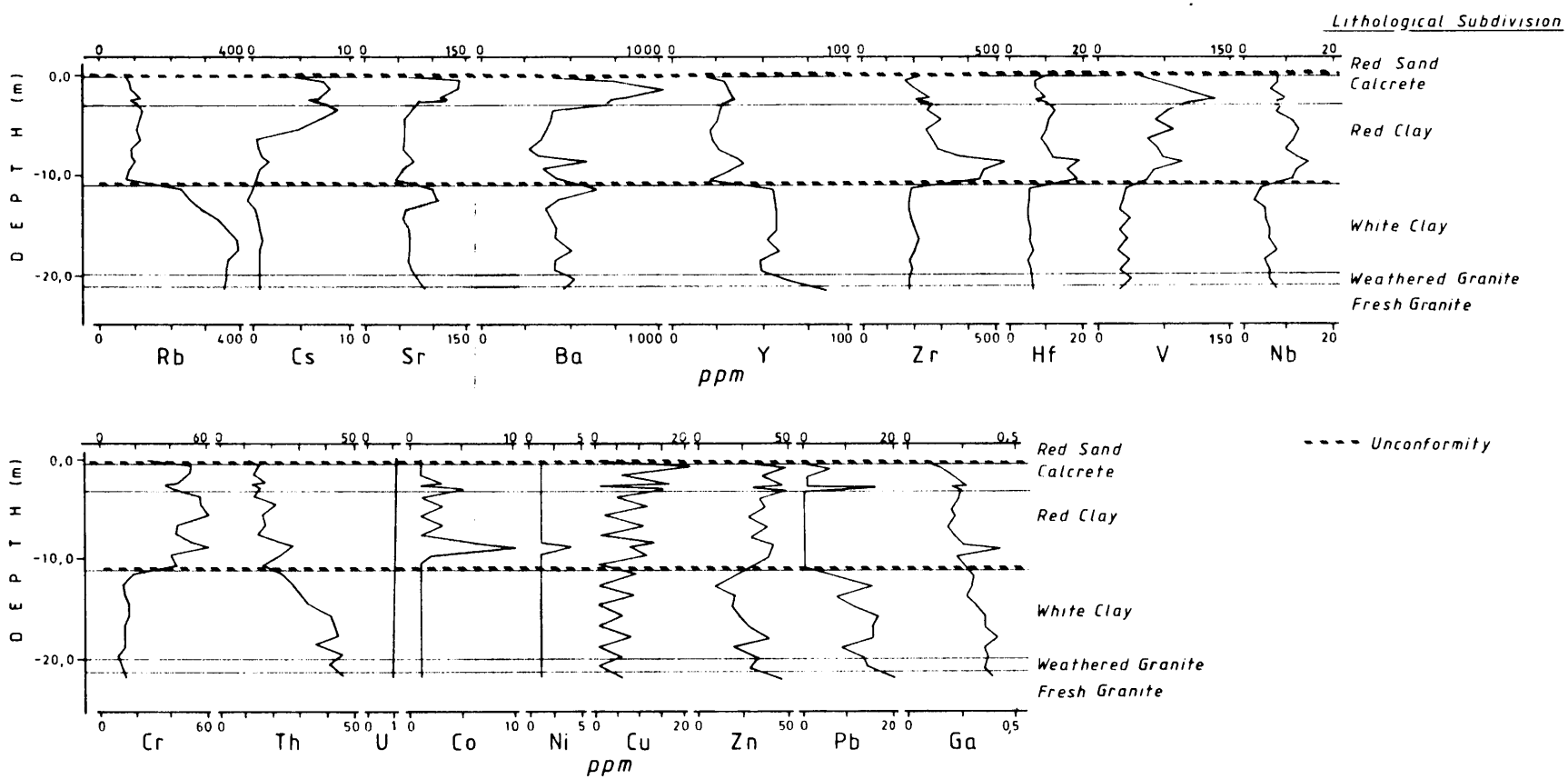

FIGURE 34

TRACE ELEMENTS VARIATION WITH DEPTH IN PERCUSSION BOREHOLE **W60 N0** ON VAALPUTS.

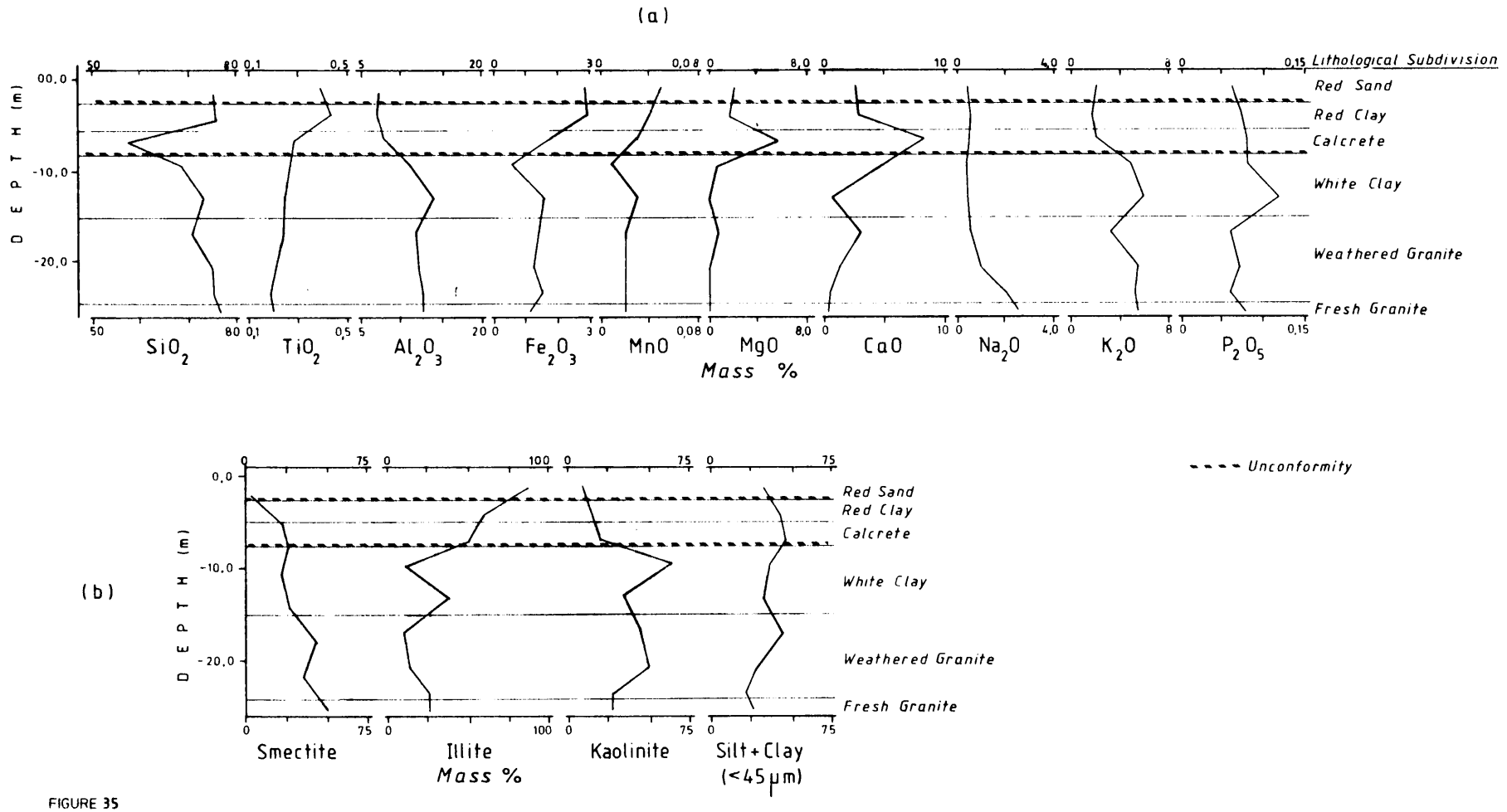

FIGURE 35

(a) MAJOR ELEMENTS VARIATION WITH DEPTH IN PERCUSSION BOREHOLE W70 N0 ON VAALPUTS.

(b) CLAY MINERAL AND TOTAL SILT AND CLAY VARIATION.

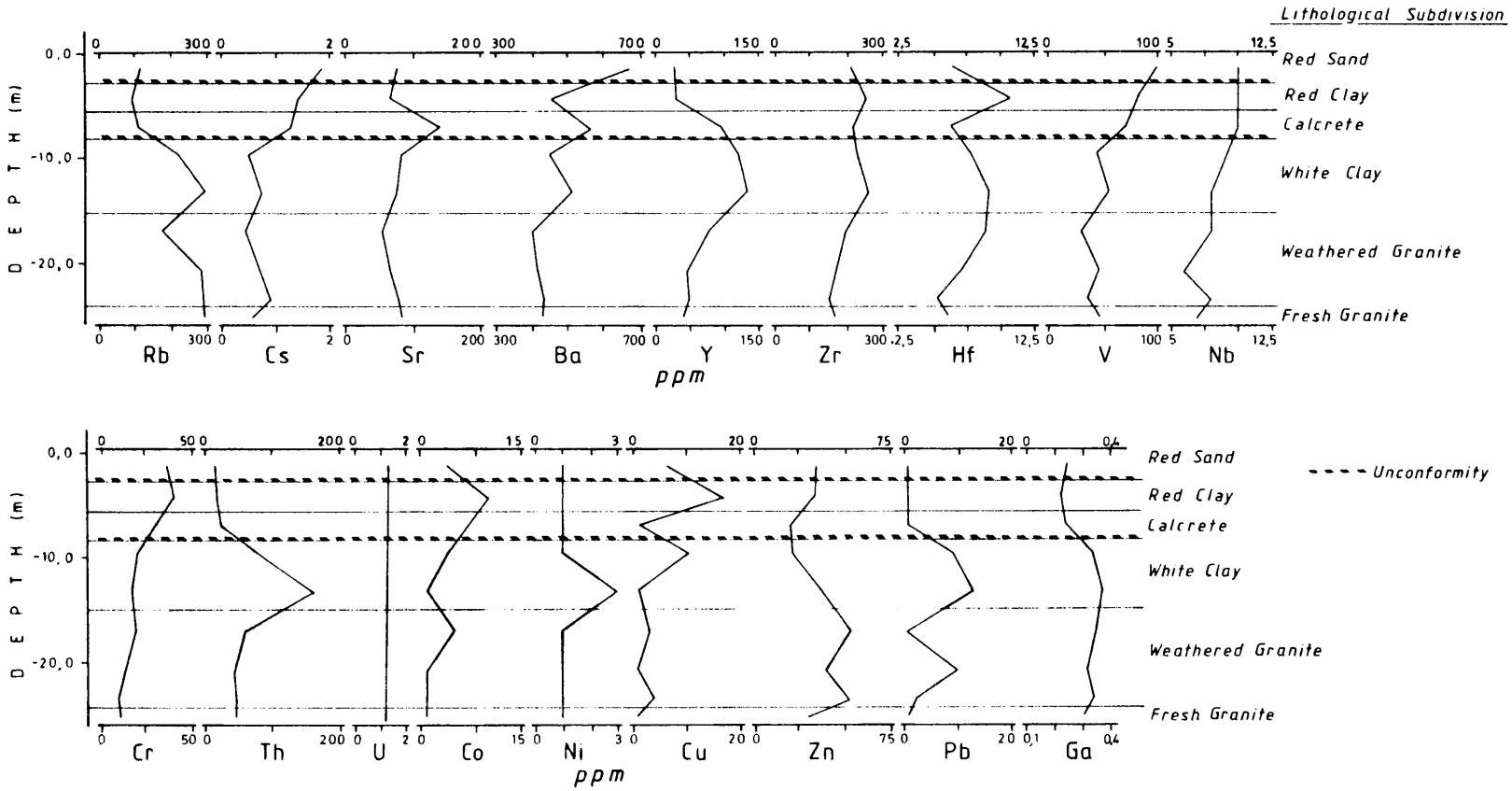

FIGURE 36

TRACE ELEMENTS VARIATION WITH DEPTH IN PERCUSSION BOREHOLE W70 N0 ON VAALPUTS.

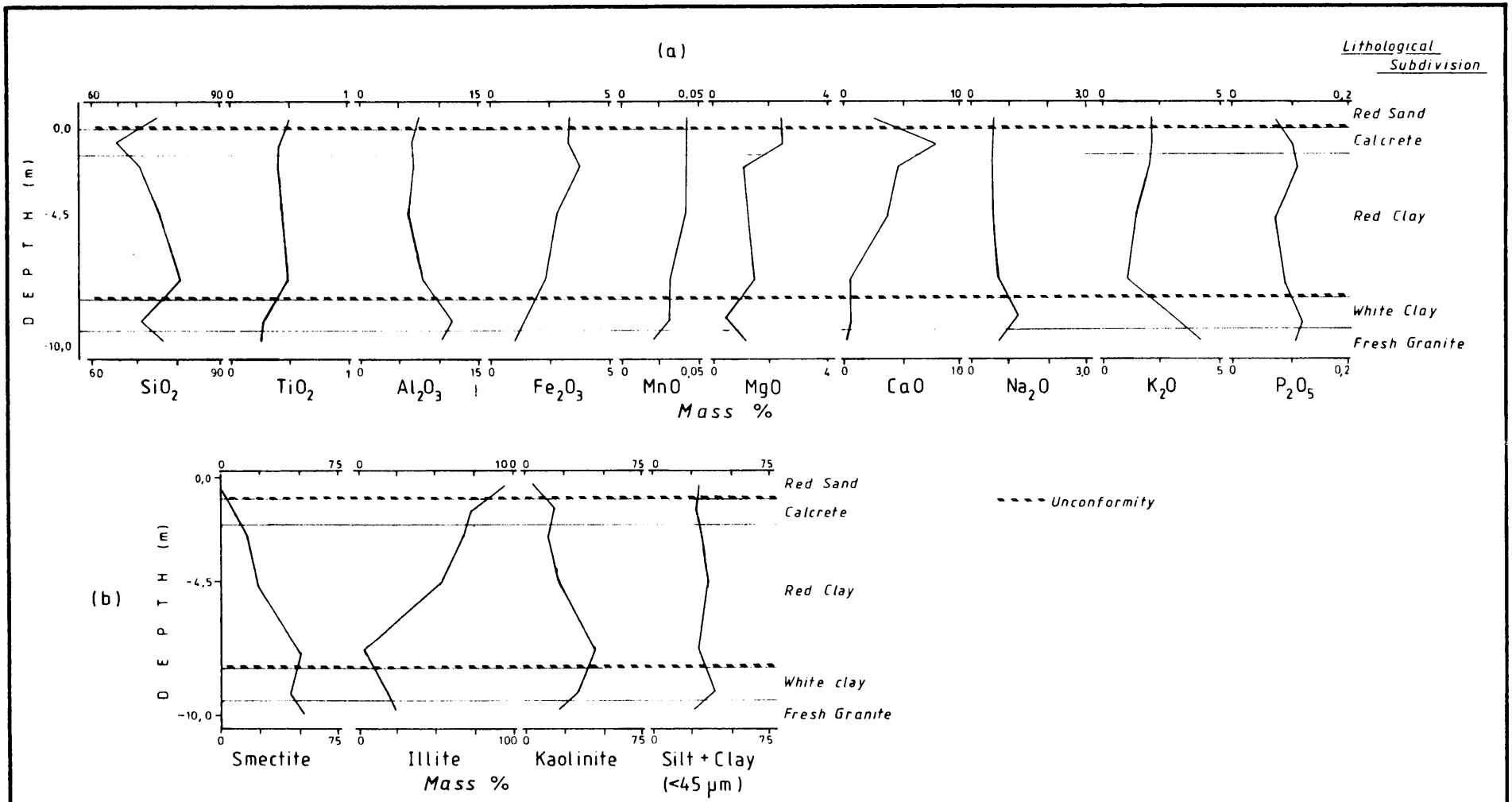

FIGURE 37

(a) MAJOR ELEMENTS VARIATION WITH DEPTH IN PERCUSSION BOREHOLE **W70 S10** ON VAALPUTS.

(b) CLAY MINERAL AND TOTAL SILT AND CLAY VARIATION.

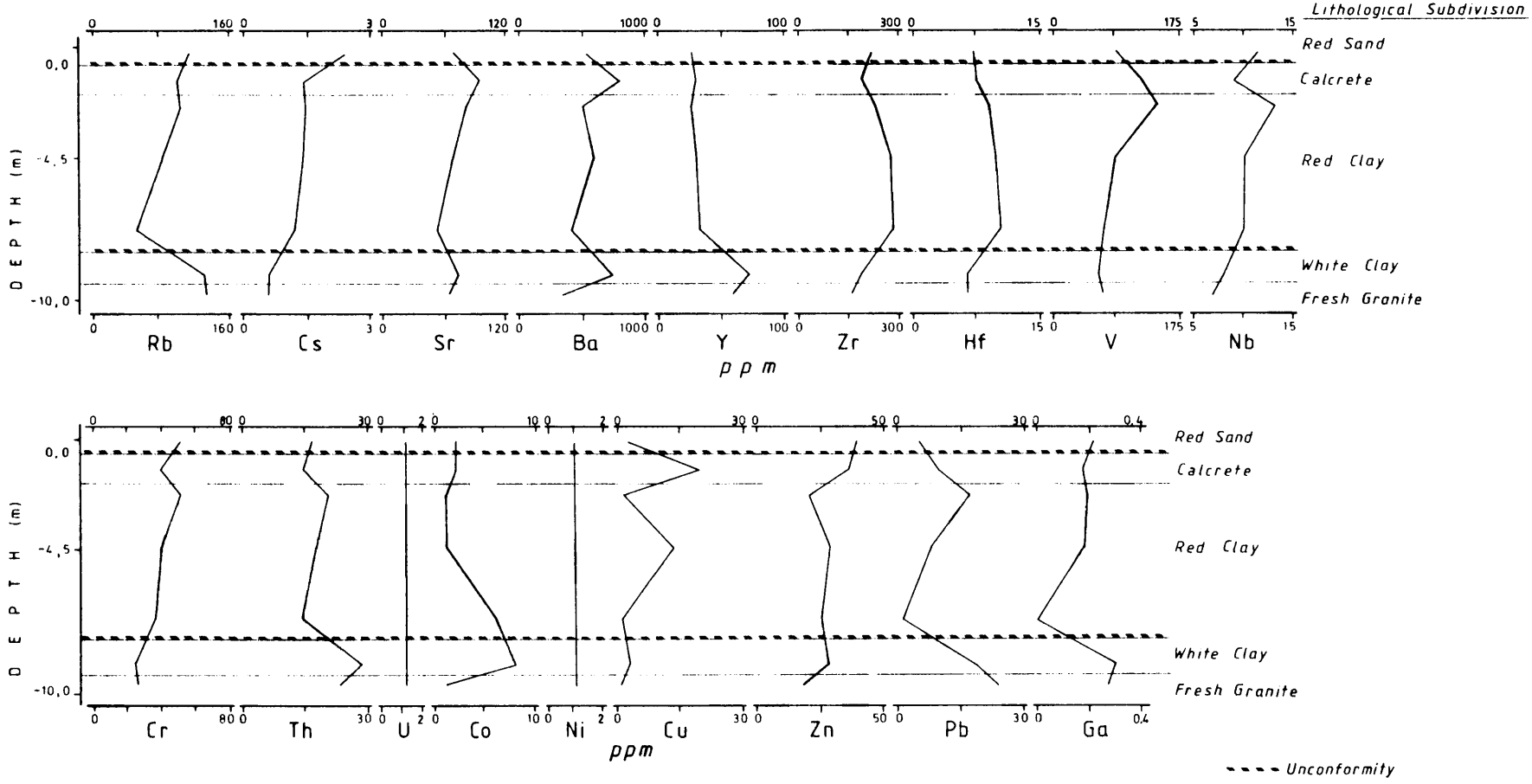

FIGURE 38

TRACE ELEMENTS VARIATION WITH DEPTH IN PERCUSSION BOREHOLE W70 S10 ON VAALPUTS.

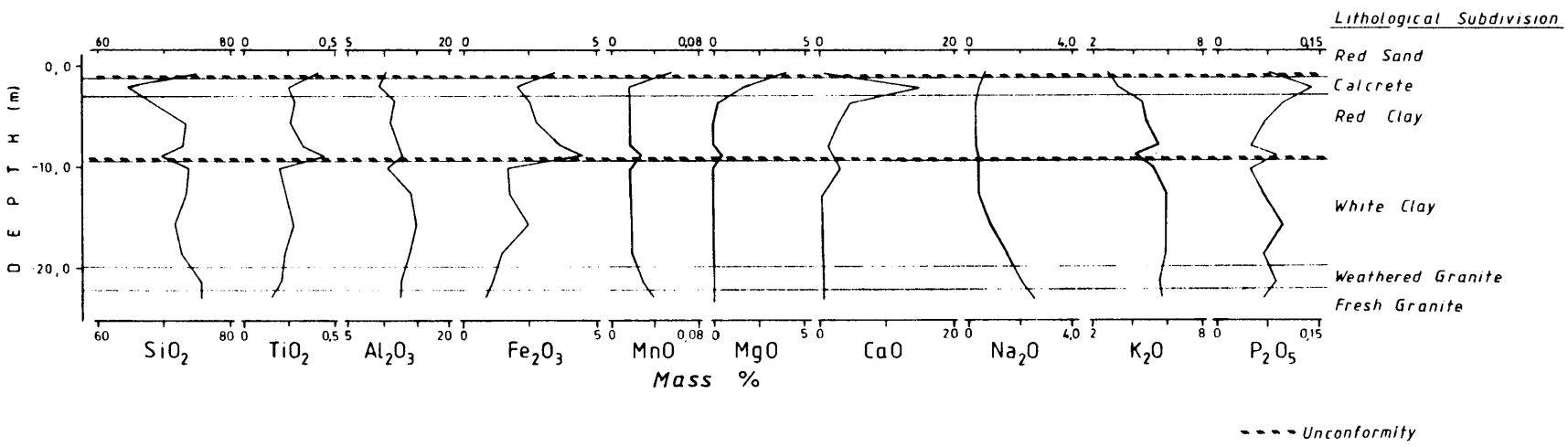

FIGURE 39

MAJOR ELEMENTS VARIATION WITH DEPTH IN PERCUSSION BOREHOLE W80 N0 ON VAALPUTS.

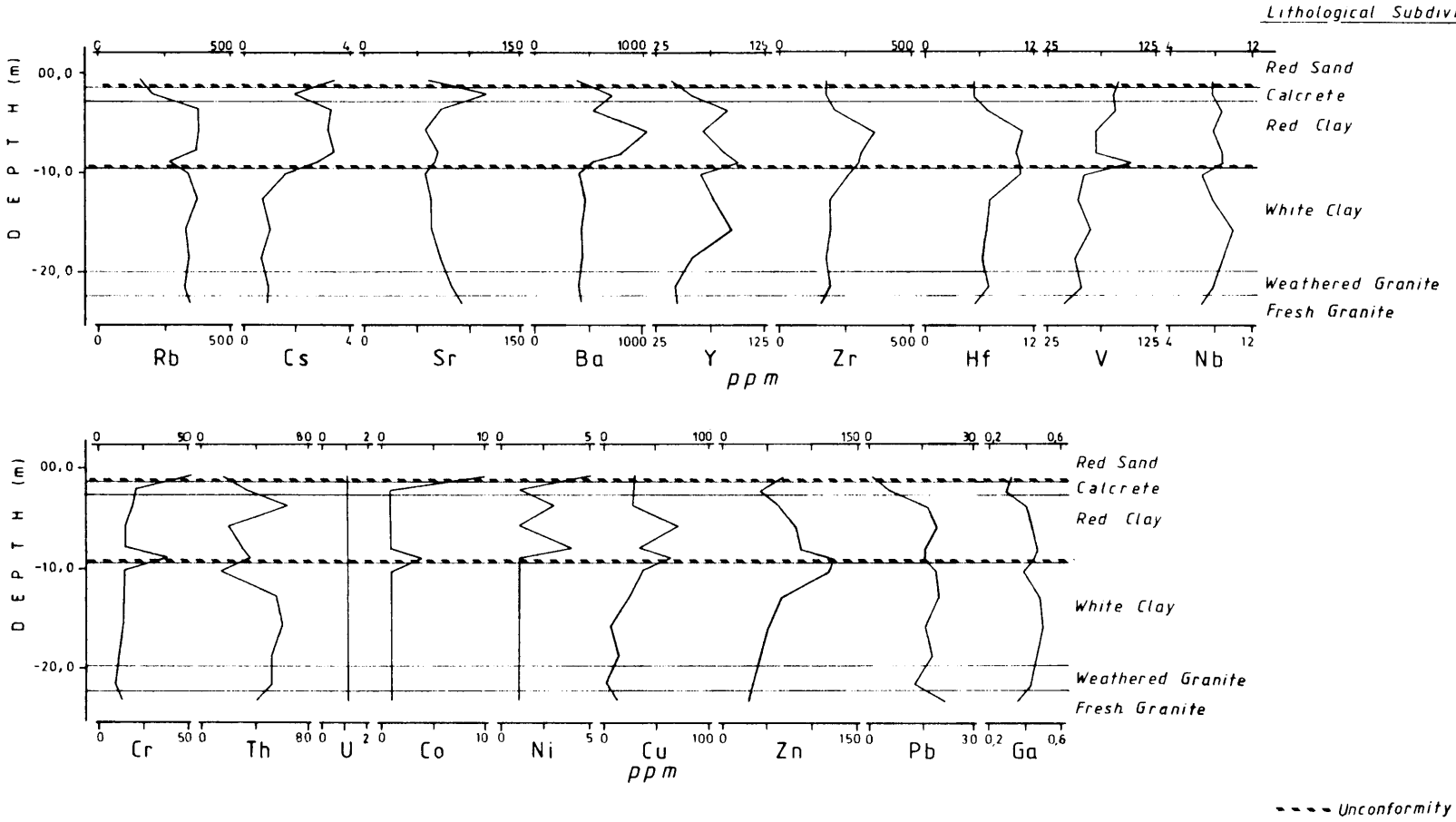

FIGURE 40

TRACE ELEMENTS VARIATION WITH DEPTH IN PERCUSSION BOREHOLE W80 N0 ON VAALPUTS.

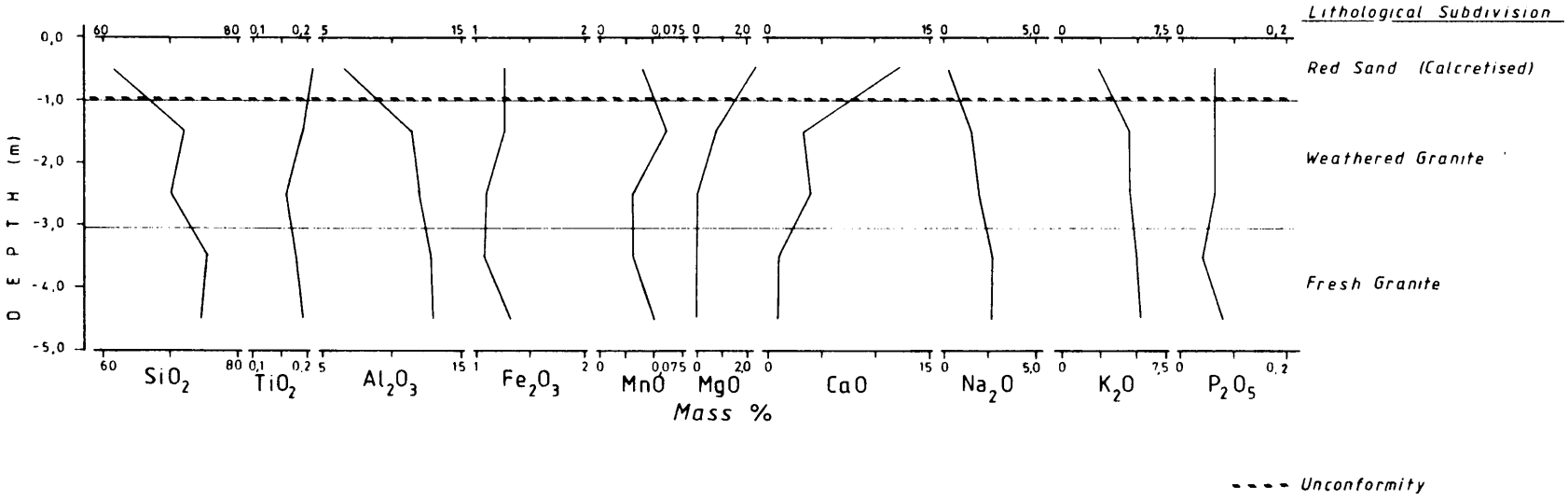

FIGURE 41

MAJOR ELEMENTS VARIATION WITH DEPTH IN PERCUSSION BOREHOLE W90 N0 ON VAALPUTS.

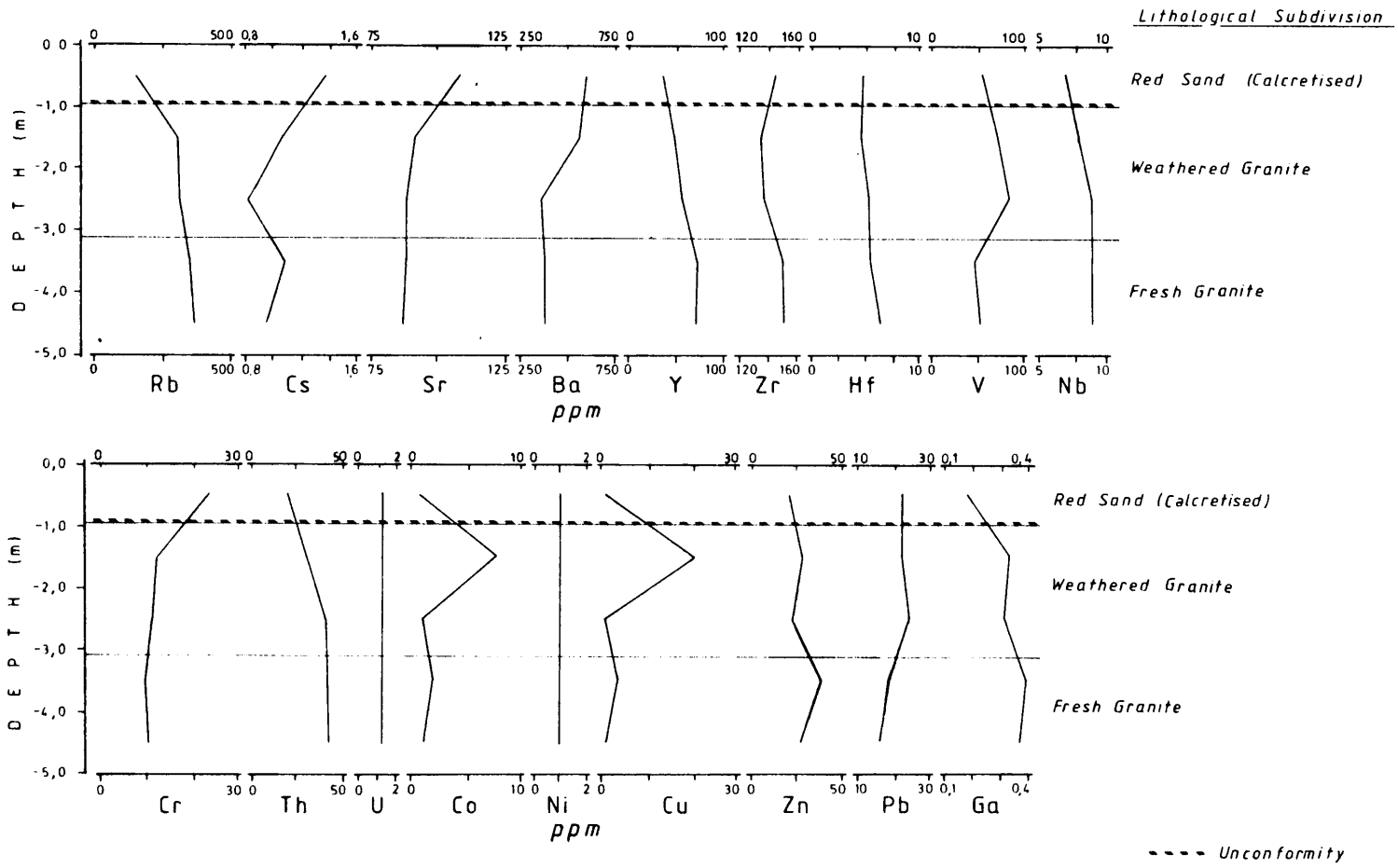

FIGURE 42

TRACE ELEMENTS VARIATION WITH DEPTH IN PERCUSSION BOREHOLE **W90 N0** ON VAALPUTS.

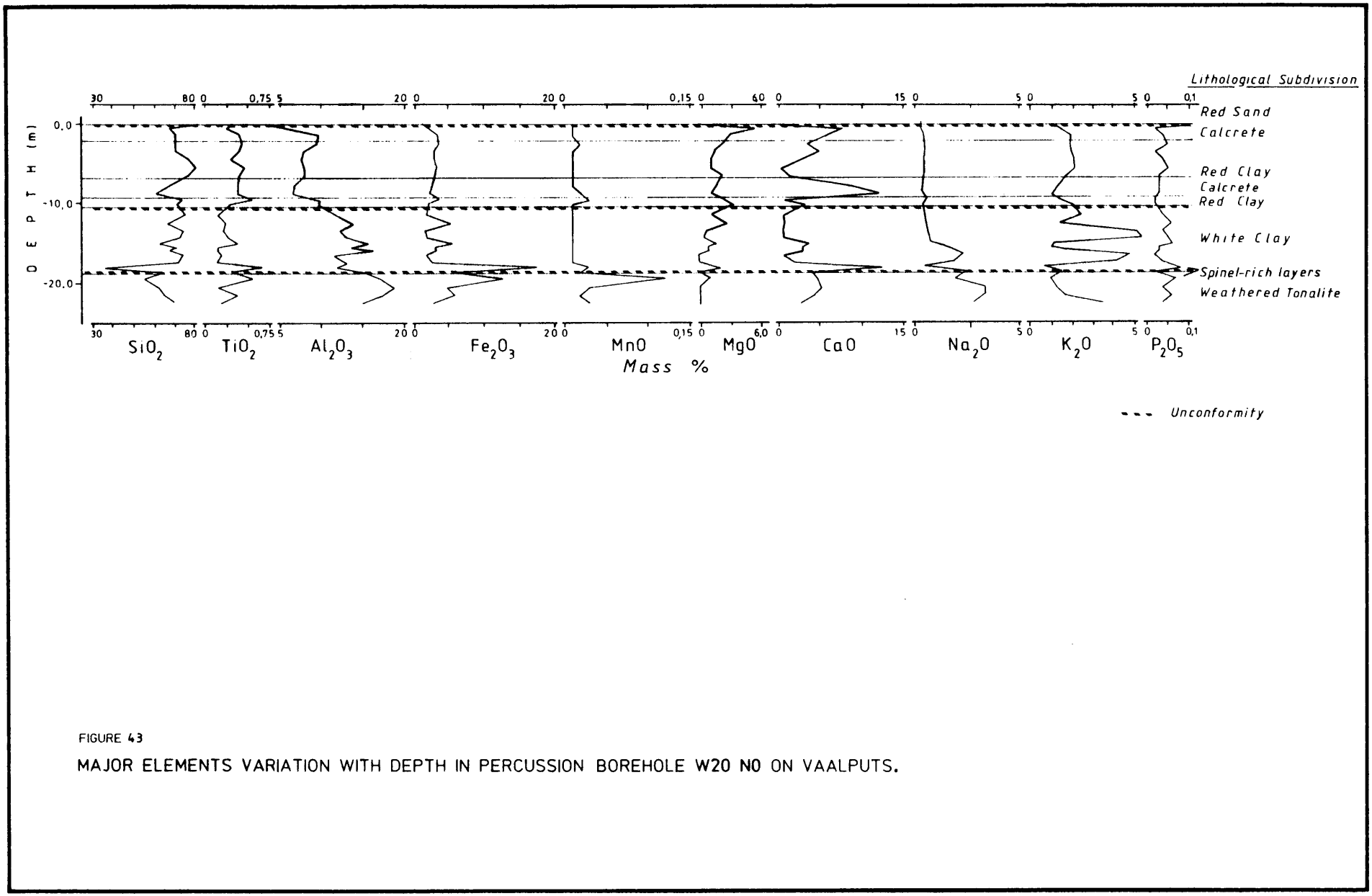

FIGURE 43

MAJOR ELEMENTS VARIATION WITH DEPTH IN PERCUSSION BOREHOLE W20 N0 ON VAALPUTS.

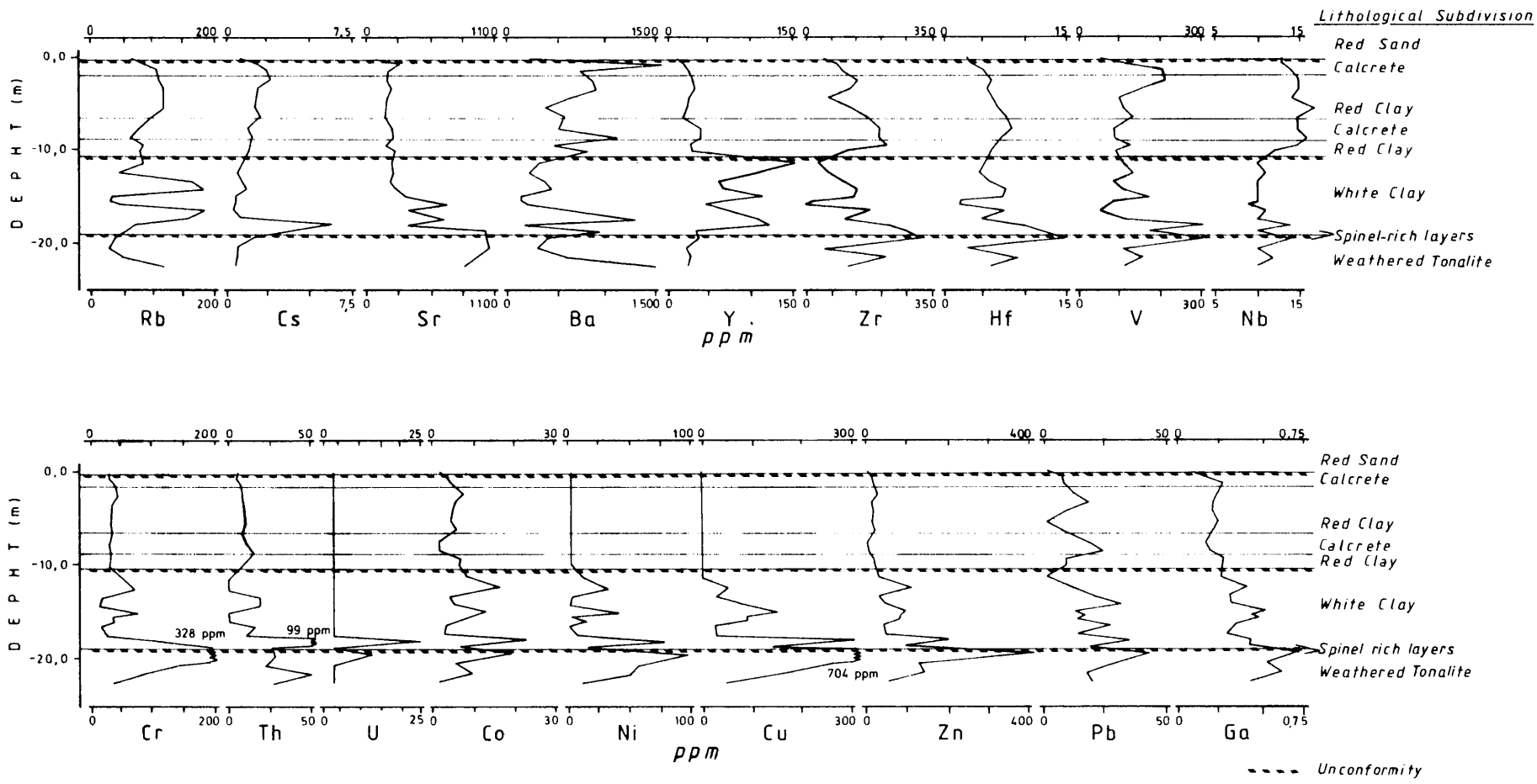

FIGURE 44

TRACE ELEMENTS VARIATION WITH DEPTH IN PERCUSSION BOREHOLE W20 N0 ON VAALPUTS.

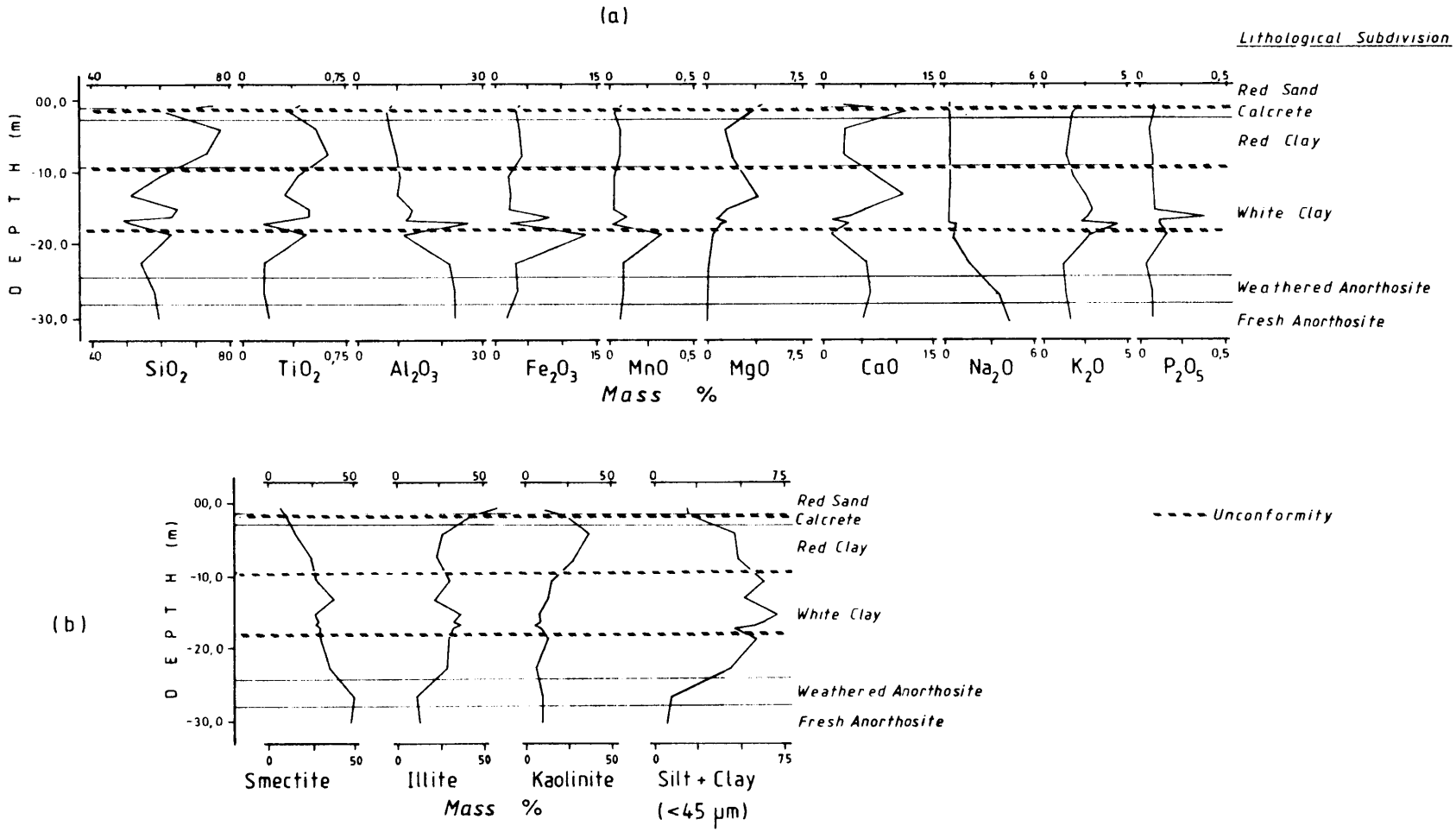

FIGURE 45

(a) MAJOR ELEMENTS VARIATION WITH DEPTH IN PERCUSSION BOREHOLE **W40 S10** ON VAALPUTS.

(b) CLAY MINERAL AND TOTAL SILT AND CLAY VARIATION.

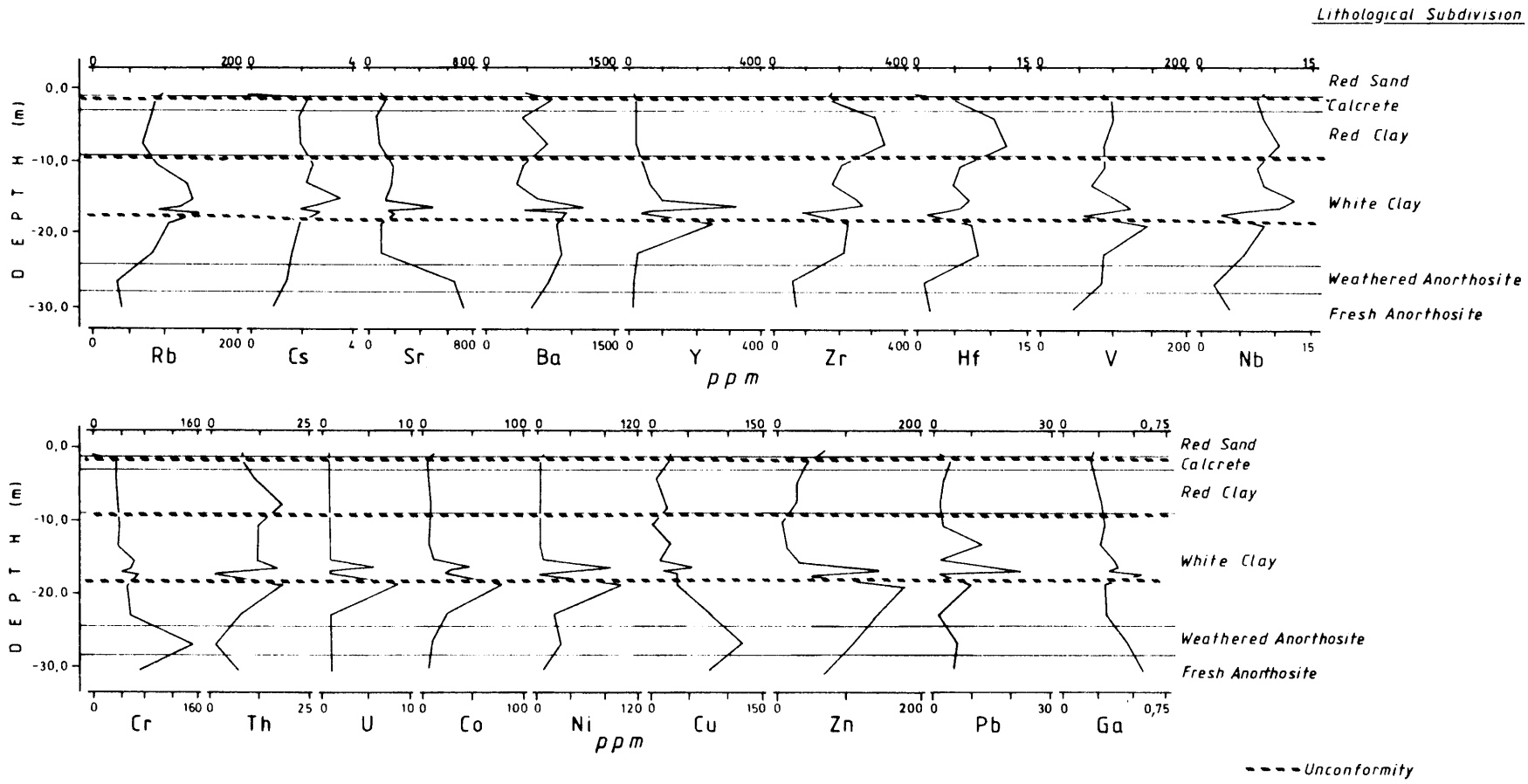

FIGURE 46

TRACE ELEMENTS VARIATION WITH DEPTH IN PERCUSSION BOREHOLE **W40 S10** ON VAALPUTS.

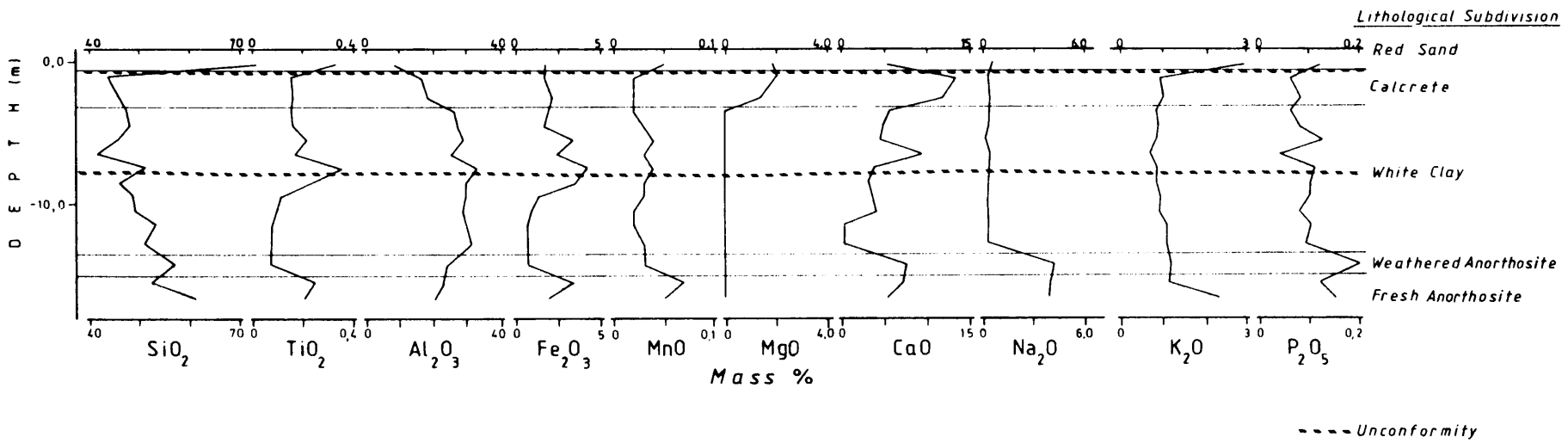

FIGURE 47

MAJOR ELEMENTS VARIATION WITH DEPTH IN PERCUSSION BOREHOLE W83 N0 ON VAALPUTS.

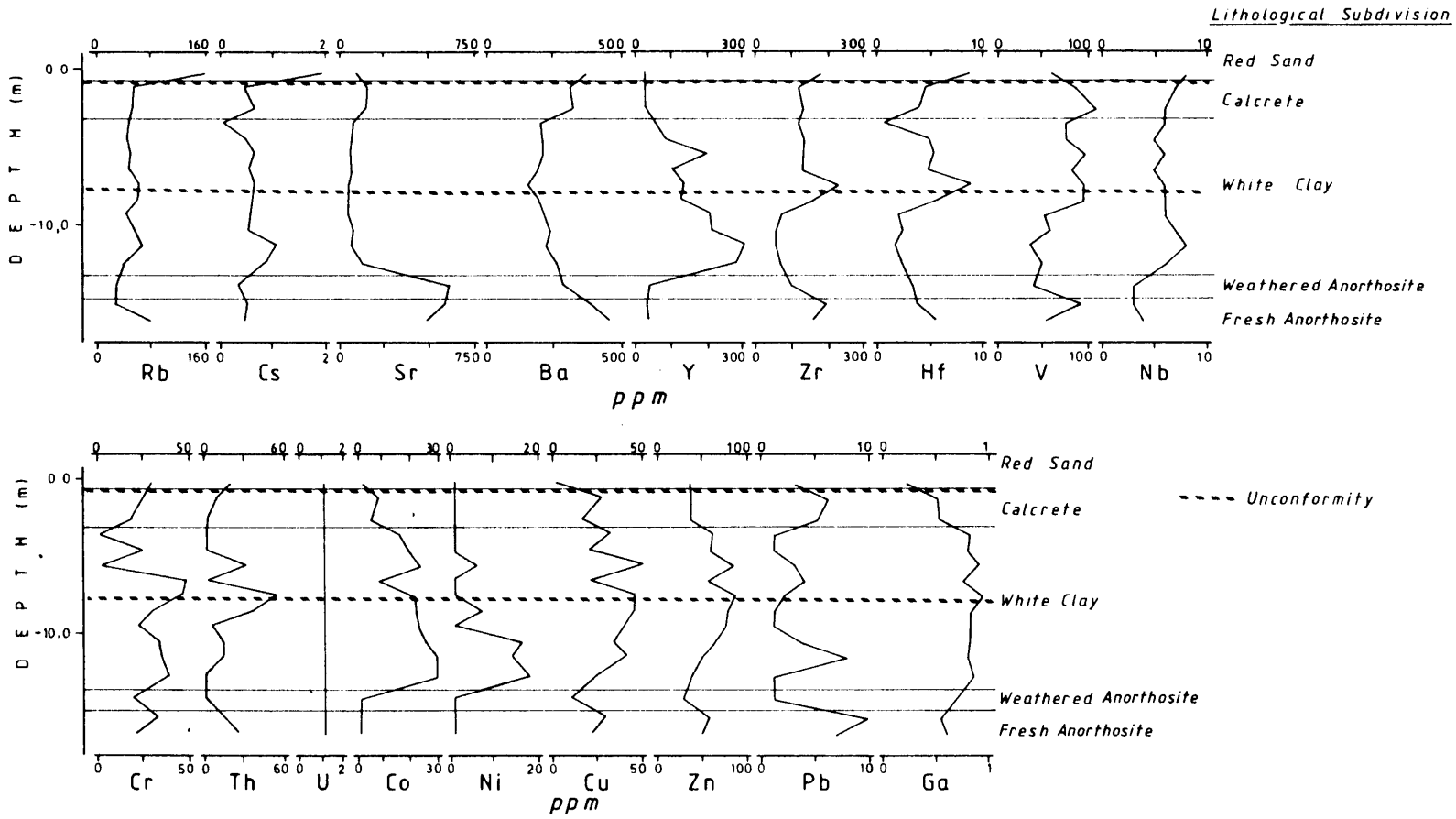

FIGURE 48

TRACE ELEMENTS VARIATION WITH DEPTH IN PERCUSSION BOREHOLE W83 N0 ON VAALPUTS.

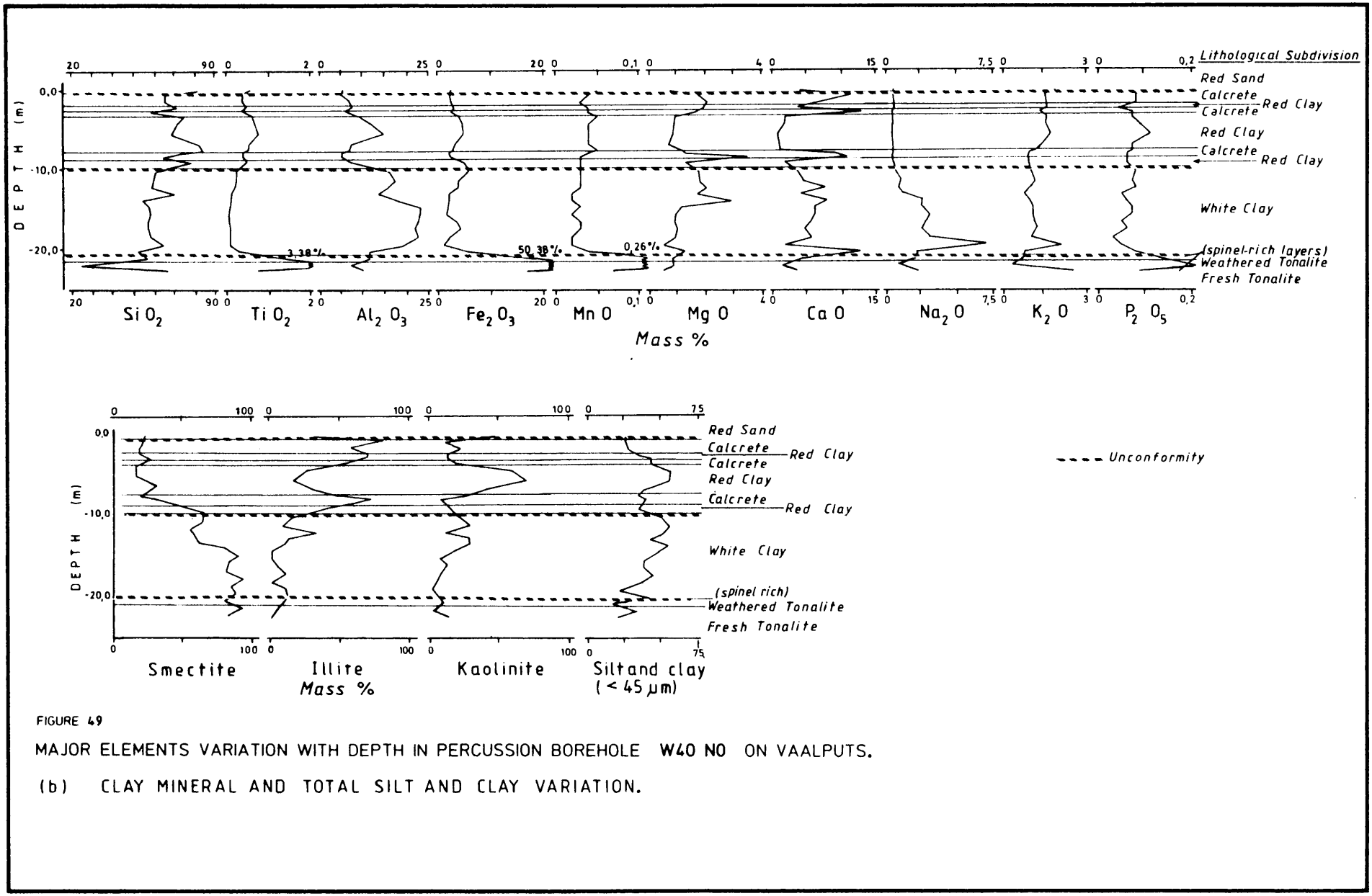

FIGURE 49

MAJOR ELEMENTS VARIATION WITH DEPTH IN PERCUSSION BOREHOLE W40 NO ON VAALPUTS.

(b) CLAY MINERAL AND TOTAL SILT AND CLAY VARIATION.

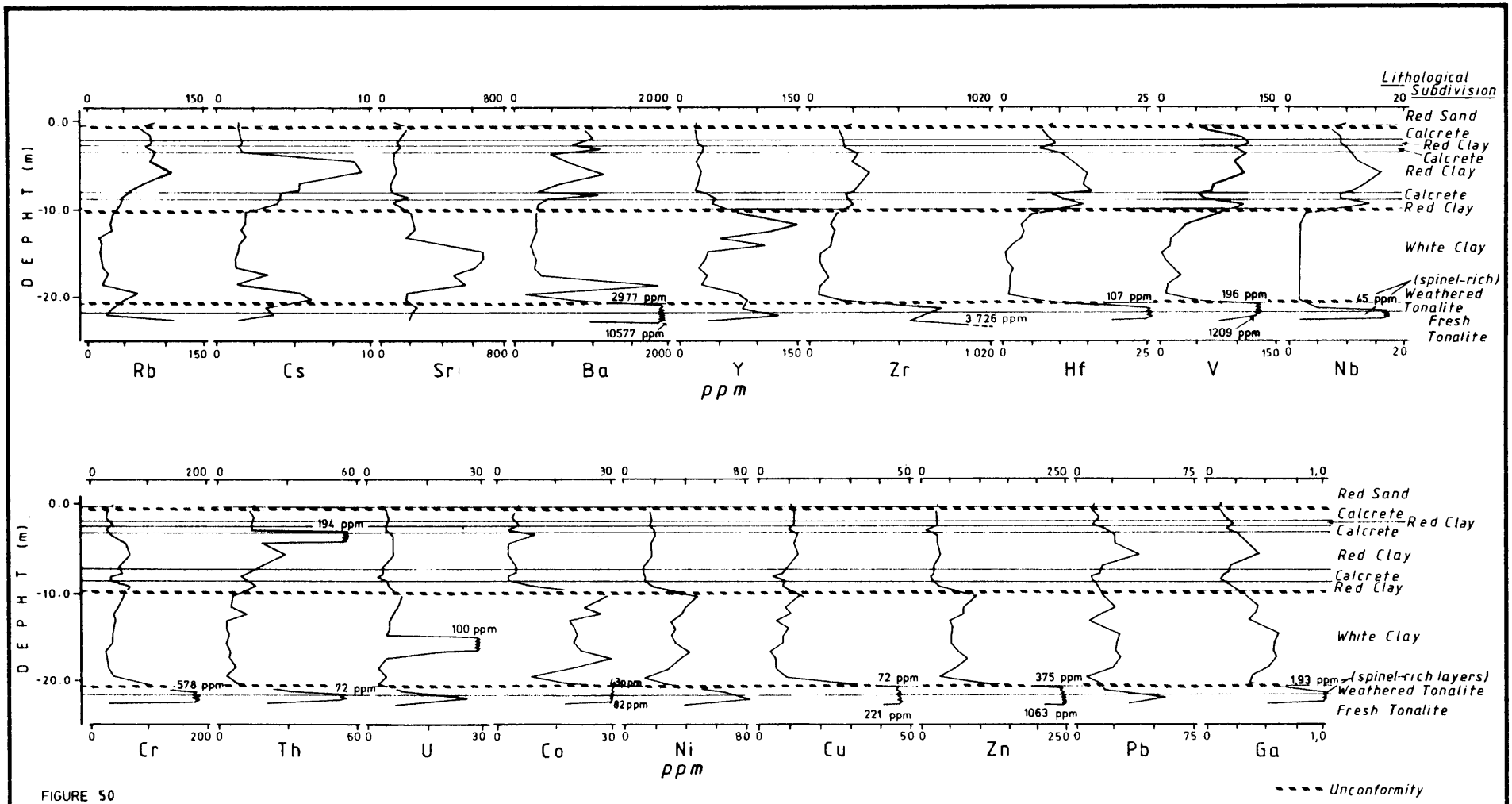

FIGURE 50

TRACE ELEMENTS VARIATION WITH DEPTH IN PERCUSSION BOREHOLE W40 N0 ON VAALPUTS.

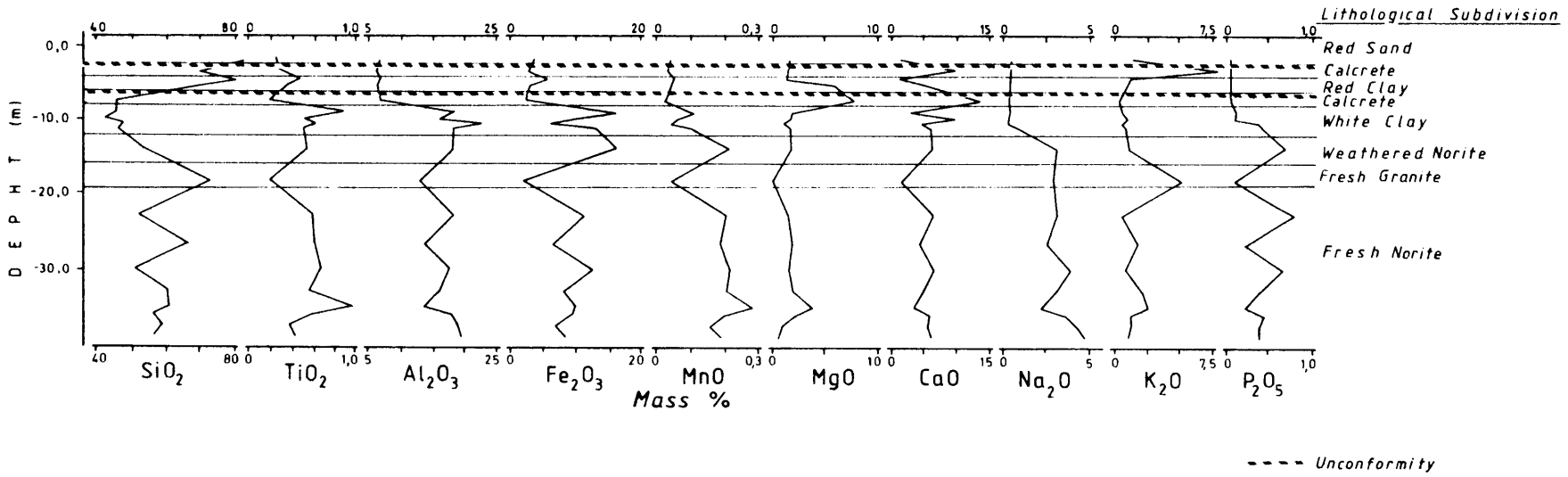

FIGURE 51

MAJOR ELEMENTS VARIATION WITH DEPTH IN PERCUSSION BOREHOLE **W49,8 N0** ON VAALPUTS.

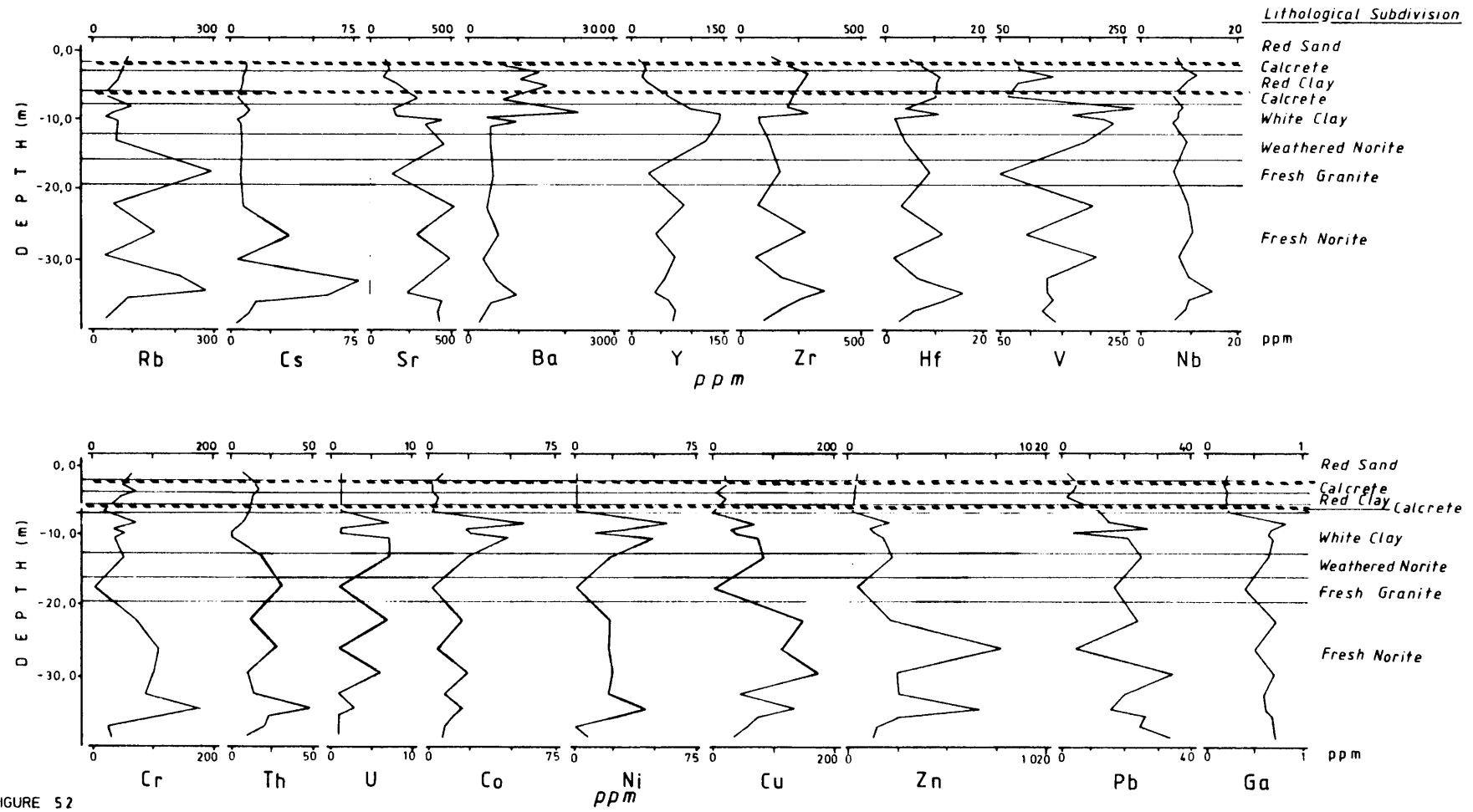

FIGURE 52

TRACE ELEMENTS VARIATION WITH DEPTH IN PERCUSSION BOREHOLE W49,8 NO ON VAALPUTS.

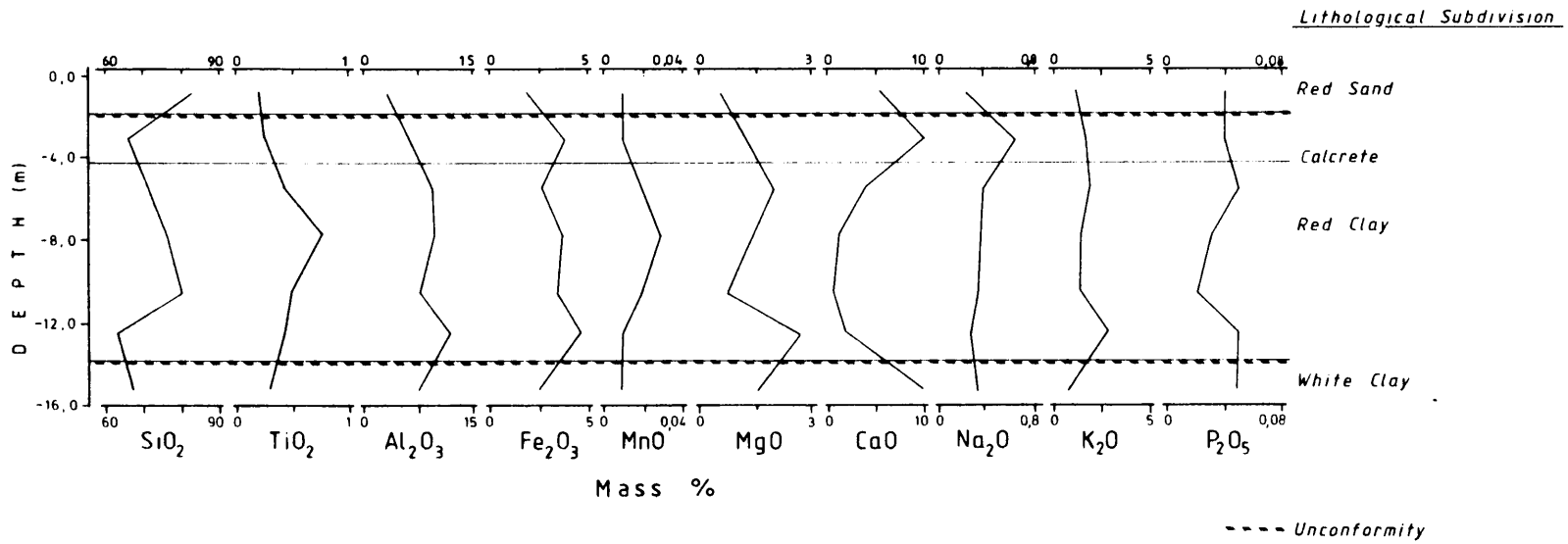

FIGURE 53

MAJOR ELEMENTS VARIATION WITH DEPTH IN PERCUSSION BOREHOLE **W30 N0** ON VAALPUTS.

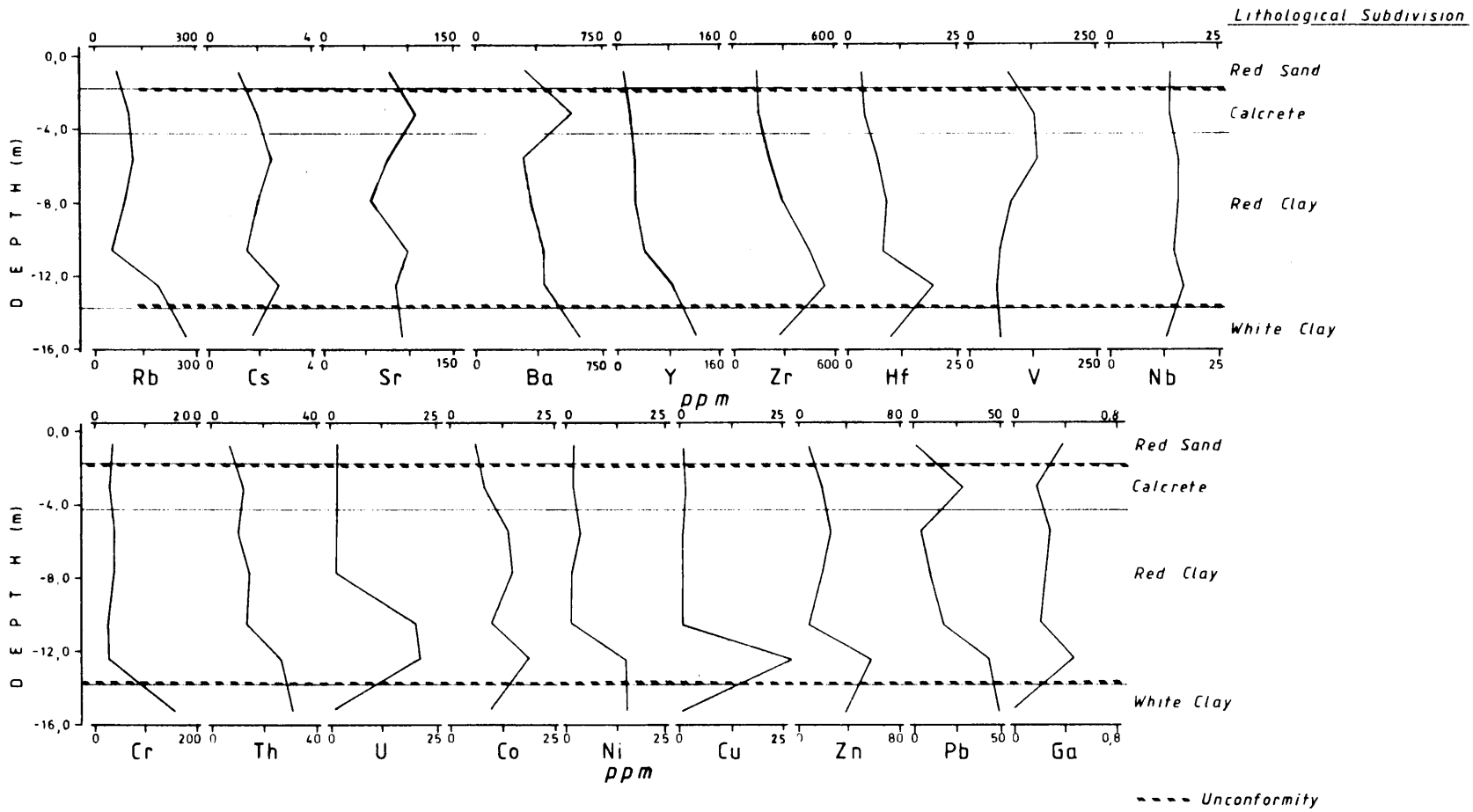

FIGURE 54

TRACE ELEMENTS VARIATION WITH DEPTH IN PERCUSSION BOREHOLE W30 N0 ON VAALPUTS.

6.4.3 Discussion

A proper understanding of the geology at Vaalputs is a prerequisite to the understanding and interpretation of the complex interrelationships of elements in the succession. Examination of the profiles in Figures 31 to 54 shows distinctive breaks in trends of the element concentrations which in most instances represent unconformities between lithological units and correspond remarkably well to lithological boundaries established during borehole logging. Another feature is the correlation of element concentration peaks within units e.g in the white clay of W83N0 and W40S10 (Figs. 47/48 and 45/46). These suggest unconformities within the rock units and influence the geochemistry profoundly. Lateritisation and subsequent calcretisation is thought to have occurred at these unconformities in W40S10 and W83N0 (Figs. 45/46 and 47/48) as suggested by high Fe_2O_3, and CaO respectively and a host of trace elements which correlate with them. In boreholes W40N0 and W20N0 accumulation of heavy minerals, particularly spinels, along the unconformity at the base of the white clay is suggested.

Principal components analysis (PCA) shows that the major element chemistry of the rock units can be conciliated with the mineralogy. The most important element oxides from an interpretative point of view are SiO_2, Al_2O_3 and CaO indicating the presence of the major rock forming components namely quartz, clay, feldspars and calcrete, with K_2O and Na_2O playing a role in distinguishing between clay minerals and feldspars. In addition Fe_2O_3, MnO and TiO_2 are thought to play a subordinate, yet important role in the concentration of some trace elements.

In the profiles of element variations at Vaalputs it can be seen that trace elements often correlate with Fe, Mn and Ti in almost all boreholes. The more obvious of these element correlations are tabulated in Table XIII. Most of the correlations occur in the oxidised red clay. In the red clay of W40N0 a peak of kaolinite coincident with the Ti, Fe and Mn peaks probably accounts for the

Rb, Sr and Ba concentrations in that unit. Zr and Hf are thought to be present in zircon and their frequent correlation with Ti, Fe and Mn can then be attributed to heavy mineral concentrations in which Fe-, Mn- and Ti-oxide minerals may occur. Thorium could be present in the zircon, but could also be adsorbed onto these oxides. In most of the boreholes the Ti, Fe and Mn peaks can be correlated with the presence of iron-oxide nodules (Fig. 9 a-l), except in the white clay of W49,8N0 and the base of the red clay in W60N0 where high concentrations of magnetite were noted. The majority of the correlated elements are considered to be adsorbed onto, or incorporated in the crystal structure of the Fe-, Mn- and Ti-oxides. Trace elements usually associated with magnetite, include Ti, Al, Cr as major constituents, Mn, V as minor constituents and Zn, Cu, Sn, Ni, Co, Pb and Mo as trace constituents (Levinson, 1974).

It is known that amorphous or poorly crystalline constituents of laterites e.g. Fe- Mn- and Ti-oxide, so called "scavengers", are able to fix elements from migrating solutions in the geological environment. The very small particle size of the material, providing a very large specific surface area and also a high degree of structural imperfection are both factors which determine their high sorption capacity and chemical reactivity (Kühnel, 1987). Iron-oxides may selectively adsorb Zn, Cu, Pb, Cr and V whereas hydrated Mn-oxide adsorbs Cu, Ni, Co and Cr (Krauskopf, 1956).

It was found by McKenzie and Taylor (1968) and Taylor (1968) that Mn-oxide nodules and stains are common constituents of the soils where alternating wet and dry conditions prevail. Most of the Mn-bearing minerals contain varying amounts of Ni, Co, Mg, Ba, Al, Na, K, Fe, Cr, Mo, Cu, Li, Ca and other elements. In soils up to 80% of Co (up to 200 ppm) in the soil is contained in the manganese minerals. The initial adsorption sequence is Cu > Co > Ni, but upon ageing Co is most strongly held. Nolan, (1976) found that elements that are probably not scavenged include Ag, Be, Ca, Ga, La, Sb, B, Cr, K, Rb, Sc, Ti, V, Zr and Y; elements weakly scavenged are Cu, Mo, Pb and Sr and elements strongly scavenged Ba, Cd, Co, Ni, Tl and

Table XIII Element correlations with peaks of Ti, Fe and Mn in element variation diagrams of Vaalputs boreholes

Borehole	Lithological unit	Major peaks	Correlated elements: Major	Correlated elements: Trace
W20NO[1]	Red clay (below calcrete)	Ti,Fe,Mn		Cs,Zr,Hf,V,Nb,Cr,Co,Zn
	White clay/ spinel-rich layer	Ti,Fe,Mn	Mg,Ca,P	Cs,Y,Zr,Hf,V,Nb,Th,Co,Ni,Cu,Zn,Pb
W30NO[2]	Calcrete	Fe	Ca,Na	Sr,Ba,V,Pb
	Red clay (base)	Fe	Al,Mg,K,P	Rb,Cs,Y,Zr,Hf,Nb,Th,U,Co,Ni,Zn,Pb,Ga
	Red clay (middle)	Ti,Mn		V,Nb,Th
W30S10[3]	Red clay	Ti, Mn		Y,Zr,Hf,Nb,Th,Co
W40NO[4]	Red clay	Ti,Fe,Mn	Al,K,P	Rb,Cs,Ba,Zr,Hf,V,Nb,Cr,Th,Cu,Zn,Pb,Ga
	Spinel-rich layer	Ti,Fe,Mn	P	Cs,Ba,Y,Zr,Hf,V,Nb,Cr,Th,U,Ni,Cu,Zn,Pb,Ga
W40S10[5]	White clay (middle)	Ti,Fe,Mn	P	Rb,Cs,Sr,Ba,Y,Zr,Hf,V,Nb,Cr,Th,Zn
		Ti,Fe,Mn	P	Rb,Cs,Ba,Y,Zr,Hf,V,Nb,Th,U,Co,Ni,Pb
W49,8NO[6]	Calcrete/red clay	Ti,Fe,Mn		Zr,Hf,V,Nb,Co,Cu
	White clay	Ti,Fe,Mn	Al	Ba,Y,Zr,Hf,V,Nb,Cr,U,Co,Ni,Cu,Zn,Pb,Ga
	Weathered norite	Ti,Fe,Mn	P	Sr,V,Nb,Cr,Th,U,Cu,Zn,Pb
W60NO[7]	Red clay	Ti,Fe,Mn	Al,Mg	Cs,Sr,Ba,Y,Zr,Hf,V,Nb,Cr,Th,Co,Ni,Cu,Zn,Ga
W70NO[8]	Red clay	Ti,Fe,Mn		Cs,Zr,Hf,V,Nb,Co,Cu,Zn
W70S10[9]	Red clay	Fe,Mn	P	Rb,Cs,Sr,Ba,V,Nb,Cr,Th,Pb
W80NO[10]	Red clay (base)	Ti,Fe,Mn	Al,Mg,P	Y,V,Nb,Cr,Th,Co,Zn,Ga,Zr?,Hf
W83NO[11]	White clay	Ti,Fe,Mn	Al,Si,P	Rb,Cs,Y,Zr,Hf,V,Nb,Th,Cr,Co,Ni,Cu,Zn,Ga
	Fresh anorthosite	Ti,Fe,Mn		Sr,Ba,Zr,V,Cr,Cu,Zn,Pb

1 Figure 43/44 2 Figure 53/54 3 Figure 31/32
4 Figure 49/50 5 Figure 45/46 6 Figure 51/52
7 Figure 33/34 8 Figure 35/36 9 Figure 37/38
10 Figure 39/40 11 Figure 47/48

Zn. Jenny (1968) concluded that the adsorption properties of Mn- and Fe-oxides are a function of the amount of crystal water present in the oxides, pH and the amount and strength of organic chelates and inorganic complex formers present in the solution.

With regard to the correlation of major and trace elements with clay minerals there are numerous instances where high element concentrations can be correlated with a particular clay mineral. Table XIV shows the most important of these correlations in the variation diagrams (Figs. 31 to 54).

Although uranium and to a lesser extent thorium contents of the sediments are generally low, some anomalous values of these elements occur, notably in boreholes W40N0, W40S10, W60N0, W70N0, W80N0 and W83N0 (Figs. 50, 46, 34, 36, 40 and 48). The Th peak in W20N0 (Fig. 44) and both the Th and U peaks in W40S10 (Fig. 46) correlate well with Zr amongst other elements. In the white clay of W40N0 only Sr correlates with the anomalous U value, but a corresponding high smectite content is evident.

If it is assumed that all the Zr in the above-mentioned samples is accounted for by zircon and if it is considered that the mineral can contain up to 5 000 ppm U (Rösler and Lange, 1972), it is clear that the anomalous U and Th contents in the above-mentioned samples cannot be accounted for by their presence in heavy minerals only. The presence of U in the clay has been illustrated in section 5.2.1. The concomittant presence of abundant smectite and illite in the above-mentioned samples where U and Th occur suggests that these elements are concentrated by these clay minerals, given locally favourable physico-chemical conditions.

In the preceding sections the probable modes of occurrence of the individual elements were discussed and it was indicated that they are usually interrelated by some geochemical process. The interpretation of multiple element associations is greatly facilitated by applying PCA, but this could lead to erroneous results without taking due cognisance of the mineralogy. The

relationships of trace elements to the rock-forming minerals is more difficult to assess and PCA plays a useful role in this regard.

Table XIV The correlation of major and trace elements with clay mineral concentrations in boreholes from Vaalputs

Borehole	Lithological unit	Major clay mineral	Correlated elements
W30S10[1]	White clay	Kaolinite	Co, Cr, Nb,Th,Zr,Hf
W40N0[2]	Red clay	Kaolinite	Ti,K,P, all trace elements except Sr,Y,Co (feldspar present)
	White clay	Smectite	Al,Ca,Ga,Sr,Pb,Co,Ni Zn,Na,U
W40S10[3]	Red clay	Kaolinite	Ba,Zr,Hf,Nb,Th,Zn Ti,Mg,Rb
	White clay (lower to middle part)	Illite/ Smectite	Fe,Ti,Mn,Mg,K,P,Rb,Cs Ba,Y,Zr,Hf,V,Nb,Th,U Co,Ni,Zn,Pb
	Calcrete/ red clay	Smectite/ Illite	Ti,Fe,Mn,Cs,Sr,Ba,Zr Hf,V,Nb,Cr,Co,Cu,Zn
	White clay (upper part)	Kaolinite	Ca,Mg,K,Sr,Y,Zr,Hf V,Cu,Pb,Ga,Nb,Cr,Co
W70N0[4]	White clay	Illite	Fe,Mn,K,P,Rb,Cs,Ba,Y Zr,Hf,V,Nb,Th,Ni,Pb,Ga
	Weathered granite	Smectite	Ca,K,Co,Cr,Zn,Ga,Rb Cs,Sr,Zr,Hf,Th,Ni,Pb
W70S10[5]	Red clay (upper part)	Illite	Ca,P,Fe,Mn,K,Rb,Cs,Sr,Ba V,Nb,Cr,Th,Zn,Pb,Ga
	White clay	Smectite	Na,P,Zr,Hf,Th,Co

1 Figure 31/32 2 Figure 49/50 3 Figure 45/46
4 Figure 35/36 5 Figure 37/38

It is concluded that eight major processes are considered to have been operating in the geological environment at Vaalputs to give rise to the present distribution of elements:

i) The concentration of elements in primary minerals by magmatic and metamorphic processes.

ii) Dissolution and virtual removal of some constituents in solution to be precipitated elsewhere.

iii) Incongruent dissolution of the rock-forming minerals and subsequent formation of clay minerals and other colloidal phases such as opal.

iv) Adsorption of certain cations by these newly formed phases, as well as by silt size grains of feldspar and quartz.

v) The formation of hydrous oxides of Fe, Mn, Ti and perhaps Al and their subsequent scavenging and/or co-precipitation of certain cations.

vi) The formation of calcrete and to a minor extent also silcrete and ferruginous nodules and their co-precipitation and/or adsorption of certain elements.

vii) Local concentration of resistate minerals in the sediments.

viii) Distribution of quartz and other minerals by aeolian processes.

Mechanisms therefore exist to significantly retard the mobility of elements, including the radionuclides present in the radioactive waste. The extent to which these elements are adsorbed and retarded are controlled by the physico-chemical conditions prevailing in the sedimentary environment.

6.5 Element Enrichment and Depletion

To assess the relative enrichment or depletion of elements in the surficial rocks at Vaalputs, normalised element variation diagrams were compiled. The procedure entailed the calculation of a weighted

mean concentration for each element in all the fresh basement rock types present at Vaalputs, omitting obviously anomalously high values from the calculation. Mean element contents for the fresh basement rocks in boreholes as well as means for 37 Vaalputs regional basement rocks were calculated. The latter group was invariably of granitic composition. Mean values for all Vaalputs rock types were then normalised through division by the mean values of 37 Vaalputs regional basement rocks. The results for both major and trace elements are presented in Figures 55 and 56 respectively. To assess the relative enrichment or depletion of elements in the surficial rocks and the weathered basement, the normalised values obtained above were further normalised through division by the mean values for fresh basement rocks in boreholes mentioned above. These results are presented for both major and trace elements in Figures 57 and 58 respectively. In all the figures the results were plotted on a logarithmic scale (to the base 10) to accommodate the large range of values, but it should be noted that this has the effect of emphasising depletions more than enrichments.

Figures 55 and 56 are useful in assessing, in particular, the composition of the basement rocks in boreholes relative to the regional basement rocks in outcrop. Figure 55 shows that the basement rocks in boreholes are distinctly enriched with respect to the major elements Ti, Al, Fe, Mn, Mg, Ca and P when compared to the regional basement rocks. They have markedly lower Na and K contents and slightly lower Si contents than the regional rocks, emphasising their predominantly basic (noritic) composition. Figure 56 indicates that the borehole basement rocks are enriched in the trace elements which are commonly abundant in basic rocks e.g. Cu, Ni, Sr, V, Y, Zn and Cr, while they are impoverished with respect to the rest of the trace elements.

Considering the diagrams, normalised to fresh basement mean values in boreholes (Fig. 57), it is noticed that the red sand is most depleted with respect to all elements except Si and Mg and calcrete is similarly depleted except for Mg and Ca. The red clay shows enrichment with respect to Ti and Mg. The marked enrichment in Mg

in all the rock types (except the weathered basement) is of interest and could be explained by its abundance in calcrete but also in smectite. The weathered basement is depleted in Mg. The strong depletion of Na in all rock types is to be expected and confirms the high mobility of this element. The depletion of Mn, however, is rather surprising in view of the fact that the element is usually immobile. The most immobile elements are Si, Ti, Al, Fe and K, but P is strongly depleted.

With respect to trace elements (Fig. 58), all the rock types seem to be depleted in most elements, but notable exceptions are Nb, V, Zr, Hf, and Ba. Elements which are distinctly depleted are Cu, Zn, Ni, Sr, Ga and Cs. The depletion of Sr is also rather surprising in view of its close association with Ca. Cobalt is enriched in the weathered basement and white clay, but also abundant in the red clay. The apparent relative enrichment of U in the white clay unit is explained by the few anomalously high values in the unit. Apart from these high values U is highly mobile and all rock units are relatively impoverished in it, except the basement rocks.

The close correlation between the variation patterns of the trace elements in weathered basement and the white clay is noticeable. The major element patterns also correlate well, with the exception of Na and Mg, which are highly mobile. This correlation is considered to be supporting evidence that the white clay was derived from in-situ weathering of the basement rocks.

In conclusion it seems that with respect to the retardation of the natural isotopes of the radionuclides, Co is best retained by the lower rock units i.e. weathered basement and the clay succession, but less efficiently by the calcrete. Strontium and cesium seem to be retained by the more favourable alkaline environment near the calcretes. Strontium also appears to be relatively immobile in the weathered basement and white clay where it probably occurs in plagioclase feldspars, but in these rock types cesium is highly depleted. Uranium, despite a few anomalously high concentrations in the white and red clay, is relatively depleted in all rock types and very mobile in the environment at Vaalputs.

6.6 Geochemical Aspects of Weathering at Vaalputs

Weathering is the process whereby pre-existing rocks are broken down physically and chemically into sedimentary material and is of importance in elucidating the geochemical processes which have resulted in the present distribution of elements at Vaalputs. Chemical weathering can be regarded as the adjustment of thermodynamically unstable minerals to the surface environment of abundant water and atmospheric gases (Brownlow, 1979). Different silicate minerals weather at different rates and Goldich (1938) pointed out that the major minerals of igneous rocks tend to have a susceptibility to weathering that is the reverse of their order of crystallisation from igneous melts, as established by Bowen. This series could be used as an overall guide to weathering, but specific exceptions occur due to differences in grain size and other factors.

6.6.1 Weathering of basement rocks

The weathering pattern of basement rocks at Vaalputs is exemplified by the profiles in boreholes W90N0, W80N0 and W70N0 (Figs. 41/42, 39/40 and 35/36). These boreholes, which were drilled to the north-west of the waste disposal site (Fig. 12) into weathered granitic basement are useful in studying <u>in</u> <u>situ</u> weathering and the consequent behaviour of elements under the present climatic conditions.

The vertical variation trends of the elements are summarised as follows: The SiO_2, Al_2O_3, K_2O and Na_2O contents decrease upwards in the profile with increasing weathering, accompanied by a decrease in the trace elements Rb, Th, Y, Nb, Ga, Zr and Hf; Ca together with Mg, Ba, Sr, Cr, V, Co, Cu and Pb increase upward in the profile. Nickel and uranium remain constant and at very low concentration levels and Fe_2O_3, MnO_2, TiO_2 and P_2O_5 variations are erratic. Zn, Ti and Cs are mutually well correlated and show variable concentrations in the profile, but Cs is sligtly enriched in the sand. They probably represent the constituents of biotite which has been altered to illite in the sandy parts where Cs

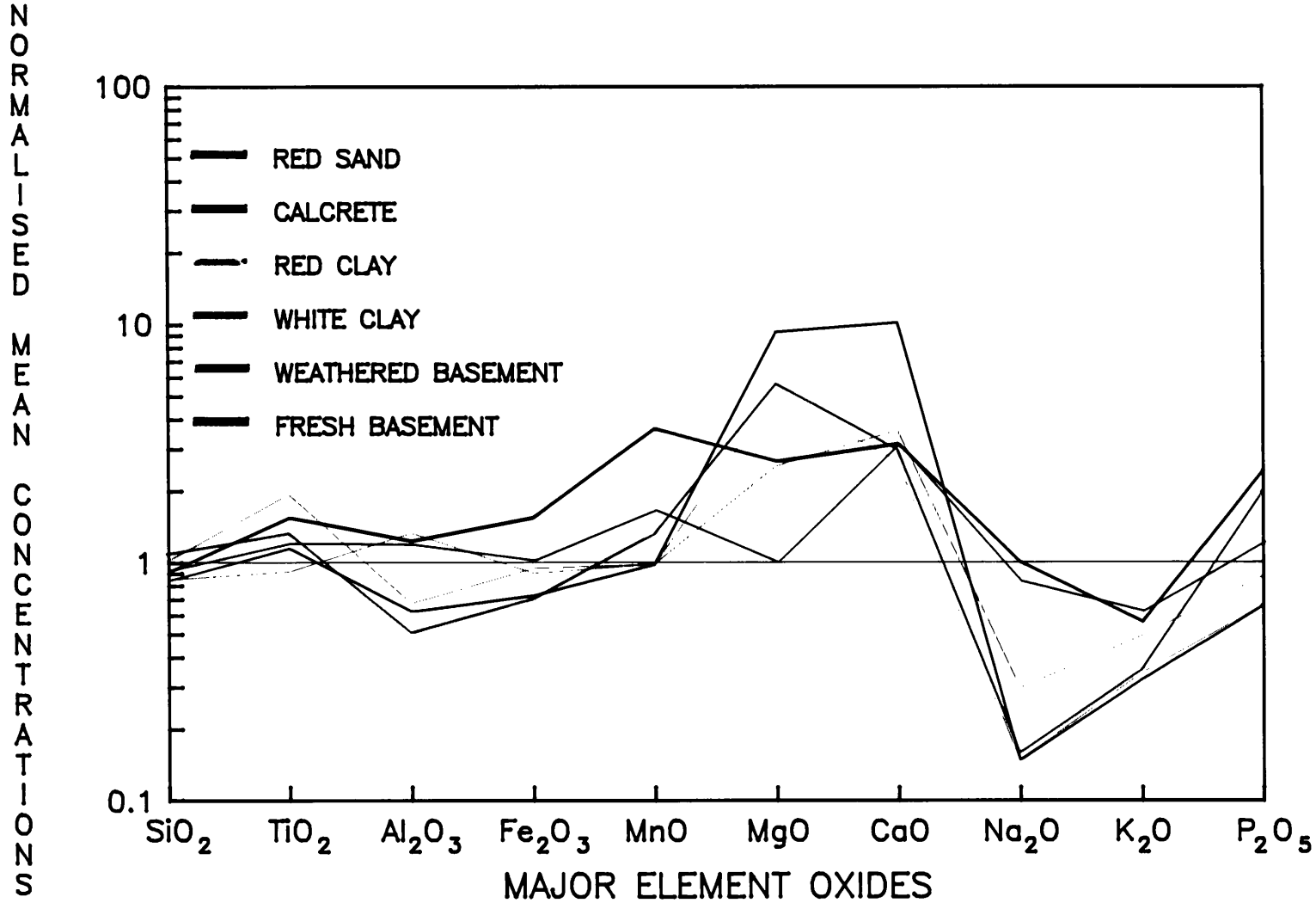

Figure 55 Major element variation diagram of Vaalputs rocks normalised to the mean value of regional basement rocks.

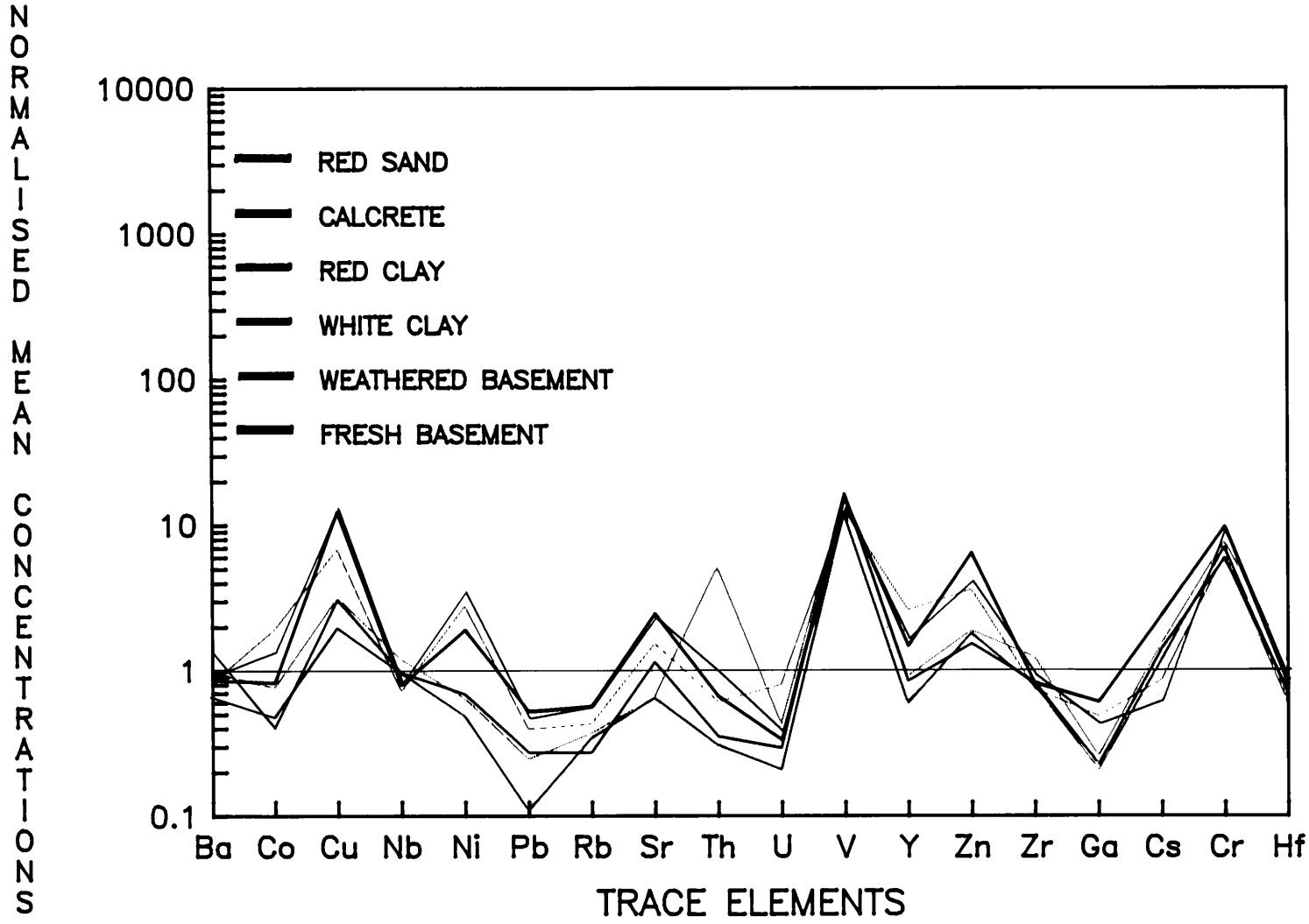

Figure 56 Trace element variation diagram of Vaalputs rocks normalised to the mean value of regional basement rocks.

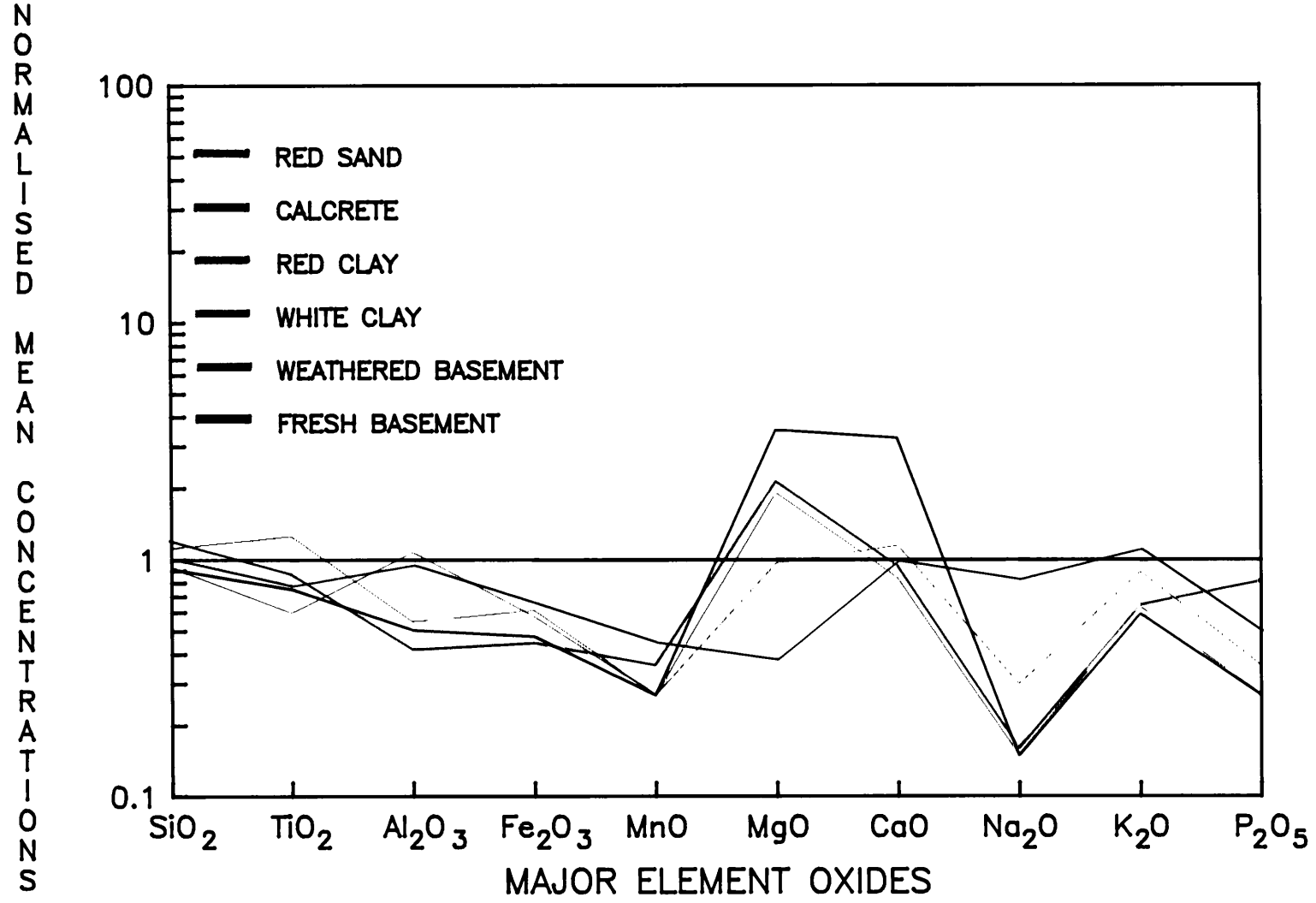

Figure 57 Major element variation diagram of Vaalputs rocks normalised to the mean value of borehole basement rocks.

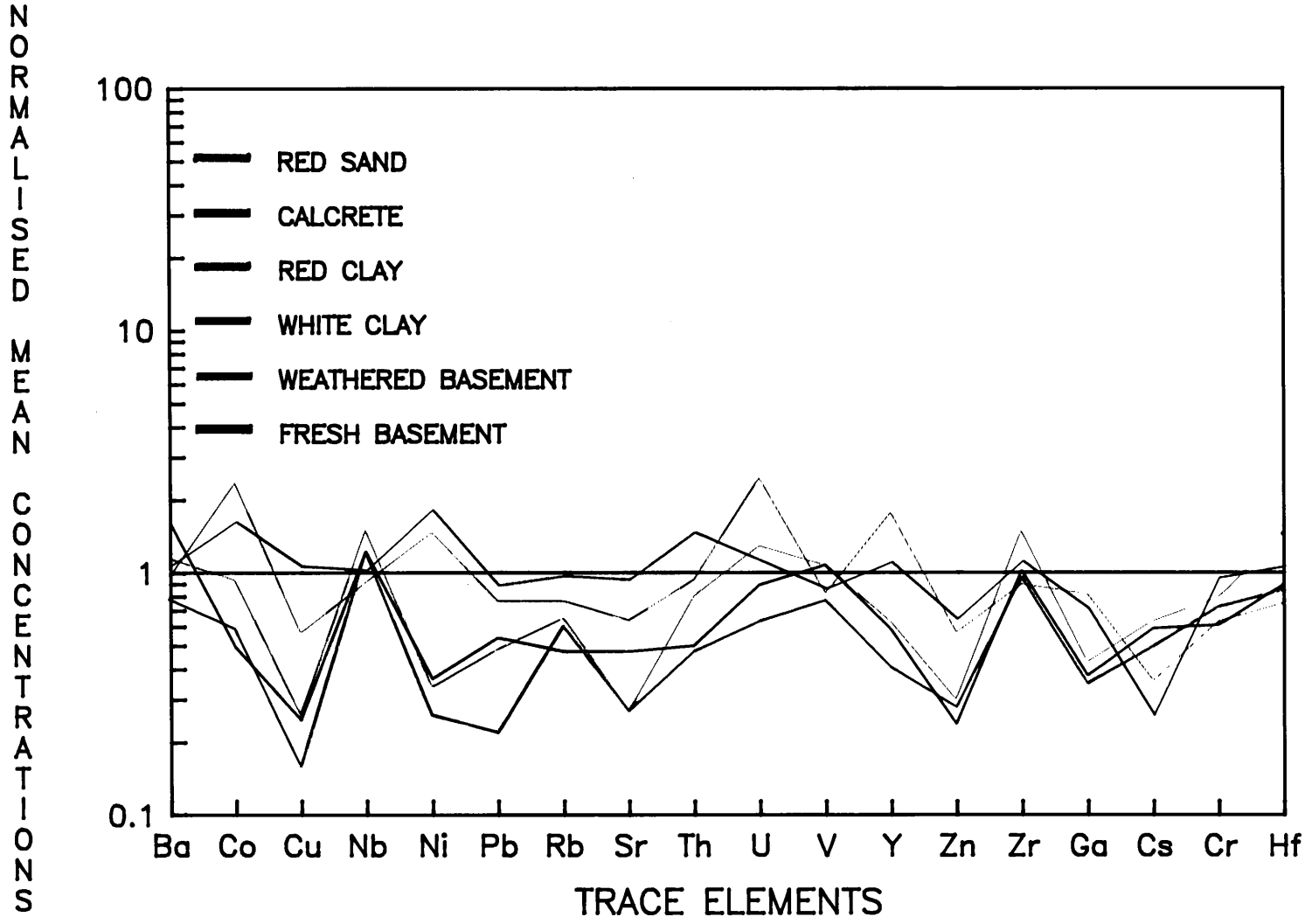

Figure 58 Trace element variation diagram of Vaalputs rocks normalised to the mean value of borehole basement rocks.

is well retained. The weathering pattern in W70N0 (Fig. 35/36) deviates slightly from the above in that Fe_2O_3 and MnO increase above the white clay unit instead of decrease as in W90N0 (Fig. 45/42) and yttrium and niobium both increase upwards in W70N0 while in W90N0 they remain either constant or show opposite trends.

Very similar trends are noted in the major and trace element variations of W70S10 (Fig. 37/38), where the trends continue through the white clay unit into the red clay unit. Minor deviations from the above-mentioned trends in W90N0 occur in W70S10 with respect to Ti, Rb, Th, and Ga, which initially decrease as in W90N0 but slightly increase upwards in the surficial rocks. The variation trends in W80N0 are also strikingly similar to those in W90N0 except for the lower CaO content of the weathered basement and white clay and the higher Fe_2O_3, TiO_2 and P_2O_5 at the boundary between the red clay and the white clay units of W80N0 (Fig. 39). The high Fe_2O_3, TiO_2, MnO and P_2O_5 contents at the boundary between the red and white clay units are due to a high magnetite content which probably accumulated on the white clay surface at the onset of deposition of the red clay. A high CaO content at the top of the white clay unit suggests calcrete formation at or near the palaeo-surface of the white clay before the deposition of the red clay. Trace elements including Y, Zr, Hf, V, Nb, Cr, Th, Co, Cu and Zn correlate with the high concentrations of Fe_2O_3 and MnO and TiO_2.

A weathering pattern different from the above-mentioned is manifested on the western portion of Vaalputs, where several flat hills with vertical cliff faces, typical of the topography of the area, are exposed. They afford a good opportunity to study in situ weathering. Five samples representing fresh to highly altered basement rocks were collected on a cliff face and these were studied chemically and mineralogically.

The major and trace element analyses are presented in Table XV. Sample FG-1 represents fresh granite and consists of perthitic microcline, albite, quartz and biotite with accessory minerals

notably zircon, ilmenite, rutile and magnetite. The degree of weathering visibly increases from sample WG-1 to WG-4. There is a distinct increase in SiO_2 content with the degree of weathering, while all the remaining major elements decrease, with the exception of MgO which shows a similar concentration in the weathered sample WG-3 as in the fresh rock. The Al_2O_3 content remains fairly constant, being highest in sample WG-2 and then decreasing markedly in WG-3 before it increases in WG-4. This trend is followed closely by Ga. There is a general decrease of all trace elements with increasing weathering with the notable exception of sample WG-2, in which Zn, Ga, Nb, Rb, Ba, Cs, Sn and W deviate from the decreasing trend and reach their highest values, except Zn. In WG-2 all the silicate minerals have been highly altered, except quartz and the accesory minerals and the sample is characterise by a high illite content, as shown by X-ray diffraction analysis, which contrasts with the high kaolinte contents of the other samples.

A similar weathering pattern was noticed in the basement to the Dasdap Formation on Rondegat, south of Vaalputs, where quartz, kaolinite and opal are the main constituents of the weathered basement. The weathering sequence as inferred from the above-mentioned description can be considered as a process of silicification and kaolinisation, during which many of the elements are leached out of the system by ground water except those which can be retained by adsorption onto clay minerals. The breakdown of this rock and subsequent transportation into a sedimentary basin constitutes a source of quartz, silicified material (silcrete) and clay minerals, mainly kaolinite. In the basement rocks which are weathering under the present day climatic conditions, the weathering products are mineralogically different from these silicified rocks and the main clay mineral formed is smectite, which affords a better barrier to element migration due to its higher cation-exchange capacity when compared to kaolinite.

6.6.2 Weathering of the surficial rocks

Although the surficial sediments are considered to be the products

Table XV Major and trace element analyses of weathered and fresh basement rocks to the west of Vaalputs.

	FG-1	WG-2	WG-3	WG-4	WG-5
		Major elements (%)			
SiO_2	72,95	74,56	74,34	82,06	82,62
TiO_2	0,23	0,21	0,23	0,00	0,02
Al_2O_3	13,99	13,49	14,09	9,96	10,52
Fe_2O_3	0,37	0,17	0,26	0,06	0,06
FeO	1,84	0,84	1,32	0,28	0,31
MnO	0,04	0,02	0,03	0,01	0,00
MgO	0,21	0,00	0,02	0,22	0,00
CaO	1,07	0,07	0,03	0,36	0,10
Na_2O	2,89	0,24	0,25	0,00	0,00
K_2O	5,68	5,15	4,32	0,51	0,65
P_2O_5	0,13	0,11	0,07	0,02	0,06
Cr_2O_3	0,00	0,00	0,00	0,03	0,04
NiO	0,00	0,00	0,00	0,00	0,00
LOI	0,40	3,64	3,57	5,01	4,05
H_2O-	0,08	0,68	0,63	0,92	0,66
TOTAL	99,88	99,18	99,16	99,44	99,09
		Trace elements (ppm)			
Zn	52	20	44	16	12
Cu	0	3	3	0	0
Ni	3	0	0	0	0
Co	0	0	4	0	0
Ga	17	18	20	13	15
Mo	4	0	0	0	0
Nb	11	10	18	5	0
Zr	212	192	160	30	60
Y	42	96	46	16	22
Sr	88	86	74	34	21
Rb	326	290	399	23	21
U	14	8	4	0	0
Th	64	59	35	0	0
Pb	48	51	40	10	9
Ba	460	553	607	143	106
Sc	10	0	0	0	0
Ce	198	145	88	35	73
Nd	58	60	42	12	26
La	75	55	41	15	0
Sn	0	0	16	0	0
W	0	0	22	0	0

FG-1 - Fresh Granite
WG-1 to WG-4 - Weathered Granite
Analyses by Rocklabs cc.

of weathering of basement rocks they are still at present subjected to weathering. The behaviour of Al_2O_3 in the surficial succession at Vaalputs is contrary to its behaviour as observed in weathering profiles in the USA (Harriss and Adams, 1966), also under arid conditions. They found that in sediments representing weathered granites, the Al_2O_3 and SiO_2 invariably show a strong inverse relationship with the former oxide increasing markedly with increasing weathering, which is opposite to the general trend at Vaalputs. However, as they point out, the apparent increase of alumina is not due to the addition of material, but rather to the loss of other constituents. At Vaalputs, Ca, Mg, Ti

and to some extent Fe and Mn and some trace elements increase upwards, which is also contrary to the above-mentioned findings and reflects the migration pattern of these elements in response to climatic conditions at Vaalputs which are favourable for calcrete formation.

The group of elements comprising K, Rb, Cs, Sr and Zn are considered by the author to be present either in K-feldspar or in the absence of the mineral to be adsorbed onto clay minerals, particularly illite, which has been shown to be abundant in the red clay. Some adsorption can possibly also take place onto kaolinite as shown in a study on the behaviour of the alkali and alkaline earth elements during weathering by Nesbitt et al. (1980). They found that during alteration of granodiorite, Sr and Ba together with Ca are lost to some extent to ground water in the early stages of weathering. Strontium is preferentially adsorbed onto clays and is not as mobile as calcium. Barium is lost to solution to some extent initially, but adsorbed onto clay minerals with advanced weathering. In contrast Rb and Cs are only lost to a minor extent during late stages of alteration when biotite is completely altered. However, in the residual material comprising kaolinite and illite, they are effectively retained by these clay minerals. The analogous behaviour of all these elements can be inferred from the element variation profiles in boreholes at Vaalputs.

The Rb/K_2O ratio was used by Nessbitt et al. (1980) to illustrate the degree of weathering in granodiorites. This ratio was shown to decrease during the early stages of alteration, and following the preferential adsorption of rubidium onto alteration products, it increased dramatically in the most altered rocks. A similar behaviour of rubidium was noted in borehole W60N0 (Fig. 59).

The element variation profile of borehole W40S10 (Fig. 45) is of interest, due to the increasing upward trend in K_2O concentration. This is interpreted as being due to the in-situ weathering of a granitic rock unit overlying one of a more basic composition, hence the upward increasing trend in constituents which

are usually more abundant in granitic rocks. In some other boreholes such as W20N0 and W40N0 (Figs. 43/44 and 49/50) the highly variable trend of element concentrations in the white clay led to the conclusion that these profiles represent heterogenous rock assemblages, as suggested by the two distinct K_2O and Rb peaks in the lower part of the white clay in borehole W20N0 (Fig. 43/44). These are interpreted as being due to the presence of boulders in the white clay or perhaps intercalations of granitic composition.

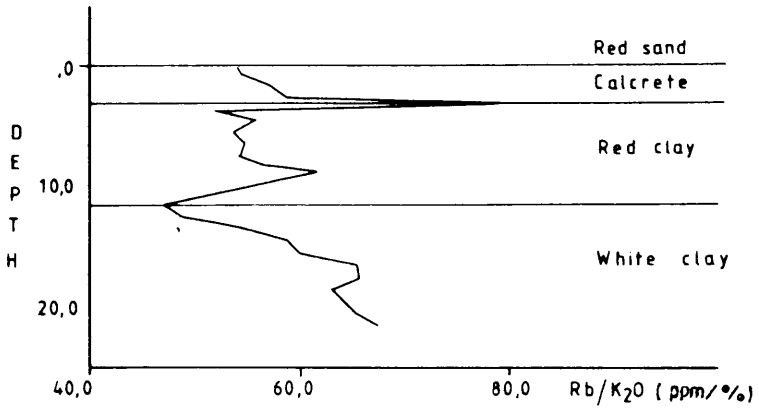

Figure 59 The variation with depth of the Rb/K_2O-ratio in borehole W60N0.

It has been noted in the section dealing with element variation that SiO_2 and Na_2O show fairly regular upward decreasing trends in boreholes W30S10, W60N0, W70N0, W80N0 and W90N0 (Figs. 31, 33, 35, 39 and 41) from fresh, through weathered basement and partially or totally into the white clay. Many other elements follow similar smooth trends, either increasing or decreasing, to a point where the trends are interrupted, possibly representing an unconformity. These trends are considered to be compelling evidence that the white clay was at least partially formed by in-situ weathering of basement at Vaalputs.

6.6.3 Physical chemistry of weathering

The physico-chemical parameters of main importance in the weathering regime are the oxidation potential, Eh, and the relative acidity or pH.

The pH-values for various rock units at Vaalputs have been determined and are presented in Table XVI. The pH in the vicinity of the calcrete layers at Vaalputs probably exceeds 8,5.

Table XVI The pH of sediments at Vaalputs

Rock unit	pH
Red sand	6,0-8,5
Calcretised red sand	8,5
Red clay	8,4
White clay	7,8

Valuable indicator elements of oxidation conditions comprise Fe and Mn, which in their reduced state are mobile in many natural environments. However, as soon as they are oxidised to their 3+ and 4+ valence states respectively, their mobilities are greatly reduced. Most reactions in the weathering environment take place in the pH range 4 - 9 and the Eh-range 0,1 - 0,6 (Fig. 60), which shows the geochemical relationship between Fe^{2+} and Fe^{3+}, also typical for some other polivalent elements e.g. Mn, U, Cu and V. The pH at which Fe^{2+} in solution precipitates as the hydroxide (pH of hydrolysis) is 5,5 (Britton, 1955 quoted by Levinson, 1974), but Figure 60 shows that this hydroxide is stable (solid part of the line) only under very reducing conditions at an Eh far below that prevailing in the weathering environment. Fe^{2+} is therefore easily oxidised to Fe^{3+}, of which the pH of hydrolysis is only 2, and ferric hydroxide immediately precipitates from solution. In the pH range 8 to 9 prevailing in the Vaalputs red clay, Fe^{3+} exists at an Eh range of +0,2 to 0,6.

Within the supergene zone, oxidation-reduction media can also be appraised by means of mineral indicators. Iron minerals are the most useful in this respect because of their bright colouring. Many minerals of trivalent iron display red, brown or yellow colours e.g. hematite, goethite and limonite, while minerals of bivalent iron are

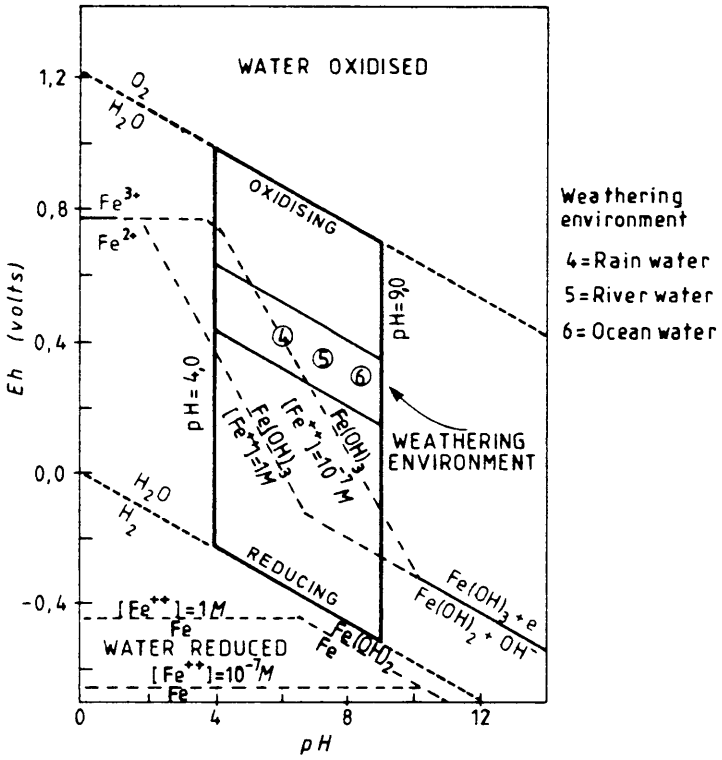

Figure 60 Diagram showing the Eh - pH conditions in the natural environment (After Levinson, 1974 and Krauskopf, 1967).

white, green or blueish (Perel'man, 1967). Such properties of iron in conjunction with its high abundance make it a good indicator of oxidising-reducing conditions. The red colour of the red clay in contrast to the white colour of the underlying white clay is therefore strongly indicative of oxidising conditions which prevailed or are still prevailing in this unit and are unfavourable for the migration of Fe^{3+}. However, in the white clay unit in which the pH is 7,8 the feldspars are distinctly free from these iron-oxide coatings, indicating that at some stage during the evolution of the Vaalputs basin, reducing conditions or low pH conditions must have prevailed in order to dissolve and transport iron out of the system.

The granitic rocks both in outcrop and those underlying the Vaalputs basin show a distinct red coloration due to hematitisation of feldspars, an indication that oxidising conditions have prevailed in them prior to the onset of the deposition of the Vaalputs sediments.

Both pH and Eh determine the concentration of an ion that will remain in solution and a change in either may be sufficient to cause precipitation. The oxidation potential may vary seasonally and may have a possible effect on the mobility of certain elements in soils (Levinson, 1974). The pH also determines the adsorption capacity of clays e.g. smectite adsorption increases with increasing alkalinity, because the hydrogen ion is preferentially adsorbed or exchanged in place of metals. Generally in a low pH environment many metals are mobile, whereas their mobility decrease as the pH increases.

6.6.4 Element mobility

Once the physico-chemical conditions in the weathering environment have been established, the relative mobilities of the constituent elements can be evaluated and compared to their observed distribution. The classification by Andrews-Jones, (1968) (Fig. 61) of element mobility is very useful in this regard and is as accurate as any classification could be, considering the great number of variables involved (Levinson, 1974).

From Figure 61 it can be seen that most of the elements that are considered in this study have very low to low mobility under all conditions that may be encountered in the geological environment at Vaalputs. The group comprising Cu, Co and Ni have medium to high mobility in oxidising and acid conditions respectively, but are immobilised at higher pH and in reducing conditions. The group consisting of Ca, Na, Mg, Sr and Zn is highly mobile in all conditions except Zn which becomes immobilised in neutral to alkaline and reducing conditions. The observed behaviour of Ca, Mg and Sr at Vaalputs, where these elements are immobile in the calcrete i.e. in an alkaline environment, contradicts this statement by Andrews-Jones (1968). Unless mechanisms existed to retain the mobile elements, Ca, Na, Mg, Zn and Sr, they would have been lost in solution during the early stages of weathering of the parent rocks from which the red clay formation had been derived. It is reasonable to assume that these sediments were highly depleted in these elements at the time of final deposition and the present day

abundance in the sediments can only be explained by upward movement from underlying white clay or basement. As mentioned previously, there are no means by which Na can be retained and it is largely lost in solution.

With regard to uranium, the observed distribution in the Vaalputs sedimentary environment is in accordance with the predictions of Andrews-Jones (1968). The high concentrations of U in some boreholes may suggest very localised reducing conditions in the rocks, where the elements could be adsorbed by clay minerals. The paucity of uranium can only be explained by its loss at very early stages of weathering while mechanisms existed to retain and ultimately fix other elements to some extent. The predicted

RELATIVE MOBILITIES	ENVIRONMENTAL CONDITIONS			
	Oxidizing	Acid	Neutral to Alkaline	Reducing
VERY HIGH			V U	
HIGH	V U Ca Na Mg Sr Zn	Ca Na Mg Sr Zn Cu Co Ni	Ca Na Mg Sr	Ca Na Mg Sr
MEDIUM	Cu Co Ni			
LOW	Si P K Pb Rb Ba Cs	Si P K Pb Rb Ba Cs Fe Mn	Si P K Pb Rb Ba Cs Fe Mn	Si P K Fe Mn
VERY LOW TO IMMOBILE	Fe Mn Al Ti Nb Cr Zr Th	Al Ti Nb Cr Zr Th	Al Ti Nb Cr Zr Th Zn Cu Co Ni	Al Ti Nb Cr Zr Th V U Zn Co Cu.Ni Pb Rb Ba Cs

Figure 61 The mobility of elements in the environment as a function of relative acidity and oxidation conditions (modified after Andrews-Jones, 1968).

behaviour of V is similar to that of U, however, its observed distribution is very dissimilar. High V concentrations in the proximity of calcrete layers were remarked on previously. The higher abundance of V together with Rb, Cs, and Ba in the vicinity of calcretes would therefore suggest not only alkaline, but also locally reducing conditions.

In addition to the chemical distribution of elements, it is believed that physical processes played a subordinate, yet important role in the dispersion of elements. The highly resistant nature with respect to attrition of zircon, magnetite, ilmenite and other accessory minerals e.g. apatite, xenotime, monazite and the titaniferous minerals and their degree of chemical inertness, prohibit the total dissolution of these minerals under the conditions which have existed at Vaalputs. A degree of physical concentration of these minerals could therefore be expected to account for some of the observed element peaks, for example Zr and Hf are often concentrated towards the base of the red clay unit where their presence in zircon has been confirmed. Other examples include iron-oxide nodules which presumably originated elsewhere and were transported into the Vaalputs sedimentary basin to form localised layers which are clearly discernible in the disposal trench walls.

In conclusion, despite the predicted high mobility of most elements in the conditions likely to be encountered in the geological environment at Vaalputs, many mechanisms exist that are able to retard element mobility, and specifically radionuclide migration in this environment.

6.6.5 Ground water chemistry

To gain insight into some of the more specific results of ground water interactions with feldspars and clays, the application of thermodynamic data within an equilibrium framework is useful. From studies of the mineralogical and chemical nature of weathered igneous rocks and from thermodynamic considerations, it is known

that the feldspar minerals are altered to clay minerals and other decomposition products. Considering only the idealised end members: K-feldspar, Na-feldspar (albite) and Ca-feldspar (anorthite), the incongruent dissolution reactions for these minerals are given by Freeze and Cherry, (1979). For the alteration of albite to kaolinite the reaction is:

$$NaAlSi_3O_8 + H^+ + 9/2H_2O \rightleftharpoons Na^+ + 2H_4SiO_4 + 0{,}5Al_2Si_2O_5(OH)_4.$$

In this reaction the major cations K, Na, Ca and pH are related to dissolved SiO_2, (as H_4SiO_4), in the pH range of 6-9, by the law of mass-action as follows:

$$K_{alb-kaol} = \frac{[Na^+]\ [H_4SiO_4]^2}{[H^+]}$$

which, expressed in logarithmic form becomes

$$\log K_{alb-kaol} = \log \frac{[Na^+]}{[H^+]} + 2\log[H_4SiO_4]$$

where the quantities in square brackets are activities.

The other reactions involving K- and Ca-feldspars can be expressed by similar relationships. These equilibrium relationships are the basis for the construction of stability field diagrams or activity-activity diagrams which are shown in Figure 62 (a,b and c). Since minerals in real systems do not have ideal chemical compositions, the stability lines based on thermodynamic data for relatively pure mineral phases probably do not accurately represent real systems. The diagrams nevertheless serve a useful purpose in the interpretation of chemical data from geohydrological systems (Freeze and Cherry, 1979).

When considering the solubilities of minerals it is important to note the effect of ionic strength. Comparison of the solubilities of minerals in pure water versus water with a high salt content indicates that the salinity increases the solubility. The increased solubility is caused by decreases in activity coefficients as a result of increased ionic strength, which is formulated as:

$$I = 0,5\Sigma(M_i Z_i^2)$$

where M_i is the molality of species i and Z_i is the valence, or charge which the ion carries. For ground water in which the six common major ions are the only ionic constituents that exist in significant concentrations, the ionic strength I is expressed as:

$$I = 0,5[(Na^+)+4(Mg^{2+})+4(Ca^{2+})+(HCO_3^-)+(Cl^-)+4(SO_4^{2-})]$$

where the quantities in parentheses are molalities. The activities of each species can be calculated or estimated from tables if the ionic strength is known.

In the law of mass action the activity coefficient for a reaction relates the activities of the components of the reaction in a simple way. These activities and the concentration of the constituent elements (expressed as molality) are again related by the relationship

$$a_i = M_i Y_i$$

where a_i is the activity of solute species i, M_i is the molality and Y_i the activity coefficient. Except for waters with extremely high salt concentrations, Y_i is less than 1 for ionic species. The activity coefficient of a given solute is the same in all solutions of the same ionic strength.

The activity coefficient for each of the species can be calculated by the Debye-Hückel equation (Garrels and Christ, 1965):

$$-\log Y_i = \frac{AZ_i^2\sqrt{I}}{1 + a_iB\sqrt{I}}$$

where Z_i and I have the designations as previously described in the definition of ionic strength and A and B are constants characteristic of the solvent at a specified temperature and pressure and can be read from published tables. The value of the quantity **a** is dependent upon the "effective diameter" of the ion in solution, and is determined largely from experiment. Published tables (Garrels and Christ, 1965; Stumm and Morgan, 1970) give the values of **a** for the most common ions. These values are usually slightly larger than ionic diameters given for ions in crystals.

Activity-activity diagrams showing stability relationships in the systems Na_2O - Al_2O_3 - SiO_2 - H_2O, CaO - Al_2O_3 - SiO_2 - H_2O, and K_2O - Al_2O_3 - SiO_2 - H_2O are shown in Figure 62 (a, b and c). Water analyses from twelve monitor boreholes (Table XVII), surrounding the waste disposal site at Vaalputs (Fig. 63) were first used to calculate the ionic strength of the ground water solution by means of the above-mentioned relationship. Having calculated the activities of cations the values were plotted on the stability-field diagrams.

The data plots show that for Na-plagioclase the dominant clay mineral which forms is Na-smectite (montmorillonite). In contact with anorthite or plagioclase of intermediate composition, kaolinite will be the stable phase. Considering the plot in the field of the K^+-ion, it is noted that the analyses cluster close to the triple junction of K-feldspar, kaolinite and illite. A low abundance of Na^+, Ca^{2+} and K^+ and a high abundance of H^+ favours formation of clay minerals from feldspars. When they form there is an increase in the abundance of Na^+, Ca^{2+} and K^+ and a decrease in the abundance of H^+. An increasing amount of dissolved silica, H_4SiO_4, favours conversion of kaolinite to montmorillonite. At concentrations above 192 ppm H_4SiO_4, amorphous silica precipitates (Brownlow, 1979).

Referring to the element variation diagrams of boreholes W30S10 and W60N0 (Figs. 31 and 33) it is noted in that the maximum development of kaolinite is in the part of the white clay where K decreases markedly and smectite is the main clay phase where Na is a maximum. In the Ca-, Mg- and Na-rich rocks of W40N0 and W40S10 (Figs. 49 and 45), smectite is the dominant clay mineral. Somewhat different results are obtained in W70N0 and W70S10 (Figs. 35 and 37) where smectite is the major clay mineral in the presence of K- and Na-rich rocks. From the above-mentioned it appears that plagioclase preferably forms smectite clay, depending upon whether Na is removed, in which instance kaolinite is the stable phase. The phase diagram for K (Fig. 62(c)) predicts that for the Vaalputs ground water composition, illite is not expected to form from K-feldspar alteration. Its presence in the surficial rocks is explained as being due to physical breakdown and chemical reconstitution of biotite and muscovite, which was shown to be possible by Brownlow, (1979). The predictions of the phase diagrams with regard to kaolinite and smectite are in accordance with the empirical data of Vaalputs .

Table XVII Water analyses of monitor boreholes around the Vaalputs Site.

Borehole	Mon 1	Mon 2	Mon3	Mon 4	Mon 5	Mon 6	Mon 7	Mon 8	Mon 9	Mon 10	Mon 11	Mon 12
					(ppm)							
F	3,4	3,3	3,2	3,1	3,0	3,2	3,0	2,9	3,0	2,8	2,9	2,6
Cl	1335,0	1327,0	1108,0	1226,0	1436,0	1227,0	1368,0	1522,0	1808,9	1531,0	1528,3	1628,7
NO_3	29,0	46,0	28,7	14,3	44,7	23,7	30,0	42,3	8,8	42,8	59,8	53,7
SO_4	338,5	329,4	293,3	298,0	356,0	313,2	341,4	356,4	390,2	365,7	372,7	386,1
Na	949,0	999,0	833,0	833,0	1034,0	781,0	1051,0	1051,0	1155,0	1068,0	963,0	1172,0
Ca	144,0	135,0	123,0	120,0	117,0	72,0	96,0	107,0	137,0	107,0	120,0	122,0
Mg	93,0	83,0	67,0	64,0	92,0	54,0	83,0	85,0	82,0	87,0	67,0	96,0
K	26,4	24,7	21,0	21,0	24,5	23,0	26,4	20,0	6,4	26,4	38,5	30,2
Si	11,4	12,6	24,0	11,5	11,0	10,3	10,4	9,4	7,5	11,9	10,6	12,0
Ionic strength	0,12	0,12	0,11	0,11	0,13	0,11	0,12	0,13	0,15	0,14	0,13	0,15
log [Na/H]	6,1	6,0	6,0	5,7	6,0	6,1	6,2	6,2	6,1	6,0	6,7	6,2
log [Ca/H]	4,8	4,6	4,7	4,4	4,5	4,6	4,6	4,6	4,6	4,4	5,3	4,7
log [K/H]	4,3	4,2	4,1	3,8	4,1	4,4	4,3	4,2	3,6	4,1	5,1	4,4
log [H_4Sio_4]	-3,4	-3,4	-3,1	-3,4	-3,4	-3,4	-3,4	-3,5	-3,6	-3,4	-3,4	-3,4
pH	7,6	7,5	7,5	7,2	7,4	7,7	7,6	7,6	7,5	7,4	8,2	7,6

Analyses by Atomic Energy Corporation of SA Ltd.

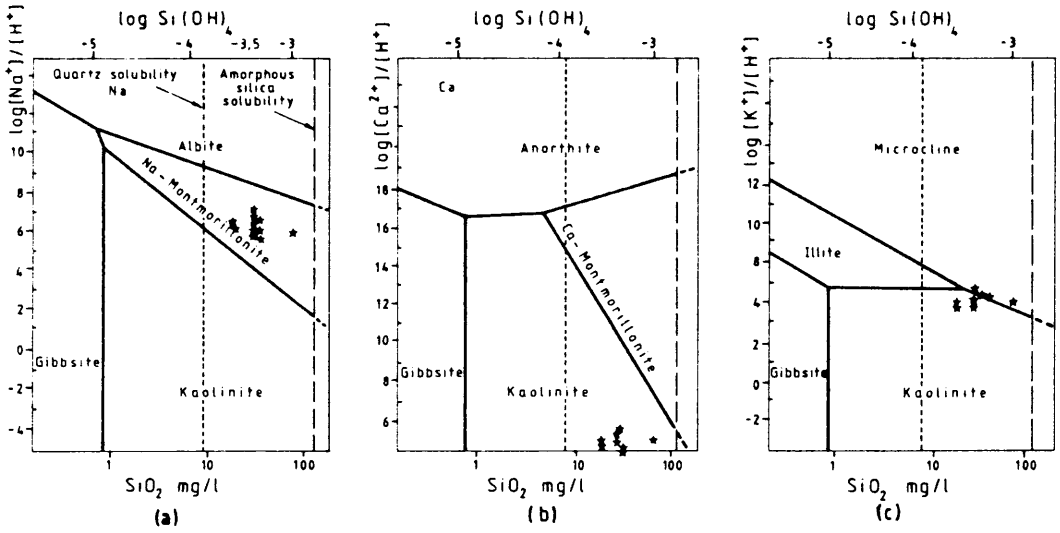

Figure 62 Activity-activity diagrams showing the stability relations of clay minerals and feldspars at 25°C and 1 bar and the plot of water analyses (indicated by stars) of monitor boreholes around the Vaalputs disposal site.

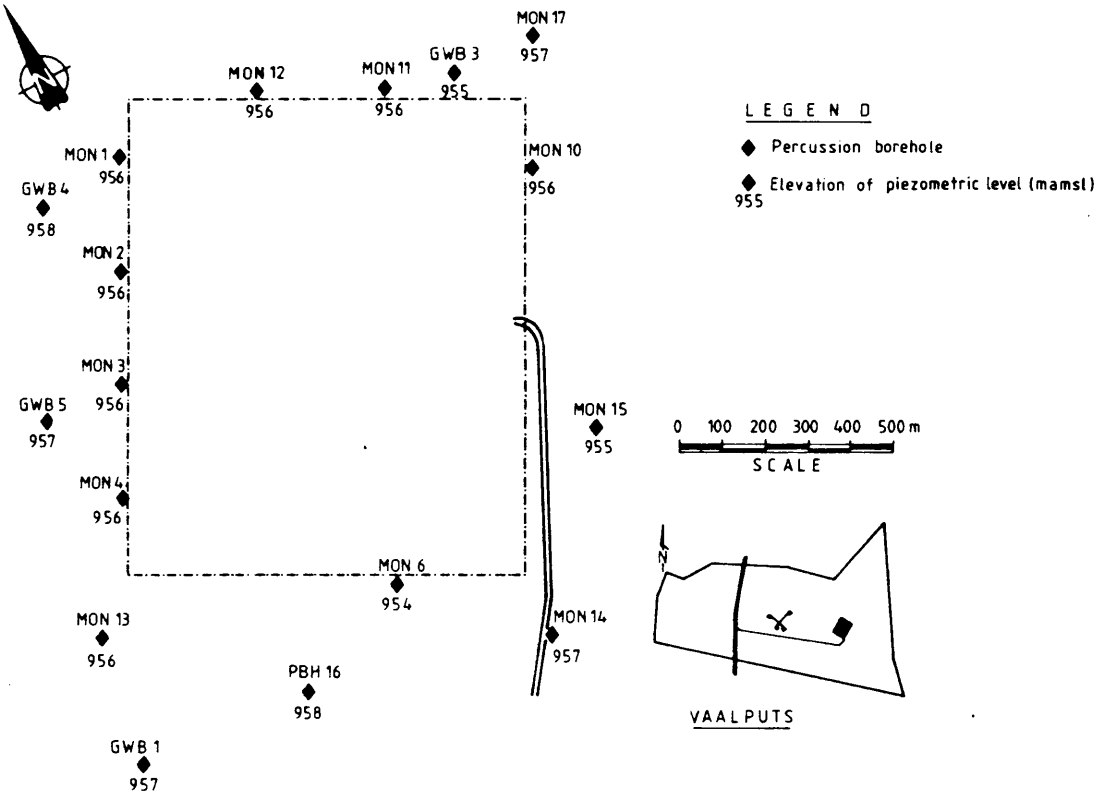

Figure 63 Map of the Vaalputs disposal site showing the location of monitor boreholes around the site

6.6.6 Discussion

During weathering and soil formation, quartz, being highly resistant to chemical disintegration processes at the temperatures prevailing in the surficial environment, is mostly physically broken down to sand or silt. A considerable proportion is also dissolved and reprecipitated during diagenesis as opal and chert. Silica from silicate minerals is far more easily released through the decomposition of these minerals.

Hydrolysis refers to those reactions of compounds with water in which a weak acid (such as H_2CO_3) or a weak base (such as NH_4OH) is formed. The weathering of silicate minerals is characterised by this type of reaction. Where the hydrolysis of aluminosilicate minerals is involved, an additional product is a clay mineral (Brownlow, 1979). Some of the silica set free in hydrolysis reactions may go into solution as colloidal silica rather than as the H_4SiO_4 molecule, but it is also possible that some of the silica precipitates as amorphous silica (Brownlow, 1979).

When the silica-alumina ratios of primary silicate minerals are compared with their clay successors, a marked decrease is evident. In K-feldspar the weight ratios of silica to alumina is 3,5:1 compared to 1,18:1 in kaolinite. There must therefore be an important outlet for dissolved silica other than by the formation of clay minerals (Goldschmidt, 1958). The solubility of silica is high under high pH conditions and this is evident in calcrete where quartz is resorbed by calcite. It is suggested that the upward decrease of SiO_2 in the profiles is the result of loss due to solution under alkaline conditions in the soil, which are conducive to the formation of calcrete. It may also be due to a dilution effect.

Opal, derived from solution (and precipitation) and possibly hydrolysis, is abundant at Vaalputs. It has been noticed microscopically in vugs in the red clay and is also associated with calcrete near the surface where it may have formed in Recent times.

It occurs in silcrete cappings overlying kaolinised basement in the western portion of Vaalputs and is abundant in the altered basement and overlying rocks belonging to the Dasdap Formation on the farm Rondegat, south of Vaalputs.

Clay minerals derived from the hydrolysis of basement rocks constitute the major components of the surficial rocks and are still forming in the basement rocks and sediments. Ion-exchange reactions are most important after initial weathering has formed clay minerals, since these minerals have a strong ability to exchange interlayer and surface ions with ions from a contacting solution. These reactions are important in the concentration of certain elements in the clay minerals, and posssibly in iron-oxides and opal. The role of oxidation in the formation of iron-oxides and their importance in concentrating elements has been discussed previously. Calcretes, formed mainly by solution and precipitation, are abundant.

The oxidation of organic carbon, iron, manganese and sulphur can be effected by micro-organisms, however, the role of organic material in the weathering process and the distribution of elements at Vaalputs is probably negligible. This is substantiated by the following observations:

- The vegetation is sparse on rocky outcrops and is likely to have been this way since the onset of sedimentation.

- After sedimentation the region was covered by aeolian Kalahari sand subsequent to which some vegetation has been established, but too little to cause the development of deep soils.

- Very little evidence of root activity or any other organic activity, except termites, is found below a depth of 60 cm. Occasional root occurrences have been detected to a depth of 7 m (the bottom of the disposal trenches) but the effect of these on the local chemistry is probably negligible.

- Termite activity is very local and is not considered to influence the role of organic activity to any great extent.

Although mechanical breakdown is considered to predominate in arid environments (Colman and Dithier, 1986), it is concluded in this study that chemical weathering has been playing a major role in the formation of the materials of the sedimentary succession at Vaalputs. The nature of this process determines the characteristics of the materials formed, their ability to retain important elements, and in this particular study, the radionuclides which may be accidentally released from the waste package. Four chemical processes have been found to be particularly important in the weathering of Vaalputs rocks, namely solution, hydrolysis, ion-exchange and oxidation. Organic reactions and mechanical breakdown of the rocks are considered to have played a minor role in this regard.

CHAPTER 7

PETROGENESIS OF BASEMENT AND SURFICIAL ROCKS

The interpretation of the petrogenesis of the Vaalputs rocks is considered here as an attempt to conciliate the observed mineralogy, geochemistry and geology of the succession.

7.1 Basement Rocks

The petrogenesis of the basement rocks is not regarded as very significant in the interpretation of the geochemical processes of the surficial succession. Suffice it to say that they originated as the result of metamorphism of ancient sediments and of syn- and post-tectonic intrusion of granitic and noritic rocks.

7.2 Surficial Rocks

7.2.1 Dasdap Formation

These sediments were interpreted by Levin et al. (1986) to have been deposited under the high energy conditions prevailing in the proximal part of an alluvial fan. The presence of Dwyka clasts in these sediments and the absence of positively identifiable Dwyka outcrops in the region suggest a time of deposition during the final stages of Dwyka erosion. The silicification of these rocks is thought to have orginated from the release of silica as a result of kaolinisation of the basement gneissic rocks. This may happen readily under humid conditions or good drainage.

The formation and evolution of iron-oxide nodules similar to those found on surfaces near Dasdap Formation rocks have been described by Nahon (1986). Their development is characterised by several stages:

- Individualisation of iron-oxyhydroxides, locally with clay from the iron-bearing parent minerals.

- Concentration of the iron into oxyhydroxide nodules.

- Formation of pseudoconglomeratic iron crusts.

This formation is characterised by two main geochemical processes:

(1) Iron accumulates, replacing quartz and kaolin by epigenetic processes, forming aluminium-bearing iron-oxyhydroxides in the shape of nodules.

2) Iron, being mobile as Fe^{2+}, migrates and leaves the kaolinite free of adsorbed iron. Variation in Eh seems to be the determining factor during this process. These variations are localised and result in small-scale migrations which are continously repeated. In the upper part of the profiles, quartz and kaolinite are progressively removed and the resultant iron-oxyhydroxides are left with aluminium in their lattice. For this process to be terminated, there must be dramatic climatic changes for sufficiently long times. Climatically affected ferricretes or laterites are presently observed in dry areas and humid areas, where iron crusts occur as relicts (Nahon, 1986).

7.2.2 White clay

The origin of the white clay could be explained by two alternative scenarios. A model for the deposition of the sediments in the Vaalputs basin has been proposed by Levin et al. (1986) from a study of the boreholes and outcrops of sedimentary rocks to the south of Vaalputs. They proposed that the sediments on Vaalputs constitute the northern distal extension of an alluvial fan originating south-west of Vaalputs. They envisage the white clay as being the equivalent of Dasdap Formation or derived largely from reworking of the Dasdap Formation. McCarthy et al. (1984) consider the

silicified weathered basement rock cappings west of Vaalputs, in which kaolinite is the main clay mineral, to represent remnants from a weathering environment which was much more humid than the present day climate or alternatively one with better drainage. The Dasdap sediments were presumably subjected to severe leaching in a similar environment. To account for the abundance of smectite in the Vaalputs white clay the hypothesis of Levin, et al. (1986) requires that the white clay in which kaolinite would have predominated, had subsequently been partially converted into smectite clay.

The partial conversion of kaolinitic clay to the present predominantly smectitic clay is likely to have happened in a fairly closed basin such as the Vaalputs Basin. The relation between porosity and pressure of compaction has been shown experimentally. At the same pressure the porosity varies considerably for the predominant clay mineral, being much higher for smectite than illite and kaolinite (Meade, 1966). Levinson (1974) states that permeability of smectite clays is higher than for illite and kaolinite respectively. It is possible that the accumulation of a thick succession of kaolinite could lead to restricted movement of fluids in the basin resulting in a build-up of the elements required for conversion of kaolinite to smectite. Elements are less mobile in poorly drained soils or soils in arid areas, which are likely to have a high pH, than in well drained soils, which are generally more acidic. In this regard Brownlow (1979) states that an increase in the amount of dissolved silica, H_4SiO_4, favours the conversion of kaolinite to smectite. This can be effected by an increase in pH.

However, little additional supporting evidence is available for the hypothesis of clay conversion. It has not been convincingly demonstrated that one clay mineral can be changed into another at ordinary temperatures, except for the change of smectite to illite. Observational evidence seems to confirm this hypothesis in some places and contradict it in others (Krauskopf, 1967). Relations between clay minerals in weathering profiles are not, as yet, well enough defined to infer a reaction relationship between minerals, or whether multiphase assemblages are stable (Velde, 1985).

Considering all the evidence it seems that the concept that the white clay is the result of in-situ weathering of basement rocks under arid conditions is more likely to be true than that of a process of smectitisation of an existing predominantly kaolinitic succession. Rocks belonging to the Dasdap Formation have been shown to have experienced considerable leaching resulting in the depletion of major elements. The white clay in contrast shows the presence of an abundance of elements and a clay mineral assemblage in which smectite is the major constituent. The chemical and morphological features of the Dasdap Formation and the white clay unit are too different to conciliate and no other hypothesis than in situ weathering can be offered as an explanation of the petrogenesis of the white clay. This is supported by the upward decreasing trend of K_2O and the loss of Rb relative to K in borehole W60NO and other boreholes. The local reworking of in situ weathered material is likely to result in the local accumulation of heavy minerals including iron-oxide nodules. An unconformity or even several, before the onset of accumulation of the overlying red clay formation in the Vaalputs basin is proposed. Signs of calcrete formation during hiatus are evident in the local concentrations of $CaCO_3$ at certain levels within the sedimentary sequence.

7.2.3 Red clay

It has been suggested by Andersen et al. (1983) that the material constituting the red clay (Vaalputs Formation) represents the distal portion of an alluvial fan which originated south-west of Vaalputs. The presence of iron-oxide nodules and blue quartz supports the notion that the material represents partially reworked Dasdap Formation rocks. There is no evidence that the iron-oxide nodules have formed in-situ in the red clay. The absence of the nodules in the white clay points to a different origin of the white clay. The abundance of SiO_2 and elements such as Zr and Hf at the base of the red clay supports an alluvial origin. During transportation of this material over some distance many of the less resistant minerals would have weathered and some of the major elements like Na, Mg, Ca and many trace elements would be largely lost. The paucity or

absence of elements such as copper and nickel leads the author to conclude that these were removed under humid conditions of weathering or good drainage of the sediments. However, the abundance of smectite, the formation of which requires low rainfall or low fluid flow, coupled with an abundance of kaolinite, suggests a depositional environment which was already arid. The abundance of smectite is explained as being the result of weathering of detrital feldspars remaining from its parent material, which was presumably different from Dasdap Formation rocks. Illite is probably the result of physical disintegration coupled with chemical reconstitution of micaceous minerals during transportation (Van der Merwe and Heystek, 1955, Brownlow, 1979). The absence of biotite in the red clay and its probable alteration to illite due to weathering is another distinguishing feature of the red clay. In addition the red clay is clearly more arenaceous than the white clay which further supports the idea that the red clay represents transported material.

7.2.4 Calcrete

Although the overall composition of carbonate sediments is relatively simple and uniform, the details of their formation and composition are quite complex. The solubility of calcite is governed by the reaction

$$CaCO_3(\text{calcite}) \rightleftharpoons Ca^{2+} + CO_3^{2-}$$

for which the solubility product, $Ksp = [Ca^{2+}][CO_3^{2-}]$ is $4{,}5 \times 10^{-9}$ at $25^{o}C$ and 1 atmosphere.

Theoretically, if at any time the product of the activity values of calcium ion and carbonate ion exceeds Ksp, calcite should precipitate. These activity values can be affected by temperature and pressure, amongst other factors. The amount of carbonate ion occurring at any place is dependent upon pH and on the amount of total dissolved carbon dioxide which in turn depends upon organic activity.

During the precipitation of calcite, important other cations can either be co-precipitated or adsorbed onto the calcite (Morse, 1986). This renders calcrete an important barrier to radionuclide migration.

The formation of calcrete involves a combination of soil forming factors namely climate, parent rock, topography, biological factors and time, which result in the migration of certain important and mobile elements to the surface to form this rock-type which is common in arid environments.

The correlation between the distribution of calcretes and climate is very marked. Well developed calcretes generally only occur where the mean annual rainfall is less than about 550 mm (Netterberg (1969). The N = 5 line of Weinert (1980), affords a good correlation with the limit of calcrete occurrence ($N = 12E_j/P_a$ where E_j = evaporation in January and P_a = annual precipitation).

Climate affects the local distribution of calcrete, for instance the preferential occurrence on certain slopes. Crowther (1930, quoted by Netterberg, 1969) found that a rise in temperature of 1 ^{o}C must be accompanied by an increase in rainfall of 33 mm in order to maintain a constant leaching effect.

Netterberg (1969) concluded that depth of calcrete is generally directly proportional to rainfall. Netterberg (1969) concludes that the maximum depth of calcrete formation for a rainfall of less than 254 mm is 1 270 mm with the mean depth in the order of 500 mm. It appears that the permeability of soil plays an important role in the depth of calcrete formation, with deeper horizons forming in more permeable soils.

Topography affects the distribution of calcrete in three ways. It creates microclimates different from the regional climate, influences runoff and erosion and, together with geology, climate and vegetation determines the position of the water table. On the whole the formation of calcretes can occur from flat ground to steep

slopes. When climatic conditions and other factors permit, calcrete would form over any parent rock which could provide the constituent elements of which calcium is the most important (Netterberg, 1969). Vegetation can influence calcrete formation by its control over the moisture regime in the soil. It can cause precipitation of carbonate by transpiration or solution of carbonate through the action of acids and carbon dioxide given off by roots.

All other factors being constant, the effect of time is to determine the stage of development of the calcrete. Boulder and hardpan calcretes are generally older than nodular calcretes, but in the instance where hardpan overlies nodular calcrete, the latter will be older because it is the precursor of the hardpan calcrete (Netterberg, 1969).

The mechanisms of formation of calcrete which have been proposed by various authors are diverse, but the most acceptable to date, for conditions prevailing in South Africa at least, is that proposed by Netterberg (1969). He proposed that solution and precipitation of calcium carbonate occurs as a result of changes in soil suction. In other words pore water pressure affects the solubility of $CaCO_3$ through its effect on P_{CO2} which is considered the most important factor in controlling solubility of $CaCO_3$.

Calcrete formation by the effect of soil suction occurs in two ways (Netterberg, 1969). The first mechanism is due to ascending ground water whereby carbonate is precipitated in the unsaturated zone above a shallow water table; the calcrete formed by this mechanism is termed non-pedogenic. The second mechanism entails the solution of existing carbonate in the upper soil horizons and its precipitation in the lower horizons at about the limit of rain infiltration; the calcrete thus formed is termed pedogenic. Many calcretes are of a complex nature, their formation having involved both mechanisms, but most South African and other calcretes are thought to be pedogenic in origin (Netterberg (1969).

The pedogenic process of calcrete formation assumes the presence of pre-existing carbonate in the soil. Assuming the hypothesis that the red clay (Vaalputs Formation) represents the distal portion of an alluvial fan, calcium being a highly mobile element, would have been largely lost from its parent material during transportation of this material to its site of deposition. The remaining calcium minerals are considered insufficient to account for the high calcium content in calcrete and calcareous layers in the present profile.

Non-pedogenic calcification due to ascending ground water could account for the formation of these calcretes, but necessitates that the ground water table at the time of formation must have been at a much higher level than at present. This could have been the case considering the hypothesis of kaolinisation and silicification during weathering of the basement rocks in palaeoclimates with higher rainfall.

The distance from the present water table to the calcrete layers is probably too great to account for their formation by the non-pedogenic process and neither are the multiple layers of calcrete explained. Calcrete nodules at various levels in the surficial formations suggest that the ground water table may have descended gradually in time, but periodically remained at a level sufficiently long to allow the formation of a thin calcrete layer.

The paucity of silcrete duricrusts at Vaalputs remains an enigma. There is general agreement that silcrete formed in a warm and more humid climate than that existing at present over much of the interior of Australia and South Africa (Leeder (1983) and Ollier (1978), quoted by Leeder, 1983). Silcretes form locally if quartz sands act as nuclei, or on a regional basis due to the accumulation and evaporation of silica-charged waters in internal drainages. Silcretes can only form as a result of prolonged pedogenic activity under stable environmental conditions. Their evolution is slow and their development is only possible under stable climatic, geological and geomorphological conditions such as occurred over much of Australia (and South Africa) in the early Cainozoic (Leeder, 1983).

7.2.5 Gordonia Formation

The petrogenesis of the red sand is considered as being merely aeolian in nature and its parent rocks could be any basement rocks in the vicinity or further afield.

In conclusion the petrogenesis of the Vaalputs rocks can be summarised as follows:

- The climate before and during deposition of the Vaalputs sediments is considered by McCarthy et al. (1984) to have been humid resulting in deep kaolinisation of the bedrock.

- During the Oligocene rapid accumulation of sediment in an extensive alluvial fan system took place.

- This was followed by the incision and degradation of the Bushmanland Plateau and degradation of fan material, giving rise to the Vaalputs sediments.

- Dune encroachment followed and later dune degradation, resulting in the present topography.

CHAPTER 8

RADIONUCLIDE RETARDATION PROCESSES

It was stated earlier that the most likely means for radionuclides to reach the biosphere is through dissolution of the waste and subsequent transport by circulating ground water. Several mechanisms exist in the geological environment to significantly constrain or delay the flow of these radionuclides. Two major processes comprise the adsorption (both physical and chemical) of radionuclides by the host rock or engineered barrier materials and secondly precipitation or incorporation of the nuclides into new mineral phases.

The primary mechanism of interaction between nuclides and host rock is adsorption-desorption which can be approached in two ways namely empirical studies of adsorption - desorption which rely on distribution coefficient measurements while mechanism studies strive to identify the processes that control nuclide retardation in the geological environment (Serne and Relyea, 1981).

8.1 Radionuclide Sorption Experiments

To quantify adsorption, the distribution of the adsorbate between the solid phase and the solution phase is measured. This value is called the distribution coefficient (K_d). Alternatively the ratio of activities can be used instead of mass. This empirical ratio does not require equilibrium conditions, quantitative reversibility or ion-exchange as the governing process, and is to be distinguished from the thermodynamic distribution coefficient which describes ideal ion-exchange.

Sorption experiments were carried out by Jakob (1983) on Vaalputs samples to determine the sorption properties of the rocks for cobalt

and uranium. The adsorption of both nuclides is highly pH dependent, being most effective at pH 6 to 7, probably by inorganic precipitation (Jakob, 1983). The pH dependency of cobalt adsorption onto three rock types from Vaalputs is shown in Figure 64. Activity ratios are plotted instead of K_d coefficients and it should be noted that a low value of A/Ao represents high adsorption and a value close to unity represents low adsorption. It can be seen from Figure 64 that adsorption of cobalt is low in the pH range 0-6, above which there is a dramatic increase in sorption for all the rock types. This implies that the calcareous portions of the white clay and the calcretes in particular should concentrate cobalt. This is indeed so in the white clay, but not in the calcrete. The calcrete samples used by Jakob were bulk samples, containing abundant clay. For most adsorption reactions the amount of cation adsorbed is proportional to the concentration of the sorbent. In the calcretes the availability of cobalt was probably low at the time of the precipitation as is seen in some profiles e.g. W40N0 (Fig. 50). Where cobalt is more abundant e.g. in red clay in W60N0, W70N0 and W80N0 (Figs. 34, 36 and 40), the cobalt concentration is indeed high in the proximity of the calcrete, although not necessarily in the calcrete itself.

With regard to uranium, the experiments by Jakob showed that uranium sorption on calcrete (Fig. 65) is a maximum at pH 4 and minimum sorption takes place at pH 5 to 6, above which there is an increase. Adsorption at pH<4, where calcrete is dissolved, is explained by a considerable clay component in this calcrete sample. In the clay, adsorption is a maximum at pH 6 (Fig. 66), above which it decreases rapidly probably as a result of complex formation. The observed uranium distribution in Vaalputs rocks, where it was noted that U is largely depleted in the sediments, is in accordance with these findings. This is confirmed by Figure 58 for calcrete, but some retention is evident in the red clay and even better retention in the white clay. It has been noted that occasional high concentrations of uranium occur in the sediments and could be attributed to locally favourable physico-chemical conditions which are conducive to its adsorption onto smectite and illite.

Experimental bulk distribution coefficients (K_d) for cobalt and uranium in some Vaalputs samples were determined by Jakob (1983) and these are listed in Table XVIII. In addition to the above, Meyer and Loots (1984) determined distribution coefficients also for other radionuclides in the Vaalputs surficial rocks and these are listed in Table XIX. The method utilised by Meyer and Loots was the batch agitation-suspension method, the most applicable for determining K_d values in the laboratory.

Table XVIII Experimental bulk distribution coefficients (K_d) for Co and U in samples of borehole W40N0

Sample	Depth (m)	pH	K_d Co	K_d U
Calcrete	1,0-2,3	8,4	1738	
Calcareous sand	8,0-8,8	8,4	1200	
Red clay	8,8-12,8	8,1	1400	
White clay	14,4-20,0	7,9	2358	
White clay	15,0-16,5	8,3		1,3
White clay	15,0-16,5	5,5		35

Jakob (1983)

Table XIX Mean K_d Values for Vaalputs rocks at pH 8,5

Rock type	U	Cs	Co	Sr
Red sand	2,5	485	1 528	9,1
Calcretised sand	2,5	589	2 295	8,4
Red clay	6,8	341	1 076	7,1
White clay	1,4	220	1 524	8,3
Weathered basement	3,0	261	578	5,5

Meyer and Loots (1984)

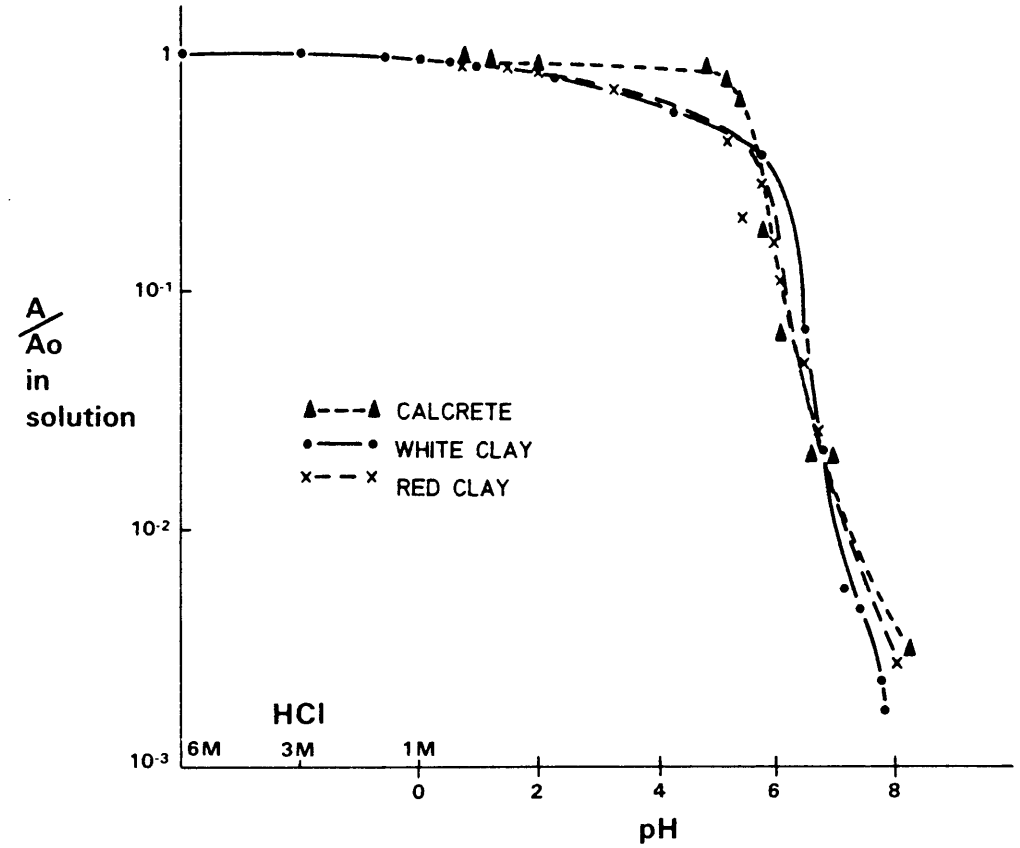

Figure 64 The adsorption of cobalt as a function of pH in bulk samples of borehole W40N0 from Vaalputs (Jakob (1983).

Ao = Initial activity of the solution

A = Final activity of the solution

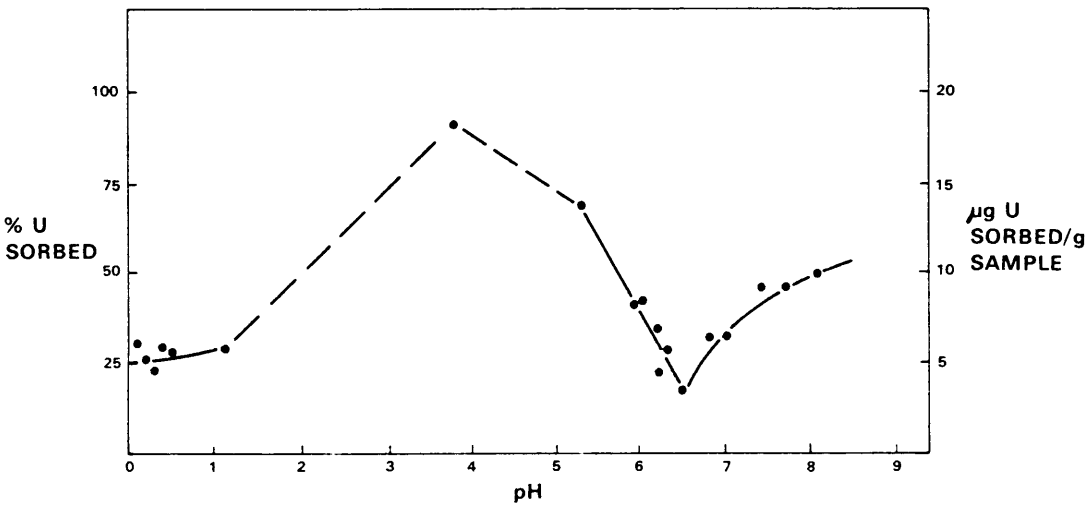

Figure 65 Uranium sorption on calcrete (0,5 - 1,0 and 2,5 - 3,2 m, in borehole W40N0 at Vaalputs after 24 h equilibration. U sorption below pH 4 is attributable to clay in sample. Total uranium used = 21,3 ppm per sample (Jakob, 1983).

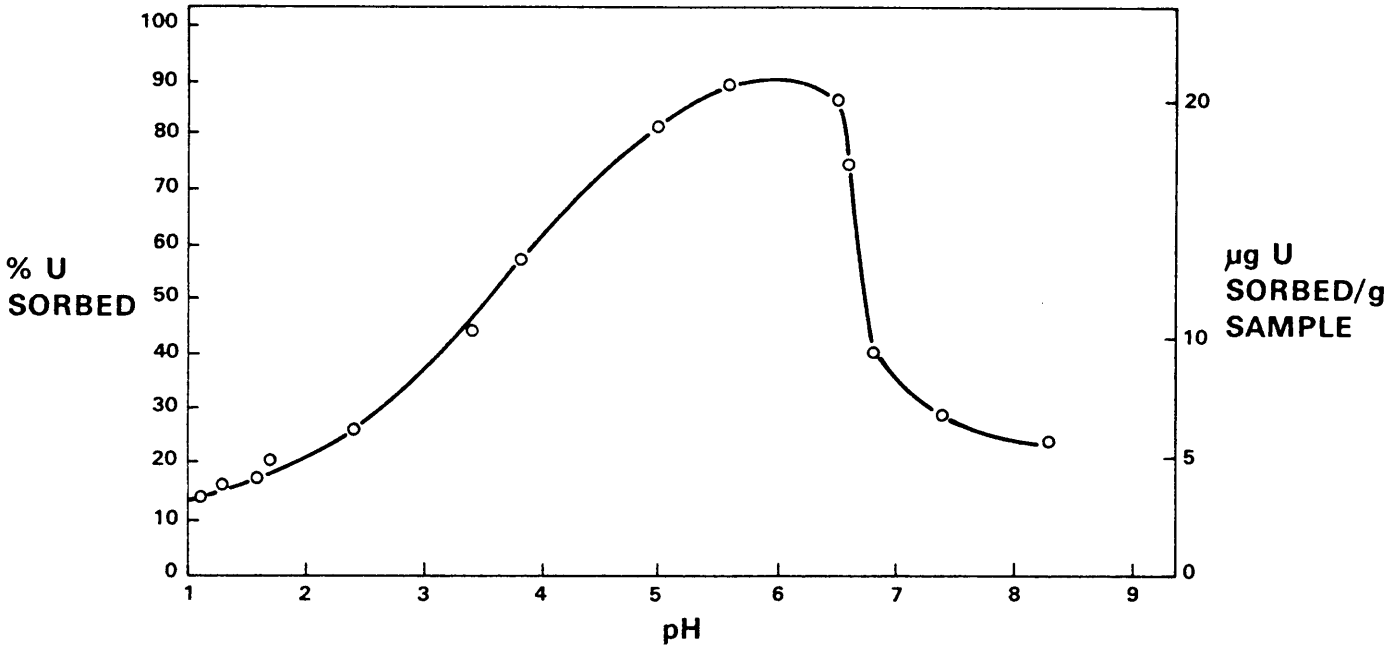

Figure 66 Uranium adsorption on clay in W40NO after 24 h equilibration. Total uranium used = 23,16 ppm per sample (Jakob, 1983).

Serne and Relyea (1981) have shown that for montmorillonite a linear relationship exists between Cs concentration and the K_d value at high Cs concentrations. Cesium adsorption onto smectite clay is strongly influenced by the presence of other competing cations. The distribution coefficient K_d for low concentrations of Cs (1,3 mg/kg) in montmorillonite at different concentrations of Na, K, Mg and Ca is shown in Figure 67. The K_d value for Cs in various potassium-bearing clay minerals as a function of potassium concentration is shown in Figure 68. It has been found that in sandy, clay-free and humus-free aquifers and in ground water saturated with varius cations, the distribution coefficient for Cs is approximately 1-500 cm^3/g and for traces of Sr, 0,5-50 cm^3/g. Therefore ^{137}Cs and ^{90}Sr migrate significantly more slowly than the groundwater flow and ^{137}Cs will in most cases migrate more slowly than ^{90}Sr. In these experiments the

distribution coefficient was determined by radiochemical analysis as the ratio of dps/g to dps/cm^3, where dps stands for disintegrations per second. K_d values measured in the laboratory

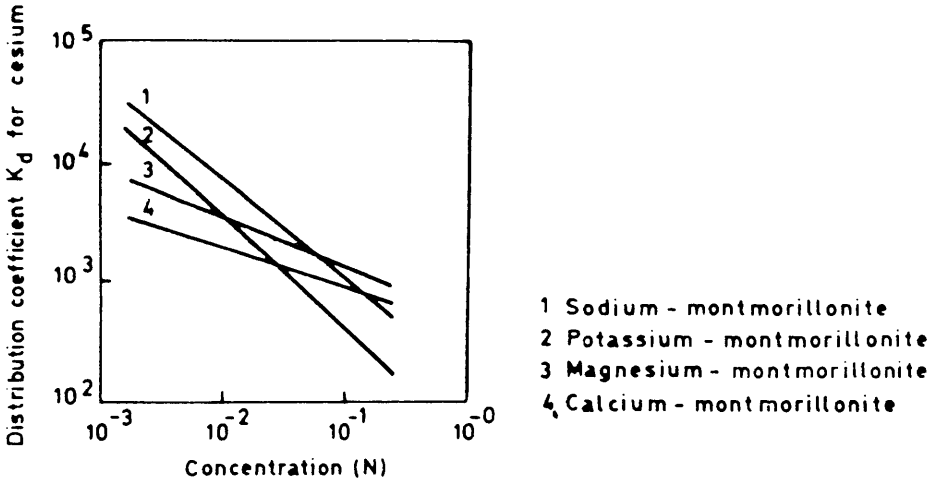

Figure 67 Distribution coefficient K_d for low concentrations of Cs in montmorillonite at different concentrations of Na, K, Mg and Ca (Wahlberg and Fishman, 1962).

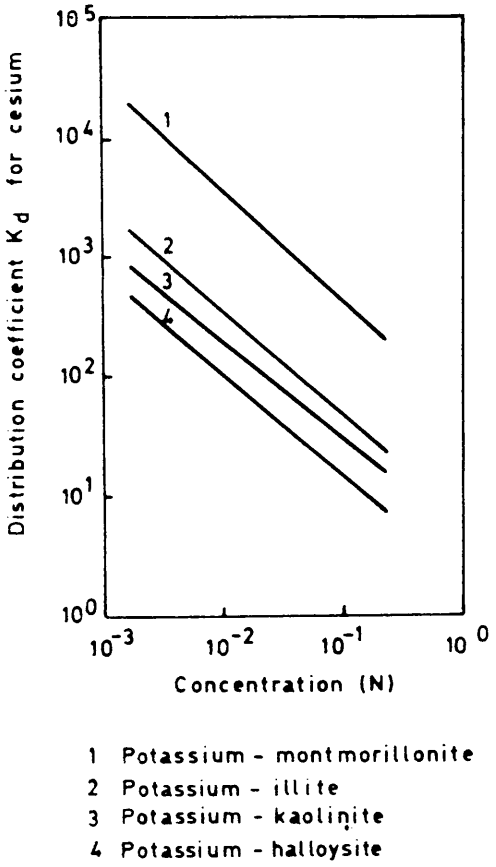

Figure 68 Distribution coefficient for low concentrations of Cs in various clay minerals as a function of K-concentration (Wahlberg and Fishman, 1962).

agree well with field observations (Matthess and Harvey, 1982, Serne and Relyea, 1981). In an intensive evaluation of the migration of ^{90}Sr and ^{137}Cs at the Chalk River Nuclear Laboratories, Canada, Jackson et al. (1980) found significant retardation of the radionuclides by exchange onto feldspars and micas, with some specifically adsorbed to Fe-, Mn- or Al-oxides or other unknown phases. Cesium retention was ascribed to adsorption and fixation onto vermiculite and biotite. There was also a significant differential movement of the radionuclides with ^{137}Cs more effectively retained than ^{90}Sr.

Sorption can be influenced by the presence of other dissolved solids. For example strontium is adsorbed better than calcium on clay minerals, nevertheless calcium strongly hinders the sorption of strontium in the soil (Mathess and Harvey, 1982). Fine calcite sand has been shown by Davis and De Wiest (1967) to have a relatively high distribution coefficient for ^{90}Sr and ^{137}Cs, the latter migrating more slowly than ^{90}Sr. Because of their different sorptive properties a separation of these cations takes place (Matthess and Harvey, 1982). The sorption and bonding strength of adsorbers such as clay minerals is a function of soil pH as found by Brown et al. (1956) and Amphlett (1958). In the low pH range, less than 5, the fraction of exchangeable alkali and alkaline earth ions amounts to more than 95% of all exchangeable metallic ions (Matthess and Harvey, 1982). In the pH range 8-12, Y, Zr and Nb again show high adsorption.

8.2 Empirical Studies

Ion exchange reactions are most important after initial weathering has formed clay minerals, since these minerals have a strong ability to exchange interlayer and surface ions with ions from a contacting solution. The normal order of preference of exchange of cations of the same valence is from strong to weak: $Cs^{+} > Rb^{+} > K^{+} > Na^{+} > Li^{+}$ and for divalents ions $Ba^{2+} > Sr^{2+} > Ca^{2+} > Mg^{2+}$. The divalent ions normally have stronger adsorption affinities than the monovalent ions, although this depends to some extent upon the

nature of the exchanger and the concentration of the solutions (Wiklander, 1964). Both affinity sequences proceed in the direction of increasing hydrated ionic radii, with strongest adsorption for the smaller hydrated ions and weakest adsorption for the largest ions. Organic materials and colloids also have good adsorption properties (Table XX) and the latter may play an important role in the retardation of elements at Vaalputs.

The abundance of smectite and illite clay at the Vaalputs site has an important bearing on its location for radioactive waste burial. The clay minerals of the smectite group have high cation-exchange capacities in comparison with kaolinite. The ion-exchange capacities of various rock types occurring at Vaalputs have been determined and are presented in Figure 69 (Jakob, 1983). The mean ion-exchange capacity (CEC) for the calcretised sand is 10 meq/100 g. The sequence of exchangeable cation is Ca>Mg>Na>K. The red clay has a similar CEC and exchangeable cation sequence. The mean CEC of the upper white clay is 31 meq/100 g and the lower portion has CEC of 20 meq/100 g. This is ascribed to the high smectite content of the white clay unit. The upper part of the white clay is characterised by a high smectite composition and this coupled with the fact that the total silt and clay content is very high in this part results in the high cation-exchange capacity.

The superior adsorption properties of clay minerals for some radionuclides have been illustrated by various investigators. The uptake of UO_2^{2+} and its hydroxocomplexes has been determined at 20°C and pH 6 for fine-grained kaolinite, illite and smectite by Borovec (1981) and a proportional relationship between adsorption capacity and cation-exchange capacity has been illustrated. At uranium concentrations below 10^{-4} mole per litre the distribution coefficients for individual minerals rise in the sequence kaolinite < illite < smectite from 50 to 10^3. The equivalence of maximum adsorption capacity with the cation-exchange capacity for smectite has also been shown by Tsunashima et al. (1981). Their experiments showed that the clay strongly preferred uranyl ions to Na^+ and K^+, but less strongly than Mg^{2+}, Ca^{2+} and Ba^{2+}.

Goldzstaub and Wey (1955) and Nuss and Wey (1956) found uranyl adsorption in the pH range 2,25 - 4,4 to be in the range 70 to 82 meq of UO_2^{2+} ions per 100 g smectite, values which approach the exchange capacity of the clay. Comparative uranium and cesium sorption studies for smectites from the Hanford site, Washington have been undertaken by Ames et al. (1982).

Uranium sorption surpassed cesium sorption and it was illustrated that temperature played an important role in sorption processes. An increase in temperature caused a decrease in cesium sorption and an increase in uranium sorption, especially in ground water with high carbonate content. The removal of excess Fe-oxide from the secondary smectite caused the uranium sorption to decrease.

TABLE XX Cation-exchange capacities of some natural substances
(in meq/100 g)

	Ion exchange capacity		
	Cations		Anions
Mineral	**Grim (1968)**	**Carroll (1959)**	**Grim (1968)**
Quartz		0,6-5,3	
Feldspar		1,0-2,0	
Kaolinite	3-15		6,6-13,3
Kaolinite (colloidal)			20,2
Nontronite			12,0-20,0
Saponite			21,0
Beidellite			21,0
Illite	10-40	10-40	
Chlorite	10-40	10-40	
Montmorillonite	80-150	70-100	23,0-31,0
Silica gel		80	
Vermiculite	100-150	100-150	4,0
Organic Substances in recent sediments	150-500		

Matthess and Harvey (1982).

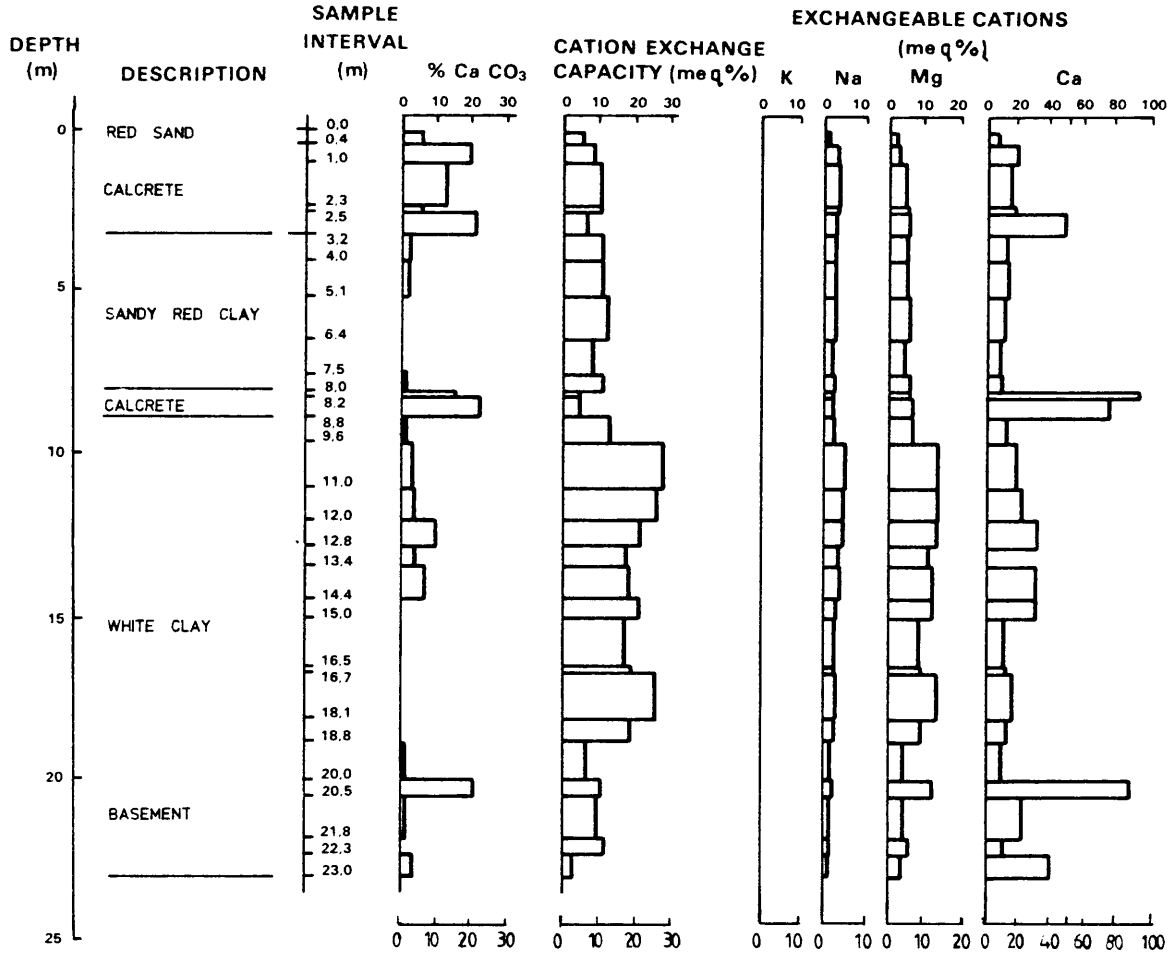

Figure 69 Depth-variation diagram showing sample interval, calcium carbonate content, cation-exchange capacity and exchangeable cations for rock types in borehole W40N0 at Vaalputs (Jakob, 1983).

Under natural conditions, the significance of clay minerals as uranium adsorbents depends upon whether they are suspended in a solution or whether they form a layer impermeable to solutions which hinders the migration and penetration of the medium. In sedimentary deposits only the smectites in fissures and joints or those finely dispersed in permeable rocks are able to adsorb large quantities of UO_2^{2+} species (Borovec, 1981).

The importance of the feldspar group minerals in adsorbing

radionuclides as illustrated by research at Whiteshell in Canada (Brown et al., 1983) is of interest to the site in question since the materials of both the basement and the surficial cover rocks contain substantial amounts of these minerals. The interaction of cesium and strontium with feldspar surfaces was studied under ambient and hydrothermal conditions i.e. in the temperature range of 130-150°C. Sorption of both cesium and strontium was observed to occur rapidly at room temperature by an ion-exchange mechanism. At higher temperature (130-150°C) secondary phases of pollucite, a cesium alumino-silicate, were formed on the surfaces of the feldspar minerals thus retarding the movement of cesium and constricting passages for the flow of groundwater which may transport other radionuclides in addition to cesium.

Several studies have been undertaken to illustrate the usefulness of iron-oxides to curb the migration of radionuclides in the geosphere. Vandergraaf et al. (1983) observed the sorption of technetium on iron-oxide inclusions in ferrous iron containing minerals such as biotite, olivine, pyroxene and hornblende and on iron-oxide coatings on micro-fractures in granite, but not on the ferrous iron minerals themselves. The studies indicated that sorption occurs only in the absence of oxygen. The bonding of ^{90}Sr in soil depends essentially on the effect of hydrated iron- and aluminum-oxides (Tamura, 1964).

In summary it can be stated that published experimental studies have shown that some of the materials constituting sediments e.g. clay minerals and iron-oxides afford an effective barrier to the migration of all radionuclides except uranium, which is of subordinate importance as a waste component. These minerals are known to occur in varying quantities in the sediments of the disposal site on Vaalputs. Although the silt and clay fractions constitute only a portion of the sediments ranging from 10% to 75% (mean value 39%) it is anticipated that these constituents will govern the geochemical behaviour of radionuclides in the event of accidental release.

The high smectite and illite contents in the vicinity of boreholes W40N0 and W40S10 (Figs. 49 and 45) and the apparent alkaline conditions prevailing in the sediments, inferred from the presence of these minerals and calcrete, favours this area for the location of the site. This area also has the highest mean percentage of clay and silt size material.

Transport of radionuclides in colloidal suspension is possible, but more study is necessary to evaluate the stability of colloids both in radiation fields and at the expected alkaline pH values of the repository. Both radionuclide solubility and sorption behaviour (and colloid stability) are highly dependent upon the environmental conditions of the repository. Temperature, pH, Eh and groundwater composition (potential complexing ligands) in particular are important factors that can control radionuclide solubility and sorption behaviour. In addition the physical and chemical characteristics of the geologic substrate are important factors in evaluating the radionuclide retardation behaviour.

CHAPTER 9

CONCLUSIONS REGARDING THE SUITABILITY OF VAALPUTS ROCKS FOR WASTE DISPOSAL

The purpose and scope of this investigation have been to study the geological environment at Vaalputs as a natural analogue to radionuclide behaviour. The criteria for the valid application of natural analogues mentioned in the introductory chapter have been met. The time scale over which element migration and retardation have taken place probably exceeds 60 million years. The physico-chemical parameters have been identified and indicate an oxidising and alkaline environment in the red clay, while in the white clay this environment is probabaly more reducing and slightly less alkaline. There appears to be no reason why the radionuclides in question will not behave chemically like the natural elements.

The geochemical processes operating in the geological environment at Vaalputs were defined, and there is no reason to believe that they will not continue to operate over the time scale in which the waste is to be stored. The major factor which could significantly change these processes is climate. The climate in Namaqualand is believed to have changed since the Cretaceous from humid to the present arid climate. However, it has not been recorded that dramatic climatic changes have occurred in a short time span or even over centuries and it is therefore concluded that this factor will probably not play an important role in changing the geochemical processes.

With regard to extraneous factors such as geological hazards which could influence the geomorphology or geohydrology, it is believed that the Vaalputs area has been tectonically stable since the mid-Tertiary times (Andreoli *et al.*, 1987). Although seismic activity has been recorded near Vaalputs this was also not considered by Andreoli *et al.* (1987) to be of significance.

McCarthy et al. (1984) concluded that geomorphologically the area is ideally suited for a waste disposal site. The location of the site near the intersection of three major watersheds ensures drainage away from the site of any hazardous radionuclides that may be present in the groundwater. The low flow rates of ground water recorded in the geohydrological environment (Levin, 1983), results in ground water of great age, up to 10 000 years. During such slow travel times any radionuclides that may be in solution will decay to safe levels before reaching the biosphere. Fracture flow could result in more rapid transport of radionuclides. The levels of concentration of natural isotopes of the hazardous nuclides are, however, known to be insignificant in the ground water and far below the permissible levels for such nuclides (Levin, 1988).

Many retardation mechanisms have been proven to exist in the Vaalputs rocks such as adsorption and ion-exchange specifically. Experimental studies elsewhere have shown that geological materials such as those found at Vaalputs are capable of significantly retarding any radionuclides that may be in solution. These observations are substantiated by empirical studies. Experimental studies of a site-specific nature at the AEC have indicated that the Vaalputs surficial rocks and minerals possess the retarding properties required for such materials for most nuclides except uranium. It was indicated that except for localised concentrations of uranium and thorium, uranium has not been retained in the sediments. Under the high pH conditions prevailing uranium easily forms carbonate complexes which are very mobile (Levinson, 1974, Garrels and Christ, 1965). Uranium is, however, not even mentioned in the list of hazardous radionuclides present in the waste package (van der Westhuizen and Moore, 1986).

Calcretes at Vaalputs are probably in chemical equilibrium with their environment and the present climate is conducive to further calcrete formation. The intermediate-level concrete waste containers will therefore also be in chemical equilibrium and it appears improbable that leaching of radionuclides would easily take place from them.

The above-mentioned discussion pertains only to low- to intermediate- level waste. With regard to high-level waste disposal entirely different concepts of storage are valid and the surficial environment will probably play an insignificant role in retaining radionuclides originating from a deep disposal facility. Analogue studies of radionuclide migration in basement rocks are nevertheless applicable to some extent. It was concluded that mechanisms exist to retard the migration of uranium significantly in oxidising conditions which are conducive to uranium migration. Under the anoxic conditions which presumably prevail in a deep repository, the factors promoting migration will be less intensive. Further research is required to assess the retarding properties of the rocks for uranium in more mobile forms such as carbonate complexes for instance, since much of the uranium present in the basement rocks are in a form not readily amenable to mobilisation e.g. uranium in refractory accessory minerals such as zircon, monazite, sphene and others.

Considering all the variables, the geological environment at Vaalputs possesses properties required to significantly retard the movement of radionuclides, relative to that of the ground water, in the event of breaching of the waste package. The Vaalputs Radioactive Waste Disposal Site has been selected following long and intensive investigations and has been proven to be eminently suitable for the purpose for which it was chosen.

ACKNOWLEDGEMENTS

This thesis forms part of studies carried out by the author during the course of his duties in the employment at the Atomic Energy Corporation of South Africa Limited. The approval of the AEC to use the results of his research for obtaining a higher degree is highly valued.

The scientific contributions of my colleagues in the Division of Earth and Environmental Technology were extensively used in the compilation of this thesis and their contributions and invaluable discussions are greatfully acknowledged.

Without the assistance of the following persons this thesis could never come to fruition and their support is greatly appreciated.

My promoters Prof C P Snyman and Prof E B Förtsch are thanked for their support and counsel.

Estelle Badenhorst and Linda Oliver for typing part of the manuscript and for their qualities of patience and tolerance to my illegible handwriting and everlasting changes.

The draughting staff, Herman van Wyk and Sheila van der Merwe for their creational abilities.

The librarians, Elize Bezuidenhout and Annatjie Bertolini for supplying research material.

Rob Heard and Nita Bath for assistance in coping with the fickle nature of computers.

My loving wife, Rita for her moral support and encouragement and my family for their sacrifice.

God my Creator and Redeemer to whom I owe gratitude for mental abilities, health and life in abundance, now and in Eternity.

REFERENCES

Ahrens, L.H. (1965). Distribution of the elements in our planet. McGraw-Hill, New York, 110pp.

Allegre, C.J., Hart, S.R., Eds. (1978). Trace elements in igneous petrology : Developments in Petrology 5. Elsevier, Amsterdam, 272 pp.

Ames, L.L., Mc Garrah, J.E., Walker, B.A., Salter, P.F. (1982). Sorption of uranium and cesium by Hanford basalts and associated secondary smectite. Chem. Geol., vol. 35, 205-225.

Amphlett, C.B. (1958). Ion exchange in clay minerals. Endeavour, vol. 17(67), 149-155.

Andersen, N.J.B., Faurie, J.N., Fernandez, L.M. (1986). Geophysical investigations on the Vaalputs Radioactive waste disposal facility in the Republic of South Africa. In : Proceedings volume : Conference on the treatment and containment of Radioactive waste and its disposal in arid environments, Cape Town, South Africa, 7-12 Sept. 1986, 57-84.

Andersen, N.J.B., Raubenheimer, E., Levin, M. (1983). The geology of the Vaalputs radioactive waste disposal site and environs. Site Selection Program for the Disposal/Storage of Radioactive Waste in S.A. Site Suitability Phase. Progress report no. 8. NUCOR Rep. PER-107, 29 pp.

Andreoli, M.A.G.; Andersen, N.J.B.; Levin, M.; Niemand, N. (1987). Geology of the Vaalputs Radioactive Waste Disposal Site in the Republic of South Africa. Explanatory notes for the Geological map of the site on the scale 1:25 000. PER-151, 40 pp.

Andrews-Jones, D.A. (1968). The application of geochemical techniques to mineral exploration. Colo. School Mines, Mineral Industr. Bull., vol. 11(6), 110pp.

Barth, T.F.W. (1962). Theoretical petrology. John Wiley & Sons, New York, 416 pp.

Berner, R.A., (1971). Principles of chemical sedimentology. Mc Graw Hill, New York, 240 pp.

Birch, G.F. (1987). The distribution of clay minerals on the continental margin off the West coast of South Africa. Trans. Geol. Soc. S.A., vol. 81(1), 23-34.

Borovec, Z. (1981). The adsorption of uranyl species by fine clay. Chem. Geol., vol. 32, 45-58.

Bradley, W.F., (1953). Analysis of mixed-layer clay mineral structures. Anal. Chem., vol. 25, 727-730.

Brown, D.L., Haines, R.I., Owen, D.G., Stanchell, F.W., Watson, D.G. (1983). Surface studies of the interaction of cesium with feldspars. In : Geochemical behavior of disposed Radioactive waste. American Chemical Society, Washington, 25-43.

Brown, R.E., Parker, H.M., Smith, J.M. (1956). Disposal of liquid wastes to the ground. Proceedings of the International Conference on the Peaceful Uses of Atomic Energy, Geneva, vol. 9, 669-675.

Brownlow, A.H. (1979). Geochemistry. Prentice Hall, New Jersey, 498 pp.

Brynard, H.J. (1983). Fission-track studies of uranium distribution in geological samples. In: ICAM 81 - Proceedings of the First International Congress on Applied Mineralogy. Spec. Publ. Geol. Soc. S. Afr., No. 3, 413-418.

Brynard, H.J. (1983). Preliminary mineralogical investigations of borehole samples from the proposed Waste Disposal Site at Vaalputs. Site Selection Program for the Disposal/Storage of radioactive waste in S.A. Site Suitability Phase. Progress report no. 15. NUCOR Rep. PER-111, 39 p.

Brynard, H.J. (1986). On the tracks of uranium. Nuclear Active, July, 25-28.

Carroll, D. (1970). Clay minerals : a guide to their X-ray identification. Spec. Pap. Geol. Soc. Amer., No. 126, Colorado, USA, 75 pp.

Carroll, D. (1959). Ion-exchange in clays and other minerals. Bull. Geol. Soc. Am., vol. 70, 749-780.

Chapman, N.A., Smellie, J.A.T. (1986). Introduction and summary of the natural analogue workshop held at Lake Geneva, Wisconsin, U.S.A., Oct. 1984. Chem. Geol., vol. 55, 167-173.

Chapman, N.A., McKinley, I.G., Smellie, J.A.T. (1984). The potential of natural analogues in assessing systems for deep disposal of high-level radioactive waste. SKAB, Stockholm, KBS Tech. Rep. TR-84-16, and NAGRA, Basel, Tech. Rep. NTB 84-41.

Colman, S.M., Dethier, D.P. (1986). Rates of chemical weathering of rocks and minerals. Academic Press, London. 600 pp.

Day, F.H. (1963). The chemical elements in nature.
Reinhold, New York, 372 pp.

Davis, S.N., De Wiest, R.J.M. (1967). Hydrology.
2nd ed. John Wiley, New York, 463 pp.

Davis, J.C. (1970). Statistics and data analysis in geology.
John Wiley, New York, 550 pp.

De Villiers, W. Van Zyl. (1983). Die bepaling van spoorelemente in uraanertse met behulp van X-straalfluoressensie-spektrometrie.
Kernkor verslag PER-80, 74 pp.

Ford, W.E. (1949) Dana's textbook of mineralogy.
4th ed., John Wiley & Sons, New York, 851 pp.

Freeze, R.A., Cherry, J.A. (1979). Groundwater.
Prentice-Hall. 604 pp.

Friedman, G.M. (1959). Identification of carbonate minerals by staining methods. Journal of Sed. Pet., vol. 299(1), 87-97.

Garrels, R.M., Christ, C.L. (1965). Solutions, minerals and equilibria. Freeman, San Francisco, 450 pp.

Garrels, R.M. (1967). Genesis of some ground waters from igneous rocks, In : Abelson, P.H., Researches in geochemistry, vol. 2, John Wiley, New York, 405-420.

Glossary of geology. (1972). American Geological Institute, Alexandria, Virginia. 805pp.

Goldich, S.S. (1938). A study in rock weathering.
J. Geol., vol. 46, 17-58.

Goldschmidt, V.M. (1958). Geochemistry,
Oxford University Press, London. 730 pp.

Goldzstaub, S., Wey, R. (1955). Adsorption of uranyl ions by clays.
Bull. Soc. Franc. Miner. Cristallogr., vol. 78, 242-248.

Graf, D.L. (1960). Geochemistry of carbonate sediments and sedimentary carbonite rocks : Part II : Sedimentary Carbonite Rocks. Illinois Geol. Surv., Circular 301, 71 pp.

Grim, R.E. (1968). Clay mineralogy,
2nd ed., McGraw-Hill, New York, 596 pp.

Harris, R.C., Adams, J.A.S. (1966). Geochemical and mineralogical studies on the weathering of granitic rocks.
Am. J. Science, vol. 264, 146-173.

Hart, R J; Andreoli, M.A.G. (1985). Geochemical and petrographic classification of the granitic rocks in the Vaalputs area. Site Selection Program for the Disposal/Storage of Radioactive Waste in South Africa. Site Suitability Phase Progress report no. 31. PER-134, 17 pp.

Hillel, D. (1971). Soil and water : physical principles and processes. Academic Press, New York. 288 pp.

Holland, J.G., Marais, J.A.H.. (1983). The significance of the geochemical signature of the Proterozoic of the Namaqualand Metamorphic Complex with special reference to the Okiep District. In: Botha, B.J.V.. Ed. Namaqualand Metamorphic Complex. Spec. Publ. no. 10. Geol. Soc. S.A., Johannesburg, 83-90.

Jackson, K.C. (1970). Textbook of lithology. McGraw Hill, New York, 551 pp.

Jackson, R.E., Inch, K.J. (1980). Hydrogeochemical processes affecting the migration of radionuclides in a fluvial sand aquifer at the Chalk River Nuclear Laboratories, N.H.R.I. Paper no. 7, Science Series no. 104, Ottawa.

Jakob, W.R.O. (1983). Preliminary geochemical studies on the soil characteristics from the Vaalputs Radioactive Waste Disposal Site. Site Selection Program for the Disposal/Storage of Radioactive Waste in South Africa. Site Suitability Phase. Progress report no. 17. (unpublished report).

Jenny, E.A. (1968). Controls on Mn, Fe, Co, Ni, Cu, and Zn concentrations in soils and water : The significant role of hydrous Mn and Fe oxides. Amer. Chem. Soc., Advances In Chemistry Series, no. 73, 337-387.

Johns, W.D., Grim, R.E., Bradley, W.F. (1954). Quantitative estimations of clay minerals by diffraction methods. J. Sedim. Petrol., vol. 24, 242-251.

Joubert, P. (1971). The regional tectonism of the gneisses of part of Namaqualand. Bull. Precamb. Res. Unit, Univ. Cape Town, vol. 10, 220 pp.

Krauskopf, K.B. (1967). Introduction to geochemistry. McGraw Hill, New York, 721 pp.

Krauskopf, K.B. (1956). Factors controlling the concentrations of thirteen rare metals in seawater. Geochim. Cosmochim. Acta, vol. 9, 1-32.

Krumbein, W.C., Sloss, L.L. (1963). Stratigraphy and sedimentation. 2nd ed., Freeman, San Francisco, 660 pp.

Kühnel, R.A. (1987). The role of cationic and anionic scavengers in laterites. Chem. Geol., vol. 60(1/4), 31-40.

Kunze, G.W. (1965). Pre-treatment for mineralogical analysis. In: Methods in soil analysis. Vol. 1, American Soc. of Agronomy, Madison Wisconsin. 568-598.

Leeder, M.R. (1983). Sedimentology. London, George Allen & Unwin, 344 pp.

Le Maitre, R.W. (1982). Numerical Petrology : Statistical interpretation of geochemical data. Developments in Petrology 8. Elsevier, Amsterdam, 281 pp.

Levinson, A.A. (1974). Introduction to exploration geochemistry. Applied Publishing, Illinois, 924 pp.

Levin, M. (1983). Geohydrological investigations of the Vaalputs radioactive waste disposal site and environs. Site-selection program for the disposal/storage of radioactive waste in S.A. Site suitability phase. Progress report no. 9. NUCOR Rep. PER-112, 37 pp.

Levin, M., Raubenheimer, E. (1983). Results of the percussion drilling program on the Vaalputs radioactive waste disposal site. Site-selection program for the disposal/storage of radioactive waste in S.A. Site suitability phase. Progress report no. 10. NUCOR Rep. PER-113, 24 pp.

Levin, M., Niemand, N., Le Roux, J.P. (1986). Reports on the Dasdap formation. Site Selection Program for the Disposal/Storage of Radioactive Waste in South Africa. Site Suitability Phase. Progress report no. 44. (Unpublished report).

Levin, M. (1988). A geohydrological appraisal of the Vaalputs radioactive waste disposal facility in Namaqualand, South Africa. Unpublished Ph.D thesis, University of the Orange Free State, 235 pp.

Lukashev, K.I.L. (1970). Lithology and geochemistry of the weathering crust. Israel Program for Scientific Translations, Jerusalem. 368 pp.

Matthess, G., Harvey, J.C. (1982). The properties of ground water. John Wiley, New York, 406 pp.

McCarthy, T.S., Levin, M., Moon, B.P. (1984). Geomorphology of the Vaalputs low-level Radioactive Waste Disposal Site and Environs. Site Selection Program for the Disposal/Storage of Radioactive Waste in S.A. Site Suitability Phase. Progress report no. 23. NUCOR Rep. PER-121, 32 pp.

McKenzie, R.M. and Taylor, R.M. (1968) The association of cobalt with manganese oxide minerals in soils. Trans. Ninth Intern. Congr. Soil Sci., vol. 2, 577-584.

Meade, R.H. (1966). Factors influencing the early stages of the compaction of clays and sands : review. J. Sed. Petrology, vol. 36, 1085-1101.

Meyer, A.J., Loots, W.G. (1984). Determination of distribution coefficients (Kd) values on samples obtained from the proposed site for intermediate - and low level waste. NUCOR Rep. PER-119. 19 pp.

Morse, J.W. (1986). The surface chemistry of calcium carbonate minerals in natural waters : an overview. Marine Chemistry, vol. 20, 91-112.

Nahon, D.B. (1986). Evolution of iron crusts in tropical landscapes. In: Colman, S.M., Dethier, D.P., Eds., Rates of chemical weathering of rocks and minerals. Academic Press, London, 169-191.

Nesbitt, H.W., Markovics, G., Price, R.C. (1980). Chemical processes affecting alkalies and alkaline earths during continental weathering. Geochim. Cosmochim. Acta, vol. 44, 1659-1666.

Netterberg, F. (1969). The geology and engineering properties of South African calcretes; Vol. 1, Summary, classification, distribution, composition and origin. D.Phil. thesis, Univ. Witwatersrand, Johannesburg, 312 pp.

Norrish, K., Hutton, J.T. (1969). An accurate x-ray spectrographic method for the analysis of a wide range of geological samples. Geochim. Consmochim. Acta, vol. 33, 431-453.

Nolan, G.A. (1976). Concretionary manganese-iron oxides in streams and their usefulness as a sample medium for geochemical prospecting. J. Geochem. Explor. vol. 6, 193-210.

Nuss, L., Wey, R. (1956). Sur l'adsorption des cations uranyles par la montmorillonite. Bull. Soc. Franc. Argiles, vol. 7, 15-19.

Partridge, T.C., Maud, R.R. (1987). Geomorphic evolution of Southern Africa since the Mezozoic. S.A. J. of Geology, vol.90(2). 179-208.

Perel'man, A.I. (1967). Geochemistry of epigenesis. Plenum Press, New York, 266 pp.

Pierce, J.W., Siegel, F.R. (1979) Quantification in clay mineral studies of sediments and sedimentary rocks. Journal of Sed. Pet., vol. 39(1). 187-193.

Price, P.B., Walker, R.M. (1962). Chemical etching of charged particle tracks. J. Appl. Phys., vol. 33, 3407.

Price, W.A. (1933). Reynosa problem of South Texas and origin of caliche. Bull. Amer. Ass. Petrol. Geol., vol. 17(5), 488-522.

Redding, S.J., Hutson, J.L. (1983). Part I : The general climate of Bushmanland. Part II : estimates of percolation at the buried waste facility, Bushmanland. Site Selection Program for the Disposal/Storage of Radioactive Waste in South Africa. Site Suitability phase. Progress report no. 16. NUCOR Rep. PER-114, 33 pp.

Reuning, E. (1930). A contribution to the geology and palaeontology of the western edge of the Bushmanland plateau. Trans. Roy. Soc. S. Afr., vol. 21, 33-39.

Robb, L.J., Schoch, A.E. (1985). Deuteric alteration and uranium mineralization processes in leucogranite intrusions from the Namaqualand Metamorphic Complex, South Africa. In : Proceedings of Symposium on high heat production (HHP) granites, hydrothermal circulation and ore genesis. Institution of Mining and Metallurgy, London, 301-314.

Robb, L.J. (1987). Fission track micro-mapping and uranium distribution in basement rocks from the Vaalputs radioactive waste disposal site. AEC unpublished report.

Rogers, A.W. (1911). Geological survey of parts of Van Rhynsdorp and Namaqualand divisions. Ann. Rep. Geol. Com., 84 pp.

Rösler, H. J., and Lange, H. (1972). Geochemical tables. Elsevier, Amsterdam, 468 pp.

Schröcke, H., Weiner, K. L. (1981). Mineralogie - Ein Lehrbuch auf systematischer Grundlage. Walter de Gruyter, Berlin, 952 pp.

Schultz, L.G. (1964). Quantitative interpretation of mineralogical composition from X-ray and chemical data for the Pierre shales. U.S. Geol. Surv. Prof. Paper. 391-C, 31 pp.

Serne, R.J. Relyea, J.F. (1981). The status of radionuclide sorption-desorption studies performed by the WRIT program. Waste Rock Interactions Technology Program, Prepared for the US Department of Energy under contract DE AC06-76RLO 1830 by the Pacific Northwest Laboratory. 79 pp.

Siever, R.,Beck, K.C., and Berner, R.A. (1965) Composition of interstitial waters of modern sediments, Jour. Geol., vol.73, 39-73.

Silk, E.C.H., Barnes, R.S. (1959). Examination of fission-fragment with an electron microscope. Phil. Mag., vol.4, 970 -971.

Spencer, P.H., Röhm, H.F., Harris, M.I.J. (1986). Radioactive waste disposal : solutions pursued in South Africa by Escom. Conference on the Treatment and Containment of Radioactive Waste and its Disposal in Arid Environments, Cape Town, South Africa. 7 - 12 Sept. 1986.

South African Committee for Stratigraphy (SACS), (1980). Stratigraphy of South Africa. Part 1 (Comp. L. E. Kent). Lithostratigraphy of the Republic of South Africa/Namibia and the Republics of Boputhatswana, Transkei and Venda: Handb. geol Surv. S. Afr., 8, 690 pp.

Stumm, W., Morgan, J.J. (1970) Aquatic chemistry - An introduction emphasizing chemical equilibria in natural waters. Wiley-Interscience, New York, 583 pp.

Tamura, T, (1964). Selective ion-exchange reactions from cesium and strontium by soil minerals. Comptes Rendus Du Colloque International sur la Rétention et la Migration d'Ions Radioactifs dans les Sols, Saclay, Paris, 1962, 95-104

Tauson, L. V., Kravchenko, L. A. (1956). Characteristics of lead and zinc distribution in minerals of Caledonian granitoids of the Susamyr Batholith in Central Tian-Shan. Geokhimiya, no. 1, 78-88.

Taylor, S.R. (1966). The application of trace element data to problems in petrology. Phys. Chem. Earth, vol. 6, 133-213.

Taylor, R.M. (1968) The association of manganese and cobalt in soil - further observations. J. Soil Sci. vol.19, 77-80.

Thiry, M., Millot, G. (1987). Mineralogical forms of silica and their sequence of formation in silcretes. J. Sedimentary Petrology, vol. 57(2), 343-352.

Tsunashima, A., Brindley, G.W., Bastovanov, M. (1981). Adsorption of uranium from solutions by montmorillonite : composition and properties of uranyl montmorillonites. Clays and Clay Minerals, vol. 29(1), 10-16.

Vandergraaf, T.T., Ticknor, K.V. , George, I.M. (1984). Reactions between technetium in solution and iron-containing minerals under oxic and anoxic conditions. In : Geochemical behavior of disposed Radioactive waste. American Chemical Society, Washington, 25-43.

Van der Merwe, C.R., Heystek, H. (1955). Clay minerals of South African soil groups: III. Soils of the desert and adjoining semiarid regions. Soil Sci., vol. 80, 479-494.

Van der Westhuizen, H.J., Moore, P.E. (1986). Radioactive waste disposal in South Africa. In : Proceedings of conference on the treatment and containment of Radioactive waste and its disposal in arid environments, 7-12 Sept., Cape Town, South Africa, 963-982.

Velde, B. (1985). Clay minerals : a physico-chemical explanation of their occurrence..Elsevier, Amsterdam, 450 pp.

Visser, J.N.J. (1985). The Dwyka formation along the north-western margin of the Karoo basin in the Cape Province, South Africa. Trans. Geol. Soc. S. Afr., vol. 88(1), 37-48.

Wahlberg, J.S., Fishman, M.J. (1962). Adsorption of cesium on clay minerals. U.S. Geological Survey Bulletin, no. 1140A, 40 pp.

Weinert, H. H., (1964) Basic igneous rocks in road foundations. Research Report 218, CSIR, Pretoria.

Whittaker, E. J. W., Muntus, R. (1970). Ionic radii for use in geochemistry. Geochim. Cosmochim. Acta, vol.34, pp.945 - 956.

Wilson, M.J. (1987). A handbook of determinative methods in clay mineralogy. Blackie, New York, 308 pp.

Znamenskii, E.B., Rodionoval, L.M., Kakhana, M.N. (1957). Distribution of niobium and tantalum in granites. Geokhimiya, no. 3, 267-270.

APPENDIX A

Locality map of regional basement rocks of which analyses were used for normalisation in element enrichment/depletion diagrams

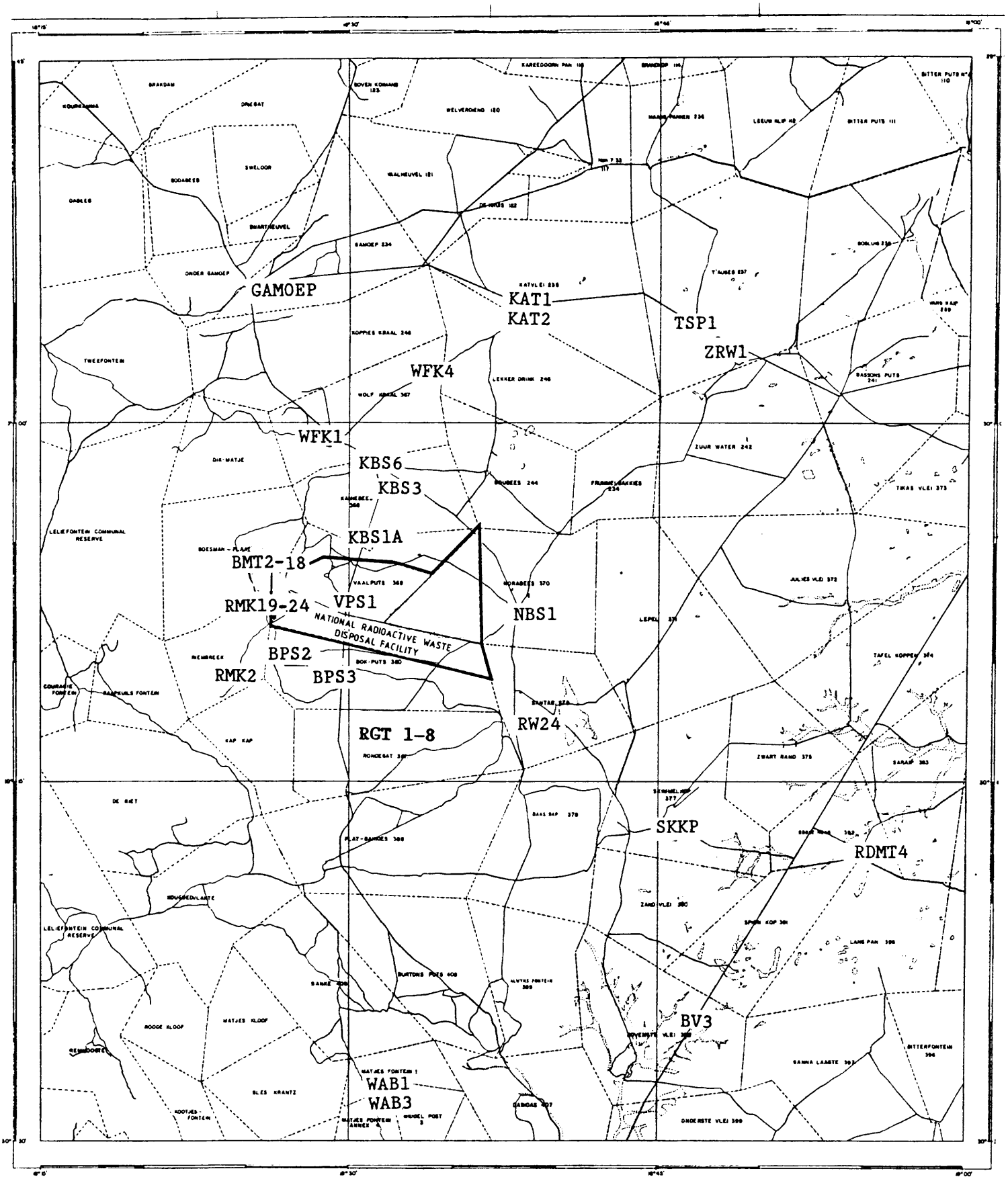

APPENDIX B

Mineralogical composition of the <2 µm clay fraction and mass percentage of the fraction <45 µm in Vaalputs boreholes

Mineralogical composition of the <2 µm clay fraction and mass percentage of the fraction <45 µm in borehole W30S10

Sample number	Sample depth (m)	Mineralogical composition of <2 µm fraction (mass %) Smectite	Illite	Kaolinite	Mass % silt and clay <45µm
RED SAND					
1	0,0-0,7	10	66	24	20,4
CALCRETE					
2	0,7-2,0	9	83	8	43,2
RED CLAY					
3	2,0-3,0	14	61	25	46,0
4	3,0-4,0	16	66	17	65,2
5	4,0-5,0	23	57	20	46,4
CALCRETE					
6	5,0-6,0	21	7	72	57,6
RED CLAY					
7	6,0-7,0	30	30	40	58,0
8	7,0-8,0	30	28	42	51,2
9	8,0-9,0	35	47	18	47,2
WHITE CLAY					
10	9,0-11,0	17	14	69	51,6
11	11,0-12,0	13	14	73	57,2
12	12,0-13,5	22	13	65	51,2
13	13,5-15,0	24	17	59	-
WEATHERED GRANITE					
14	15,0-15,7	42	19	39	38,4
FRESH GRANITE					
15	15,7-17,0	40	19	41	39,6

Mineralogical composition of the <2 µm clay fraction and mass percentage of the fraction <45 µm in borehole W40N0

Sample number	Sample depth (m)	Mineralogical composition of <2 µm fraction (mass %) Smectite	Illite	Kaolinite	Mass % silt and clay <45 µm
RED SAND					
1	0,0-0,4	21	32	47	26,0
CALCRETE					
2	0,4-1,0	5	83	12	26,8
3	1,0-2,3	18	59	23	29,2
RED CLAY					
4	2,3-2,5	16	71	13	36,4
CALCRETE					
5	2,5-3,2	17	70	13	44,8
RED CLAY					
6	3,2-4,0	25	56	19	45,6
7	4,0-5,1	14	27	59	58,8
8	5,1-6,4	15	17	69	58,4
9	6,4-7,5	29	31	40	40,0
10	7,5-8,0	24	49	26	36,4
CALCRETE					
11	8,0-8,2	18	74	8	41,2
12	8,2-8,8	27	63	10	39,2
RED CLAY					
13	8,8-9,6	44	41	15	36,0
WHITE CLAY					
14	9,6-11,0	63	16	21	52,4
15	11,0-12,0	62	9	29	58,0
16	12,0-12,8	54	34	12	52,8
17	12,8-13,4	57	14	29	44,8
18	13,4-14,4	59	11	30	56,8
19	14,4-15,0	78	2	20	50,0
20	15,0-16,5	88	2	9	40,0
21	16,5-16,7	81	6	13	38,8
22	16,7-18,1	79	12	9	46,0
23	18,1-18,8	92	2	6	38,4
24	18,8-20,0	84	12	4	22,0
25	20,0-20,5	87	13	0	43,2
WEATHERED TONALITE					
26	20,5-21,8	79	10	11	17,6
SPINEL-RICH LAYER					
27	21,8-22,3	92	4	4	34,4
FRESH TONALITE					
28	22,3-23,0	82	2	16	21,2

Mineralogical composition of the <2 µm clay fraction and mass percentage of the fraction <45 µm in borehole W40S10

Sample number	Sample depth (m)	Mineralogical composition of <2 µm fraction (Mass %) Smectite	Illite	Kaolinite	Mass % silt and clay <45 µm
RED SAND					
1	0,0-1,0	7	87	6	21,8
CALCRETE					
2	1,0-2,0	12	72	16	22,4
RED CLAY					
3	2,0-6,0	18	55	27	50,0
4	6,0-9,0	27	51	22	52,8
WHITE CLAY					
5	9,0-12,0	30	59	11	67,2
6	12,0-14,0	40	50	11	56,0
7	14,0-16,0	29	66	5	75,2
8	16,0-16,5	31	63	6	67,6
9	16,5-16,8	30	66	4	62,8
10	16,8-17,0	32	62	6	50,4
11	17,0-20,0	32	58	10	63,6
12	20,0-25,0	37	59	4	48,4
WEATHERED ANORTHOSITE					
13	25,0-28,0	54	37	9	12,4
FRESH ANORTHOSITE					
14	28,0-32,0	51	40	9	9,6

Mineralogical composition of the <2 µm clay fraction and mass percentage of the fraction <45 µm in borehole W60N0

Sample number	Sample depth (m)	Mineralogical composition of <2 µm fraction (Mass %) Smectite	Illite	Kaolinite	Mass % silt and clay <45 µm
RED SAND					
1	0,0-0,3	3	85	12	8,8
CALCRETE					
2	0,3-1,0	11	81	8	27,2
3	1,0-2,1	14	55	31	26,0
4	2,1-2,6	13	61	26	46,4
5	2,6-27	11	81	8	46,0
RED CLAY					
6	2,7-3,1	20	70	10	49,6
7	3,1-4,2	16	68	16	46,8
8	4,2-5,0	21	44	35	33,6
9	5,0-6,0	32	48	20	35,6
10	6,0-7,0	30	42	28	37,6
11	7,0-8,0	44	25	31	42,4
12	8,0-8,5	29	20	51	49,2
13	8,5-9,0	29	24	47	53,6
14	9,0-10,0	29	20	51	41,2
15	10,0-10,9	36	27	37	30,0
WHITE CLAY					
16	10,9-12,0	36	24	40	26,8
17	12,0-13,0	24	10	66	22,4
18	13,0-14,0	23	15	62	24,0
19	14,0-15,0	20	7	73	20,4
20	15,0-16,0	30	24	46	21,6
21	16,0-17,0	33	15	52	24,0
22	17,0-18,0	35	6	59	28,4
23	18,0-19,0	39	12	48	21,6
24	19,0-19,8	38	15	46	21,6
WEATHERED GRANITE					
25	19,8-21,0	43	28	29	19,6
FRESH GRANITE					
26	21,0-22,0	37	27	36	21,2

Mineralogical composition of the <2 µm clay fraction and mass percentage of the fraction <45 µm in borehole W70N0

Sample number	Sample depth (m)	Mineralogical composition of <2 µm fraction (Mass %) Smectite	Illite	Kaolinite	Mass % silt and clay <45 µm
RED SAND					
1	0,0-2,3	3	89	7	31,6
RED CLAY					
2	2,3-6,0	24	62	14	42,4
CALCRETE					
3	6,0-7,8	27	53	19	46,8
WHITE CLAY					
4	7,8-11,5	22	12	65	36,8
5	11,5-15,0	27	39	34	32,4
WEATHERED GRANITE					
6	15,0-19,0	44	11	44	44,4
7	19,0-22,5	36	15	48	28,4
8	22,5-24,5	48	26	26	21,6
FRESH GRANITE					
9	24,5-26,5	28	42	31	26,8

Mineralogical composition of the <2 µm clay fraction and mass percentage of the fraction <45 µm in borehole W70S10

Sample number	Sample depth (m)	Mineralogical composition of <2 µm fraction (Mass %) Smectite	Illite	Kaolinite	Mass % silt and clay <45 µm
RED SAND					
1	0,0-1,0	0	96	4	29,2
CALCRETE					
2	1,0-2,0	9	72	19	27,2
RED CLAY					
3	2,0-3,0	18	67	15	31,2
4	3,0-6,0	31	50	19	35,6
5	6,0-8,5	50	5	45	28,8
WEATHERED GRANITE					
6	8,5-9,5	47	18	35	39,6
FRESH GRANITE					
7	9,5-10,0	65	26	9	26,4

APPENDIX C

Mass percentage variation with depth of seven grain size fractions from borehole W40N0 and total mass percentage of silt and clay fractions (<45 µm)

Sample depth(m)	Mass percentages of grain size fractions							Total mass % silt and clay (<45 µm)
	+45 µm	+63 µm	+125 µm	+250 µm	+425 µm	+850 µm	+1700 µm	
0,0-0,4	3,2	8,4	17,6	20,4	28,0	15,3	7,1	81,9
0,4-1,0	4,6	10,9	20,1	21,0	22,0	13,3	8,1	74,0
1,0-2,3	1,9	4,7	8,2	8,5	12,0	54,1	54,1	81,8
2,3-2,5	2,2	6,4	11,8	12,6	15,4	12,4	39,4	70,3
2,5-3,2	4,4	8,4	15,9	17,0	18,8	11,2	24,2	54,9
3,2-4,0	3,5	8,6	17,7	18,8	29,6	15,9	5,9	51,8
4,0-5,1	4,8	8,5	15,6	15,6	25,5	16,9	12,9	46,4
5,1-6,4	3,0	12,4	17,6	20,6	19,0	11,5	16,1	39,2
6,4-7,5	3,5	8,6	17,0	17,1	23,7	14,2	16,0	66,4
7,5-8,0	3,0	8,0	20,6	23,6	24,5	13,5	6,9	62,6
8,0-8,2	3,8	10,9	21,6	17,3	25,8	14,1	6,5	54,2
8,2-8,8	2,9	11,8	16,7	21,3	23,1	15,1	9,1	68,9
8,8-9,6	4,7	11,5	18,8	22,0	21,8	13,5	7,7	63,3
9,6-11,0	7,9	11,4	16,9	15,9	17,8	11,2	18,9	42,1
11,0-12,0	9,7	15,7	16,1	21,7	15,1	9,7	11,9	41,2
12,0-12,8	6,2	13,1	14,6	24,4	15,7	9,4	16,6	40,1
12,8-13,4	5,0	7,9	16,8	24,4	23,4	18,6	3,9	48,6
13,4-14,4	7,9	17,4	16,8	27,2	13,6	11,5	5,7	47,1
14,4-15,0	7,8	26,9	18,3	31,9	11,4	2,7	1,0	53,8
15,0-16,5	7,5	22,6	19,4	30,1	15,8	3,8	0,9	58,9
16,5-16,7	10,2	22,2	20,4	30,4	13,1	3,0	0,7	56,1
16,7-18,1	7,1	21,2	19,1	30,3	16,2	4,4	1,7	52,9
18,1-18,8	8,0	22,8	17,9	32,3	13,1	4,4	1,6	60,7
18,8-20,0	4,7	10,9	16,8	20,5	22,6	15,0	9,6	72,7

APPENDIX D

MAJOR ELEMENT ANALYSES OF VAALPUTS BOREHOLE SAMPLES

Borehole W20N0

	SiO_2	TiO_2	Al_2O_3	Fe_2O_3	MnO	MgO	CaO	Na_2O	K_2O	P_2O_5	LOI	H_2O-	TOTAL	$CaCO_3$
							(%)							
RED SAND														
1	81,97	0,32	3,75	1,27	0,01	0,00	0,41	0,31	1,28	1,38	1,38	0,28	92,36	1,00
CALCRETE														
2	68,30	0,27	6,16	2,19	0,01	5,29	7,54	0,33	1,58	0,02	9,29	1,99	102,97	13,50
3	71,09	0,42	9,98	3,53	0,01	2,85	5,88	0,43	2,04	0,04	8,12	2,33	106,72	9,40
RED CLAY														
4	70,84	0,46	9,76	3,58	0,02	2,33	3,46	0,47	2,03	0,05	6,37	1,71	101,08	5,50
5	71,15	0,42	8,24	2,99	0,01	1,46	4,82	0,55	2,09	0,02	6,64	1,23	99,62	8,70
6	76,57	0,32	7,81	2,83	0,01	1,09	2,83	0,51	2,19	0,04	4,67	1,05	99,92	4,50
7	79,98	0,49	8,25	3,19	0,01	1,05	0,45	0,47	2,22	0,05	2,92	1,07	100,15	1,00
8	76,88	0,43	8,14	3,16	0,01	2,15	1,45	0,50	1,84	0,03	4,23	1,72	100,54	1,50
CALCRETE														
9	67,69	0,41	6,95	2,57	0,01	1,65	8,77	0,40	1,42	0,03	9,98	1,30	101,09	15,30
10	61,19	0,41	6,78	2,45	0,02	1,20	12,26	0,35	1,10	0,03	13,00	1,08	99,87	22,20
RED CLAY														
11	73,81	0,56	10,05	3,65	0,03	2,58	0,96	0,54	1,53	0,02	5,07	1,97	100,77	0,50
12	71,65	0,31	9,90	2,16	0,01	3,33	3,15	0,45	2,12	0,02	7,61	1,31	102,02	7,70
WHITE CLAY														
13	75,36	0,17	11,94	1,74	0,01	1,18	0,73	0,47	2,52	0,04	4,55	1,24	99,95	0,50
14	66,94	0,26	13,97	5,27	0,01	2,67	0,81	0,63	1,53	0,06	6,16	4,34	102,65	0,50
15	74,43	0,22	12,49	1,59	0,01	0,68	0,55	0,68	5,23	0,04	3,08	1,01	100,01	0,50
16	72,62	0,28	13,20	1,84	0,01	0,39	0,63	0,75	5,47	0,05	3,05	0,66	98,95	0,50
17	63,02	0,39	15,69	5,41	0,01	1,63	3,57	0,79	1,29	0,06	7,45	2,13	101,44	4,90
18	71,00	0,17	13,81	3,01	0,01	0,85	2,96	1,45	1,13	0,03	4,13	1,07	99,62	1,40
19	67,61	0,16	16,35	3,04	0,01	0,84	3,00	1,88	1,70	0,03	3,14	1,01	98,77	0,50
20	74,00	0,19	11,67	1,73	0,01	0,00	0,75	2,28	4,86	0,02	1,13	0,33	96,97	1,00
21	71,79	0,15	13,12	2,76	0,01	0,00	1,92	1,91	4,23	0,04	2,38	0,55	98,86	1,00
22	37,24	0,68	11,93	17,64	0,03	2,07	12,51	0,61	0,76	0,08	15,59	1,89	101,03	0,50
23	64,56	0,33	15,31	5,93	0,02	0,07	4,12	2,40	1,66	0,02	2,54	0,52	97,48	1,90
WEATHERED SPINEL-ANORTHOSITE														
24	55,53	0,57	17,22	12,73	0,12	0,81	4,69	2,03	0,98	0,07	3,23	0,87	98,85	0,50
WEATHERED TONALITE														
25	62,27	0,17	18,76	4,65	0,03	0,00	5,16	3,41	1,30	0,04	1,72	0,43	97,94	2,00
26	64,78	0,39	17,41	5,71	0,02	0,00	4,34	3,42	1,70	0,06	1,28	0,28	99,39	2,80
27	69,86	0,19	14,96	2,90	0,03	0,00	2,77	2,89	3,50	0,04	1,00	0,17	98,31	1,00

Borehole W30N0

	SiO_2	TiO_2	Al_2O_3	Fe_2O_3	MnO	MgO	CaO	Na_2O	K_2O	P_2O_5	LOI	H_2O-	TOTAL	$CaCO_3$
							(%)							
RED SAND														
1	82,20	0,20	3,47	1,82	0,01	0,64	5,25	0,26	1,01	0,04	5,89	0,49	101,28	10,20
CALCRETE														
2	65,41	0,24	6,53	3,84	0,01	1,34	10,07	0,68	1,55	0,04	11,45	1,04	102,20	18,50
RED CLAY														
3	70,76	0,43	10,06	2,67	0,02	2,04	3,82	0,39	1,86	0,05	7,53	1,41	101,04	7,00
4	75,83	0,75	10,12	3,85	0,03	nd	1,12	nd	1,37	0,03	5,31	1,24	99,65	0,00
5	79,77	0,49	8,12	3,52	0,02	0,82	0,61	0,35	1,34	0,02	3,96	0,76	99,78	1,00
6	63,01	0,44	12,42	4,78	0,01	2,73	1,95	0,28	2,86	0,05	13,19	0,98	102,70	20,60
WHITE CLAY														
7	67,30	0,30	7,81	2,64	0,01	1,61	10,19	0,33	0,81	0,05	6,88	0,95	98,88	2,00

Borehole W30S10

	SiO_2	TiO_2	Al_2O_3	Fe_2O_3	MnO	MgO	CaO	Na_2O	K_2O	P_2O_5	LOI	H_2O-	TOTAL	$CaCO_3$
							(%)							
RED SAND														
1	86,66	0,58	6,33	2,92	0,01	0,33	0,17	0,38	1,53	0,03	1,89	0,68	101,51	0,50
CALCRETE														
2	59,19	0,38	8,93	3,31	0,01	2,79	10,51	0,39	1,75	0,02	12,63	1,99	101,90	19,10
RED CLAY														
3	68,45	0,43	8,93	3,26	0,02	1,16	6,67	0,76	2,18	0,04	8,76	1,46	102,12	11,30
4	75,39	0,56	9,36	3,61	0,03	1,67	2,13	0,47	1,97	0,04	5,24	1,72	102,19	3,90
5	73,17	0,52	7,94	4,13	0,02	1,99	3,29	0,40	1,65	0,02	5,81	1,62	100,56	5,90
CALCRETE														
6	63,60	0,52	7,20	3,32	0,02	1,27	11,14	0,29	1,22	0,03	12,86	1,27	102,74	18,50
RED CLAY														
7	79,49	0,46	7,63	3,32	0,02	1,25	1,81	0,34	1,39	0,04	4,50	1,23	101,48	2,90
8	75,32	0,65	7,10	2,73	0,01	1,20	3,83	0,28	1,03	0,03	6,19	1,34	99,71	7,00
9	82,11	0,78	7,11	2,50	0,03	1,99	0,36	0,37	0,87	0,02	3,47	1,45	101,06	0,50
WHITE CLAY														
10	65,24	0,70	14,16	0,55	0,01	0,95	4,81	0,18	0,31	0,04	10,86	0,73	98,54	9,90
11	63,81	0,34	16,09	2,46	0,01	0,45	3,31	0,25	0,50	0,03	10,00	0,53	97,78	6,80
12	66,49	0,32	15,72	2,57	0,01	0,07	2,39	0,23	3,92	0,06	6,58	0,48	98,84	4,00
13	69,47	0,31	14,63	3,20	0,01	0,05	1,06	0,62	4,99	0,07	4,11	0,52	99,04	1,00
WEATHERED GRANITE														
14	71,62	0,57	11,75	6,42	0,01	0,00	0,93	1,53	3,85	0,03	2,25	0,27	99,23	0,50
FRESH GRANITE														
15	72,47	0,41	12,32	4,44	0,01	0,00	1,03	1,55	1,56	0,06	2,45	0,33	96,63	1,00

nd = not determined
Analyses by Atomic Energy Corporation of SA Ltd.
MgO and Na_2O by Rocklabs cc.

Borehole W40N0

	SiO_2	TiO_2	Al_2O_3	Fe_2O_3	MnO	MgO	CaO	Na_2O	K_2O	P_2O_5	LOI	H_2O-	TOTAL	$CaCO_3$
							(%)							
RED SAND														
1	81,20	,56	5,67	2,08	,05	1,27	3,97	,43	1,79	,09	5,46	,07	102,64	6,90
CALCRETE														
2	65,55	,39	5,37	1,95	,04	2,57	11,51	,47	1,43	,08	13,01	,27	102,64	20,40
3	65,34	,35	6,52	2,26	,03	3,51	9,87	,55	1,46	,08	12,91	,50	103,38	17,40
RED CLAY														
4	71,02	,45	7,26	2,69	,04	3,52	3,45	,57	1,52	,04	12,18	1,19	103,93	6,00
CALCRETE														
5	58,82	,36	6,10	2,23	,04	2,27	14,46	,39	1,22	,07	14,84	1,77	102,57	27,00
RED CLAY														
6	74,79	,60	9,79	3,52	,05	1,34	1,96	,40	1,51	,07	5,40	1,54	100,97	2,00
7	70,92	,68	12,65	4,36	,04	,82	1,84	,42	1,47	,09	6,27	1,42	100,98	3,00
8	68,24	,76	15,56	4,56	,04	,54	1,13	,39	1,62	,11	6,71	1,36	101,02	1,00
9	81,30	,55	7,65	3,02	,04	1,33	1,12	,42	1,32	,07	3,77	1,32	101,91	1,50
10	82,75	,51	6,79	2,50	,05	2,32	1,17	,44	1,07	,07	4,38	1,91	103,96	1,50
CALCRETE														
11	72,99	,38	5,40	1,96	,04	1,81	8,52	,43	,88	,06	9,46	1,47	103,40	24,20
12	64,31	,38	5,17	2,28	,03	4,35	10,85	,33	,80	,06	13,61	1,20	103,37	24,40
RED CLAY														
13	77,64	,48	7,11	4,67	,03	2,38	1,77	,46	,87	,06	4,88	1,80	102,15	2,50
WHITE CLAY														
14	60,49	,24	16,07	5,70	,03	2,14	4,77	,65	,95	,08	9,05	3,41	103,58	6,40
15	59,69	,24	18,14	3,75	,03	2,35	4,51	,96	1,08	,07	7,63	3,32	101,77	3,90
16	58,81	,20	17,11	3,61	,03	2,16	5,58	,80	,94	,08	11,36	2,32	103,00	7,40
17	69,59	,11	14,43	1,95	,02	1,83	3,54	1,06	,72	,05	6,73	2,35	102,38	3,00
18	54,28	,13	18,75	1,94	,02	2,31	7,90	2,54	,90	,06	9,88	2,56	101,27	9,90
19	57,73	,10	23,32	1,67	,03	1,52	6,00	2,47	1,03	,07	3,58	1,77	99,29	0,50
20	58,08	,07	23,93	1,51	,02	1,08	6,18	2,99	1,04	,07	3,18	1,39	99,54	0,50
21	56,72	,07	23,59	3,39	,03	,84	5,42	2,85	1,08	,05	5,10	1,13	100,27	1,00
22	57,09	,10	22,60	4,22	,03	1,44	5,47	2,57	1,16	,06	4,29	1,52	100,55	0,50
23	58,33	,08	23,50	1,89	,02	1,25	5,81	3,06	,98	,03	2,59	1,62	99,16	0,50
24	64,26	,08	20,59	,99	,02	0,00	1,74	7,05	2,05	,05	2,39	,28	99,50	1,50
25	52,37	,29	11,88	5,65	,04	1,35	11,98	2,19	,76	,08	12,02	1,20	99,81	23,10
WEATHERED TONALITE														
26	56,09	1,51	11,79	19,95	,15	,91	3,47	2,21	,67	,15	2,59	,39	99,88	1,00
SPINEL-RICH LAYER (Zn-SPINEL AND MAGNETITE)														
27	25,60	3,38	6,90	50,38	,26	2,02	1,36	,91	,32	,21	2,34	,80	94,48	0,50
FRESH TONALITE														
28	66,32	,74	10,55	16,99	,07	,15	3,71	2,06	2,43	,09	3,05	,11	106,27	4,00

Borehole W40S10

	SiO_2	TiO_2	Al_2O_3	Fe_2O_3	MnO	MgO	CaO	Na_2O	K_2O	P_2O_5	LOI	H_2O-	TOTAL	$CaCO_3$
							(%)							
RED SAND														
1	75,49	,43	8,30	3,39	,06	4,42	2,67	,41	1,92	,09	5,92	1,85	104,95	3,90
CALCRETE														
2	60,26	,35	7,47	2,84	,04	3,78	11,65	,40	1,64	,09	13,27	2,12	103,91	20,60
RED CLAY														
3	78,30	,57	8,36	3,30	,06	1,49	2,89	,49	1,48	,06	5,61	1,23	103,84	4,90
4	73,42	,66	9,88	3,90	,06	1,99	2,75	,40	1,24	,08	6,94	1,28	102,60	3,90
WHITE CLAY														
5	60,07	,42	10,37	1,66	,03	3,11	7,24	,47	1,71	,08	12,86	1,30	99,32	16,60
6	51,44	,32	9,92	2,10	,03	4,13	11,07	,31	2,43	,09	17,25	,80	99,89	29,30
7	64,79	,51	13,45	1,89	,03	1,43	5,43	,35	2,90	,09	8,86	1,34	101,07	10,10
8	63,49	,51	12,79	8,14	,10	,85	3,66	,36	2,66	,38	7,46	,94	101,34	6,40
9	48,99	,30	12,07	6,60	,05	1,62	1,19	,37	2,24	,12	15,58	1,05	90,18	24,00
10	51,02	,15	26,77	2,14	,03	1,14	3,42	,80	4,31	,12	9,59	1,68	101,17	5,90
11	63,26	,49	11,61	14,34	,30	,45	1,08	,73	2,60	,16	5,74	,42	101,18	1,50
12	54,10	,15	22,08	3,11	,07	,10	6,03	2,01	1,16	,04	6,55	,26	95,66	5,90
WEATHERED ANORTHOSITE														
13	58,08	,16	23,68	3,34	,08	0,00	6,49	4,34	1,30	,07	1,57	,07	99,18	0,50
FRESH ANORTHOSITE														
14	59,56	,19	23,66	1,66	,06	0,00	5,60	5,05	1,55	,07	1,46	,04	98,90	0,50

Analyses by Atomic Energy Corporation of SA Ltd.
MgO and Na_2O by Rocklabs cc.

Borehole W49,8N0

	SiO_2	TiO_2	Al_2O_3	Fe_2O_3	MnO	MgO	CaO	Na_2O	K_2O	P_2O_5	LOI	H_2O-	TOTAL	$CaCO_3$
							(%)							
RED SAND														
1	81,75	,31	7,10	3,07	,05	1,71	1,48	,45	1,51	,07	4,93	1,32	103,75	1,50
CALCRETE														
2	69,38	,34	6,65	2,45	,04	1,45	9,62	,32	8,02	,07	10,67	,83	109,84	16,80
RED CLAY														
3	80,04	,59	7,12	5,31	,06	1,29	1,10	,36	1,24	,08	4,53	,86	102,58	1,00
4	68,10	,43	6,65	2,61	,05	6,07	5,27	,37	,99	,07	11,42	1,69	103,72	15,70
CALCRETE														
5	45,85	,24	7,13	1,93	,03	7,86	13,54	,28	,39	,07	22,38	,97	100,67	40,60
WHITE CLAY														
6	45,48	1,11	18,54	15,89	,12	1,97	2,88	,33	,61	,13	11,51	3,02	101,59	4,00
7	42,27	,64	16,35	9,49	,07	1,88	9,60	,24	,92	,11	16,41	1,46	99,44	18,50
8	47,27	,77	22,76	5,73	,05	1,25	4,65	,31	,65	,39	13,53	3,30	100,66	7,70
9	46,31	,64	18,53	13,00	,11	1,88	6,17	,94	,79	,44	9,91	2,10	100,82	6,50
WEATHERED NORITE														
10	53,23	,69	18,36	15,99	,22	2,01	6,30	3,10	1,10	,69	3,22	,48	105,39	1,00
FRESH GRANITE														
11	72,93	,23	13,43	1,79	,05	0,00	1,34	2,90	5,22	,10	1,49	-,19	99,29	1,00
FRESH NORITE														
12	52,30	,75	18,45	11,26	,21	1,58	6,58	3,10	,59	,79	2,46	,18	98,25	1,00
13	66,22	,77	14,00	6,64	,19	2,00	4,41	2,57	1,79	,24	1,51	-,15	100,19	1,00
14	51,29	,84	17,80	12,61	,22	1,73	6,47	3,90	,79	,65	,82	-,22	96,90	1,00
15	60,46	,70	16,15	8,23	,21	1,94	4,84	3,09	2,18	,38	,93	-,29	98,82	0,50
16	61,06	1,21	13,99	9,98	,28	3,76	3,40	2,27	2,56	,21	1,25	-,25	99,72	0,50
17	56,40	,76	18,09	9,55	,20	2,34	5,70	3,63	1,28	,44	1,04	-,26	99,17	0,50
18	58,58	,49	19,04	7,03	,16	,94	5,62	4,38	1,32	,38	1,24	-,19	98,99	0,50
19	56,57	,55	19,67	8,37	,19	,63	6,10	4,76	1,10	,39	,42	-,27	98,48	0,50

Borehole W60N0

	SiO_2	TiO_2	Al_2O_3	Fe_2O_3	MnO	MgO	CaO	Na_2O	K_2O	P_2O_5	LOI	H_2O-	TOTAL	$CaCO_3$
							(%)							
RED SAND														
1	91,36	,46	4,11	1,57	,04	0,00	,14	0,35	1,32	,07	1,34	,14	100,90	0,50
CALCRETE														
2	57,24	,34	7,89	2,72	,04	4,10	11,31	,43	1,55	,08	16,73	2,64	105,07	25,50
3	56,96	,35	7,46	2,70	,04	4,19	14,53	,42	1,55	,10	14,77	2,63	105,70	20,50
4	62,63	,43	9,19	2,98	,04	2,49	8,48	,48	1,91	,05	11,66	2,39	102,73	15,00
5	52,20	,33	7,53	2,37	,03	2,45	15,79	,39	1,50	,06	17,47	1,94	102,06	29,00
RED CLAY														
6	51,84	,33	6,09	2,08	,03	2,57	3,53	,51	1,39	,05	33,21	2,05	103,68	8,50
7	75,50	,46	8,58	2,69	,04	1,76	3,31	,56	2,37	,07	6,10	1,42	102,86	5,50
8	80,86	,49	7,25	3,13	,04	1,04	1,35	,52	2,01	,07	4,02	,76	101,54	2,00
9	80,60	,53	7,19	3,81	,04	,99	1,22	,55	1,93	,03	4,11	,88	101,88	2,00
10	80,89	,50	7,09	2,63	,04	,99	1,46	,60	2,09	,07	3,96	,79	101,11	2,00
11	79,27	,53	7,31	3,06	,04	,95	2,56	,51	1,64	,06	5,36	1,06	102,35	4,40
12	75,46	,72	9,99	4,16	,05	1,08	1,70	,51	1,58	,08	5,89	1,32	102,54	2,50
13	70,62	,91	12,28	5,10	,06	,58	,31	,47	1,61	,06	5,87	1,29	99,16	0,50
14	79,96	,74	8,25	3,57	,05	,53	,49	,46	1,48	,06	4,14	,64	100,37	1,00
15	86,03	,71	5,88	2,91	,04	,66	,32	,47	1,50	,07	3,06	,39	102,04	1,00
WHITE CLAY														
16	77,00	,21	9,94	,60	,02	,12	2,93	,41	4,93	,08	4,54	,25	101,03	5,00
17	69,97	,14	9,75	,15	,02	0,00	6,34	,30	5,33	,05	7,06	,04	99,15	11,90
18	76,55	,15	10,31	,34	,02	0,00	2,99	,34	5,36	,07	4,54	,02	100,69	5,50
19	76,90	,15	10,89	,57	,02	0,00	,79	,40	5,74	,06	2,82	-,02	98,32	1,00
20	75,17	,18	11,84	,45	,02	0,00	1,26	,53	6,06	,06	3,32	,03	98,92	2,00
21	74,57	,20	13,02	,84	,02	0,00	1,27	,57	5,98	,08	3,77	,11	100,43	2,50
22	74,78	,20	12,77	,94	,02	0,00	,92	,64	6,04	,05	2,71	,53	99,60	1,50
23	77,80	,15	11,15	,64	,02	0,00	1,31	,84	5,81	,06	2,39	,42	100,59	2,00
24	75,88	,19	11,39	1,21	,03	0,00	1,88	1,07	5,56	,07	2,77	,44	100,49	3,00
WEATHERED GRANITE														
25	75,53	,20	12,39	1,62	,04	0,00	1,15	2,28	5,51	,08	1,46	,29	100,55	1,00
FRESH GRANITE														
26	75,33	,21	12,51	1,12	,03	0,00	,96	2,73	5,25	,07	,85	,16	99,22	1,00

Analyses by Atomic Energy Corporation of SA Ltd.
MgO and Na_2O by. Rocklabs cc.

Borehole W70N0

	SiO_2	TiO_2	Al_2O_3	Fe_2O_3	MnO	MgO	CaO	Na_2O	K_2O	P_2O_5	LOI	H_2O-	TOTAL	$CaCO_3$
							(%)							
RED SAND														
1	76,85	,40	6,99	2,83	,05	2,24	2,68	,49	1,99	,06	5,15	1,06	100,79	5,00
RED CLAY														
2	78,19	,44	6,93	2,89	,04	1,72	2,88	,64	1,62	,07	5,73	1,65	102,80	2,90
CALCRETE														
3	57,81	,29	7,90	1,66	,03	5,70	8,38	,61	1,99	,08	14,42	1,86	100,73	23,30
WHITE CLAY														
4	69,22	,27	11,17	,58	,01	,67	4,91	,40	4,80	,08	6,97	,69	99,77	9,80
5	73,56	,25	13,91	1,57	,03	0,00	,72	,46	6,00	,12	3,16	,70	100,48	1,00
WEATHERED GRANITE														
6	70,94	,24	11,79	1,39	,02	,78	2,97	,63	3,23	,06	5,72	1,34	99,11	4,40
7	75,19	,21	12,10	1,29	,02	0,00	1,16	1,05	5,63	,07	2,45	,58	99,75	1,50
8	75,50	,19	12,64	1,54	,02	0,00	,46	2,19	5,28	,06	1,64	,47	99,99	0,50
FRESH GRANITE														
9	76,82	,20	12,73	1,13	,02	0,00	,36	2,63	5,61	,08	,88	,30	100,76	0,50

Borehole W70S10

	SiO_2	TiO_2	Al_2O_3	Fe_2O_3	MnO	MgO	CaO	Na_2O	K_2O	P_2O_5	LOI	H_2O-	TOTAL	$CaCO_3$
							(%)							
RED SAND														
1	77,53	,50	7,51	3,52	,04	2,28	2,52	,64	2,09	,07	4,73	1,38	102,81	3,90
CALCRETE														
2	69,68	,41	6,50	3,48	,04	2,25	7,83	,61	2,06	,10	8,72	,65	102,33	14,40
RED CLAY														
3	74,25	,40	6,72	3,96	,04	1,01	4,59	,58	1,93	,11	6,00	,76	100,35	7,90
4	77,91	,45	6,17	2,92	,04	1,16	3,74	,58	1,42	,07	5,36	1,23	101,05	6,80
5	82,00	,48	7,94	2,40	,03	1,35	,46	,72	1,06	,09	3,60	1,87	102,00	0,50
WHITE CLAY														
6	74,84	,30	11,79	1,46	,03	,40	,62	1,29	3,29	,12	2,54	1,03	97,71	0,50
FRESH GRANITE														
7	78,96	,27	10,61	1,08	,02	1,03	,23	,73	4,23	,11	2,96	1,21	101,44	0,50

Borehole W80N0

	SiO_2	TiO_2	Al_2O_3	Fe_2O_3	MnO	MgO	CaO	Na_2O	K_2O	P_2O_5	LOI	H_2O-	TOTAL	$CaCO_3$
							(%)							
RED SAND														
1	74,87	,42	10,16	3,48	,06	4,13	,45	,67	2,82	,08	4,14	2,77	104,05	1,00
CALCRETE														
2	64,80	,25	9,25	2,05	,02	1,60	14,85	,44	3,34	,14	13,17	,96	110,87	23,70
RED CLAY														
3	68,46	,29	11,66	2,53	,02	,31	4,25	,32	4,71	,10	6,56	1,16	100,37	4,40
4	73,37	,26	10,96	2,78	,02	,01	2,55	,29	5,01	,07	4,19	,25	99,76	3,40
5	72,96	,34	12,14	3,67	,02	,01	,89	,28	5,61	,05	3,12	,41	99,50	,50
6	69,89	,45	12,87	4,48	,03	,33	2,00	,40	4,37	,09	5,25	1,28	101,44	2,40
WHITE CLAY														
7	73,92	,20	10,75	1,68	,02	,01	2,99	,40	5,38	,05	4,52	,26	100,18	4,90
8	73,46	,24	14,36	1,76	,02	,01	,23	,43	6,13	,07	2,82	,31	99,84	1,00
9	71,85	,28	15,06	2,50	,02	,01	,29	,86	6,07	,10	2,84	,43	100,31	1,00
10	72,81	,23	14,13	1,43	,02	,01	,31	1,45	5,98	,07	2,06	,29	98,79	1,00
WEATHERED GRANITE														
11	75,87	,21	12,80	1,09	,03	,01	,44	2,05	5,60	,09	1,33	,18	99,70	1,00
FRESH GRANITE														
12	75,97	,15	12,76	,87	,04	,01	,47	2,54	5,80	,07	,86	,13	99,67	1,00

Analyses by Atomic Energy Corporation of SA Ltd.
MgO and Na_2O by Rocklabs cc.

Borehole W83N0

	SiO_2	TiO_2	Al_2O_3	Fe_2O_3	MnO	MgO	CaO	Na_2O	K_2O	P_2O_5	LOI	H_2O-	TOTAL	$CaCO_3$
							(%)							
RED SAND														
1	73,56	,33	8,21	1,83	,05	1,91	5,57	,61	2,94	,12	6,36	1,04	102,53	9,30
CALCRETE														
2	43,83	,15	16,46	1,77	,02	2,02	13,85	,40	,93	,06	18,15	2,74	100,38	22,10
3	46,11	,16	18,04	2,14	,02	1,44	12,19	,43	1,02	,08	16,86	3,03	101,52	18,60
WHITE CLAY														
4	47,49	,15	26,37	1,97	,02	0,00	5,80	,37	,82	,06	14,32	2,12	99,49	9,40
5	48,12	,16	27,48	1,75	,03	0,00	5,07	,34	,86	,08	14,14	1,77	99,80	8,40
6	46,02	,21	28,94	3,41	,04	0,00	4,80	,21	,83	,12	14,48	1,36	100,42	7,70
7	41,86	,17	25,30	2,52	,03	0,00	9,65	,36	,70	,04	17,55	1,55	99,73	14,60
8	51,62	,35	33,15	4,35	,04	0,00	3,98	,30	,86	,11	13,77	1,41	109,94	5,40
9	46,34	,23	29,58	3,68	,03	0,00	3,33	,25	,83	,10	13,62	1,43	99,42	5,90
10	48,80	,11	29,76	1,36	,03	0,00	3,62	,25	,96	,10	13,51	1,99	100,49	5,80
11	49,15	,09	28,41	,89	,02	0,00	4,23	,16	,90	,08	13,76	1,54	99,23	7,30
12	53,42	,08	29,60	,69	,02	0,00	,35	,27	1,09	,10	11,53	1,43	98,58	1,50
13	51,24	,08	31,28	,75	,03	0,00	,35	,26	1,09	,09	11,68	3,39	100,24	0,50
WEATHERED ANORTHOSITE														
14	57,18	,07	24,29	,69	,03	0,00	7,73	4,15	1,19	,20	2,06	,39	97,98	1,50
FRESH ANORTHOSITE														
15	52,72	,25	23,08	3,48	,07	0,00	7,30	3,89	1,18	,12	2,13	,37	94,59	2,00
16	61,65	,21	20,34	1,97	,05	0,00	5,54	3,94	2,32	,15	1,70	,34	98,21	1,50

Borehole W90N0

	SiO_2	TiO_2	Al_2O_3	Fe_2O_3	MnO	MgO	CaO	Na_2O	K_2O	P_2O_5	LOI	H_2O-	TOTAL	$CaCO_3$
							(%)							
RED SAND (CALCRETISED)														
1	61,77	,21	6,62	1,26	,04	2,20	12,55	,46	2,76	,08	12,54	,71	101,20	23,10
WEATHERED GRANITE														
2	72,26	,19	11,69	1,26	,06	,72	3,64	1,77	5,07	,08	3,98	,44	101,16	4,80
3	70,42	,16	12,23	1,09	,03	,04	4,20	2,09	5,13	,08	4,02	,39	99,88	5,80
FRESH GRANITE														
4	75,52	,18	13,13	1,07	,03	0,00	1,21	2,82	5,63	,07	,95	,24	100,85	1,00
5	74,56	,19	13,12	1,32	,05	0,00	1,03	2,74	5,78	,09	,81	,24	99,93	0,50

Analyses by Atomic Energy Coporation Ltd.
MgO and Na_2O by Rocklabs cc.

APPENDIX E

TRACE ELEMENT ANALYSES OF VAALPUTS BOREHOLE SAMPLES

Borehole W2ONO

Sample	Ba	Co	Cu	Nb	Ni	Pb	Rb	Sr	Th
					(ppm)				
RED SAND									
1	210,00	4,00	1,00	13,00	1,00	1,00	62,00	31,00	7,00
CALCRETE									
2	1561,00	8,00	1,00	13,00	1,00	7,00	80,00	104,00	6,00
3	733,00	11,00	1,00	14,00	1,00	8,00	104,00	75,00	9,00
RED CLAY									
4	869,00	19,00	4,00	15,00	1,00	12,00	109,00	70,00	10,00
5	901,00	14,00	1,00	15,00	1,00	18,00	116,00	84,00	11,00
6	634,00	12,00	1,00	14,00	1,00	9,00	117,00	69,00	11,00
7	373,00	11,00	1,00	17,00	1,00	1,00	117,00	62,00	12,00
8	573,00	15,00	1,00	15,00	1,00	8,00	97,00	61,00	10,00
CALCRETE									
9	512,00	4,00	1,00	15,00	1,00	19,00	75,00	82,00	12,00
10	1106,00	5,00	1,00	16,00	1,00	24,00	63,00	87,00	16,00
RED CLAY									
11	463,00	17,00	1,00	15,00	1,00	9,00	83,00	62,00	12,00
12	809,00	16,00	1,00	12,00	1,00	9,00	78,00	93,00	8,00
WHITE CLAY									
13	314,00	21,00	1,00	10,00	12,00	1,00	83,00	80,00	1,00
14	209,00	42,00	52,00	11,00	32,00	12,00	44,00	87,00	1,00
15	377,00	10,00	26,00	10,00	3,00	21,00	162,00	76,00	20,00
16	442,00	13,00	78,00	10,00	1,00	32,00	181,00	91,00	20,00
17	139,00	34,00	152,00	10,00	41,00	13,00	32,00	122,00	1,00
18	136,00	26,00	90,00	10,00	2,00	17,00	29,00	190,00	1,00
19	199,00	20,00	92,00	9,00	14,00	14,00	43,00	244,00	1,00
20	621,00	8,00	24,00	11,00	1,00	27,00	184,00	130,00	17,00
21	1301,00	7,00	27,00	10,00	7,00	14,00	155,00	243,00	12,00
22	165,00	59,00	309,00	14,00	78,00	35,00	70,00	130,00	99,00
23	935,00	16,00	143,00	10,00	16,00	19,00	59,00	368,00	27,00
WEATHERED SPINEL-ANORTHOSITE									
24	415,00	49,00	704,00	14,00	97,00	43,00	38,00	373,00	29,00
WEATHERED TONALITE									
25	306,00	14,00	261,00	10,00	57,00	28,00	30,00	383,00	23,00
26	610,00	24,00	171,00	12,00	50,00	18,00	52,00	342,00	52,00
27	1513,00	4,00	46,00	10,00	11,00	20,00	120,00	303,00	27,00

Sample	U	V	Y	Zn	Zr	Ga	Cs	Cr	Hf
					(ppm)				
RED SAND									
1	1,00	56,00	11,00	2,00	136,00	0,09	0,79	28,50	4,57
CALCRETE									
2	1,00	117,00	18,00	16,00	160,00	0,17	1,75	29,90	4,79
3	1,00	209,00	26,00	20,00	175,00	0,27	2,43	39,30	6,19
RED CLAY									
4	1,00	215,00	31,00	29,00	205,00	0,24	2,61	44,20	7,14
5	1,00	149,00	33,00	13,00	192,00	0,22	1,87	33,90	6,62
6	1,00	99,00	25,00	19,00	144,00	0,21	0,00	0,00	0,00
7	1,00	109,00	23,00	13,00	192,00	0,24	1,76	32,10	7,71
8	1,00	130,00	29,00	22,00	225,00	0,22	1,98	34,20	8,62
CALCRETE									
9	1,00	86,00	40,00	5,00	253,00	0,17	1,29	29,90	9,18
10	1,00	87,00	40,00	7,00	247,00	0,20	1,55	32,60	8,16
RED CLAY									
11	1,00	128,00	27,00	17,00	265,00	0,28	1,46	31,40	7,63
12	1,00	90,00	29,00	21,00	183,00	0,28	1,37	30,20	7,09
WHITE CLAY									
13	1,00	109,00	156,00	34,00	123,00	0,26	0,99	49,90	6,51
14	1,00	136,00	110,00	114,00	145,00	0,41	0,60	69,60	5,92
15	1,00	85,00	62,00	34,00	176,00	0,32	0,90	20,60	6,81
16	1,00	110,00	68,00	46,00	204,00	0,33	1,18	15,70	8,57
17	1,00	171,00	115,00	98,00	197,00	0,53	0,58	75,30	8,40
18	1,00	82,00	69,00	89,00	111,00	0,46	0,45	34,90	4,05
19	1,00	74,00	45,00	85,00	98,00	0,49	0,45	37,20	3,89
20	1,00	52,00	70,00	42,00	230,00	0,36	0,35	14,90	8,53
21	1,00	113,00	109,00	49,00	180,00	0,30	0,82	27,10	6,21
22	10,00	306,00	124,00	202,00	266,00	0,44	6,37	117,80	10,50
23	1,00	175,00	32,00	98,00	299,00	0,44	4,03	223,25	12,55
WEATHERED SPINEL-ANORTHOSITE									
24	5,00	306,00	36,00	414,00	331,00	0,75	1,68	328,70	14,60
WEATHERED TONALITE									
25	1,00	109,00	22,00	126,00	136,00	0,54	0,55	140,20	4,72
26	1,00	158,00	28,00	141,00	261,00	0,62	0,51	79,10	9,78
27	1,00	113,00	24,00	56,00	186,00	0,45	0,43	34,40	7,18

Analyses by Geological Survey of South Africa
Ga, Cs, Cr and Hf analyses by Atomic Energy Corporation of SA Ltd.

Borehole W30N0

Sample	Ba	Co	Cu	Nb	Ni	Pb	Rb	Sr	Th
					(ppm)				
RED SAND									
1	278,00	6,00	1,00	14,00	1,00	1,00	54,00	79,00	7,00
CALCRETE									
2	555,00	8,00	2,00	14,00	1,00	28,00	89,00	107,00	13,00
RED CLAY									
3	272,00	14,00	1,00	16,00	3,00	4,00	106,00	75,00	11,00
4	320,00	15,00	1,00	16,00	1,00	9,00	82,00	54,00	15,00
5	394,00	10,00	1,00	15,00	1,00	17,00	47,00	98,00	14,00
6	398,00	19,00	26,00	17,00	15,00	44,00	186,00	84,00	27,00
WHITE CLAY									
7	609,00	10,00	1,00	13,00	16,00	50,00	266,00	93,00	32,00

Sample	U	V	Y	Zn	Zr	Ga	Cs	Cr	Hf
					(ppm)				
RED SAND									
1	1,00	79,00	13,00	9,00	115,00	0,38	1,10	35,10	3,53
CALCRETE									
2	1,00	131,00	23,00	19,00	137,00	0,18	1,83	31,80	4,36
RED CLAY									
3	1,00	133,00	29,00	27,00	201,00	0,29	2,35	38,60	7,42
4	1,00	82,00	29,00	20,00	274,00	0,25	1,89	38,10	9,38
5	20,00	60,00	44,00	10,00	441,00	0,21	1,48	27,40	8,43
6	21,00	54,00	87,00	57,00	540,00	0,48	2,72	27,40	20,20
WHITE CLAY									
7	1,00	62,00	123,00	38,00	267,00	0,00	1,69	154,60	10,20

Borehole W30S10

Sample	Ba	Co	Cu	Nb	Ni	Pb	Rb	Sr	Th
					(ppm)				
RED SAND									
1	227,00	3,00	1,00	9,00	1,00	1,00	84,00	38,00	10,00
CALCRETE									
2	688,00	4,00	21,00	9,00	1,00	12,00	97,00	115,00	10,00
RED CLAY									
3	724,00	1,00	13,00	8,00	1,00	8,00	112,00	81,00	10,00
4	470,00	10,00	27,00	9,00	1,00	1,00	101,00	59,00	9,00
5	647,00	7,00	8,00	9,00	1,00	5,00	89,00	61,00	9,00
CALCRETE									
6	516,00	1,00	18,00	10,00	1,00	8,00	65,00	72,00	15,00
RED CLAY									
7	267,00	7,00	7,00	8,00	1,00	1,00	75,00	52,00	7,00
8	419,00	7,00	15,00	11,00	1,00	7,00	56,00	55,00	12,00
9	278,00	14,00	6,00	13,00	1,00	1,00	47,00	40,00	13,00
WHITE CLAY									
10	202,00	19,00	16,00	15,00	1,00	14,00	23,00	65,00	29,00
11	205,00	16,00	1,00	11,00	1,00	11,00	62,00	44,00	19,00
12	493,00	9,00	18,00	13,00	1,00	33,00	263,00	65,00	32,00
13	662,00	5,00	1,00	9,00	9,00	35,00	289,00	85,00	29,00
WEATHERED GRANITE									
14	525,00	13,00	17,00	10,00	3,00	30,00	236,00	76,00	30,00
FRESH GRANITE									
15	594,00	6,00	5,00	9,00	6,00	30,00	241,00	72,00	22,00

Sample	U	V	Y	Zn	Zr	Ga	Cs	Cr	Hf
					(ppm)				
RED SAND									
1	1,00	76,00	16,00	33,00	242,00	0,19	2,08	45,10	7,65
CALCRETE									
2	1,00	88,00	26,00	48,00	165,00	0,25	2,11	42,62	8,81
RED CLAY									
3	1,00	101,00	27,00	42,00	232,00	0,26	2,13	37,67	11,14
4	1,00	108,00	27,00	55,00	245,00	0,27	2,22	35,20	12,30
5	1,00	130,00	32,00	35,00	266,00	0,26	1,70	31,00	10,70
CALCRETE									
6	1,00	87,00	37,00	33,00	287,00	0,21	1,82	34,90	11,55
RED CLAY									
7	1,00	86,00	21,00	31,00	248,00	0,21	1,94	38,80	12,40
8	1,00	65,00	26,00	32,00	335,00	0,22	1,29	32,70	13,50
9	1,00	64,00	32,00	28,00	469,00	0,20	1,65	32,70	18,10
WHITE CLAY									
10	1,00	29,00	42,00	33,00	405,00	0,42	0,54	23,50	15,40
11	1,00	41,00	87,00	33,00	340,00	0,61	1,61	14,10	11,40
12	3,00	41,00	130,00	46,00	311,00	0,61	2,39	15,10	11,50
13	1,00	51,00	100,00	40,00	273,00	0,72	2,22	16,10	10,60
WEATHERED GRANITE									
14	3,00	39,00	81,00	79,00	342,00	0,99	1,67	15,40	13,00
FRESH GRANITE									
15	1,00	63,00	62,00	59,00	270,00	0,64	1,62	14,60	9,72

Analyses by Geological Survey of South Africa
Ga, Cs, Cr and Hf analyses by Atomic Energy Corporation of SA Ltd.

Borehole W40N0

Sample	Ba	Co	Cu	Nb	Ni	Pb	Rb	Sr	Th
					(ppm)				
RED SAND									
1	356,00	6,00	11,00	10,00	16,00	13,00	88,00	85,00	16,00
CALCRETE									
2	912,00	5,00	12,00	7,00	17,00	11,00	67,00	169,00	13,00
3	1025,00	4,00	12,00	9,00	18,00	16,00	82,00	137,00	15,00
RED CLAY									
4	759,00	6,00	12,00	9,00	16,00	12,00	83,00	99,00	14,00
CALCRETE									
5	1106,00	3,00	10,00	10,00	19,00	20,00	77,00	121,00	14,00
RED CLAY									
6	469,00	10,00	13,00	11,00	20,00	26,00	89,00	82,00	194,00
7	709,00	3,00	12,00	12,00	17,00	26,00	81,00	81,00	19,00
8	1157,00	3,00	13,00	16,00	18,00	42,00	110,00	103,00	29,00
9	532,00	5,00	10,00	13,00	13,00	18,00	73,00	63,00	18,00
10	332,00	5,00	8,00	11,00	13,00	16,00	57,00	61,00	13,00
CALCRETE									
11	1098,00	3,00	5,00	9,00	14,00	11,00	53,00	84,00	10,00
12	411,00	3,00	9,00	9,00	14,00	12,00	46,00	170,00	12,00
RED CLAY									
13	316,00	9,00	8,00	14,00	19,00	15,00	44,00	74,00	16,00
WHITE CLAY									
14	296,00	29,00	14,00	3,00	48,00	18,00	33,00	191,00	6,00
15	288,00	23,00	9,00	2,00	40,00	26,00	30,00	210,00	5,00
16	284,00	27,00	11,00	2,00	37,00	17,00	31,00	218,00	12,00
17	256,00	19,00	6,00	2,00	31,00	9,00	15,00	162,00	3,00
18	221,00	20,00	10,00	2,00	34,00	19,00	18,00	431,00	3,00
19	245,00	21,00	8,00	2,00	31,00	29,00	17,00	665,00	4,00
20	293,00	20,00	8,00	2,00	34,00	27,00	18,00	665,00	3,00
21	272,00	22,00	4,00	2,00	43,00	26,00	20,00	613,00	5,00
22	341,00	30,00	6,00	2,00	36,00	29,00	25,00	469,00	4,00
23	1866,00	20,00	6,00	2,00	29,00	25,00	18,00	558,00	7,00
24	152,00	9,00	9,00	2,00	14,00	7,00	66,00	176,00	3,00
25	849,00	18,00	29,00	2,00	28,00	16,00	45,00	164,00	8,00
WEATHERED TONALITE									
26	2977,00	43,00	72,00	5,00	66,00	19,00	31,00	236,00	31,00
SPINEL-RICH LAYER (Zn-SPINEL AND MAGNETITE)									
27	10577,00	82,00	221,00	45,00	83,00	58,00	23,00	197,00	72,00
FRESH TONALITE									
28	986,00	18,00	41,00	2,00	39,00	35,00	113,00	181,00	21,00

Sample	U	V	Y	Zn	Zr	Ga	Cs	Cr	Hf
					(ppm)				
RED SAND									
1	4,00	39,00	21,00	31,00	282,00	,12	1,43	38,10	9,14
CALCRETE									
2	5,00	50,00	20,00	29,00	191,00	,11	1,44	28,00	7,04
3	6,00	105,00	22,00	29,00	219,00	,16	1,54	27,70	8,16
RED CLAY									
4	5,00	116,00	23,00	31,00	224,00	,23	1,77	37,80	9,52
CALCRETE									
5	5,00	98,00	31,00	12,00	239,00	,18	1,43	25,50	6,85
RED CLAY									
6	7,00	112,00	29,00	31,00	319,00	,27	1,76	32,80	10,70
7	7,00	96,00	22,00	31,00	280,00	,35	9,01	61,40	12,50
8	7,00	110,00	27,00	37,00	288,00	,47	9,50	67,80	15,00
9	4,00	71,00	23,00	25,00	326,00	,22	5,44	48,60	14,40
10	4,00	68,00	20,00	25,00	291,00	,19	5,42	53,70	15,80
CALCRETE									
11	3,00	51,00	35,00	20,00	249,00	,16	4,19	33,00	9,06
12	5,00	59,00	45,00	22,00	257,00	,13	4,19	34,20	10,70
RED CLAY									
13	6,00	109,00	42,00	33,00	292,00	,20	3,99	68,20	14,30
WHITE CLAY									
14	9,00	74,00	77,00	97,00	174,00	,34	1,95	55,30	5,26
15	8,00	32,00	153,00	75,00	133,00	,46	1,93	45,90	3,43
16	7,00	25,00	121,00	76,00	166,00	,44	1,61	39,30	3,78
17	6,00	15,00	55,00	52,00	149,00	,37	1,93	41,00	3,30
18	6,00	12,00	110,00	56,00	135,00	,51	1,52	38,70	1,80
19	5,00	2,00	36,00	54,00	70,00	,63	1,50	36,20	,71
20	100,00	7,00	33,00	54,00	64,00	,59	1,24	36,10	1,05
21	20,00	18,00	26,00	66,00	86,00	,58	1,31	24,40	1,87
22	5,00	27,00	37,00	82,00	114,00	,61	3,38	27,40	1,50
23	3,00	9,00	29,00	60,00	63,00	,54	1,35	29,10	1,50
24	5,00	7,00	77,00	33,00	54,00	,40	5,43	35,70	1,32
25	3,00	48,00	90,00	113,00	217,00	,37	6,27	83,60	6,78
WEATHERED TONALITE									
26	9,00	196,00	81,00	375,00	856,00	,93	3,28	144,00	27,20
SPINEL-RICH LAYER (Zn-SPINEL AND MAGNETITE)									
27	26,00	1209,00	129,00	1063,00	3726,00	1,93	3,76	578,50	107,00
FRESH TONALITE									
28	7,00	77,00	36,00	215,00	655,00	,53	1,50	29,40	19,10

Analyses by Geological Survey of South Africa
Ga, Cs, Cr and Hf analyses by Atomic Energy Corporation of SA Ltd

Borehole W40S10

Sample	Ba	Co	Cu	Nb	Ni	Pb	Rb	Sr	Th
					(ppm)				
RED SAND									
1	443,00	7,00	22,00	9,00	5,00	1,00	95,00	96,00	8,00
CALCRETE									
2	768,00	1,00	21,00	8,00	1,00	4,00	84,00	144,00	8,00
RED CLAY									
3	408,00	2,00	3,00	9,00	1,00	2,00	79,00	62,00	11,00
4	706,00	5,00	16,00	11,00	1,00	1,00	68,00	83,00	18,00
WHITE CLAY									
5	412,00	3,00	1,00	8,00	1,00	2,00	89,00	199,00	12,00
6	344,00	3,00	23,00	9,00	1,00	12,00	129,00	187,00	12,00
7	597,00	8,00	9,00	13,00	5,00	1,00	135,00	131,00	12,00
8	1136,00	43,00	54,00	11,00	87,00	16,00	121,00	499,00	17,00
9	434,00	25,00	14,00	6,00	44,00	22,00	91,00	157,00	8,00
10	944,00	20,00	33,00	3,00	1,00	1,00	147,00	209,00	1,00
11	815,00	76,00	34,00	9,00	96,00	9,00	105,00	99,00	18,00
12	896,00	23,00	81,00	6,00	19,00	1,00	82,00	99,00	8,00
WEATHERED ANORTHOSITE									
13	726,00	8,00	125,00	2,00	27,00	6,00	32,00	679,00	1,00
FRESH ANORTHOSITE									
14	521,00	5,00	77,00	4,00	8,00	5,00	39,00	753,00	7,00

Sample	U	V	Y	Zn	Zr	Ga	Cs	Cr	Hf
					(ppm)				
RED SAND									
1	1,00	88,00	20,00	61,00	163,00	,22	0,00	0,00	0,00
CALCRETE									
2	1,00	97,00	22,00	47,00	148,00	,21	2,25	34,00	5,16
RED CLAY									
3	1,00	100,00	24,00	34,00	295,00	,24	1,85	34,10	10,70
4	1,00	87,00	25,00	34,00	325,00	,29	1,96	36,00	12,40
WHITE CLAY									
5	1,00	89,00	44,00	12,00	197,00	,31	2,45	38,80	5,99
6	1,00	71,00	63,00	20,00	170,00	,27	2,20	37,50	5,05
7	1,00	111,00	101,00	36,00	243,00	,40	3,51	64,20	7,18
8	6,00	123,00	316,00	146,00	259,00	,42	2,53	57,80	6,25
9	1,00	93,00	72,00	86,00	167,00	,37	1,96	43,30	3,89
10	1,00	59,00	42,00	55,00	83,00	,61	2,66	69,40	1,45
11	9,00	147,00	246,00	181,00	217,00	,33	1,94	52,80	7,65
12	1,00	86,00	28,00	141,00	205,00	,34	1,65	56,90	8,53
WEATHERED ANORTHOSITE									
13	1,00	84,00	14,00	109,00	55,00	,51	1,39	156,00	1,14
FRESH ANORTHOSITE									
14	1,00	46,00	13,00	72,00	62,00	,63	,82	71,30	2,00

Analyses by Geological Survey of South Africa
Ga, Cs, Cr and Hf analyses by Atomic Energy Corporation of SA Ltd.

Borehole W49,8N0

Sample	Ba	Co	Cu	Nb	Ni	Pb	Rb	Sr	Th
					(ppm)				
RED SAND									
1	244,00	7,00	19,00	8,00	1,00	1,00	82,00	65,00	7,00
CALCRETE									
2	1438,00	1,00	23,00	9,00	1,00	4,00	73,00	94,00	15,00
RED CLAY									
3	1042,00	1,00	7,00	12,00	1,00	3,00	67,00	58,00	17,00
4	1562,00	5,00	22,00	10,00	1,00	1,00	58,00	135,00	14,00
CALCRETE									
5	666,00	1,00	1,00	7,00	1,00	11,00	27,00	264,00	12,00
WHITE CLAY									
6	2206,00	59,00	67,00	9,00	57,00	14,00	91,00	117,00	8,00
7	336,00	22,00	31,00	8,00	33,00	26,00	49,00	133,00	4,00
8	934,00	25,00	40,00	8,00	13,00	3,00	28,00	420,00	1,00
9	429,00	48,00	76,00	7,00	48,00	20,00	62,00	314,00	1,00
WEATHERED NORITE									
10	439,00	23,00	86,00	10,00	22,00	24,00	54,00	439,00	19,00
FRESH GRANITE									
11	472,00	1,00	3,00	7,00	1,00	16,00	291,00	117,00	32,00
FRESH NORITE									
12	362,00	20,00	148,00	10,00	22,00	23,00	50,00	498,00	12,00
13	610,00	5,00	113,00	11,00	21,00	4,00	148,00	274,00	28,00
14	272,00	24,00	174,00	8,00	24,00	34,00	29,00	483,00	10,00
15	577,00	9,00	47,00	10,00	21,00	19,00	213,00	331,00	14,00
16	993,00	20,00	136,00	15,00	44,00	15,00	281,00	217,00	48,00
17	469,00	15,00	73,00	10,00	26,00	26,00	88,00	440,00	23,00
18	331,00	9,00	55,00	9,00	1,00	24,00	59,00	410,00	20,00
19	206,00	7,00	34,00	7,00	8,00	33,00	33,00	422,00	9,00

Sample	U	V	Y	Zn	Zr	Ga	Cs	Cr	Hf
					(ppm)				
RED SAND									
1	1,00	75,00	18,00	57,00	126,00	,21	8,58	62,30	4,85
CALCRETE									
2	1,00	84,00	29,00	42,00	205,00	,17	6,89	48,00	8,68
RED CLAY									
3	1,00	140,00	24,00	35,00	276,00	,21	5,87	70,70	11,20
4	1,00	82,00	32,00	38,00	258,00	,19	5,75	44,00	10,50
CALCRETE									
5	1,00	65,00	69,00	31,00	216,00	,22	2,41	17,10	10,20
WHITE CLAY									
6	7,00	275,00	103,00	246,00	195,00	,82	10,30	70,30	4,04
7	1,00	173,00	151,00	133,00	281,00	,67	6,67	34,40	10,90
8	1,00	222,00	150,00	163,00	78,00	,63	2,79	51,40	1,81
9	7,00	241,00	147,00	214,00	81,00	,68	4,53	35,50	2,00
WEATHERED NORITE									
10	7,00	191,00	127,00	275,00	123,00	,64	5,40	50,70	4,08
FRESH GRANITE									
11	1,00	52,00	32,00	57,00	165,00	,39	4,49	5,20	8,98
FRESH NORITE									
12	7,00	205,00	93,00	268,00	74,00	,71	6,06	73,20	3,07
13	1,00	95,00	43,00	944,00	270,00	,50	34,70	110,00	11,60
14	6,00	211,00	75,00	298,00	62,00	,70	4,06	103,00	1,51
15	1,00	128,00	59,00	313,00	167,00	,59	78,10	86,90	6,46
16	3,00	128,00	41,00	811,00	354,00	,61	59,50	179,00	15,80
17	1,00	139,00	62,00	298,00	248,00	,67	14,50	108,60	11,70
18	1,00	122,00	75,00	172,00	165,00	,68	11,30	27,20	5,36
19	1,00	142,00	71,00	159,00	96,00	,70	2,43	30,80	2,53

Analyses by Geological Survey of South Africa
Ga, Cs, Cr and Hf analyses by Atomic Energy Corporation of SA Ltd.

Borehole W60N0

Sample	Ba	Co	Cu	Nb	Ni	Pb	Rb	Sr	Th
					(ppm)				
RED SAND									
1	213,00	1,00	1,00	9,00	1,00	1,00	71,00	31,00	11,00
CALCRETE									
2	745,00	1,00	35,00	9,00	1,00	7,00	84,00	145,00	15,00
3	1027,00	1,00	10,00	8,00	1,00	2,00	88,00	142,00	13,00
4	811,00	3,00	27,00	11,00	1,00	2,00	112,00	116,00	17,00
5	725,00	1,00	2,00	9,00	1,00	17,00	88,00	127,00	12,00
RED CLAY									
6	711,00	5,00	25,00	10,00	1,00	1,00	110,00	88,00	15,00
7	401,00	1,00	8,00	9,00	1,00	1,00	123,00	72,00	13,00
8	387,00	3,00	19,00	12,00	1,00	1,00	112,00	63,00	21,00
9	364,00	1,00	3,00	13,00	1,00	1,00	103,00	64,00	16,00
10	336,00	3,00	18,00	12,00	1,00	1,00	114,00	63,00	17,00
11	264,00	1,00	2,00	11,00	1,00	1,00	89,00	61,00	14,00
12	323,00	6,00	22,00	13,00	1,00	1,00	90,00	71,00	22,00
13	600,00	10,00	13,00	15,00	4,00	1,00	99,00	76,00	27,00
14	349,00	2,00	19,00	13,00	1,00	1,00	85,00	59,00	23,00
15	428,00	1,00	1,00	12,00	1,00	1,00	78,00	48,00	15,00
WHITE CLAY									
16	657,00	1,00	15,00	6,00	1,00	8,00	231,00	104,00	23,00
17	423,00	1,00	1,00	5,00	1,00	16,00	260,00	108,00	27,00
18	362,00	1,00	14,00	7,00	1,00	8,00	292,00	65,00	30,00
19	389,00	1,00	1,00	7,00	1,00	12,00	337,00	58,00	33,00
20	424,00	1,00	10,00	8,00	1,00	17,00	364,00	68,00	41,00
21	414,00	1,00	1,00	8,00	1,00	16,00	391,00	67,00	43,00
22	509,00	1,00	13,00	9,00	1,00	16,00	396,00	68,00	44,00
23	414,00	1,00	1,00	7,00	1,00	9,00	367,00	66,00	36,00
24	407,00	1,00	9,00	8,00	1,00	14,00	357,00	70,00	46,00
WEATHERED GRANITE									
25	528,00	1,00	1,00	8,00	1,00	15,00	360,00	80,00	41,00
FRESH GRANITE									
26	461,00	1,00	10,00	9,00	1,00	21,00	354,00	89,00	46,00

Sample	U	V	Y	Zn	Zr	Ga	Cs	Cr	Hf
					(ppm)				
RED SAND									
1	1,00	59,00	18,00	23,00	227,00	,13	3,71	27,70	10,80
CALCRETE									
2	1,00	84,00	30,00	49,00	159,00	,18	7,53	52,00	7,25
3	1,00	123,00	32,00	36,00	179,00	,22	8,22	51,00	7,25
4	1,00	177,00	35,00	47,00	248,00	,28	7,26	44,40	10,20
5	1,00	176,00	33,00	31,00	196,00	,23	6,17	37,60	7,26
RED CLAY									
6	1,00	135,00	29,00	49,00	256,00	,26	7,68	42,10	11,00
7	1,00	105,00	27,00	35,00	238,00	,26	8,80	57,10	12,70
8	1,00	88,00	26,00	38,00	291,00	,23	7,23	56,90	10,70
9	1,00	115,00	23,00	28,00	236,00	,23	5,37	60,50	10,60
10	1,00	75,00	24,00	39,00	261,00	,21	1,35	43,70	9,11
11	1,00	91,00	27,00	30,00	280,00	,23	1,55	42,70	10,80
12	1,00	98,00	37,00	43,00	371,00	,27	1,89	52,20	12,40
13	1,00	126,00	40,00	42,00	535,00	,41	2,31	62,20	19,60
14	1,00	84,00	33,00	40,00	457,00	,25	1,45	39,60	16,20
15	1,00	76,00	22,00	31,00	438,00	0,28	1,21	42,50	19,20
WHITE CLAY									
16	1,00	44,00	57,00	20,00	179,00	,31	,92	18,30	5,56
17	1,00	40,00	58,00	9,00	174,00	,30	,34	12,90	5,32
18	1,00	33,00	59,00	21,00	176,00	,28	1,07	13,60	4,89
19	1,00	51,00	59,00	19,00	183,00	,32	1,29	16,50	5,39
20	1,00	35,00	60,00	24,00	197,00	,35	1,40	16,30	5,72
21	1,00	45,00	55,00	28,00	214,00	,35	1,89	13,60	5,27
22	1,00	31,00	61,00	40,00	193,00	,40	1,47	14,00	6,19
23	1,00	48,00	50,00	20,00	178,00	,35	1,51	13,90	5,13
24	1,00	33,00	51,00	34,00	188,00	,36	1,52	10,40	5,87
WEATHERED GRANITE									
25	1,00	51,00	65,00	29,00	177,00	,35	1,51	11,90	6,16
FRESH GRANITE									
26	1,00	33,00	87,00	47,00	175,00	,38	1,49	13,40	6,45

Analyses by Geological Survey of South Africa
Ga, Cs, Cr and Hf analyses by Atomic Energy Corporation of SA Ltd.

Borehole W70N0

Sample	Ba	Co	Cu	Nb	Ni	Pb	Rb	Sr	Th
					(ppm)				
RED SAND									
1	663,00	4,00	6,00	10,00	1,00	1,00	111,00	78,00	14,00
RED CLAY									
2	450,00	10,00	16,00	10,00	1,00	1,00	87,00	69,00	18,00
CALCRETE									
3	553,00	7,00	1,00	10,00	1,00	1,00	98,00	140,00	25,00
WHITE CLAY									
4	445,00	4,00	10,00	9,00	1,00	9,00	213,00	85,00	78,00
5	508,00	1,00	1,00	8,00	3,00	13,00	289,00	77,00	160,00
WEATHERED GRANITE									
6	402,00	5,00	3,00	8,00	1,00	1,00	171,00	56,00	59,00
7	413,00	1,00	1,00	6,00	1,00	10,00	280,00	68,00	44,00
8	434,00	1,00	4,00	8,00	1,00	2,00	289,00	81,00	47,00
FRESH GRANITE									
9	428,00	1,00	1,00	7,00	1,00	1,00	290,00	84,00	45,00

Sample	U	V	Y	Zn	Zr	Ga	Cs	Cr	Hf
					(ppm)				
RED SAND									
1	1,00	96,00	27,00	35,00	212,00	,23	1,86	35,50	6,45
RED CLAY									
2	1,00	79,00	30,00	34,00	256,00	,21	1,40	39,30	10,70
CALCRETE									
3	1,00	68,00	96,00	20,00	220,00	,23	1,28	28,60	6,33
WHITE CLAY									
4	1,00	41,00	122,00	22,00	234,00	,32	,48	19,10	7,70
5	1,00	53,00	135,00	38,00	260,00	,37	,74	16,60	9,07
WEATHERED GRANITE									
6	1,00	28,00	77,00	54,00	194,00	,34	,43	19,10	8,82
7	1,00	46,00	45,00	39,00	167,00	,32	,73	12,40	7,13
8	1,00	35,00	48,00	53,00	151,00	,34	,90	9,50	5,29
FRESH GRANITE									
9	1,00	46,00	42,00	30,00	166,00	,30	,59	10,10	6,11

Borehole W70S10

Sample	Ba	Co	Cu	Nb	Ni	Pb	Rb	Sr	Th
					(ppm)				
RED SAND									
1	563,00	2,00	2,00	11,00	1,00	5,00	113,00	72,00	16,00
CALCRETE									
2	825,00	2,00	19,00	9,00	1,00	10,00	99,00	97,00	14,00
RED CLAY									
3	519,00	1,00	1,00	13,00	1,00	17,00	101,00	83,00	20,00
4	609,00	1,00	13,00	10,00	1,00	8,00	80,00	71,00	17,00
5	426,00	6,00	1,00	10,00	1,00	1,00	51,00	55,00	14,00
WHITE CLAY									
6	750,00	8,00	3,00	8,00	1,00	19,00	132,00	76,00	28,00
FRESH GRANITE									
7	346,00	1,00	1,00	7,00	1,00	24,00	135,00	67,00	23,00

Sample	U	V	Y	Zn	Zr	Ga	Cs	Cr	Hf
					(ppm)				
RED SAND									
1	1,00	88,00	26,00	40,00	216,00	,23	2,44	49,00	7,46
CALCRETE									
2	1,00	122,00	29,00	37,00	189,00	,19	1,48	37,80	7,75
RED CLAY									
3	1,00	144,00	26,00	21,00	232,00	,21	1,54	50,00	9,31
4	1,00	85,00	30,00	30,00	278,00	,19	1,44	38,80	10,00
5	1,00	69,00	33,00	26,00	281,00	0,00	1,22	35,90	10,50
WHITE CLAY									
6	1,00	64,00	73,00	29,00	185,00	,32	,60	23,70	6,60
FRESH GRANITE									
7	1,00	69,00	60,00	19,00	161,00	,28	,60	25,50	6,47

Analyses by Geological Survey of South Africa
Ga, Cs, Cr and Hf analyses by Atomic Energy Corporation of SA Ltd.

Borehole W80N0

Sample	Ba	Co	Cu	Nb	Ni	Pb	Rb	Sr	Th
					(ppm)				
RED SAND									
1	329,00	10,00	29,00	8,00	5,00	1,00	160,00	61,00	17,00
CALCRETE									
2	668,00	1,00	27,00	8,00	1,00	6,00	208,00	115,00	34,00
RED CLAY									
3	500,00	1,00	28,00	9,00	3,00	17,00	380,00	72,00	66,00
4	1019,00	1,00	71,00	8,00	1,00	19,00	381,00	57,00	21,00
5	775,00	1,00	34,00	9,00	4,00	16,00	371,00	69,00	32,00
6	505,00	4,00	63,00	9,00	1,00	16,00	275,00	67,00	36,00
WHITE CLAY									
7	386,00	1,00	37,00	7,00	1,00	19,00	342,00	58,00	15,00
8	433,00	1,00	24,00	8,00	1,00	20,00	375,00	63,00	57,00
9	414,00	1,00	6,00	10,00	1,00	16,00	336,00	64,00	62,00
10	426,00	1,00	15,00	9,00	1,00	18,00	344,00	73,00	53,00
WEATHERED GRANITE									
11	395,00	1,00	1,00	8,00	1,00	13,00	329,00	83,00	53,00
FRESH GRANITE									
12	426,00	1,00	13,00	7,00	1,00	22,00	345,00	92,00	41,00

Sample	U	V	Y	Zn	Zr	Ga	Cs	Cr	Hf
					(ppm)				
RED SAND									
1	1,00	94,00	38,00	70,00	171,00	,31	3,44	51,90	5,83
CALCRETE									
2	1,00	89,00	56,00	43,00	168,00	,28	1,91	21,30	5,77
RED CLAY									
3	1,00	91,00	91,00	64,00	207,00	,40	3,32	19,50	7,46
4	1,00	72,00	68,00	84,00	350,00	,43	3,19	14,70	11,20
5	1,00	73,00	90,00	89,00	304,00	,46	3,45	14,60	10,50
6	1,00	106,00	102,00	127,00	298,00	,44	2,82	38,50	10,90
WHITE CLAY									
7	1,00	61,00	66,00	122,00	256,00	,38	1,55	14,90	11,10
8	1,00	54,00	80,00	68,00	190,00	,48	,70	13,50	7,54
9	1,00	67,00	97,00	52,00	195,00	,50	1,03	13,90	7,04
10	1,00	52,00	58,00	44,00	175,00	,46	,69	11,00	6,50
WEATHERED GRANITE									
11	1,00	57,00	44,00	35,00	191,00	,43	,94	9,14	7,30
FRESH GRANITE									
12	1,00	41,00	46,00	29,00	160,00	,35	,92	13,10	5,55

Analyses by Geological Survey of South Africa
Ga, Cs, Cr and Hf analyses by Atomic Energy Corporation of SA Ltd.

Borehole W83N0

Sample	Ba	Co	Cu	Nb	Ni	Pb	Rb	Sr	Th
					(ppm)				
RED SAND									
1	376,00	1,00	2,00	8,00	1,00	3,00	162,00	93,00	18,00
CALCRETE									
2	317,00	7,00	27,00	7,00	1,00	6,00	56,00	152,00	9,00
3	330,00	4,00	16,00	6,00	1,00	5,00	54,00	141,00	3,00
WHITE CLAY									
4	205,00	15,00	33,00	6,00	1,00	1,00	49,00	75,00	1,00
5	214,00	19,00	21,00	5,00	1,00	1,00	45,00	64,00	1,00
6	215,00	23,00	51,00	6,00	6,00	3,00	52,00	52,00	30,00
7	194,00	8,00	22,00	5,00	1,00	4,00	49,00	68,00	2,00
8	157,00	21,00	46,00	6,00	1,00	2,00	62,00	45,00	54,00
9	198,00	22,00	46,00	6,00	7,00	1,00	61,00	46,00	36,00
10	221,00	23,00	41,00	6,00	1,00	1,00	43,00	50,00	6,00
11	241,00	26,00	35,00	7,00	16,00	4,00	55,00	71,00	14,00
12	227,00	30,00	42,00	8,00	14,00	8,00	68,00	63,00	14,00
13	269,00	30,00	25,00	6,00	18,00	1,00	41,00	128,00	1,00
WEATHERED ANORTHOSITE									
14	292,00	1,00	11,00	3,00	1,00	1,00	30,00	615,00	1,00
FRESH ANORTHOSITE									
15	392,00	1,00	30,00	3,00	1,00	10,00	29,00	588,00	14,00
16	463,00	1,00	23,00	4,00	1,00	7,00	79,00	493,00	25,00

Sample	U	V	Y	Zn	Zr	Ga	Cs	Cr	Hf
					(ppm)				
RED SAND									
1	1,00	60,00	32,00	34,00	184,00	,23	1,90	31,70	8,53
CALCRETE									
2	1,00	87,00	31,00	36,00	118,00	,51	,44	26,20	4,42
3	1,00	110,00	30,00	37,00	130,00	,54	,65	20,40	3,73
WHITE CLAY									
4	1,00	76,00	61,00	62,00	117,00	,82	,05	2,69	,40
5	1,00	77,00	91,00	59,00	138,00	,81	,49	26,40	4,76
6	1,00	96,00	205,00	85,00	135,00	,91	,63	3,83	5,08
7	1,00	83,00	107,00	57,00	134,00	,76	,54	50,30	4,63
8	1,00	99,00	141,00	88,00	230,00	,95	,65	48,20	8,85
9	1,00	97,00	132,00	78,00	156,00	,84	,60	31,10	5,64
10	1,00	53,00	213,00	77,00	69,00	,82	,57	23,70	1,97
11	1,00	58,00	217,00	63,00	54,00	,82	,53	35,90	2,23
12	1,00	36,00	310,00	50,00	54,00	,80	1,05	36,30	1,69
13	1,00	51,00	285,00	39,00	66,00	,86	,86	39,70	2,22
WEATHERED ANORTHOSITE									
14	1,00	40,00	43,00	29,00	102,00	0,70	,34	19,70	3,35
FRESH ANORTHOSITE									
15	1,00	95,00	31,00	58,00	114,00	,55	,53	33,20	3,79
16	1,00	55,00	36,00	51,00	160,00	,60	,46	21,50	5,68

Borehole W90N0

Sample	Ba	Co	Cu	Nb	Ni	Pb	Rb	Sr	Th
					(ppm)				
RED SAND (CALCRETISED)									
1	621,00	1,00	1,00	7,00	1,00	22,00	163,00	109,00	19,00
WEATHERED GRANITE									
2	575,00	8,00	21,00	8,00	1,00	22,00	316,00	92,00	30,00
3	368,00	1,00	1,00	9,00	1,00	24,00	320,00	89,00	41,00
FRESH GRANITE									
4	379,00	2,00	4,00	9,00	1,00	18,00	355,00	89,00	42,00
5	382,00	1,00	1,00	9,00	1,00	16,00	367,00	87,00	42,00

Sample	U	V	Y	Zn	Zr	Ga	Cs	Cr	Hf
					(ppm)				
RED SAND (CALCRETISED)									
1	1,00	56,00	34,00	22,00	148,00	,19	1,41	24,30	4,96
WEATHERED GRANITE									
2	1,00	73,00	47,00	29,00	137,00	,35	1,08	12,60	4,91
3	1,00	85,00	56,00	23,00	138,00	,33	,83	11,50	5,52
FRESH GRANITE									
4	1,00	48,00	74,00	39,00	152,00	,41	1,10	9,86	5,52
5	1,00	54,00	73,00	27,00	151,00	,39	,96	10,40	6,39

Analyses by Geological Survey of South Africa
Ga, Cs, Cr and Hf analyses by Atomic Energy Corporation of SA Ltd.

APPENDIX F

MAJOR AND TRACE ELEMENT ANALYSES OF VAALPUTS CALCRETE WHOLE ROCK SAMPLES AND DETRITAL FRACTIONS

ANALYSES OF CALCRETE WHOLE ROCKS

	Major elements (%)											
Sample	SiO_2	TiO_2	Al_2O_3	Fe_2O_3	MnO	MgO	CaO	Na_2O	K_2O	P_2O_5	H_2O	LOI	TOTAL
1T1	5,16	0,05	1,18	0,43	0,01	0,78	51,23	0,24	0,04	0,01	0,46	39,46	100,91
1T1B	4,93	0,04	0,89	0,32	0,01	0,79	52,17	0,21	0,04	0,01	0,41	40,90	100,75
1T2	8,00	0,08	1,04	0,42	0,01	0,57	49,85	0,21	0,07	0,01	0,41	39,02	100,33
1T2B	8,27	0,06	1,14	0,47	0,03	0,44	50,20	0,22	0,10	0,01	0,25	39,61	100,81
1T2C	8,86	0,09	1,26	0,50	0,01	0,50	49,61	0,22	0,14	0,01	0,23	38,93	100,39
1T3	13,33	0,15	1,91	1,36	0,02	0,41	45,96	0,22	0,12	0,01	0,38	36,50	100,40
1T3B	17,60	0,18	1,98	1,19	0,01	0,37	43,81	0,24	0,30	0,01	0,37	34,46	100,57
1T3C	17,04	0,16	2,30	0,70	0,01	0,56	44,11	0,25	0,16	0,01	0,56	34,23	100,55
1T4	20,07	0,13	2,76	1,12	0,02	0,64	41,00	0,24	0,38	0,01	0,70	33,64	100,79
1T4B	15,92	0,10	2,44	0,93	0,01	0,83	43,77	0,25	0,27	0,01	0,80	35,17	100,57
1T4C	62,57	0,40	11,40	4,08	0,03	3,22	1,59	0,50	1,64	0,05	6,49	7,74	99,77
2T1	70,74	0,37	9,10	3,47	0,16	2,59	0,49	0,72	1,97	0,08	5,89	4,48	100,25
2T2	21,82	0,17	3,49	1,25	0,01	1,08	38,14	0,28	0,59	0,04	1,12	30,44	100,55
2T3	12,58	0,10	2,06	0,72	0,01	0,91	46,35	0,25	0,22	0,01	0,99	36,53	101,11
2T4	12,58	0,11	1,86	0,76	0,01	0,80	46,30	0,24	0,17	0,02	0,69	36,20	100,96
2T4B	10,63	0,06	1,56	0,48	0,02	1,22	46,68	0,27	0,15	0,01	1,12	37,18	100,31
2T4C	8,79	0,06	1,81	0,64	0,01	0,96	47,52	0,32	0,08	0,02	1,22	38,65	100,12
2T4D	10,06	0,05	1,66	0,41	0,01	1,33	47,79	0,24	0,08	0,01	1,16	38,18	101,21
2T5	13,18	0,10	1,50	0,64	0,02	0,64	45,80	0,23	0,18	0,01	0,61	36,40	99,88
2T5B	12,66	0,12	2,09	0,63	0,01	1,04	45,25	0,21	0,10	0,01	1,06	37,22	100,42
2T5C	10,79	0,08	2,05	0,69	0,00	0,83	47,30	0,25	0,09	0,01	0,70	37,88	100,68
2T5D	14,24	0,11	2,76	1,06	0,02	0,79	43,58	0,26	0,12	0,03	1,02	35,46	99,89
2T6	20,67	0,14	2,76	1,03	0,01	0,73	39,76	0,34	0,36	0,01	0,99	34,12	100,98

	Trace elements (ppm)									
Sample	Zn	Cu	Ni	Co	Ga	Nb	Zr	Y	Sr	Rb
1T1	7,8	10,6	6,7	1,9	2,4	0,1	23,3	103,8	201,4	3,4
1T1B	6,7	6,0	0,9	1,0	0,0	4,0	18,6	98,5	128,9	1,1
1T2	4,8	6,3	2,1	0,0	0,0	2,6	34,4	82,7	124,2	8,2
1T2B	7,0	7,6	3,6	0,0	0,0	1,8	48,1	103,3	97,1	8,9
1T2C	6,8	9,3	6,0	0,0	3,0	2,2	59,7	101,7	164,4	11,3
1T3	13,7	7,4	4,7	0,2	0,3	4,5	89,2	149,4	125,6	10,5
1T3B	7,8	8,6	6,8	1,3	2,6	8,0	95,7	109,9	142,1	12,5
1T3C	7,1	8,2	3,6	0,0	3,5	6,2	113,7	171,2	148,0	8,9
1T4	14,7	8,0	6,6	0,5	3,4	1,8	67,8	52,6	111,7	27,5
1T4B	12,9	9,9	7,2	0,0	0,3	3,1	57,0	112,5	118,2	19,3
1T4C	41,7	12,4	13,5	2,3	16,5	8,4	198,4	36,7	51,0	93,3
2T1	37,7	23,5	71,0	60,9	11,6	10,5	172,9	274,5	104,7	99,0
2T2	15,8	9,9	10,4	2,0	8,1	6,5	65,6	85,7	261,2	29,5
2T3	7,7	9,6	9,8	2,9	0,0	5,3	44,3	97,4	178,0	18,2
2T4	10,5	8,2	5,2	0,0	0,0	4,8	50,7	126,0	164,8	13,4
2T4B	6,2	6,0	3,9	0,3	2,7	4,9	40,0	156,3	185,5	6,2
2T4C	11,5	4,0	9,6	0,0	0,0	3,0	30,2	114,9	126,8	9,4
2T4D	7,8	8,0	6,8	2,4	0,4	5,2	30,3	136,3	126,7	7,5
2T5	11,9	9,2	3,9	0,5	0,0	6,1	58,2	126,2	163,1	14,3
2T5B	17,4	7,0	7,6	1,4	6,4	6,6	54,0	146,1	127,1	12,1
2T5C	10,8	7,7	4,1	0,9	3,4	5,8	50,4	143,4	133,3	9,7
2T5D	11,8	9,3	6,3	2,4	2,2	8,0	64,5	145,5	147,5	17,8
2T6	10,9	7,7	6,0	1,2	0,8	3,9	65,7	60,2	92,6	28,6

	Trace elements (ppm)										
Sample	U	Th	Pb	Cr	V	Ba	La	Ce	Nd	S	Cl
1T1	0,0	4,2	0,0	168,8	17,2	15990,5	172,7	56,5	67,1	1183,0	3684,0
1T1B	0,9	0,0	6,1	149,4	16,7	123,2	160,2	55,5	116,7	1207,0	568,0
1T2	0,0	0,0	0,0	157,0	16,8	5189,6	69,9	55,1	68,4	1063,0	1474,0
1T2B	2,7	0,0	7,9	178,0	16,5	158,4	217,1	54,6	72,0	1277,0	442,0
1T2C	0,0	0,0	4,4	165,5	16,4	2110,6	146,3	54,4	154,6	1156,0	1020,0
1T3	0,0	9,0	10,9	179,2	16,1	122,0	151,6	90,2	137,7	1244,0	566,0
1T3B	0,0	4,3	9,9	230,7	15,8	334,1	111,4	51,6	224,4	1235,0	564,0
1T3C	0,0	5,8	5,6	203,2	15,8	3610,1	226,0	52,9	257,0	1314,0	1194,0
1T4	2,3	0,5	3,9	185,1	15,1	137,8	41,4	50,6	41,7	1131,0	737,0
1T4B	1,6	15,8	8,4	153,7	115,4	190,0	76,2	30,3	78,1	1347,0	279,0
1T4C	1,2	0,0	6,4	173,5	15,3	111,3	213,4	51,6	107,9	769,0	622,0
2T1	5,6	14,0	11,6	208,1	132,3	1144,2	289,5	701,2	302,5	2149,0	506,0
2T2	1,7	1,1	0,0	172,9	15,5	18345,4	203,5	91,2	203,5	1473,0	3733,0
2T3	0,0	0,0	5,7	172,7	15,6	3082,5	16,2	136,2	109,8	1338,0	1568,0
2T4	0,0	0,0	0,9	179,0	16,1	10465,7	169,3	54,0	124,9	1135,0	2525,0
2T4B	5,0	1,3	5,5	142,8	16,4	8069,3	256,7	54,0	197,1	1391,0	1861,0
2T4C	0,0	0,2	5,7	135,1	15,9	111,1	191,9	53,6	122,3	1319,0	555,0
2T4D	0,4	0,0	1,8	146,1	16,1	1530,6	41,7	53,7	154,1	801,0	828,0
2T5	0,0	1,5	0,0	193,3	16,2	4940,2	174,4	53,5	129,1	1154,0	1291,0
2T5B	0,0	0,0	8,5	172,2	15,5	223,9	135,6	51,7	215,4	1256,0	558,0
2T5C	5,1	0,0	4,6	145,0	15,8	85,9	196,1	53,7	132,1	1003,0	385,0
2T5D	0,0	0,0	6,0	184,6	15,7	3454,8	172,6	52,1	153,3	1343,0	1040,0
2T6	4,7	3,6	0,9	158,4	14,8	186,9	73,6	49,3	28,4	1198,0	693,0

Analyses by Rocklabs cc.

Sample	Major elements (%) SiO_2	TiO_2	Al_2O_3	Fe_2O_3	MnO	MgO	CaO	Na_2O	K_2O	P_2O_5	H_2O	LOI	TOTAL
1T1	47,19	0,33	10,49	3,53	0,04	5,38	4,27	0,30	0,75	0,23	8,62	13,31	99,96
1T1B	46,07	0,26	8,59	2,90	0,03	3,62	7,10	3,20	0,76	0,16	5,62	21,67	100,61
1T2	54,11	0,37	6,86	2,52	0,05	2,85	7,84	1,26	0,87	0,08	3,39	18,75	101,30
1T2B	57,20	0,43	7,65	2,92	0,09	2,41	5,26	3,08	1,07	0,14	3,28	17,07	100,88
1T2C	57,66	0,41	9,49	3,11	0,04	2,84	3,60	0,25	0,80	0,09	10,29	12,78	101,44
1T3	69,31	0,63	9,46	3,55	0,04	2,03	2,02	0,33	1,05	0,15	4,67	7,64	100,98
1T3B	69,30	0,55	8,63	4,43	0,04	2,18	2,31	0,38	1,29	0,15	1,30	8,73	99,35
1T3C	57,00	0,59	7,64	1,99	0,03	2,48	6,38	0,27	0,76	0,08	1,66	19,29	99,61
1T4	68,32	0,42	8,95	3,51	0,03	1,94	1,95	0,36	1,55	0,12	1,98	11,41	100,60
1T4B	70,29	0,42	12,75	4,15	0,03	3,33	1,93	0,26	1,25	0,25	1,26	4,52	101,20
1T4C	65,39	0,36	11,78	4,32	0,03	3,29	0,32	0,24	1,23	0,04	1,83	10,03	98,91
2T1	68,27	0,32	8,08	2,91	0,14	1,24	0,41	0,26	1,38	0,09	2,89	13,90	99,97
2T2	53,55	0,32	8,65	2,90	0,03	3,12	6,87	0,35	1,60	0,09	1,66	17,25	100,78
2T3	43,42	0,22	6,65	2,12	0,02	3,40	9,94	0,27	0,99	0,07	3,69	28,41	99,87
2T4	59,99	0,48	8,31	4,52	0,04	3,18	2,45	0,38	1,12	0,18	2,57	10,44	99,91
2T4B	50,63	0,25	7,87	1,88	0,02	5,79	6,71	0,27	0,65	0,09	3,28	19,91	101,05
2T4C	63,25	0,37	11,65	4,00	0,02	3,50	1,91	0,27	1,24	0,11	3,22	10,03	100,32
2T4D	58,13	0,24	9,07	2,41	0,03	6,37	3,19	0,25	0,71	0,10	3,91	15,19	100,96
2T4E	65,43	0,49	10,72	4,65	0,04	3,41	1,00	0,28	1,16	0,10	2,26	9,78	100,60
2T5	47,33	0,31	5,00	2,09	0,03	2,22	11,31	0,32	0,90	0,05	1,90	26,06	100,67
2T5B	43,81	0,31	7,23	2,47	0,03	2,62	6,86	0,08	0,61	0,09	13,86	21,21	99,76
2T5C	56,05	0,42	9,39	3,20	0,02	3,18	5,02	0,28	0,90	0,11	6,96	12,43	100,70
2T5D	44,25	0,37	8,11	2,77	0,03	2,42	10,57	0,21	0,74	0,08	2,59	27,54	100,83
2T6	66,24	0,42	8,33	3,24	0,03	1,47	2,00	0,39	1,85	0,08	1,74	13,27	100,90

Sample	Trace elements (ppm) Zn	Cu	Ni	Co	Ga	Nb	Zr	Y	Sr	Rb
1T1	52,1	27,0	66,8	0,0	15,2	9,6	130,1	933,0	503,7	55,9
1T1B	75,0	13,0	20,0	200,0	0,0	25,0	169,0	935,0	85,0	55,0
1T2	48,0	15,0	15,0	38,0	8,0	12,0	372,0	696,0	120,0	66,0
1T2B	79,0	11,0	20,0	293,0	0,0	6,0	303,0	825,0	100,0	52,0
1T2C	30,7	11,8	20,6	0,0	12,0	12,4	267,8	592,0	46,4	52,5
1T3	36,7	9,8	27,8	0,0	10,5	20,3	389,5	886,9	39,7	59,1
1T3B	36,0	10,2	20,8	0,0	10,8	17,3	389,7	545,0	45,6	73,5
1T3C	23,0	5,2	13,1	0,0	7,2	14,4	330,7	584,7	104,4	39,4
1T4	34,8	9,5	15,0	0,4	10,0	13,9	208,1	169,4	36,6	85,2
1T4B	39,6	13,4	14,0	3,3	15,9	10,4	205,8	353,6	43,5	65,3
1T4C	41,3	12,3	12,7	1,6	15,8	11,9	175,8	28,6	32,6	75,7
2T1	32,1	13,9	40,2	44,9	7,1	10,7	139,9	160,4	56,7	74,4
2T2	33,5	16,7	18,8	2,2	6,8	7,9	130,3	186,1	298,0	77,7
2T3	27,5	6,0	10,2	2,5	5,8	8,3	112,9	309,1	88,8	60,9
2T4	32,8	22,7	31,7	0,0	9,0	12,5	187,0	434,4	346,3	60,8
2T4B	18,6	9,9	12,3	1,0	8,6	6,3	118,1	519,7	212,2	33,5
2T4C	42,2	13,9	20,6	0,0	15,8	14,9	193,4	525,4	62,3	82,4
2T4D	23,9	9,3	13,5	0,0	17,0	9,0	128,6	566,9	104,4	42,7
2T4E	37,2	15,2	22,8	0,0	15,9	16,0	265,6	642,5	111,9	63,1
2T5	22,5	9,4	12,4	1,1	4,7	6,5	153,9	343,6	187,3	42,2
2T5B	28,0	6,7	14,9	0,4	9,7	13,2	182,3	719,1	90,2	33,3
2T5C	31,8	14,3	27,3	0,0	8,0	9,0	241,8	675,9	199,4	51,4
2T5D	25,7	8,5	11,8	2,0	11,2	10,0	154,2	432,7	109,5	44,5
2T6	38,3	9,4	14,7	0,1	8,7	9,4	191,6	174,2	36,1	88,2

Sample	Trace elements (ppm) U	Th	Pb	Cr	V	Ba	La	Ce	Nd	S	Cl
1T1	9,1	17,4	0,0	67,8	28,2	48427,8	793,2	69,1	1012,2	1735,2	8018,0
1T1B	0,0	0,0	25,0	65,3	40,7	3155,1	605,0	145,9	780,6	3698,0	948,0
1T2	0,0	13,0	12,0	231,5	42,2	10170,4	582,0	252,1	633,7	1873,0	1505,0
1T2B	0,0	12,0	30,0	150,8	43,7	5165,9	920,5	155,5	555,3	3274,0	1384,0
1T2C	10,0	15,2	17,3	209,1	34,6	685,6	590,8	49,4	743,7	1324,0	274,0
1T3	9,6	30,8	24,1	319,0	46,6	433,8	837,2	212,1	1135,1	1644,0	252,0
1T3B	7,9	28,8	28,8	177,4	92,5	353,4	654,5	143,9	801,9	1499,0	232,0
1T3C	7,7	17,0	10,4	145,0	29,0	12444,1	650,2	65,4	848,1	2061,0	3139,0
1T4	1,4	12,7	12,7	140,0	91,3	318,3	270,6	44,7	201,9	1337,0	397,0
1T4B	6,5	19,9	15,8	89,3	39,8	854,3	155,5	47,3	241,4	2157,0	371,0
1T4C	1,9	11,8	7,3	139,8	105,4	199,5	31,7	52,4	16,2	1438,0	256,0
2T1	1,1	12,2	15,5	108,9	98,4	937,7	225,0	478,3	155,3	1629,0	304,0
2T2	0,0	12,5	0,0	112,0	49,1	38481,3	349,6	54,0	324,9	1552,0	7047,0
2T3	2,1	6,6	11,1	106,7	32,2	5463,5	587,1	94,9	473,3	1345,0	1358,0
2T4	0,0	15,5	0,0	94,6	41,6	54921,3	515,2	32,0	509,1	1964,0	9455,0
2T4B	3,1	12,8	0,0	69,4	10,1	32641,9	690,6	32,2	715,2	1735,0	6091,0
2T4C	6,3	14,9	14,5	143,4	57,9	6050,7	651,8	81,6	671,6	1492,0	1275,0
2T4D	0,0	6,0	6,6	78,7	47,3	11550,6	755,6	29,5	827,4	1540,0	2154,0
2T4E	4,5	17,7	9,3	112,3	55,6	10859,3	929,9	170,6	1077,5	1433,0	1799,0
2T5	0,0	7,1	2,0	100,6	36,1	27639,0	391,2	70,5	419,3	1220,0	4769,0
2T5B	0,7	13,8	10,9	128,3	26,4	4740,3	582,4	51,1	756,3	1203,0	873,0
2T5C	0,0	17,1	7,3	191,8	28,0	23932,9	755,6	109,3	902,8	1626,0	3996,0
2T5D	0,0	14,4	8,1	92,3	29,8	9723,6	519,7	138,3	647,3	1128,0	2112,0
2T6	5,9	14,2	14,4	262,2	90,4	339,9	227,6	96,3	156,0	1462,0	420,0

Analyses by Rocklabs cc.